Design, Synthesis, Characterization, and Reactivity of Group III *ansa*-Metallocenes Containing Bulky Alkyl and Silyl Substituents

Thesis by

Michael B. Abrams

In Partial Fulfillment of the
Requirements for the Degree of
Doctor of Philosophy

Division of Chemistry
and Chemical Engineering

California Institute of Technology
Pasadena, California

1998
(Submitted January 6, 1998)

For my parents

Acknowledgments

I have been very fortunate to have been able to work for and with John Bercaw during my stay at Caltech, and I am deeply appreciative of the support, guidance, and generosity that he has provided over the course of my graduate career. I consider myself very lucky to have been able to work for an advisor who granted me the freedom to explore what I found interesting, both in and out of the laboratory.

I can not thank my family enough for their assistance and enthusiasm. My parents have been sources of unwavering support, and I am truly indebted to them for all that they have provided. I've also truly appreciated the kind thoughts and deeds of my grandparents.

I would especially like to thank my brother for being a true confidant. He has always been there for me with a receptive ear and a much-enjoyed and appreciated perspective on just about everything. In addition, the almost frightening ability of Le Chèvre to motivate me to drop everything and run to Tucson, Las Vegas, San Francisco, Berkeley, Oakland, and other locales in North America too numerous to mention have resulted in some of my most enjoyable memories and outrageous stories of the last several years.

The Bercaw Mafia has provided a unique assortment of people with whom I am happy to have spent the last seven (?) years. Bryan Coughlin (SB#1) taught me all that I ever wanted to know about vacuum line techniques; I blame him personally for getting me started in organosilicon chemistry. Andy Kiely, in addition to being a terrific linemate and softball coach, is one of the few people who truly knows what does and what does not go into a whiskey sour (viva Diver Cocktails™!). It has also been a pleasure to share a vacuum line with Chris (Jag) Brandow, whose dance moves are overshadowed only by his fine singing voice. Many thanks to Alex Muci for not booting me off the vac line while he was getting started, and for reading the next to last installment of allyl misery.

Donnie Cotter's Organometallics seminar was the first one I saw here at Caltech, and his unabashed mid-seminar belch certainly made me take notice

of the Bercaw group; he also took me on my first backpacking trip in the Sierras, and the beauty of Little Five Lakes Basin and the Kaweah Gap more than made up for me wanting to kill him during every step of the entire 3000+ foot slog up and over Black Rock Pass. Roger Quan taught me how to rule the Blue Box with an iron fist (glove?), and demonstrated the subtleties involved in throwing a softball from third to first base. I always enjoyed Eric Kelson's presence on backpacking trips and at softball games. I can't thank Sharad (Bahooka) Hajela enough for his help in and out of lab; he's a great person with whom to talk chemistry, and his home has provided fantastic food, usually way too much drink, and shelter from the occasional Hurricane. Bob Blake knew the importance of and introduced me to Big Wednesday, as well as Little Thursday. As well as being a fine chemist and a source of fruitful discussions, Tim (Vandalism is Cool) Herzog is a close friend and was a great roommate (may the Disco Party pictures survive forever!) and hiking partner. Thanks to Eva Birnbaum for helping motivate me to go to New Mexico, and to Shannon Stahl for relentless cheerfulness on backpacking trips and for debates on the nature of fish tacos. Many thanks to Susan (Donut Dilemma) Brookhart, my running partner, sometimes climbing partner, and faithful dream analyzer. It's been amazing to work in the same labs as Antek Wong-Foy, who is poised to lead the Bercaw Mafia into the 21st century; thanks for your enthusiasm both on and off of the 2nd floor of Noyes. My fourth year as a grad. student provided a litter of new Hogs: in addition to the previously mentioned WWF, we gained Cory Nelson and Steve Miller, with whom I have had the pleasure of sharing multiple Hogball innings. Jeff (A.J., Turbo, Sparky) Yoder, my partner in allyl crime, has been a great person with whom to discuss all things fluxional, preferably over a steaming trough of Phillips BBQ. It's been really fun sharing the Nook™ with Deanna Zubris (despite her choice of calendars) and going to P-Chem seminars with Paul (Notorious) Chirik. Many thanks to Annita Zhong for not giving me grief about my progress writing props, and to Seva (Can You Dope It?) Rostovtsev for harassing me on a nearly daily basis about my progress writing props.

Numerous Postdocs have influenced my life here at Caltech. Gui Bazan introduced me to the wonders of the Dining Society, Gerrit Luinstra was in the San Francisco hotel room when Screaming Weasels were invented/discovered/born, and Dave Antonelli showed me how the hell to find The Room. I really enjoyed trying to understand Jon (Limus) Mitchell talk chemistry over the roar of the vac lines and glove box and stereo back when we were in 201; also great fun was trying to understand him talk about anything in our frequent forays outside of Noyes. Eugene Mueller, Stephanie Chacon, and Antonio Pastor kept conversations in the Orange Room lively, and I'm indebted to Lin Wang for being a great Beer Coach, and to (Where's) Jim Gilchrist for discussions on all things organic, at BI social hours, and at parties in the toilet seat statue. Matt Holtcamp has killed, skinned, and eaten one of almost every animal on this planet, and it was fun having someone with whom to commiserate while interviewing for jobs. Cyrille Loeber added enantiomerically pure metallocenes to the confusion of allyl rearrangements. Thanks to Shigenobu Miyake for continuing to bring fame and fortune to compounds containing Adamantyl substituents, and to Dario Veghini for dinner parties, discussions about chemistry, runs to Lucky Baldwin's, and for aiding my fluency in Italian. Chris Levy arrived just in time to make and enliven this year's hike in the Sierras, and I hope that rest of the group drags him along on several more (or vice versa); I am forever indebted to him, as well, for braving Crenshaw Blvd. on New Years Eve for a mid-thesis Phillips run.

There are also several people outside of my research group who I'd like to thank. Chris Kenyon and Ken Brameld have been fantastic climbing partners and occasionally as successful poker players, without whom grad school would have been no fun whatsoever. Mike (Aeropuerto) Woolf , Ken and Jen Butvill, Alison McCurdy, Chris Karp, Maria Khader, Eric Rubinstein, Arnel Fajardo, Tom (P) Shields, Dave (Slug) Lauterbach, and all the deadbeats who showed up for Poker Nights™ truly helped make life fun.

Abstract

The preparations of a series of silyl-bridged bis(cyclopentadiene) complexes containing bulky alkyl and silyl substituents are reported. Incorporation of tertiary alkyl groups are required in order to direct trimethylsilyl groups exclusively adjacent to the silyl linkers. This 1,2,4- substitution is crucial for the directed syntheses of chiral *ansa*-metallocenes. Transmetallation of $Me_2Si\{2\text{-}SiMe_3\text{-}4\text{-}[2\text{-}(2\text{-}CH_3\text{-}C_{10}H_{14})]\text{-}C_5H_2\}_2^{2-}$ affords exclusively *racemo*-(chiral) Group III metallocenes, whereas transmetallation of $Me_2Si\{3\text{-}[2\text{-}(2\text{-}CH_3\text{-}C_{10}H_{14})]\text{-}C_5H_3\}_2^{2-}$ (lacking the α-TMS groups) proceeds with the opposite enantioselectivity, generating exclusively *meso*- (achiral) metallocenes.

Treatment of *meso*-$Me_2Si\{3\text{-}[2\text{-}(2\text{-}CH_3\text{-}C_{10}H_{14})]\text{-}C_5H_3\}_2MCl\text{-}(LiCl)\text{-}(THF)_2$ (*meso*-AdpMCl-(LiCl)-$(THF)_2$) with allylmagnesium bromide affords *meso*-AdpM(η^3-C_3H_5) (M = Sc, Y). Hydrogenolyses of these *meso*-metallocenes generate highly reactive 14-electron d^0 metal hydride complexes. The methyladamantyl substituents on the Cp rings inhibit formation of bridging hydride dimers, enabling the reactive *meso*-AdpMH monomers to react readily with available solvent or metallocene C-H bonds.

Treatment of $[rac\text{-}Me_2Si\{2\text{-}SiMe_3\text{-}4\text{-}[2\text{-}(2\text{-}CH_3\text{-}C_{10}H_{14})]\text{-}C_5H_2\}_2Y(\mu\text{-}Cl)]_2$ ([*rac*-AbpY(μ-Cl)]$_2$) with $LiCH(SiMe_3)_2$ affords the bulky yttrium-alkyl complex *rac*-AbpY$CH(SiMe_3)_2$. This alkyl complex readily polymerizes ethylene, but does not react with α-olefins. Hydrogenolysis of *rac*-AbpY$CH(SiMe_3)_2$ generates the homochiral hydride dimer [*rac*-AbpY(μ-H)]$_2$. The bulk of the methyladamantyl substituents inhibits formation of the heterochiral hydride dimer. Efforts are made to assess the ability of the methyladamantyl groups to inhibit the hydride monomer-dimer equilibria that deactivates previously reported group III Ziegler-Natta catalysts. The hydride dimer [*rac*-AbpY(μ-H)]$_2$ is an α-olefin hydrogenation catalyst, but does not oligomerize or polymerize α-olefins. [*rac*-AbpY(μ-H)]$_2$ also reacts readily with dihydrogen, allene, and 2-butyne; examples of σ-bond metathesis, alkyne insertion, and β-hydride elimination have been observed for [*rac*-AbpY] complexes.

The fluxional behavior exhibited by a series of d^0-metallocene η^3-allyl complexes is investigated. Lineshape analysis of NMR studies performed on these complexes indicates activation barriers of ~8-14 kcal/mol for processes involving dissociation of the allyl C=C double bond as the rate determing step. Investigation of C_s-symmetric linked scandocenes and yttrocenes allows elucidation of a second allyl rearrangement mechanism which operates concurrently with olefin dissociation: in-plane rotation rotation of the intact η^3-allyl ligand. Allyl rotation is generally fast relative to the rate of olefin dissociation. Ligand, metal, and solvent effects on the observed rates are discussed.

Table of Contents

List Of Figures

Chapter 1:

Chapter 2:

Chapter 3:

Chapter 4:

LIST OF TABLES

Chapter 4:

Appendix C: Variable Temperature ^1H NMR Data for 15-18

Appendix D: Selected gNMR Data

LIST OF SCHEMES

Chapter 3:

Chapter 4:

Chapter 1

Discovery and Development of Homogeneous Ziegler-Natta Catalysis

Abstract

A brief introduction to the discovery of and recent developments in the field of Ziegler-Natta catalysis is provided in order to provide context for the experiments described in Chapters 2, 3, and 4.

Introduction

The discovery that group IV transition metal-halides and certain aluminum alkyls may be used to catalyze the polymerization of ethylene was made by Karl Ziegler more than 40 years ago.[1] The extension of this type of catalyst mixture to the polymerization of α-olefins was made shortly thereafter in the laboratories of Giulio Natta.[2] Since then, intense research on heterogeneous α-olefin polymerization systems have lead to the development of catalysts with remarkable activities and regio- and stereochemical selectivities; billions of pounds of polyolefins are produced annually using these Ziegler-Natta catalysts.[3] Complicating characterization of the active site of and detailed mechanistic studies on these systems are the heterogeneous nature of the polymerization reactions and the fact that the catalysts are often poorly-defined mixture of $MgCl_2$-supported metal halide, trialkylaluminum, and ester or amine donor species.

Efforts to develop homogeneous catalysts that rivaled the activities and selectivities of the heterogeneous systems, yet which proved more amenable to mechanistic investigation and rational catalyst design, were prompted by the observation that solutions of titanocene dichloride and alkyl aluminum species could be used to catalyze the polymerization of ethylene.[4,5] A major breakthrough in the development of homogeneous catalysts was the discovery by Sinn and Kamisnky[6] that the addition of methylaluminoxane (MAO) to any of a variety of group IV metallocenes generated highly active olefin polymerization catalysts. The MAO cocatalyst, generated by the addition of exactly one equivalent of water to trimethylaluminum, presumably consists of a mixture of linear and cyclic oligomers containing the -Al(O)(CH_3)- repeat unit.[7]

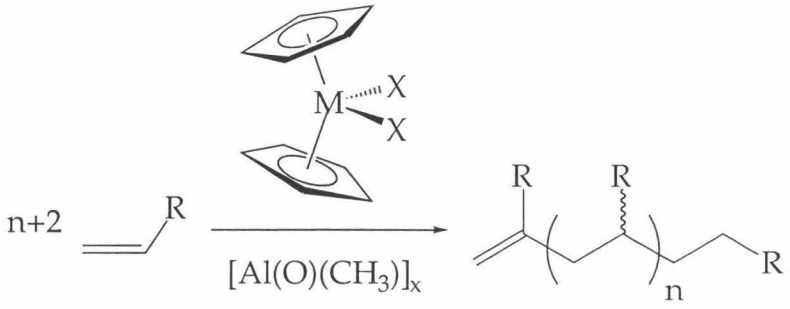

Another significant advance in the use of metallocenes as Ziegler-Natta catalysts was the finding by Brintzinger[8] that chiral metallocenes could be utilized as the precursors to catalysts for the stereospecific polymerization of propylene and other α-olefins. The use of rigid C_2-symmetric group IV metallocenes, such as *racemo*-ethylenebis(tetrahydroindenyl)zirconium dichloride (*rac*-EBTHIZrCl_2, **1**), in conjunction with sufficient MAO to afford ~1000-fold excesses of Al:Zr were found to catalyze the polymerization of propylene to isotactic polypropylene. Both the activity and stereospecificity of this system approached those of the commercially employed heterogeneous systems.

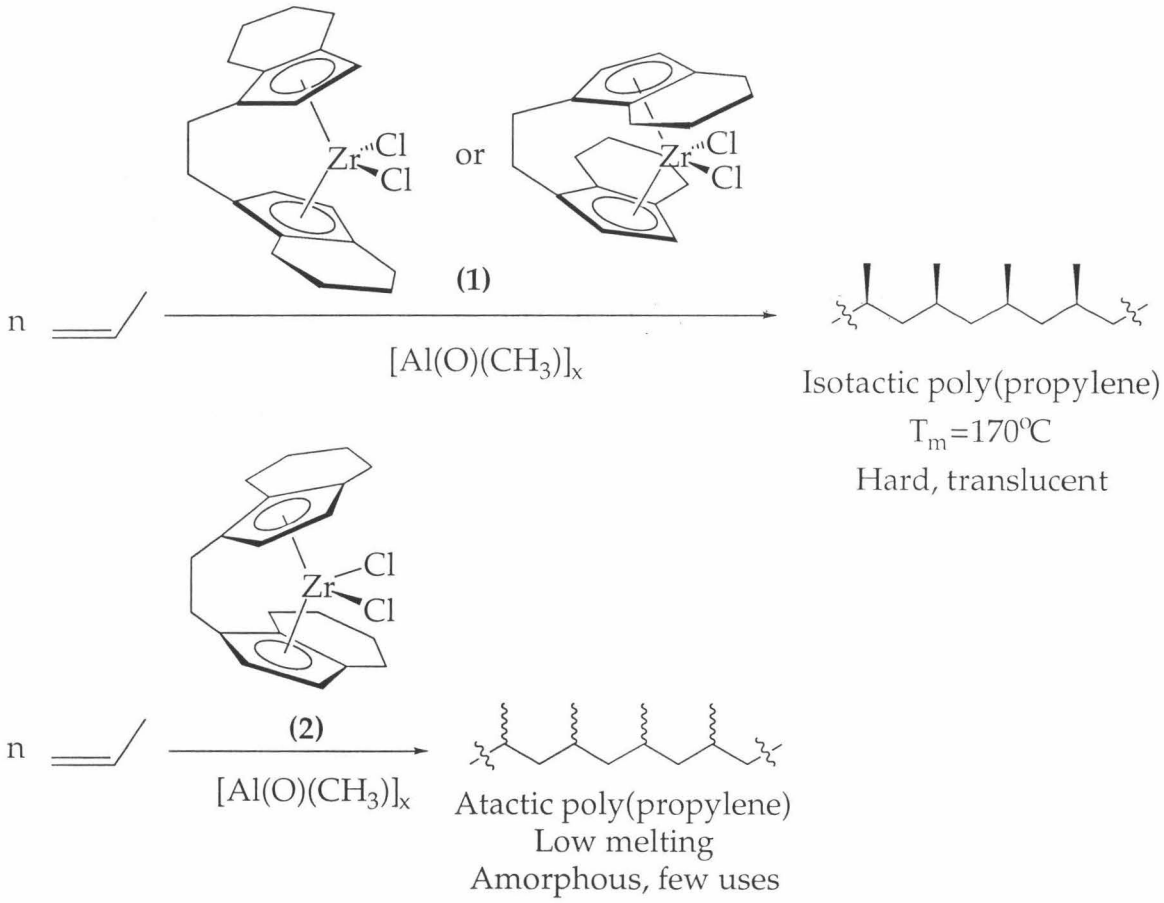

One drawback to the use of this type of chiral catalyst was the fact that isolation of the *racemo*- isomers was a prerequisite for the production of isotactic polypropylene. The achiral *meso*- conformer (**2**), which was typically formed in two-fold to ten-fold excesses along with the desired *racemo*-metallocenes, generate atactic polypropylene. Although methods were

developed for the purification and isolation of exclusively the C_2-symmetric isomers, these separations were typically tedious and resulted in significantly diminished yields of available catalyst precursors.

Investigations into the electronic requirements for the generation of active homogeneous metallocene catalysts indicate that part of the role of the MAO cocatalyst is to generate a cationic 14-electron d^0-metallocene alkyl.[9-11] Watson first demonstrated that 14-electron d^0-metal complexes could act as ethylene polymerization catalysts.[12] The use of $Cp^*_2LuCH_3$, which is isolectronic with cationic $[Cp_2M\text{-}R]^+$ (M=group IV), to demonstrate olefin insertion, β-H elimination, β-methyl elimination, and σ-bond metathesis showed that neutral metallocenes could be used as model complexes for the fundamental steps involved in olefin polymerization, supporting the notion of 14-electron d^0 active sites for the group IV systems.

Further support for the involvement of 14-electron metal centers as the active polymerization catalysts came from research in which a single alkyl substituent was removed from neutral group IV metallocenes to generate complexes of the form $[Cp_2M\text{-}R]^+ [A]^-$ (M=Ti, Zr, Hf; A="weakly coordinating" counterion), which initiate olefin polymerization. Convenient methods for the removal of an alkyl group involve protonolysis by dimethylanilinium ($C_6H_5NH(CH_3)_2$) salts, first developed by Turner,[13-15] or by abstraction using the highly Lewis acidic trityl cation ($(C_6H_5)_3C^+$).[16,17] Fluorophenylborate counterions ($B(Ar_F)_4^-$) such as $[B(C_6F_5)_4]^-$[14,18] and $[B(C_6F_4SiR_3)_4]^-$[19] have proven less prone to side reactions with or deactivation of the metal cation than have conventional counterions such as $[BF_4]^-$, $[PF_6]^-$, and $[BPh_4]^-$.[20] The highly Lewis acidic $B(C_6F_5)_3$ may be alternately be used to generate complexes such as **3** which are active for ethylene and propylene polymerization.[21,22]

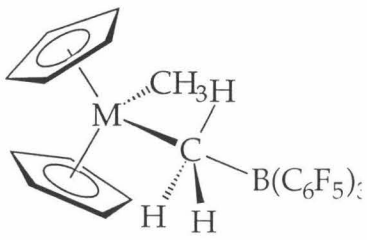

(3)

Uncertainties in the roles of the various counterions in the initiation, propagation, and termination of polymerization by the $[Cp_2MR]^+[B(Ar_F)_4]^-$ catalysts are obviated by the use of isoelectronic neutral group III metallocene complexes as Z-N catalysts. Previous work in the Bercaw group has shown that scandocene and yttrocene derivatives may act as single component catalysts for the polymerization of ethylene and the stereospecific polymerization of α-olefins.

At low temperatures, the permethylscandocene methyl complex **4** was shown to be an active catalyst for the living polymerization of ethylene.[23,24] Although **4** reacts with propylene, σ-bond metathesis results in the generation of methane and the vinylic complex **5**. Unfavorable steric interactions between the bulky pentamethylcyclopentadienyl ligands and the alkyl group of incoming monomer explain the inability of $Cp^*_2Sc\text{-}CH_3$ to oligomerize, or even insert, propylene (Figure 1).

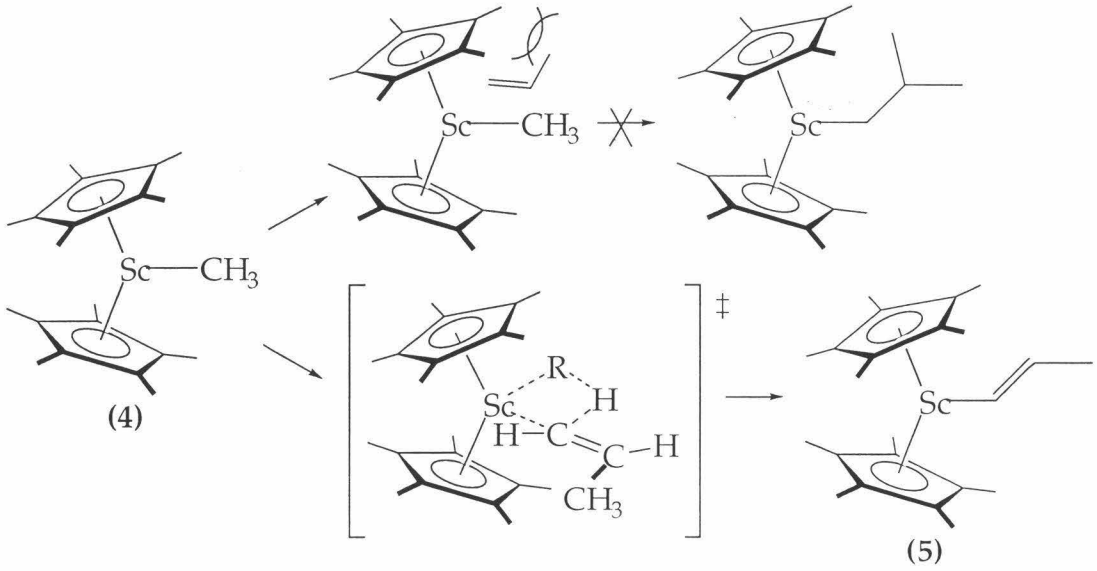

Figure 1. Olefin insertion vs. σ-bond metathesis for $Cp^*_2Sc\text{-}CH_3$ (**4**).

The use of dimethylsilyl linked cyclopentadienyls to reduce the effective steric congestion at the metal center has been demonstrated by the ability of $Me_2Si(C_5Me_4)_2Sc(H)PMe_3$ (**6**, OpScH(PMe_3)) to catalyze the head-to-tail dimerization of α-olefins and the cyclization of α,ω-dienes.[25] A similar reactivity towards olefinic substrates was observed for [*meso*-$Me_2Si(3\text{-}CMe_3\text{-}C_5H_3)_2Sc(\mu\text{-}H)]_2$ (**7**, [*meso*-DpSc(μ-H)$_2$]), whose reduction in steric crowding at

the metal center is manifested by the dimerization of the electron-deficient monomeric Sc-H species responsible for catalysis.

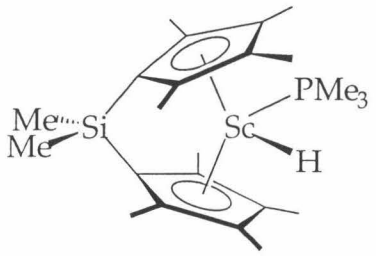

(6)

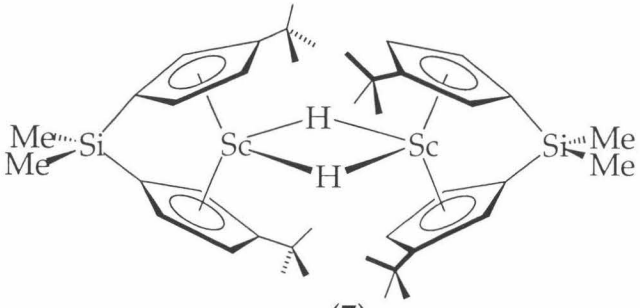

(7)

Further reductions to the bulk of the ancillary ligand array was achieved by replacement of one of the cyclopentadienyl rings with an alkylamido fragment, resulting in derivatives of $Me_2Si(C_5Me_4)[N(CMe_3)]$ (abbreviated Cp*SiNR) such as **8** $([Cp^*SiNRSc(\mu\text{-}H)(PMe_3)]_2$ and **9** $([Cp^*SiNRSc(\mu\text{-}CH_2CH_2CH_2CH_3)]_2$.[26,27] The Cp*SiNRSc systems polymerize ethylene and propylene at room temperature, and were the first examples of single component α-olefin polymerization catalysts. The group IV derivatives utilizing the Cp*SiNR and related ligand arrays have generated considerable interest as possible commercial ethylene/1-alkene copolymerization catalysts.[28-30]

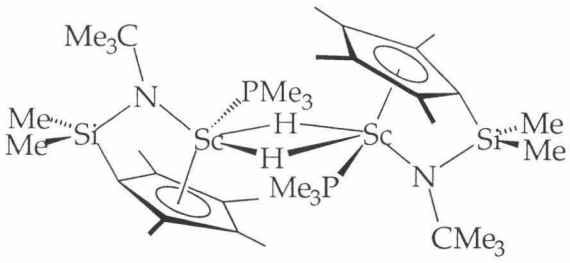

(8)

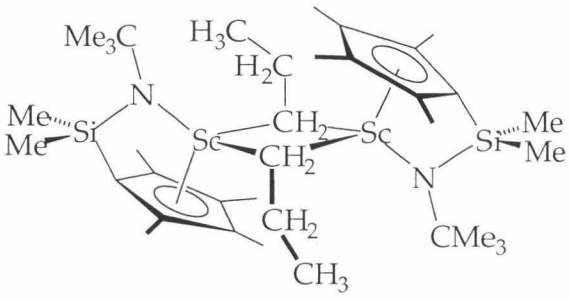

(9)

The introduction of additional silyl substituents to the cyclopentadienyl rings can be used to generate single component isospecific olefin polymerization catalysts. The C_2-symmetric yttrocene **10** ($\{rac\text{-}[Me_2Si(2\text{-}SiMe_3\text{-}4\text{-}CMe_3\text{-}C_5H_2)_2Y(\mu\text{-}H)\}_2$, $[BpY(\mu\text{-}H)]_2$) catalyzes the stereospecific polymerization of propylene, 1-butene, 1-pentene, and 1-hexene to isotactic poly(α-olfins).[31]

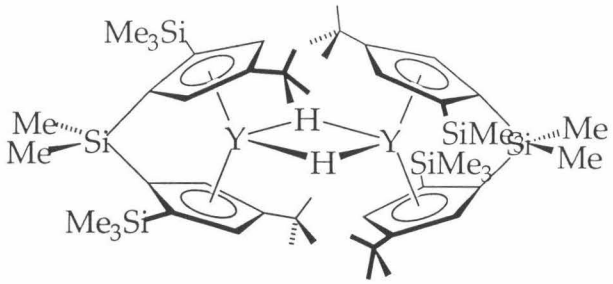

(10)

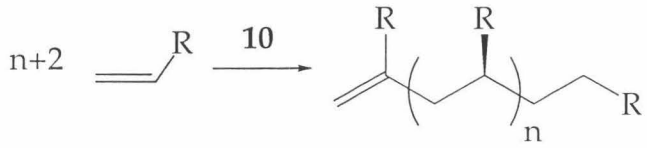

Synthesis of the [Bp] ligand array proved to be a major breakthrough in the construction of chiral metallocenes, as exclusively *racemo*-metallocenes are formed upon metallation of $[Bp]^{2-}$ (M=Sc, Y, La, Ti, Zr),[32,33] thus eliminating the need for tedious separation of *racemo*- from undesired *meso* conformers. Unfavorable steric interactions between the trimethylsilyl groups in the narrow portion of the metallocene wedge are believed to direct the syntheses of exclusively C_2-symmetric (*racemo*) metallocenes.

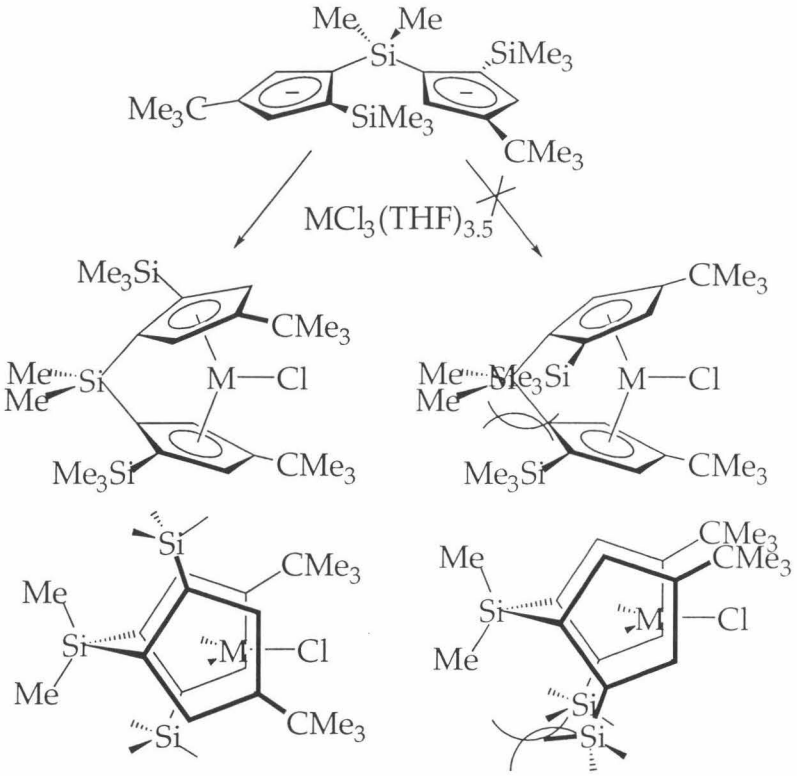

The use of trimethylsilyl groups adjacent to a silyl- linking unit may be employed to direct the formation of *racemo*-metallocenes incorporating linkers other than the dimethylsilyl moiety in [Bp]. The use of an enantiomerically pure 1,1′-bi-2-naphthol to generate a chiral linking unit resulted in the directed synthesis of diastereomerically pure metallocenes.[34] In addition to the TMS-TMS interactions in the narrow portion of the metallocene wedge preventing formation of *meso*-metallocenes, steric interactions between the TMS groups and the 3,3′-methine positions of the naphthalene rings are thought to induce enantioselective metallation of the $[(C_{20}H_{12}O_2)Si(2\text{-}SiMe_3\text{-}4\text{-}CMe_3\text{-}C_5H_2)_2]^{2-}$ ($[BnBp]^{2-}$) ligand array.

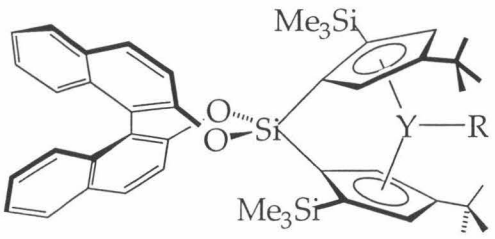

R,S-[BnBp]Y-R

(11)

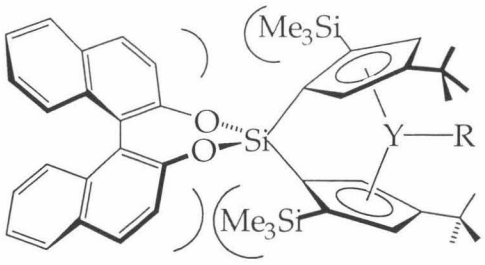

S,S-[BnBp]Y-R

(not observed)

Initial mechanisms for the C-C bond forming step in olefin polymerization invoked direct addition of the olefin across the M-alkyl bond (Figure 2), the so-called Cossee-Arlman mechanism.[35,36] This mechanism, however, did not account for the empirical observation that two vacant metallocene orbitals appeared to be a prerequisite for olefin insertion; although they contain d^0 metal centers, 16-electron metal dialkyls such as $Cp_2Zr(CH_3)_2$ do not insert olefins.

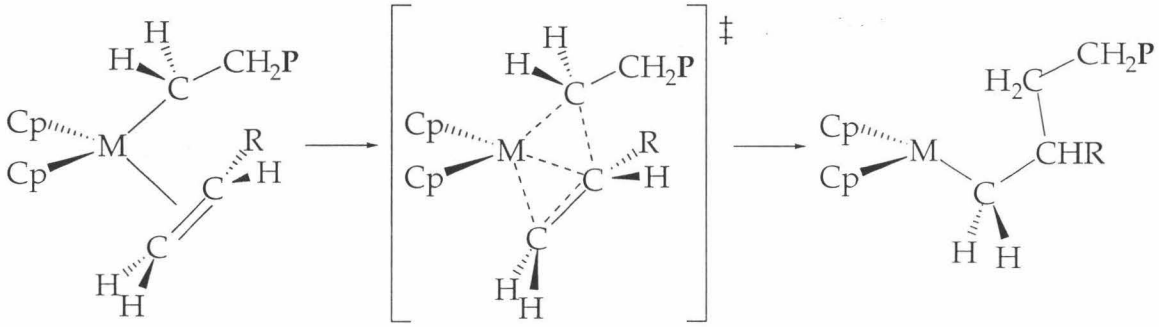

Figure 2. The Cossee-Arlman mechanism for olefin insertion.

Rooney and Green[37,38] noted the availability of multiple oxidation states for the group V metals, and proposed a mechanism in which there is α-elimination from a M-alkyl species; subsequent cyclization and reductive elimination would serve to regenerate a propagating metal-alkyl (Figure 3). The fact that cationic group IV and neutral single component group III and lanthanide metallocene complexes, which can not undergo the formal oxidation resulting from α-elimination, are active polymerization catalysts efficiently refutes this proposed mechanism.

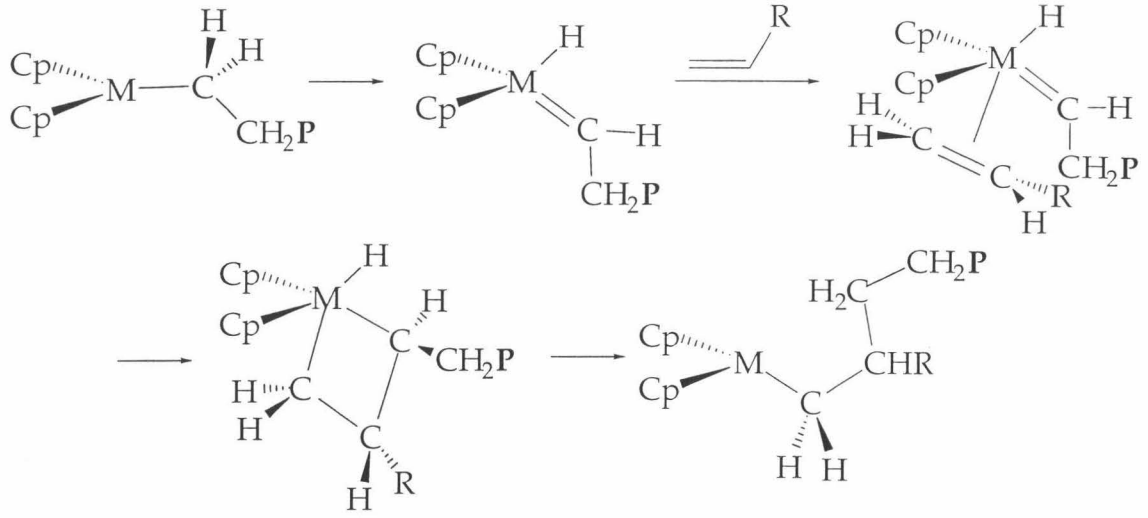

Figure 3. The original Green-Rooney mechanism (M=Group V).

In a modification to the Green-Rooney mechanism, Green and Brookhart[39] proposed that one vacant orbital was required for olefin coordination and that a second vacant orbital accommodates an α-agostic interaction which facilitates olefin insertion into the metal-alkyl bond (Figure 4). The requirement for α-agostic assistance in olefin insertion has generated considerable debate. While Bercaw,[40,41] Brintzinger,[42,43] and Stille[44] have developed systems which provide evidence for α-agostic interactions, other experiments devised in the laboratories of Grubbs[45] and Brintzinger[43] show no evidence for such interactions, and implicate a transition state such as **A** as that for olefin insertion.

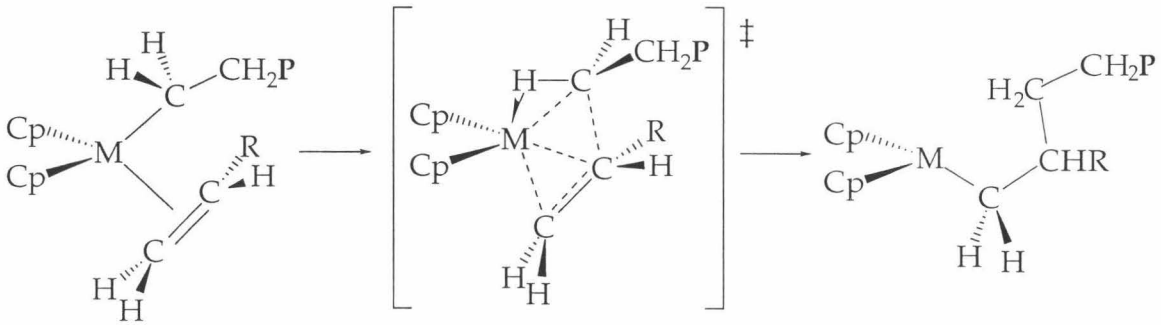

Figure 4. The modified Green-Rooney mechanism.

One drawback to mechanistic studies on **7-11** results from the tendency of the highly electron deficient metal hydrides and alkyls to dimerize. Although the bridging hydride dimers **10** and that of **11** promote the

stereospecific polymerization of α-olefins, the polymerizations are slow; typical reactions produce enchainment of several hundred monomer units after days in neat olefin. This sluggishness is attributed to the low concentration of 14-electron monomeric Y-H species in solution, a direct result of the monomer-$(\mu\text{-H})_2$ dimer equilibria which heavily favor the inactive 16-electron dimers. It has been shown that bridging d^0f^n- metal-hydrides react ~ 10^8-10^{10} times slower than the corresponding terminal hydrides.[46] The equilibria for metallocenes incorporating *tert*-butyl substituents in the open portion of the wedge (such as **7**, **10**, and **12**) is sufficiently weighted towards the dimer so that monomeric Y-H species are never observed in solution by ^{1}H NMR spectroscopy.

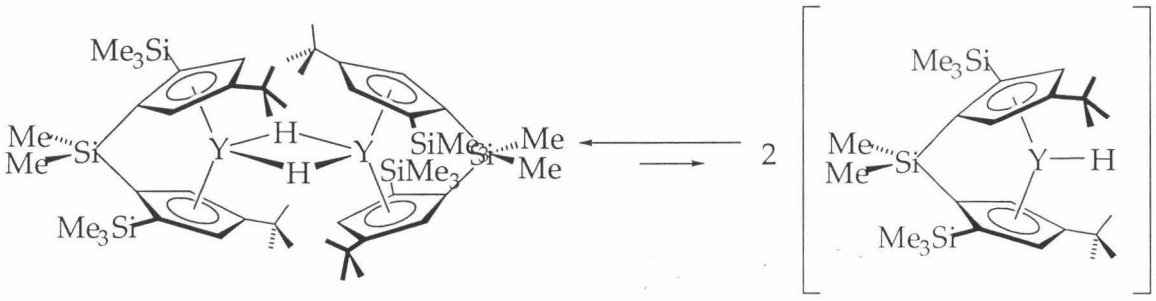

(never observed directly)

Although the advent of single component catalysts allowed kinetic studies on systems that afforded atactic polyolefins, similar investigations had not been performed on isospecific systems. The availability of a monomeric C_2-symmetric Y-H species would be invaluable for such mechanistic studies. Rates of processes such as olefin insertion into metal hydride (initiation), insertion into metal alkyls (propagation), β-H or β-Me elimination (termination) could then be measured directly by techniques such as NMR spectroscopy. In addition, insertion of an unsymmetric *gem*-disubstituted olefin to a M-H species would result in a chiral alkyl unit in a chiral metallocene framework, ideal for characterization by techniques such as X-Ray diffraction. The stabilities of the previously observed $(\mu\text{-H})_2$ dimers had prevented studies such as those described above.

The replacement of the *tert*-butyl groups in the open portion of the metallocene wedge with more extensive alkyl substituents was proposed to be a means of perturbing the monomer-dimer equilibria to disfavor formation

of the $(\mu\text{-H})_2$ dimers, thus favoring formation of the active 14-electron monomers. Crucial to the directed syntheses of C_2-symmetric metallocenes, however, was the placement of the trimethylsilyl substituents adjacent to the silyl linker; the results of such changes in alkyl substitution on ligand syntheses, and the abilities of the resultant metallocenes to insert α-olefins, remained to be investigated.

Chapter 2 describes the syntheses of such ligand arrays incorporating cyclohexyl-, 2-adamantyl-, and 2-(2-methyl)-adamantyl- substituents, and the contents of Chapter 3 concern the elucidation of the ability of 2-(2-methyl)-adamantyl substituents to perturb monomer-dimer equilibria and prevent formation of (μ-H) dimers. Chapter 4 is a mechanistic study on allyl rearrangement processes that arose initially from the characterization of several complexes derived from ligand arrays incorporating methyladamantyl groups.

References and Notes

1. Ziegler, K.; Holzkamp, E.; Breil, H.; Martin, H. *Angew. Chem.* **1955**, *67*, 541.

2. Natta, G. *Angew. Chem.* **1956**, *68*, 393.

3. Thayer, A. N. *Chem. Eng. News.* **1995**, *73*, 15.

4. Natta, G.; Pino, P.; Mazzanti, G.; Giannini, U. *J. Am. Chem. Soc.* **1957**, *79*, 2975.

5. Breslow, D. S.; Newburg, N. R. *J. Am. Chem. Soc.* **1957**, *79*, 5072.

6. Andersen, A.; Cordes, H. G.; Herwig, J.; Kaminsky, W.; Merck, A.; Mottweiler, R.; Pein, J.; Sinn, H.; Vollmer, H. J. *Angew. Chem., Int. Ed. Engl.* **1976**, *15*, 630.

7. Mason, M. R.; Smith, J. M.; Bott, S. G.; Barron, A. R. *J. Am. Chem. Soc.* **1993**, *115*, 4971.

8. Kaminsky, W.; Külper, K.; Brintzinger, H. H.; Wild, F. R. W. P. *Angew. Chem. Int. Ed. Engl.* **1985**, *24*, 507.

9. Jordan, R. F. *Adv. Organomet. Chem.* **1991**, *32*, 325.

10. Long, W. P.; Breslow, D. S. *Liebigs. Ann. Chem.* **1975**, 463.

11. Harlan, C. J.; Bott, S. G.; Barron, A. R. *J. Am. Chem. Soc.* **1995**, *117*, 6465.

12. Watson, P. L. *J. Am. Chem. Soc.* **1982**, *104*, 337.

13. Hlatky, G. G.; Turner, H. W.; Eckman, R. R. *J. Am. Chem. Soc.* **1989**, *111*, 2728.

14. Turner, H. H. *Eur. Pat. Appl.* **1988**, 277004.

15. Hlatky, G. G.; Turner, H. W. *Eur. Pat. Appl.* **1988**, 277003.

16. Ewen, J. A.; Elder, M. J. *Eur. Pat. Appl.* **1991**, 426637, 426638.

17. Chien, J. C. W.; Tsai, W.-M.; Rausch, M. D. *J. Am. Chem. Soc.* **1991**, *113*, 8570.

18. Turner, H. W. *Chem. Abstr.* **1989**, *110*, 58290a.

19. Lia, L.; Yang, X.; Ishihara, A.; Marks, T. J. *Organometallics* **1995**, *14*, 3135.

20. Bochmann, M. *J. Chem. Soc., Dalton Trans.* **1996**, 255.

21. Yang, X.; Stern, C. L.; Marks, T. J. *J. Am. Chem. Soc.* **1991**, *113*, 3623.

22. Yang, X.; Stern, C. L.; Marks, T. J. *J. Am. Chem. Soc.* **1994**, *116*, 10015.

23. Thompson, M. E.; Baxter, S. M.; Bulls, A. R.; Burger, B. J.; Nolan, M. C.; Santarsiero, B. D.; Schaefer, W. P.; Bercaw, J. E. *J. Am. Chem. Soc.* **1987**, *109*, 203.

24. Burger, B. J.; Thompson, M. E.; Cotter, W. D.; Bercaw, J. E. *J. Am. Chem. Soc.* **1990**, *112*, 1566.

25. Bunel, E. E., Ph.D. Thesis, California Institute of Technology, **1989**.

26. Shapiro, P. J.; Bunel, E. E.; Schaefer, W. P.; Bercaw, J. E. *Organometallics* **1990**, *9*, 867.

27. Shapiro, P. J.; Cotter, W. D.; Schaefer, W. P.; Labinger, J. A.; Bercaw, J. E. *J. Am. Chem. Soc.* **1994**, *116*, 4623.

28. Canich, J. M. *Eur. Pat. Appl.* **1990**, 420436.

29. Canich, J. M.; Hlatky, G. G.; Turner, H. W. *U. S. Patent* **1990**, 542236.

30. Stevens, J. C.; Timmers, F. J.; Wilson, D. R.; Schmidt, G. F.; Nickias, P. N.; Rosen, R. K.; Knight, G. W.; Lai, S. *Eur. Pat. Appl.* **1990**, 416815.

31. Coughlin, E. B.; Bercaw, J. E. *J. Am. Chem. Soc.* **1992**, *114*, 7606.

32. Coughlin, E. B., Ph.D. Thesis, California Institute of Technology, **1994**.

33. Chacon, S. T.; Coughlin, E. B.; Henling, L. M.; Bercaw, J. E. *J. Organomet. Chem.* **1995**, *497*, 161.

34. Mitchell, J. P.; Hajela, S.; Brookhart, S. K.; Hardcastle, K. I.; Henling, L. M.; Bercaw, J. E. *J. Am. Chem. Soc.* **1996**, *118*, 1045.

35. Cossee, P. J. *J. Catal.* **1964**, *3*, 80.

36. Arlman, E. J. *J. Catal.* **1964**, *3*, 99.

37. Brookhart, M.; Green, M. L. H. *J. Organomet. Chem.* **1983**, *250*, 395.

38. Laverty, D. T.; Rooney, J. J. *J. Chem. Soc. Faraday Trans.* **1983**, *79*, 869.

39. Brookhart, M.; Green, M. L. H.; Wong, L. *Prog. Inorg. Chem.* **1988**, *36*, 1.

40. Piers, W. E.; Bercaw, J. E. *J. Am. Chem. Soc.* **1990**, *112*, 9406.

41. Piers, W. E.; Köhn, R. D.; Herzog, T. A.; Bercaw, J. E. . Manuscript in preparation.

42. Leclerc, M. K.; Brintzinger, H. H. *J. Am. Chem. Soc.* **1995**, *117*, 1651.

43. Brintzinger, H. H.; Krauledat, H. *Angew. Chem. Int. Ed. Engl.* **1990**, *29*, 1412.

44. Barta, N. S.; Kirk, B. A.; Stille, J. R. *J. Am. Chem. Soc.* **1994**, *116*, 8912.

45. Clawson, L.; Soto, J.; Buchwald, S. J.; Steigerwald, M. L.; Grubbs, R. H. *J. Am. Chem. Soc.* **1985**, *107*, 3377.

46. Stern, D.; Sabat, M.; Marks, T. J. *J. Am. Chem. Soc.* **1990**, *112*, 9558.

Chapter 2

Design of Sterically Tailored bis-(Cyclopentadienyl) Ligand Arrays with Extensive β-Alkyl Substituents for Syntheses of Group III *ansa*-Metallocenes

Abstract

The preparations of a series of dimethylsilyl-bridged bis(cyclopentadiene) complexes are reported. Double deprotonation of $Me_2Si[(SiMe_3)(C_6H_{11})C_5H_3]_2$ (**25**), $Me_2Si[(SiMe_3)$-$(2$-$C_{10}H_{15})$-$C_5H_3]_2$ (**28**), or $[(\pm)C_{20}H_{12}O_2]Si[(SiMe_3)$-$(2$-$C_{10}H_{15})$-$C_5H_3]_2$ (**38**) result in the formation of a mixture of products, assigned as constitutional isomers of the desired dianionic ligands. Double deprotonation of $Me_2Si\{[SiMe_3]$-$[2$-$(2$-CH_3-$C_{10}H_{14})]$-$C_5H_3\}_2$ (**45**) affords exclusively $[Me_2Si\{2$-$(SiMe_3)$-4-$[2$-$(2$-CH_3-$C_{10}H_{14})]$-$C_5H_2\}_2]M_2$ (M = Li (**46**); K (**47**)), indicating that tertiary alkyl groups are required to direct the trimethylsilyl groups exclusively adjacent to the silyl linkers. Transmetallation of **47** with $MCl_3(THF)_{3.5}$ (M=Sc, Y) provides exclusively *racemo*- scandocenes and yttrocenes; steric interactions between the trimethylsilyl substituents in the narrow portion of the [Cp-M-Cp] wedge preclude the formation of *meso*- complexes. Transmetallation of $[Me_2Si\{3$-$[2$-$(2$-$CH_3)$-$C_{10}H_{14}]$-$C_5H_3\}_2]Li_2$ (**46**) results in the formation of exclusively *meso*-group III metallocene complexes *meso*-$[Me_2Si\{3$-$[2$-$(2$-CH_3-$C_{10}H_{14})]$-$C_5H_3\}_2]ScCl$-$(LiCl)$-$(THF)_2$ (**48**) and *meso*-$[Me_2Si\{3$-$[2$-$(2$-CH_3-$C_{10}H_{14})]$-$C_5H_3\}_2]YCl$-$(LiCl)$-$(THF)_2$ (**49**), proceeding with enantioselectivity opposite to that observed for **47**.

Introduction

The appeal of using chiral organometallic compounds as catalysts for enantioselective transformations has prompted the development of a wide variety of chiral metallocenes. Chiral early transition-metal cyclopentadienyl-based complexes have found considerable success as stereospecific Ziegler-Natta α-olefin polymerization catalysts.[11] Similar Cp-based compounds have proven successful in promoting transformations related to organic synthesis, such as the asymmetric hydrogenation of imines,[2,3] enamines,[4] and olefins,[5] and the enantioselective hydrosilylation of ketones.[6] From the search for chiral catalysts have evolved several strategies for the construction of chiral Cp-based organometallic complexes.

Unlinked substituted cyclopentadienyls, such as those depicted in Figure 1, may adopt both chiral and achiral conformations. The freedom of the Cp rings to rotate about the M-centroid axis permits interconversion between C_2-symmetric (and chiral) structures, in which the Cp substituents are staggered, and C_s-symmetric (and achiral) structures, in which the Cp substituents adopt eclipsing conformation. Equilibration between these limiting structures is generally rapid on the NMR timescale, thus diminishing the possible stereodirecting effects of the chiral conformer. A judicious choice of Cp substituents, however, may be used to exploit this

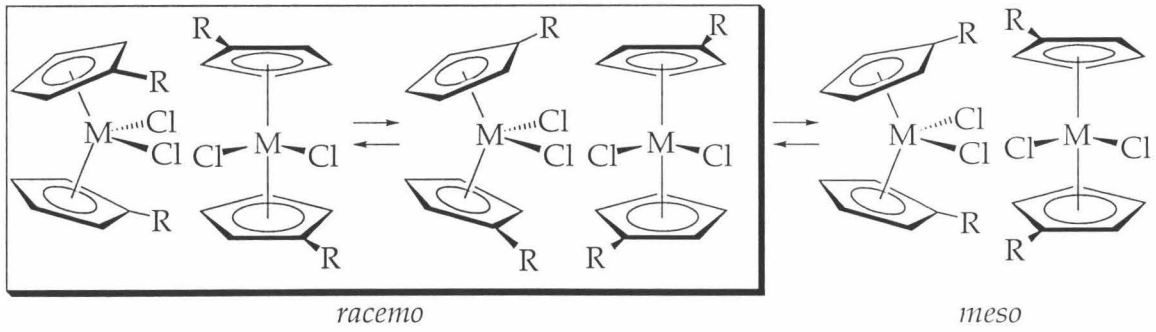

Figure 1. Racemic and meso conformations of singly-substituted unlinked metallocenes (M = group IV).

chiral-achiral interconversion to observe new and potentially useful reactivities; if exchange between the C_2 and C_s structures is slow on the polymerization timescale, polymers containing blocks of both isotactic and atactic sequences may be produced. Erker[7-9] has used chiral substituents on

Cp rings, and Waymouth[10,11] has employed achiral phenylindenyl ligands, to generate catalysts that appear to function in this manner.

Linking the two cyclopentadienyls with a short tether effectively inhibits these rotations. Organometallic complexes with such tethered linked arrays are commonly referred to as "*ansa*"-metallocenes.[12] Incorporation of a single substituent onto one of the Cp rings results in an overall C_1-symmetric complex (Figure 2). Marks has successfully utilized chiral R substituents (menthyl, neomenthyl, phenylmenthyl) in order to induce diastereoselective metallation in a variety of metallocenes; the group III, group IV, and lanthanide metallocenes. Derivatives of these C_1-symmetric complexes have found use as olefin hydrogenation, hydroamination/cyclization,[13,14] and polymerization[15] catalysts.

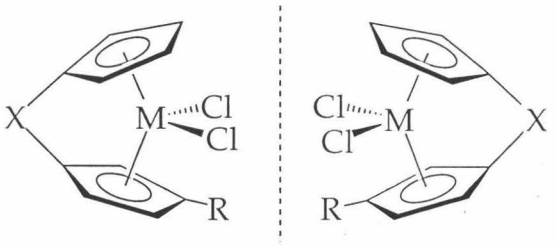

Figure 2. Linked mixed-ring Cp complexes as chiral *ansa*- metallocenes.

Although additional methods have been developed for generation of chiral metallocenes,[16-18] the most prevalent means is through the use of a short tether to connect a pair of symmetrically substituted Cp rings. Incorporation of a transannular linker does not necessarily result in the formation of chiral complex, as C_s- (*meso*) and C_2-symmetric (*rac*) isomers of a given *ansa*-metallocene are possible. Major drawbacks in the use of *ansa*-metallocenes are the facts that both *rac*- and *meso*- complexes are typically formed upon metallation, and that separation and isolation of the *racemo*-isomer is required for asymmetric catalysis. Modification of both the inter-Cp tether and the Cp substituents themselves have been employed in order to encourage formation of the *rac*- isomer.

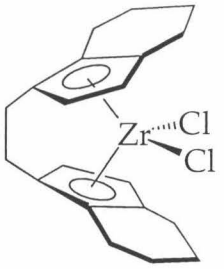

1

The catalyst originally reported by Brintzinger for the stereospecific polymerization of propylene to isotactic poly(propylene) utilizes the ethano-bridged bis(tetrahydroindenyl) zirconium dichloride **1**. Metallocenes incorporating such a 2-carbon linker are particularly attractive because of the ease with which the linker is incorporated into the ligand framework. Synthesis of bridged metallocenes of this sort typically involve treatment of two equivalents of the appropriate Cp anion with 1,2-dibromoethane. Although the 2-atom interannular bridge significantly hinders rotation of the Cp rings between *rac* and *meso* isomers, several energetically discernible conformations of -(CH_2CH_2)- linked metallocenes have been observed crystallographically and detected using dynamic NMR techniques;[19,20] interconversion between the various isomers is generally rapid in solution.

The use of a transition metal halide and the alkali metal salt of the appropriate ligand is commonly used to generate *ansa*- metallocenes.[21] These metallations typically generate both *rac* and *meso* products, the exact ratio of which is often dependent not only on the particular metal and ligand substituents, but also the workup procedure. For ethano-bridged Cps containing only β-alkyl substitutents,[22] the selectivity for formation of *racemo*- metallocenes is generally poor, with equimolar quantities of *rac* and *meso* complexes formed irrespective of the bulk of the β-alkyl group (Table 1, R = -CH_3, -CH_2CH_3, -$CH(CH_3)_2$, -$C(CH_3)_3$).

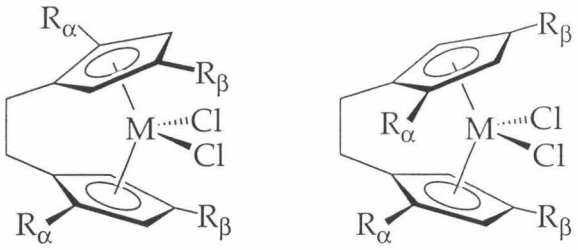

racemo *meso*

2

	M	R_α	R_β	Synthetic		Photostationary	
				rac	meso	rac	meso
2a[22]	Ti	H	CH_3	1	1.3	*	*
2b [22]	Ti	H	CH_2CH_3	1	1.5	*	*
2c[22]	Ti	H	$CH(CH_3)_2$	1	1.8	*	*
2d[22]	Ti	H	$C(CH_3)_3$	1	2.0	*	*
2e[23]	Ti	CH_3	CH_3	2	1	2.5	1
2f[23]	Ti	CH_3	CH_2CH_3	2.6	1	4	1
2g[23]	Ti	CH_3	$C(CH_3)_3$	1.6	1	15	1

Table 1. Metallation enantioselectivities for a series of ethylene-bridged group IV metallocenes. * = not investigated

The substituent adjacent to the linker is able to exert considerably more influence on the metallation enantioselectivity than is the β- substituent, as observed by incorporation of methyl groups α- to the ethano linker.[23] These ratios may occasionally be further enhanced by photoisomerization of the original mixtures, permitting isolation of pure *racemo*- complexes by fractional crystallization or by column chromatography.

Incorporation of a more sterically demanding linker results in only a modest improvement in the observed *rac*:*meso* ratios, as shown for a related series of tetramthylethano-bridged titanocenes and zirconocenes (Table 2).[24] The effects of different reaction conditions and workup procedures are illustrated by the range of multiple *rac*:*meso* ratios denoted as multiple entries in Table 2.

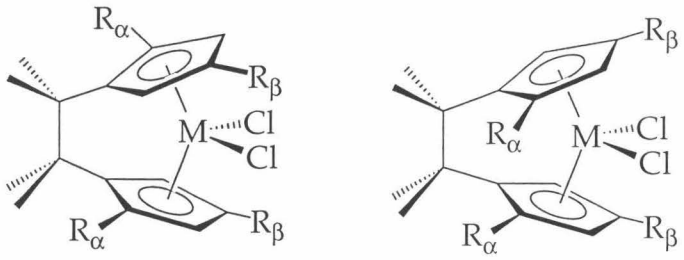

racemo *meso*

3

	M	R_α	R_β	rac	meso
3a	Ti	H	$C(CH_3)_3$	2.5	1
3b	Ti	H	$Si(CH_3)_3$	0.6	1
				1.8	1
3c	Ti	H	$CH(CH_3)_2$	1	1
3d	Ti	H	$CH_2C_6H_5$	1	1
3e	Ti	H	$C(CH_3)_2C_6H_5$	1.2	1
				2.2	1
3f	Ti	H	$C(CH_3)_2C_6H_5$	1.2	1
				2.2	1
3g	Zr	H	$C(CH_3)_3$	1.5	1
				2	1
3h	Zr	H	$Si(CH_3)_3$	1.5	1
				2	1

Table 2. Racemic/meso ratios for tetramethylethano-bridged group IV metallocenes[24]

Silyl linking units have found widespread use as a result of the simplicity with which they are incorporated into ligand ensembles, and because of their ability to "tie back" the Cp rings, often affording an effective reduction in steric bulk in the front of the metallocene wedge. The insertion of a single-atom silyl-linker is often obtained through the use of dichlorodimethylsilane rather than 1,2-dibromoethane in the ligand synthesis.

As is observed for the ethano-bridged complexes, *rac:meso* ratios for the group IV metallocenes employing a dimethylsilyl linker are largely unaffected by the nature of the β-alkyl substituent when the α-substituent is a hydrogen. Increasing the steric bulk of the α-substituent generally results in a considerable increase in selectivity for the racemo metallocene, with smaller effects imparted by modification of the β- substituent (Table 3).

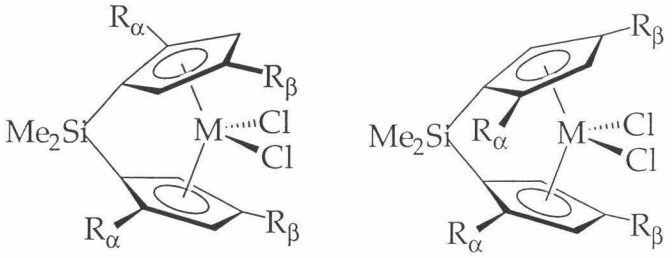

4

	M	R_α	R_β	rac	meso
4a[25]	Zr	H	$C(CH_3)_3$	1	1
4b[25]	Zr	H	$Si(CH_3)_3$	1	1
4c[25]	Zr	H	$C(CH_3)_2C_6H_5$	1	1
4d[25]	Zr	H	$C(CH_2)_5C_6H_5$	1	1
4e[25]	Zr	CH_3	$C(CH_3)_3$	2	1
4f[25]	Zr	CH_3	$CH(CH_3)_2$	6	1
4g[26]	Ti	$Si(CH_3)_3$	$C(CH_3)_3$	1	*
4h[26]	Zr	$Si(CH_3)_3$	$C(CH_3)_3$	1	*

Table 3. Racemic/meso ratios for dimethylsilyl bridged group IV metallocenes; * = not observed

A major breakthrough in the synthesis of chiral metallocenes was the discovery that incorporation of a trimethylsilyl group adjacent to the silyl linker results in the exclusive formation of C_2-symmetric metallocenes. The ligand is constructed by the procedure outlined in Figure 3. The ligand array, abbreviated [Bp], exists in its doubly protonated form ([BpH_2]) as a mixture of rapidly interconverting isomers, due to facile silyl- and hydrogen- migrations about the cyclopentadiene rings.[27] Double deprotonation yields exclusively

$[Me_2Si(2\text{-}SiMe_3\text{-}4\text{-}CMe_3\text{-}C_5H_2)_2]^{2-}$ ($[Bp]^{2-}$), the isomer in which the silyl groups reside α- to the silyl linker.

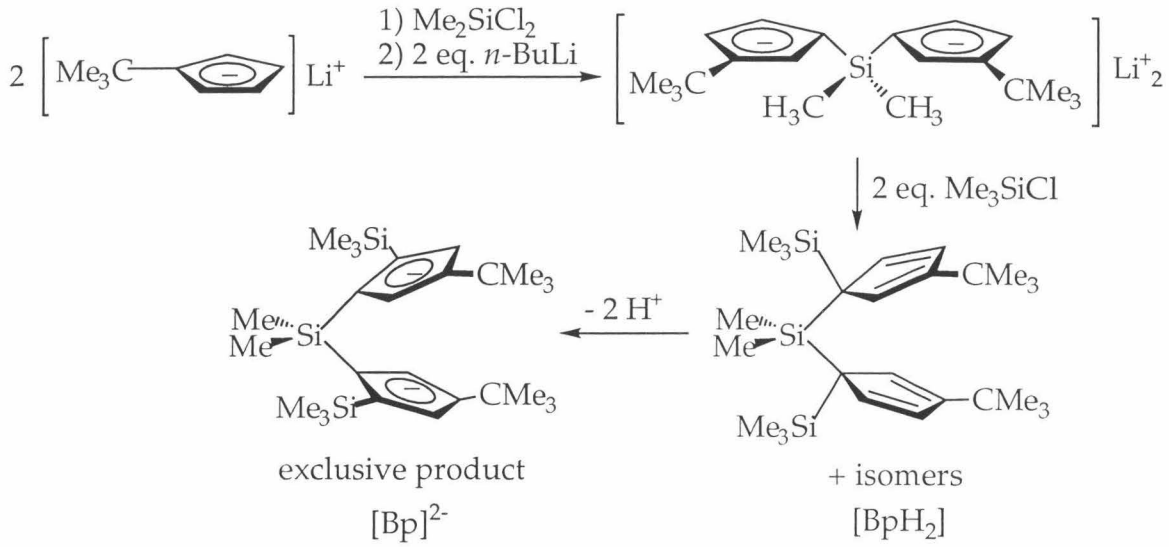

Figure 3. Synthesis of $[Me_2Si(2\text{-}SiMe_3\text{-}4\text{-}CMe_3\text{-}C_5H_2)_2]^{2-}$ ($[Bp]^{2-}$).

Transmetallation of $[Bp]^{2-}$ affords exclusively *racemo*- metallocenes. Unfavorable steric interactions between the trimethylsilyl groups in the narrow portion of the metallocene wedge precludes formation of the *meso*-isomer. This is true not only for the group IV metallocenes, but also for the group III derivatives (Table 4).

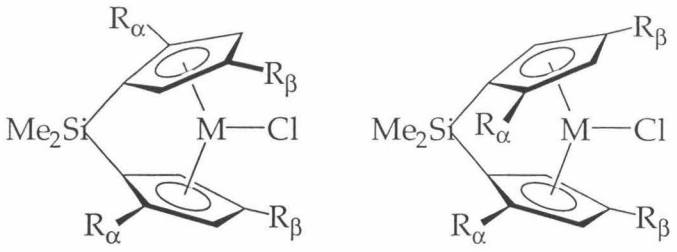

racemo *meso*

5

	M	R_α	R_β	rac	meso
5a[28]	Sc	H	$C(CH_3)_3$	*	1
5b[29]	Y	H	$C(CH_3)_3$	1	1
5c[30]	Sc	$Si(CH_3)_3$	$C(CH_3)_3$	1	*
5d[31]	Y	$Si(CH_3)_3$	$C(CH_3)_3$	1	*
5e[32]	La	$Si(CH_3)_3$	$C(CH_3)_3$	1	*

Table 4. Observed group III enantioselectivities for dimethylsilyl-bridged ligands; * = not observed

In the absence of the metallation-directing α-trimethylsilyl groups, additional steric congestion on the Cp rings serves to increase the metallation selectivity, as shown in Table 5. The most substantial effects, again, result from incorporation of increasing steric bulk in the position adjacent to the Si-linker.

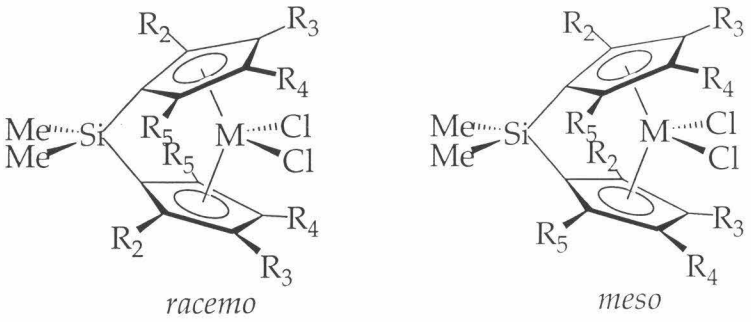

6

	M	R_2	R_3	R_4	R_5	rac	meso
6a	Zr	CH_3	CH_3	H	CH_3	5.6	1
6b	Zr	CH_3	H	CH_3	H	15.7	1
6c	Zr	H	$C(CH_3)_3$	H	H	2.7	1
6d	Zr	H	CH_3	H	H	7.3	1
6e	Hf	CH_3	CH_3	H	CH_3	13.3	1
6f	Hf	CH_3	H	CH_3	H	100	1
6g	Hf	H	H	H	H	1	2.8
6h	Hf	H	CH_3	H	H	1.1	1

Table 5. Racemic/meso ratios for additional dimethylsilyl bridged group IV metallocenes[33]

Chiral metallocenes incorporating indenyl- and indenyl-derived rings have often resulted in catalysts with especially high activities and/or stereospecificities. The metallocene dichloride precursors to these catalysts, however, are formed with generally poorer enantioselectivity than the formally Cp-based complexes described previously (Table 6).

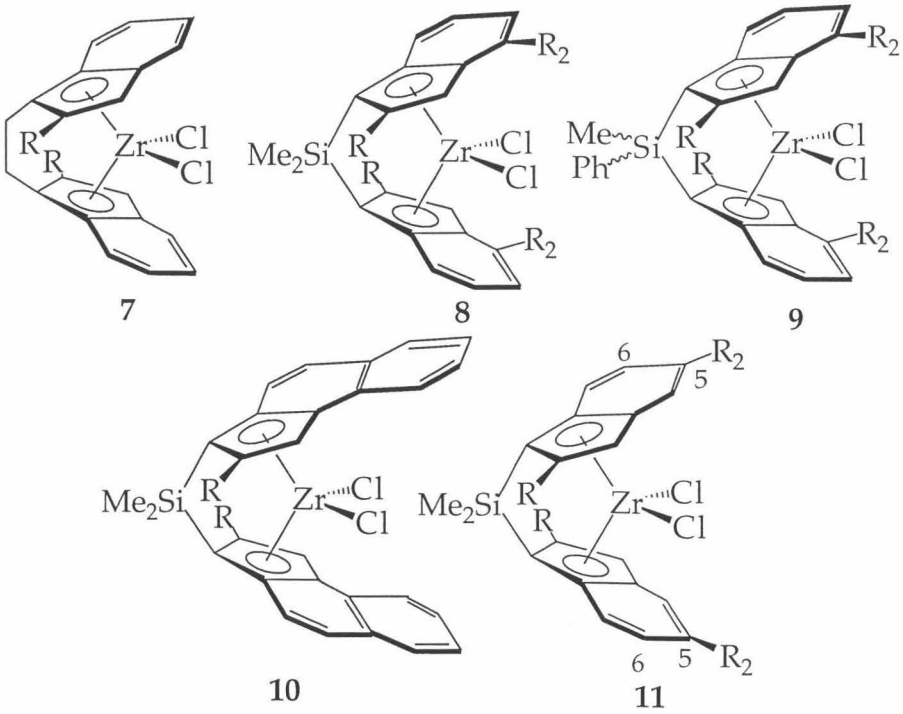

	M	R	R_2	rac	meso
7[34]	Zr	H		1	2-10
8a[35,36]	Zr	H	H	1	1
8b[35,36]	Zr	CH_3	H	1	1
8c[35]	Zr	CH_2CH_3	H	1	1
8d[35]	Zr	CH_3	$CH(CH_3)_2$	1	1
8e[37]	Zr	H	C_6H_5	1	1
8f[37]	Zr	CH_3	C_6H_5	1	1
8g[37]	Zr	CH_3	1-naphthyl	1	1
9[37]	Zr	CH_3	C_6H_5	1	2
10a[36,37]	Zr	H		1	*
10b[36,37]	Zr	CH_3		1	1
11[‡37]	Zr	CH_3	C_6H_5	[Δ]	[Δ]

Table 6. Racemic/meso ratios for indene- and indenyl-based *ansa*-metallocenes; *= not observed; [‡] = mixture of 5- and 6- indenyl substituted metallocenes were inseparable; [Δ] = mixture observed, but *rac/meso* ratio was not reported

The use of chiral linking units to induce not only enantioselectivity (*rac* vs. *meso*) but diastereoselectivity in the metallation step has been, until recently, met with little success. Ligands employed in initial studies resulted in either mixtures of *rac* and *meso* (ligand **12**)[38] or exclusively *meso* (ligand **13**)[39] metallocenes, and generally low overall yields.

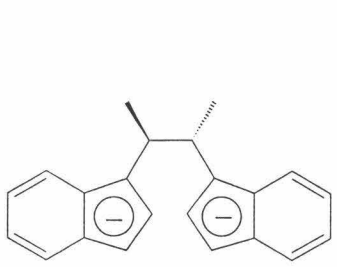

12

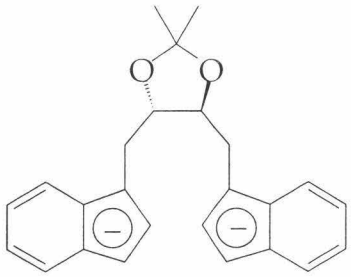

13

The chiral binaphthyl-bridged ligand (**14**)[40] affords exclusively chiral metallocenes, although X-Ray diffraction indicates that the steric constraints of the linker result in considerable deviations from the desired C_2-metallocene symmetry. The use of enantiomerically pure cyclacene ligand **15** affords only one *rac*- metallocene (M=Ti);[41] a crystal structure indicates an unsymmetric disposition of the indenyl ligands, despite their apparent equivalence in solution (^{1}H NMR). The use of a 2,2'-biphenyl linker (**16**; R=H, CH_3)[42] results in the formation of diastereomerically pure metallocenes, although in low overall (c.a. 3-18%) yield.

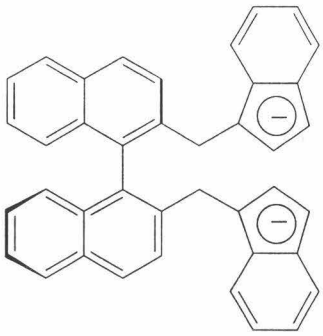

14

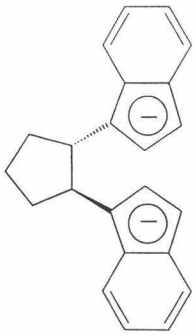

15

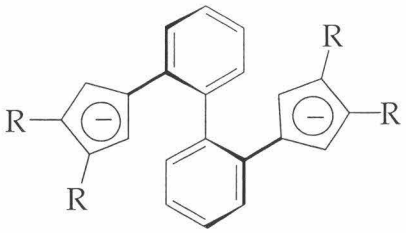

16

Considerably more successful are the use of chiral cyclohexane linkers and silyl linkers containing chiral binaphthol-derived substituents (Figure 4). **17** metallates in high yield to give a single metallocene as a result of steric

interactions between the indenyl moieties and the isopropyl groups on the cyclohexane linker;[43] the high diastereoselectivity of **18** is a result of steric interactions between the α-trimethylsilyl substituents on the Cp rings (interactions between which are responsible for enantioselective metallation), and the 3,3′-naphthalene methine positions.[44]

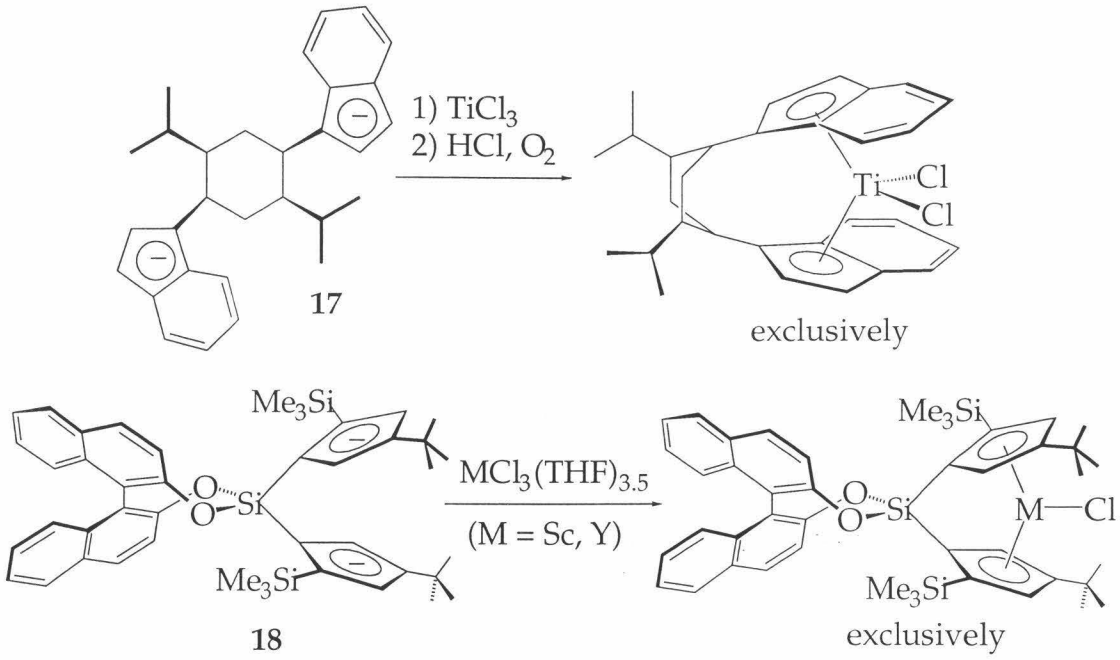

Figure 4. Tailored ligand arrays for diastereoselective metallocene syntheses.

As described in Chapter One, a monomeric chiral group III complex would be invaluable for mechanistic studies on a single component isospecific catalyst. Generation of such a complex hinges on the ability to prevent formation of bridging-hydride dimers commonly observed for group III and lanthanide metallocene derivatives. We reasoned that replacement of the *tert* butyl substituents in **5** and **18** with more extensive alkyls may perturb the hydride monomer-dimer equilibrium by virtue of intermolecular steric interactions between these new β-substituents. The choice of substituent must induce the 1-(linker)-2-($SiMe_3$)-4-(alkyl) Cp substitution required to generate exclusively *racemo*- metallocenes (as in compounds **4g**. **4h**, **5c-e**, **18**), thus eliminating the need for separation of *meso* and *rac* isomers. The synthesis of several novel ligand arrays incorporating extensive β-substituents is reported herein, as are the resultant group III metallation enantioselectivities.

Results and Discussion

Efforts to generate *ansa*- metallocenes with extensive alkyl substituents in the β- positions focused initially on the synthesis of the cyclohexyl-substituted analogue to the [Bp] ligand array, as shown in Figure 5.

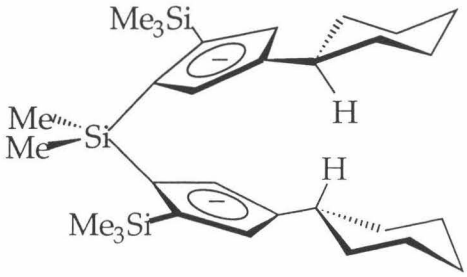

Figure 5. Initial cyclohexyl-substituted target ligand array.

Following the general protocol for the parent system,[32] the initial steps of the ligand synthesis involved construction of alkyl-substituted cyclopentadienyls. Pentamethylenefulvene (**19**), synthesized using the procedure of Stone and Little,[45] is easily reduced using borohydride reagents such as $LiB(CH_2CH_3)_3H$ (Super-Hydride) and $KB[CH(CH_3)CH_2CH_3]_3H$ (K-Selectride), resulting in trialkylborane adducts of cyclohexylcyclopentadienyllithium (**20**) and -potassium (**21**) (75-80% yields, Figure 6). The coordinated trialkylboranes are not removed either by repeated washings of the complexes with petroleum ether or by extended heating under dynamic vacuum.

Attempts to generate cyclohexyl-substituted ligand arrays from the trialkylborane adducts **20-$(BR_3)_n$** and **21-$(BR_3)_n$** ultimately proved unsuccessful. The coordinated trialkylborane appears to interfere in the linking reaction of **20-$(BR_3)_n$** and **21-$(BR_3)_n$** with Me_2SiCl_2, as the borane free salts **20** and **21** may be successfully employed to generate the dimethylsilyl-bridged **22** (*vide infra*). Dichlorodimethylsilane reacts readily with **20-$(BR_3)_n$**,

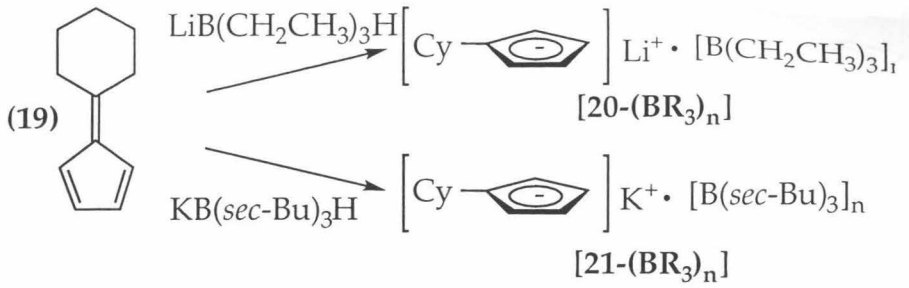

Figure 6. Syntheses of cyclohexylcyclopentadienyl-trialkylborane adducts.

yet does not consistently generate **22**. The mixture of resultant products may be a mixture of **22**, the mono-cyclopentadiene product **23**, and species resulting from deprotonation of **23** by additional equivalents of **20-(BR$_3$)$_n$**; more thorough analyses of linking reactions are presented later (*vide infra*).

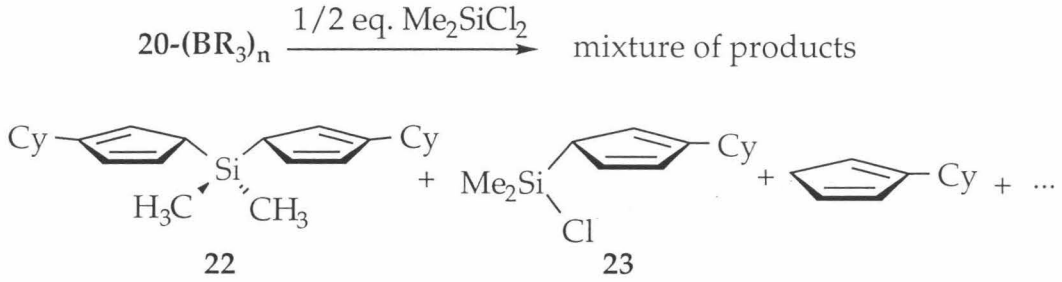

Figure 7. Dichlorodimethylislane fails to cleanly link **20-(BR$_3$)$_n$**.

The trimethylsilyl- substituted Cp **24** ([1-SiMe$_3$-3-Cy-C$_5$H$_3$]K; Cy = cyclohexyl = C$_6$H$_{11}$) is obtained from the treatment of **20-(BEt$_3$)$_n$** with chlorotrimethylsilane and subsequent deprotonation with potassium-*tert*-butoxide (Figure 8), the reaction of this dipotassium salt with 1/2 equivalent of dichlorodimethylsilane failed to generate the diprotio- form of the desired ligand array, **25.** The origin of the difficulties in obtaining **25** from the route shown in Figure 8 was not investigated in great detail, but analogous linking reactions on 2-adamantyl-substituted cyclopentadienyls indicates that 1-trimethylsilyl-3-(secondary alkyl)-cyclopentadienyls are too sterically congested to permit linking with Me$_2$SiCl$_2$ (*vide infra*).

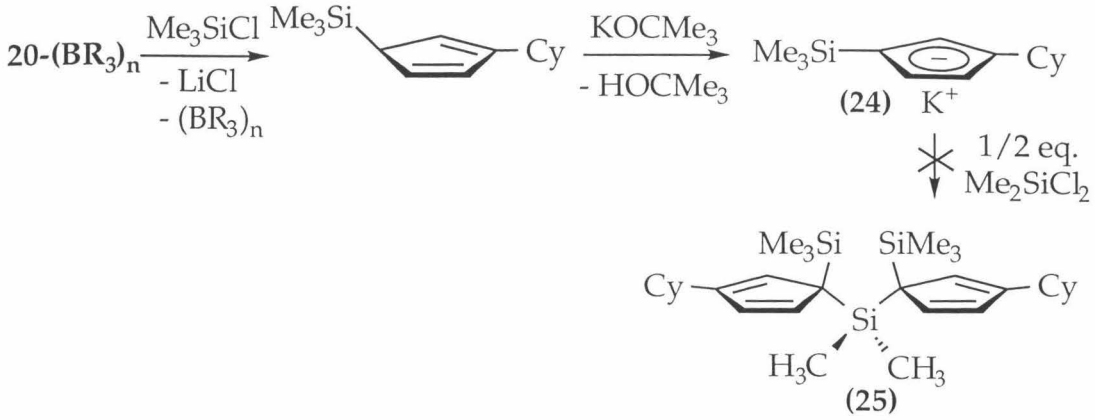

Figure 8. Alternate synthetic attempts to obtain $Me_2Si[(Cy)(SiMe_3)\text{-}C_5H_3)]_2$ (**25**).

Alternate routes into the synthesis of **20/21** were investigated in the hopes of obtaining borane-free lithium- or potassium cyclopentadienyl salts. Albeit in low yield (≤ 30%), Diels-Alder dimers of cyclohexylcyclopentadiene

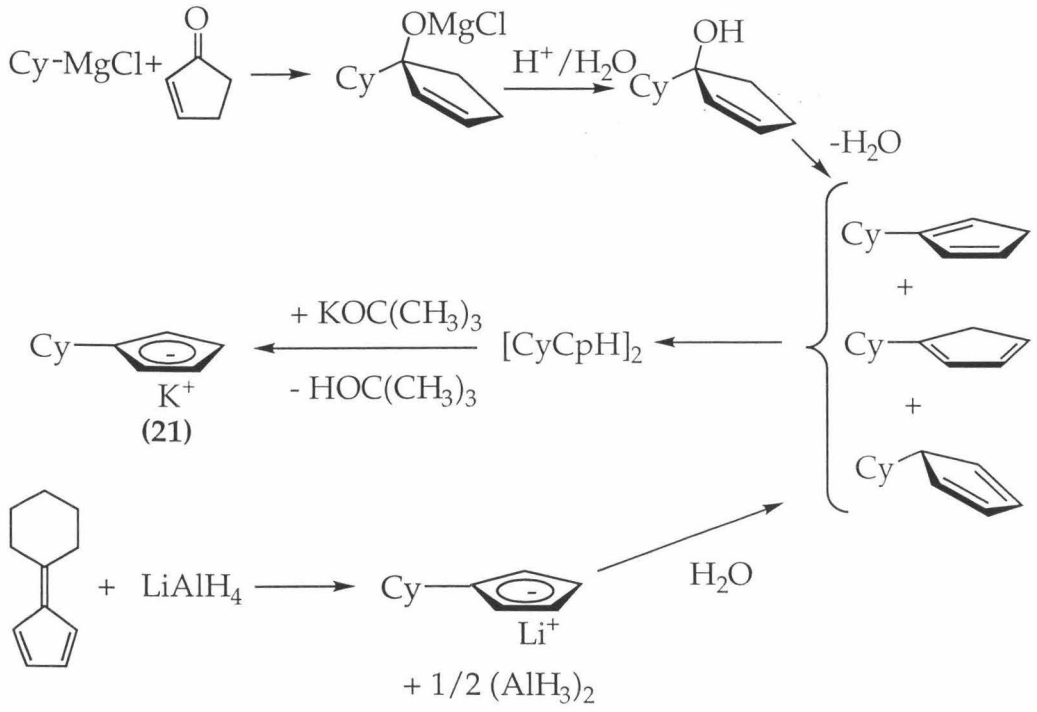

Figure 9. Alternate syntheses of **20** and **21**.

($[CyCpH]_2$) are generated cleanly from the reaction of the appropriate Grignard reagent with cyclopenten-2-one (Figure 9). Improved yields (>70%) of $[CyCpH]_2$ are obtained from use of $LiAlH_4$ in conjunction with **19**.

Either the lithium salt resulting from the reaction of **19** with $LiAlH_4$ or the potassium salt generated from treatment of CyCpH with $KOCMe_3$ may be used to generate the linked complex $Me_2Si(Cy\text{-}C_5H_4)_2$ (**22**) by the slow warming from -78 °C to 25 °C of a tetrahydrofuran solution of the appropriate anion with 0.5 equivalents of Me_2SiCl_2. A single regioisomer $Li_2[Me_2Si(3\text{-}Cy\text{-}C_5H_3)_2]$ (**26**) is obtained as a white petroleum ether insoluble powder (60% yield), from deprotonation of **22** (Figure 10) with two equivalents of *n*-butyllithium.

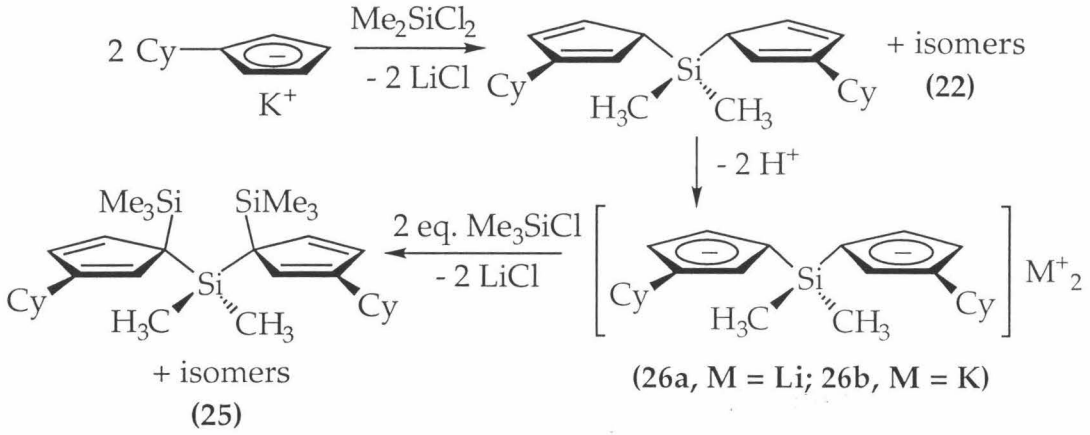

Figure 10. Synthesis of doubly protonated cyclohexyl-substituted ligand array.

Trimethylsilyl- groups are introduced to the Cp rings by treatment of **26** with a slight excess of chlorotrimethylsilane. As is common for silyl-substituted cyclopentadienes, the multiply silylated complex **25** exists in solution as a mixture of regioisomers due to facile silyl and hydrogen migrations about the cyclopentadiene ring, although the silyl substituents tend to reside on sp^3-hybridized ring carbons.[27,32] ^1H NMR spectroscopy indicates a mixture of products; complete assignments were not made because of multiple overlapping resonances (> 18 Cp, 9 Me_2Si signals). Resonances for the major product (by integration of the -$SiMe_3$ resonances, (δ 0.10 to -0.10, C_6D_6) are consistent with those expected for the isomer of **25** drawn in Figure 10, in which all silyl substituents reside on sp^3- hybridized carbons. Mass spectroscopy on the interconverting isomers provides a parent peak at (m/z) = 496 (molecular weight of $C_{30}H_{52}Si_3$ = 497.09 g/mol).

In contrast to the *tert*-butyl-substituted [Bp] ligand array, which deprotonates to give a single regioisomer (Figure 10),[32] the doubly-protonated cyclohexyl-substituted ligand array **25** reacts with a variety of deprotonating agents (e.g. *n*-BuLi, $LiCH_2SiMe_3$, $KOCMe_3$, $KN(TMS)_2$, $LiN(TMS)_2$, etc.) to afford a mixture of products. Presumably, this mixture includes not only the desired $Me_2Si(2\text{-}SiMe_3\text{-}4\text{-}Cy\text{-}C_5H_2)_2$ isomer (**27a**), but also regioisomers **27b** ($Me_2Si(3\text{-}SiMe_3\text{-}4\text{-}Cy\text{-}C_5H_2)_2$) and the mixed (1,2,4)(1,3,4)-substituted complex **27c** (see Figure 11). Also possible are structures analogous to **27a-c** in which the cyclohexyl groups reside adjacent to the dimethylsilyl linker rather than to the trimethylsilyl group.

Various permutations of deprotonating agent, solvent, and reaction temperature fail to result in the exclusive formation of the desired isomer **27a**; the most successful set of reaction conditions towards the formation of a single isomer is the slow warming from -78 °C to 25 °C of a THF solution of $KOCMe_3$ and **25**. The major regioisomer is then be obtained in approximately 20-25% yield after repeated (>3) recrystallizations from cold THF/petroleum ether solutions.

The failure of the cyclohexyl-substituted ligand array to provide a single geometric isomer upon deprotonation is attributed to the inability of the cyclohexyl group to exclusively direct the trimethylsilyl group adjacent to the dimethylsilyl linker prior to deprotonation. Figure 11 shows some of the possible isomers of **25**, and the results of deprotonation thereof; an alkyl substituent that is not sufficiently bulky to disfavor the sampling of the isomers indicated in the two leftmost columns will result in a mixture of undesired constitutional isomers upon deprotonation.

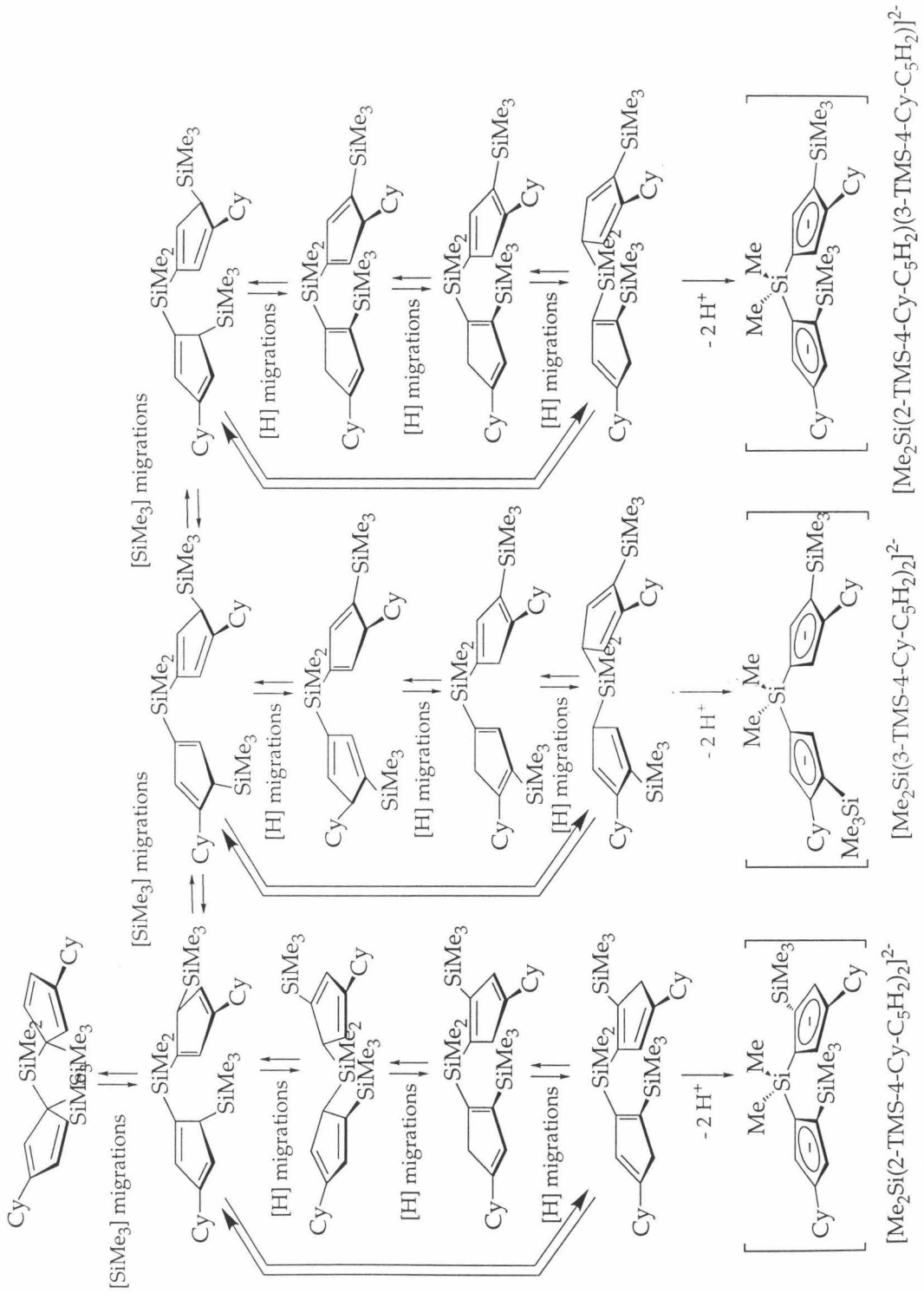

Figure 11. Some of the possible constitutional isomers of **25**. The ability of the cyclohexyl groups to direct the -$SiMe_3$ substituents adjacent to the Si- linker will determine whether **27a** is the exclusive deprotonation product.

It was hoped that replacement of the cyclohexyl groups with even larger alkyl substituents, namely 2-Adamantyl (Ad) groups, could provide a ligand array that could be deprotonated to afford the single $Me_2Si(2\text{-}SiMe_3\text{-}4\text{-}alkyl\text{-}C_5H_2Li)_2$ isomer (**29**).

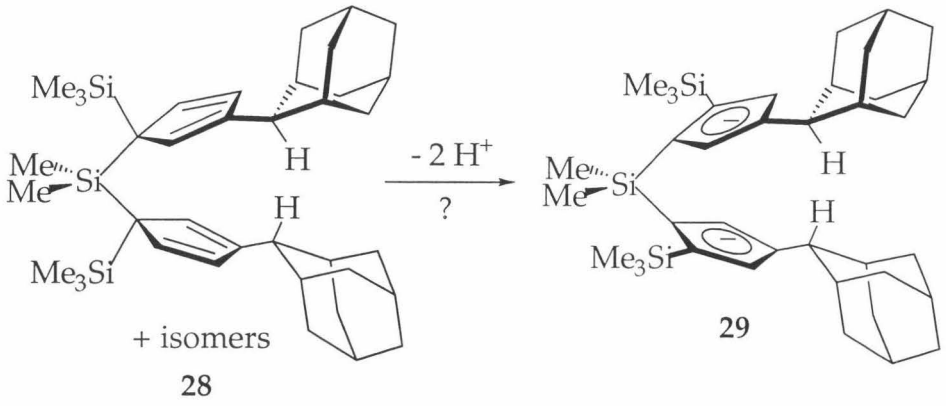

Figure 12. Target ligand incorporating 2-Adamantyl substituents.

Condensation of 2-Adamantanone with freshly cracked cyclopentadiene provides fulvene **30**, a bright yellow crystalline solid, in high yield (>90%, Figure 13). Reduction of the fulvene with borohydride reagents gives results similar to those observed with pentamethylenefulvene:

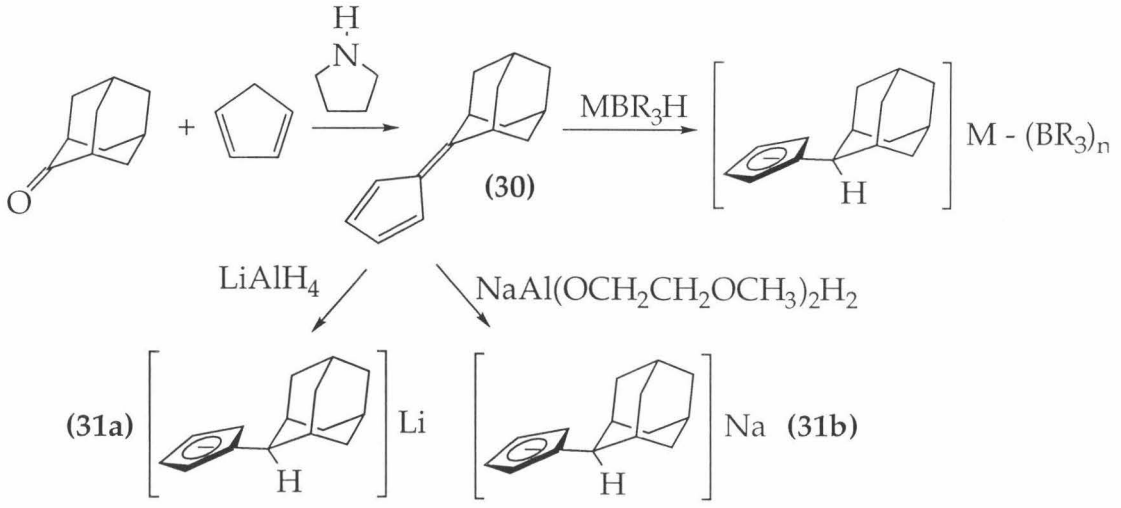

Figure 13. Syntheses of 2-Adamantyl substituted cyclopentadienyl anions. (M = Li, R = $-CH_2CH_3$; M = K, R = $CH(CH_3)CH_2CH_3$)

alkylborane - Cp adducts of the desired alkyl-substituted cyclopentadienes. Borane-free (2-Ad)-C_5H_4Li (**31**) and (2-Ad)-C_5H_4Na is obtained from treatment of **30** with $LiAlH_4$ or $NaAl(OCH_2CH_2OCH_3)_2H_2$, respectively (2-Ad = 2-Adamantyl = 2-($C_{10}H_{15}$)).

The (2-Ad)-C_5H_4Li and Na salts react readily with chlorosilane reagents to give (2-Ad)(silyl)-substituted cyclopentadienes. ^1H NMR spectroscopy indicates that both **32** and **33** (Figure 14) exist as single isomers in solution (THF-d_8, C_6D_6). **32** shows three vinylic and one allylic cyclopentadiene protons, a single $SiMe_3$ group, and a single set of Ad resonances; **33** shows similar cyclopentadiene resonances and a doublet for the diastereotopic Si-Me groups. **32** is converted to [1-$SiMe_3$-3-(2-Ad)-C_5H_3]Li (**34**) by treatment with excess *n*-BuLi. Similarly, **34** is obtained from treatment of **33** with excess CH_3Li, both deprotonating the cyclopentadiene ring and reacting with the remaining Si-Cl group. In contrast to both the *tert*-butyl- and cyclohexyl-systems, (2-Ad)-C_5H_4Li can *not* be linked using dichlorodimethylsilane; treatment of 2 equivalents of **31** with Me_2SiCl_2 results only in the formation of **33**, with the second equivalent of Li salt failing to react at room

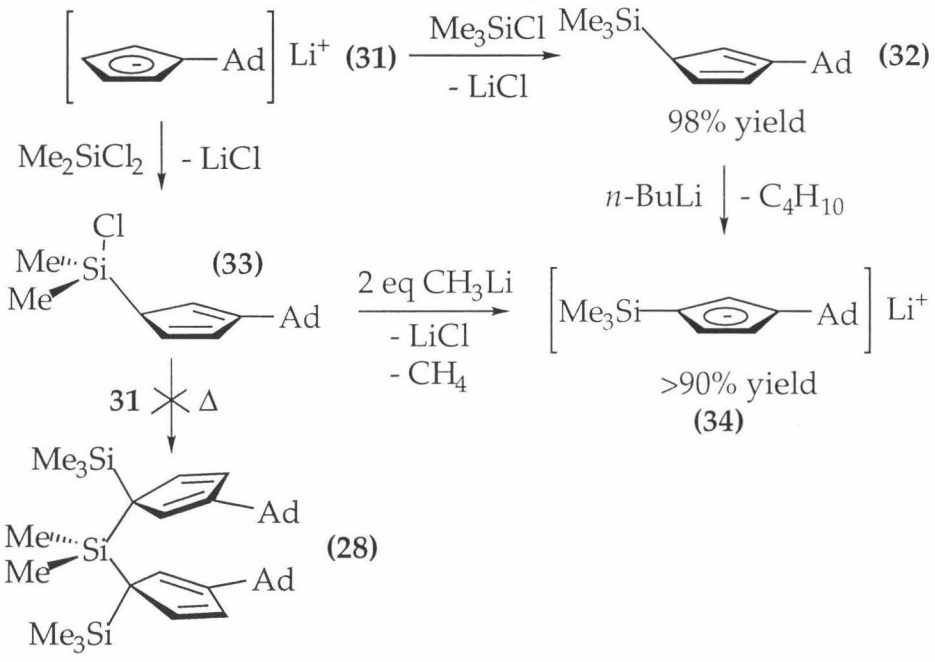

Figure 14. Syntheses of [1-$SiMe_3$-3-(2-Adamantyl)-C_5H_3]Li, **34**.

temperature. Heating a **31/33** mixture (80 °C, THF) results only in decomposition of the starting materials.

The exact nature of the side reaction/decomposition mechanism operating in this system is not known, although the presence of appreciable quantities of AdCpH (*protonated* staring material) in the product mixture supports the two pathways shown in Figure 15. After generation of the chlorosilyl- substituted cyclopentadiene **33**, additional equivalents of cyclopentadienyllithium may react with the remaining Si-halide functional group (pathway **i**) to give the desired linked species **28**; the remaining **31** may alternately serve to deprotonate the doubly allylic cyclopentadiene hydrogen in **33** (pathway **ii**), thus generating one equivalent of AdCpH (the other products are unlikely to be identified due to subsequent decomposition). Competing pathways analogous to (**i**) and (**ii**) are presumed to account for the inability to cleanly link **24** with Me_2SiCl_2, as described previously.

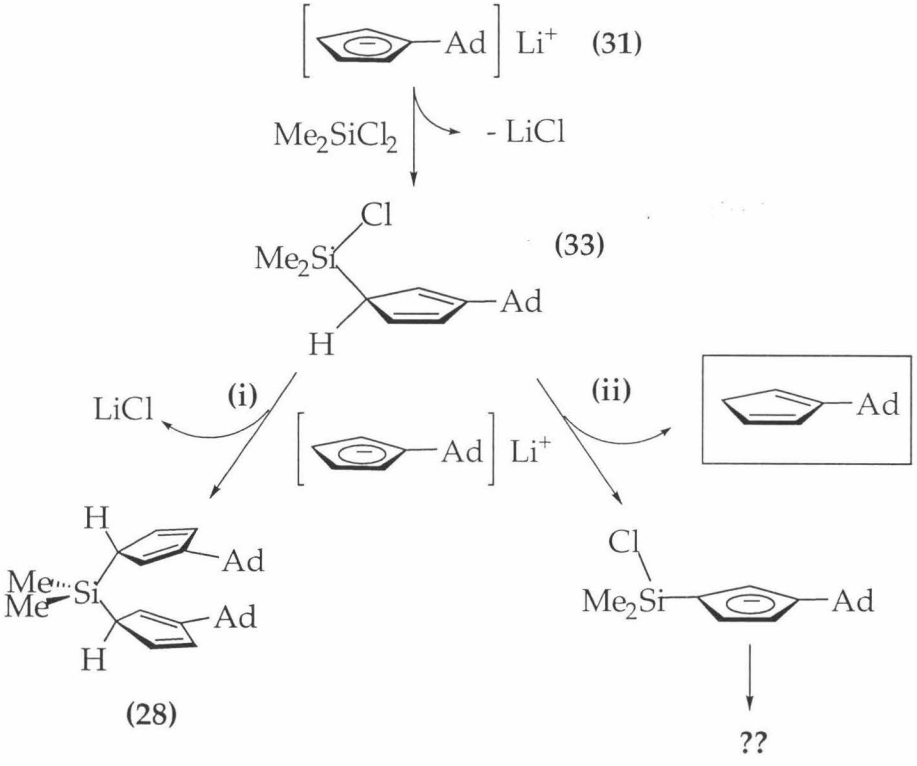

Figure 15. Possible reactivity pathways for **33**.

The tendency for silyl- groups to reside on sp^3-hybridized cyclopentadiene ring carbons may, however, be exploited in order to disfavor the side reaction arising from pathway (**ii**). The trimethylsilyl-substituted complex **34** reacts with Me_2SiCl_2 to generate the doubly-silylated complex **35**; the single isomer of **35** observed in solution is that with both silyl

substituents residing on the same sp^3-hybridized carbon. This isomer has no allylic (i.e. acidic) hydrogens available for deprotonation by additional equivalents of **34**, and should therefore be expected to resist deprotonation/decomposition (pathway **ii**) in a manner analogous to that shown in Figure 15.

Indeed, deprotonation of **35** is found to be slow; there is, in fact, no additional reaction between **35** and additional equivalents of **34** at room temperature. Extended heating (days at 80 °C) results in the slow decomposition of the starting materials to give a mixture of intractable, unidentifiable products. The resistance of **35** to deprotonation is a consequence of the desire of multiple silyl substituents to reside on a single sp^3-hybridized cyclopentadiene carbon. The stability of the Si-Cl bond is attributed to a combination of steric influences from the adjacent methyl groups on the potential linker and those of the alkyl and silyl substituents on **34**.

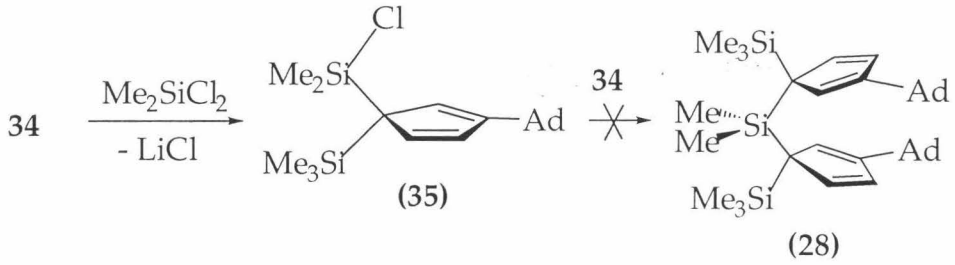

Figure 16. Reaction of **34** with Me_2SiCl_2 generates a robust doubly silylated cyclopentadiene, **35**.

An alternate route into the synthesis of **28** involves synthesis of a silyl-linked complex whose linker unit is subsequently functionalized after the linking step. The unlinked, (trimethylsilyl)(trichlorosilyl)- substituted complex **36** is generated from the reaction of equimolar quantities of **31** and $SiCl_4$ (Figure 17); the single isomer of **36** observed in solution is, again, that with both silyl substituents residing on the same sp^3-hybridized carbon. Additional equivalents of **31** react with the $-SiCl_3$ moiety of **36** within 24 hours (25 °C, THF) to generate the dichlorosilylene bridged complex **37**, as an air and moisture sensitive pale yellow solid. The dimethylsilylene bridged species **28** is obtained as a mixture of rapidly interconvering isomers[27] from treatment of **37** with an excess of CH_3Li followed by quenching with methanol

and an aqueous workup, similar to the procedure reported by Marks and coworkers.[46]

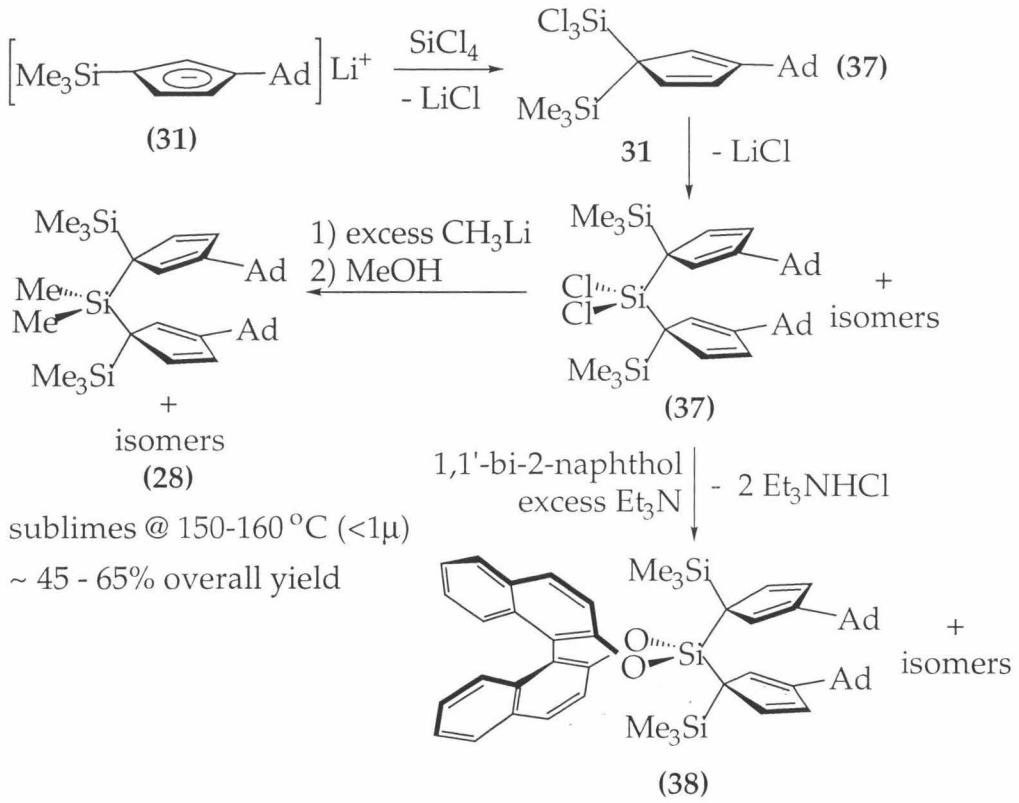

Figure 17. Syntheses of doubly protonated, 2-Adamantyl substituted ligand arrays (**28**, **38**).

No deprotonation of **36** by **31** is observed. Based in part on the stability of **35**, the robustness of the Si-Cl functional group in **36** is attributed to steric protection by the adjacent silyl methyl groups, although steric effects are not easily separated from electronic effects of switching from Me_2SiCl to $SiCl_3$ substituents.

It was hoped that **37** would prove to be a versatile building block for a variety of metallocene precursors due to the presence of reactive Si-Cl bonds in the Cp linking unit. In addition to reacting with small nucleophiles such as CH_3Li, **37** reacts with (±)1,1'-bi-2-naphthol, resulting presumably in the $C_{20}H_{12}O_2Si$-linked bis(cyclopentadiene) **38**. The chelating nature of the binaphthol moiety should favor formation of **38** over structures in which only one of the binaphthol O-H bonds reacts, or polymeric structures in

which Bn groups bridge multiple Si- linkers. Unfortunately, positive identification by ^{1}H NMR of the product mixture is complicated by the silyl and hydrogen migrations that rapidly interconvert the various regioisomers of **39**,[27] and positive identification by deprotonation to give a recognizable BnSi(Ad-TMS-Cp)$_2$ dianion is unsuccessful (*vide infra*).

As is observed for the mixture of isomers of **25**, deprotonation of the 2-Adamantyl-substituted ligand precursors **28** fails to produce single isomers of the desired dianionic ligands. Mixtures of products are obtained when **28** is treated with any one of a variety of alkyllithium reagents, amides, or alkoxides (e.g. CH_3Li, *n*-BuLi, $LiCH_2SiMe_3$, $LiCH(SiMe_3)_2$, $LiN(SiMe_3)_2$, $KN(SiMe_3)_2$, $KOCMe_3$, $NaOCMe_3$). Analogous mixtures of products are obtained upon deprotonation of the binaphthol-containing ligand precursor **38**.

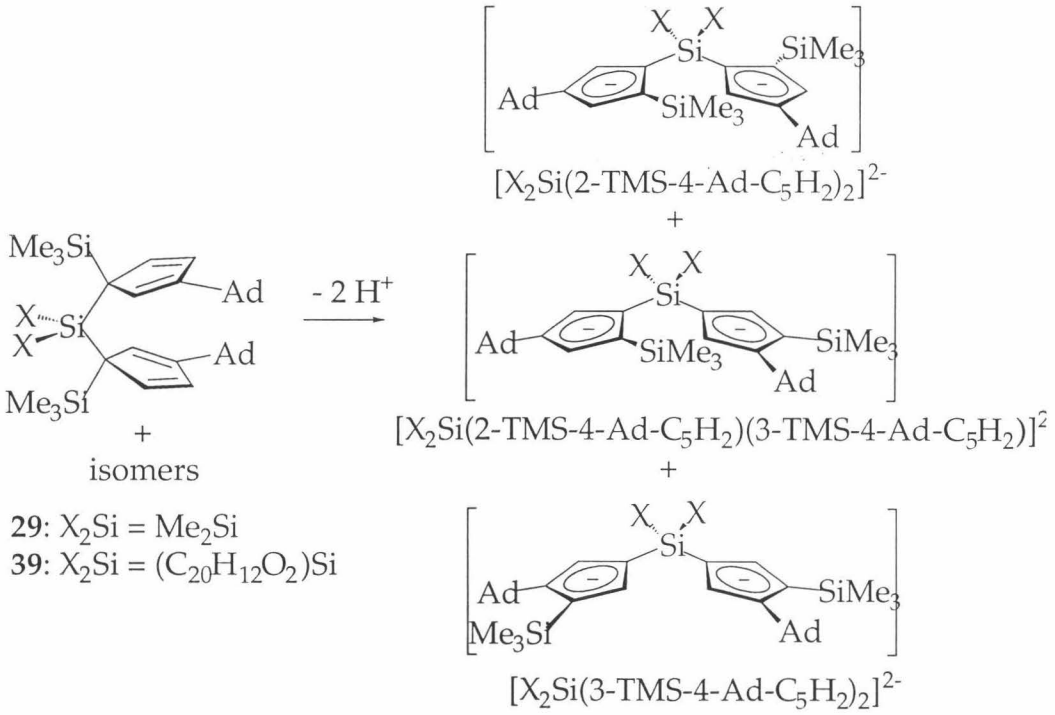

29: $X_2Si = Me_2Si$
39: $X_2Si = (C_{20}H_{12}O_2)Si$

Figure 18. Deprotonation of 2-Adamantyl-substituted ligand precursors **28, 38** result in mixtures of constitutional isomers.

If the mixture of products observed upon deprotonation are merely the kinetic products and are different from the thermodynamic deprotonation products, then an equilibration to the thermodynamically favored isomers may be feasible by introduction of a small amount of a proton source,

followed by subsequent deprotonation. Multiple cycles of this sequence should eventually convert all of the initially formed species to the thermodynamically favored species. Attempts to drive the observed deprotonation mixture to such a product (or products) by addition of a small amount of **28** to either the lithio- or potassium deprotonation products (days at 80 °C, THF-d_8) result only in the observation of unidentifiable additional products.

The failures of the secondary alkyl (cyclohexyl- and 2-Adamantyl) substituents to direct the trimethylsilyl substituents exclusively adjacent to the Si- linker, and the success of the *tert*-butyl groups in inducing such regioselectivity,[32,44] suggests that tertiary alkyls are necessary in order to obtain the 1,2,4- substitution required for the directed synthesis of exclusively C_2-symmetric *racemo*- metallocenes.

Accordingly, three tertiary alkyls are considered for incorporation into ligand ensembles directed towards the generation of monomeric C_2-symmetric Group III metallocene hydride complexes: methylcyclohexyl, 1-Adamantyl, and 2-(2-Methyl)-Adamantyl groups.

Methylcyclohexylcyclopentadienyllithium is prepared pentamethylenefulvene and CH_3Li; it is important that the reaction mixture remain cold (petroleum ether/diethyl ether, ≤0 °C) in order to prevent deprotonation of the fulvene to yield methane and (cyclohex-1-ene)cyclopentadienyllithium.

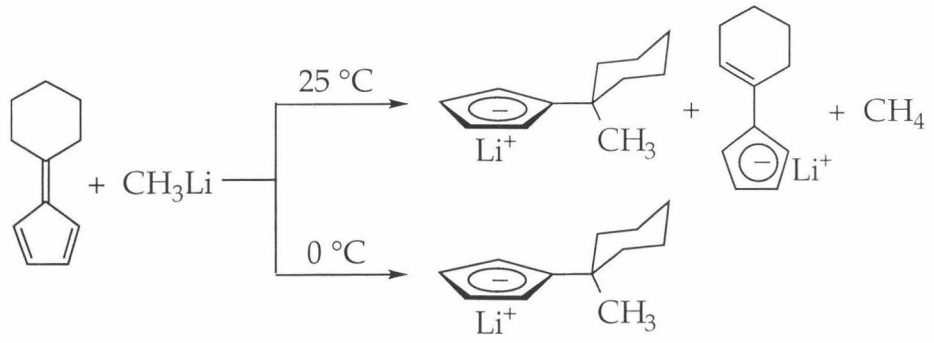

Figure 19. Synthesis of methylcyclohexylcyclopentadienyllithium.

Although the appropriate starting material could be made cleanly, efforts to synthesize a complete ligand array incorporating MeCy substituents were terminated at this point due to the likelihood of cyclohexane chair-chair interconversion perturbing the stereospecificity of any eventual catalyst derived from this tertiary alkyl. The high stereospecificities of **4g**, **4h**, and **5d**, and catalysts derived from **18** are believed to result, in part, from the rigidity of the ligand arrays; the fact that methylcyclohexyl-derived ligand arrays are likely to possess more than one energetically accessible conformation (i.e. methyl group axial versus methyl group equatorial, as shown in Figure 20) prompted the search for a more rigid tertiary alkyl substituent.

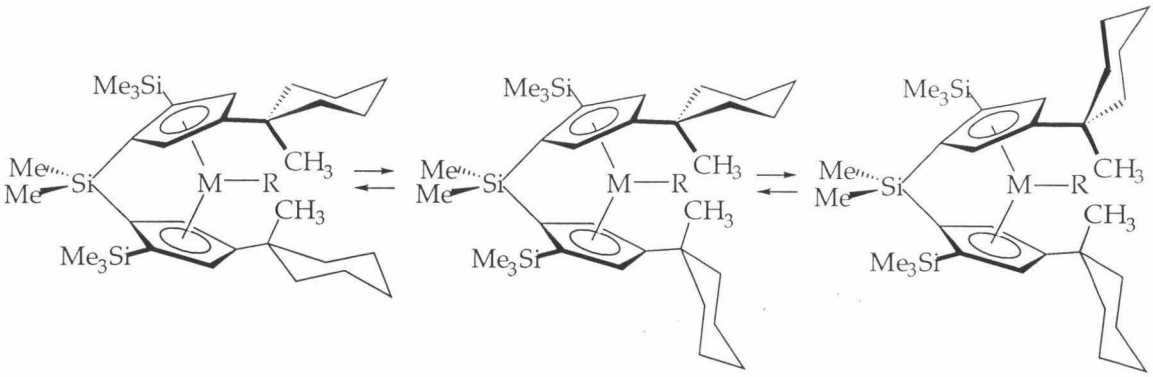

Figure 20. Possible methylcyclohexyl-Cp chair-chair interconversions.

A ligand array incorporating 1-Adamantyl groups as the β-alkyl substituents would provide the desired steric rigidity; synthesis of such a ligand is not currently feasible, however, as a result of difficulties encountered in forming a 1-Adamantyl - cyclopentadienyl C-C bond. Almost entirely unsuccessful are attempts to couple 1-AdMgBr and cyclopenten-2-one. GC/MS analysis indicates that only approximately 2% of the highly reactive 1-AdMgBr, generated *in situ* ,[47,48] reacted with cyclopenten-2-one to give (1-adamantyl)cyclopenten-1-ol or 1-adamantylcyclopentadiene. The vast majority of the product mixture (>97%) had NMR spectra and mass spectral (m/z) ratios consistent with adamantane and adamantane dimers. Also unsuccessful are attempts to generate (1-Ad)-CpH from 1-AdLi and cyclopenten-2-one and from NaCp and 1-bromoadamantane.

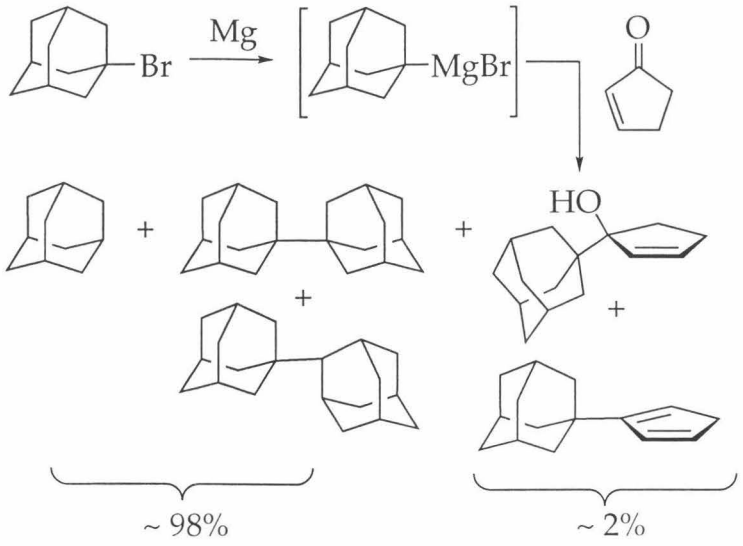

Figure 21. Synthesis of 1-adamantyl-cyclopentadiene.

The rigid tertiary alkyl most amenable to incorporation into *ansa* metallocenes is the 2-(2-methyl)-adamantyl group, whose **5a,b** and **5c-e** analogues $[Me_2Si\{3\text{-}[2\text{-}(2\text{-}CH_3\text{-}C_{10}H_{14})]\text{-}C_5H_3\}_2]^{2-}$ and $(Me_2Si\{2\text{-}SiMe_3\text{-}4\text{-}[2\text{-}(2\text{-}CH_3\text{-}C_{10}H_{14})]\text{-}C_5H_3\}_2)^{2-}$, abbreviated $[Adp]^{2-}$ and $[Abp]^{2-}$, respectively) are shown below. Although the [Adp] ligand array is not expected to result in exclusively *racemo*- metallocenes (due to the absence of $-SiMe_3$ groups adjacent to the linker), metallocenes derived from this ligand array may be utilized to gauge the ability of the methyladamantyl groups to perturb group III hydride monomer-dimer equilibria.

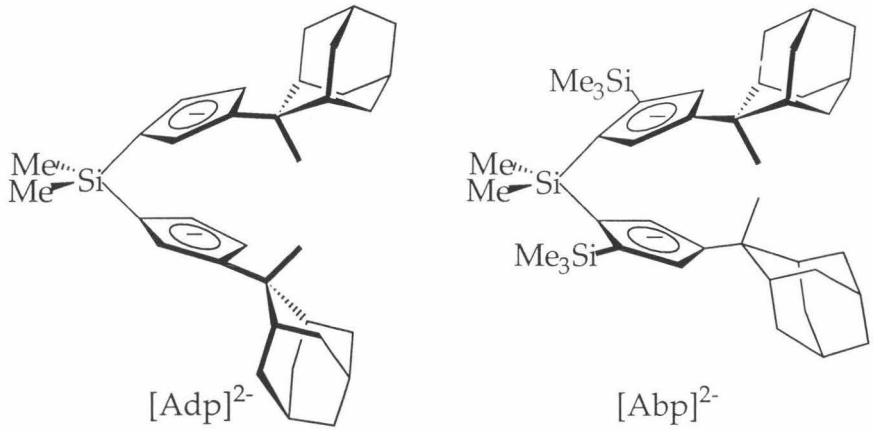

Figure 22. Target [Adp] ($[Me_2Si\{3\text{-}[2\text{-}(2\text{-}CH_3\text{-}C_{10}H_{14})]\text{-}C_5H_3\}_2]$) and [Abp] ($(Me_2Si\{2\text{-}SiMe_3\text{-}4\text{-}[2\text{-}(2\text{-}CH_3\text{-}C_{10}H_{14})]\text{-}C_5H_3\}_2)$ dianions.

Although considerably slower than the previous borohydride and LAH reductions, 30-40 gram quantities of [2-(2-methyl)-adamantyl]-cyclopentadienyllithium (**39**) are obtained in high yield (>90%) from the reaction of CH_3Li with fulvene **30**. Slightly more convenient for subsequent manipulations are the DME and TMEDA adducts of **39** (**39-DME** and **39-TMEDA**, respecitively), which are obtained from the addition of the appropriate ether or amine prior to isolation of the Li salt.

Efforts to obtain a methyladamantyl-substituted dichlorosilyl-linked species analogous to **37** were undertaken, as such a complex would be of considerable synthetic utility due to the large number of metallocene precursors readily available from functionalization of the $SiCl_2$ linker. **40** is obtained upon treatment of **39** with Me_3SiCl, filtration of LiCl, and subsequent deprotonation with *n*-butyllithium. The dimethoxyethane and tetramethylethylenediamine adducts **40-DME** and **40-TMEDA** are more easily manipulated species than the DME-free complex, as the former precipitate readily from petroleum ether, thus facilitating isolation and purification; the free salt **40** forms a viscous paste in petroleum ether, from which residual butyllithium can not be removed.

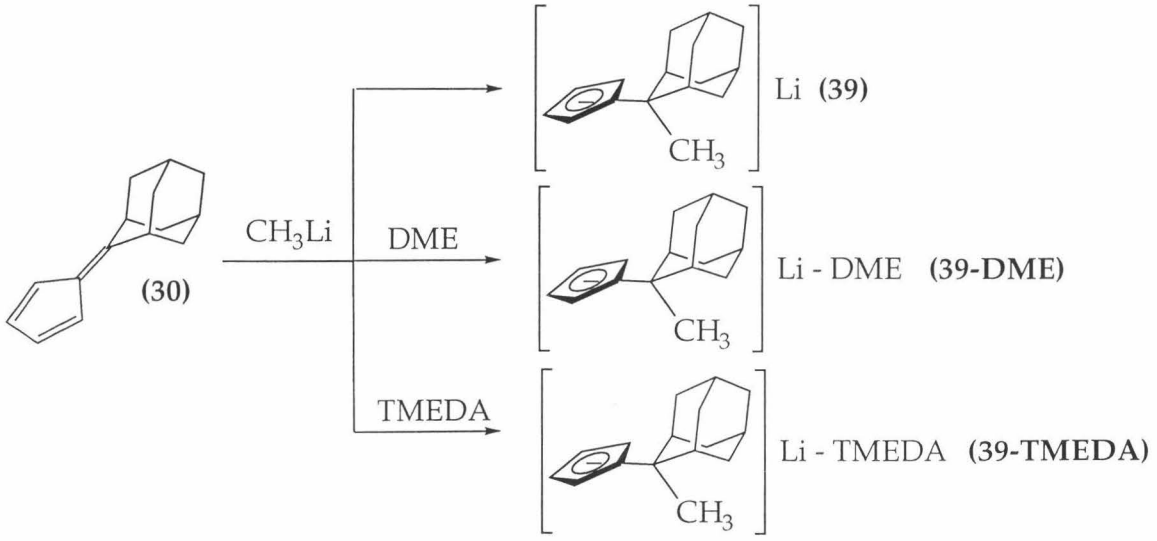

Figure 23. Syntheses of [2-(2-Methyl)-Adamantyl] cyclopentadienyls.

Unfortunately, all attempts to generate linked bis(Cp) complexes from **40** (or the DME or TMEDA adducts) and Me_2SiCl_2 or $SiCl_4$ are unsuccessful, irrespective of the presence or absence of chelating ethers or amines. **40**-

complexes react readily with Me_2SiCl_2 and $SiCl_4$, yet often result in a mixture of products analogous to those formed via the pathways indicated in Figure 15.

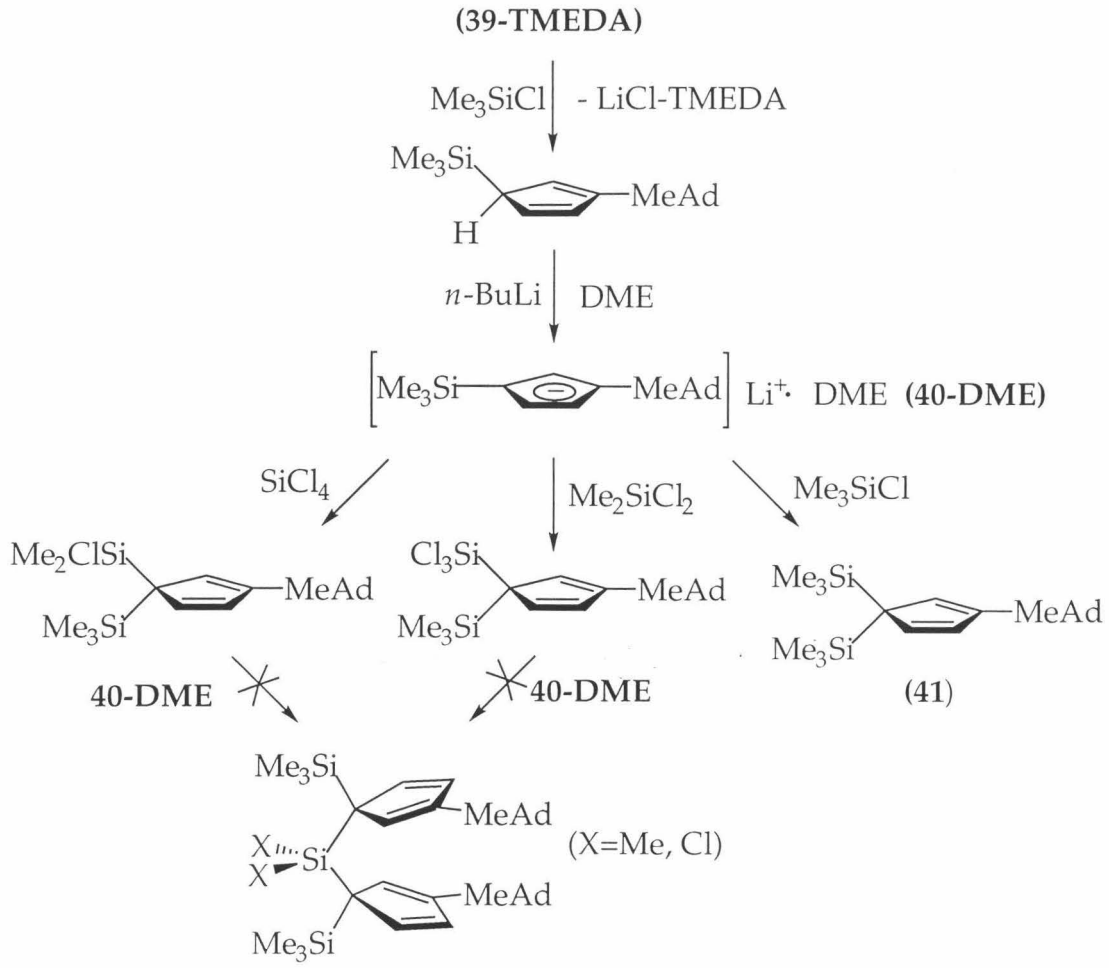

Figure 24. Unsuccessful attempts to generate 2-(2-methyl)-Adamantyl substituted analogues to **28** and **38**. MeAd = 2-(2-methyl)-Adamantyl); TMEDA = N,N,N',N'-tetramethylethylenediamine; DME = 1,2-dimethoxyethane.

The regiochemistry upon deprotonation of the multiple silylated cyclopentadienes provides a means of ascertaining the relative bulk of the methyladamantyl substituents. Of interest is the ability of the methyladamantyl groups to direct various silyl- substituents about the ring, relative to that of both the cyclohexyl- and 2-adamantyl substituents employed previously. The doubly silylated cyclopentadiene **41** exists as a single isomer in solution (determined by ^{1}H NMR). Upon deprotonation, the

resultant cyclopentadienyllithium salt shows only 1,2-$(SiMe_3)_2$-4-MeAd substitution (MeAd = 2-(2-methyl)-Adamantyl); none of the 1,3-$(SiMe_3)_2$-4-MeAd regioisomer, in which the two vinylic Cp and the two trimethylsilyl groups are inequivalent, is observed in the ^1H NMR of even the crude reaction mixture. This indicates that the 2-MeAd substituents should be sufficiently bulky to direct trimethylsilyl groups exclusively α- to the silyl linking unit to generate $[Abp]^{2-}$.

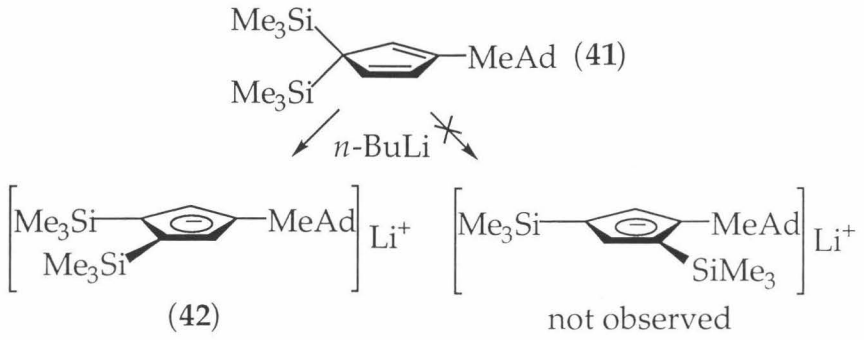

Figure 25. Deprotonation of **41** affords exclusively [1,2-$(SiMe_3)_2$-4-(MeAd)-C_5H_2]Li (**42**).

Using the strategy employed successfully for **25**, dichlorodimethylsilane is used to link two equivalents of **39-TMEDA**. Slow warming from -78 °C of a THF solution of **39-TMEDA** and Me_2SiCl_2 yields multigram quantities of the doubly protonated ligand **43**, H_2[Adp], in c.a. 80% yield after removal of LiCl-TMEDA by extraction of **43** into petroleum ether and Kugelröhr distillation. The success of this reaction is somewhat surprising, given the failure of Me_2SiCl_2 to cleanly link the 2-adamantyl-substituted **31**; the origin of this discrepancy is unclear.

Deprotonation of **43** provides $Li_2[Me_2Si(3\text{-}MeAd\text{-}C_5H_3)_2]$ (Li_2Adp, **44**) as a white petroleum ether insoluble powder (~50% yield after recrystallization). Trimethylsilyl groups are incorporated onto each ring by addition of a slight excess of Me_3SiCl to **44** (THF). After a purification procedure which involves deprotonation with $KOCMe_3$ and then hydrolysis, H_2Abp (**45**) may be isolated as a tan air and moisture-stable solid (38% yield).

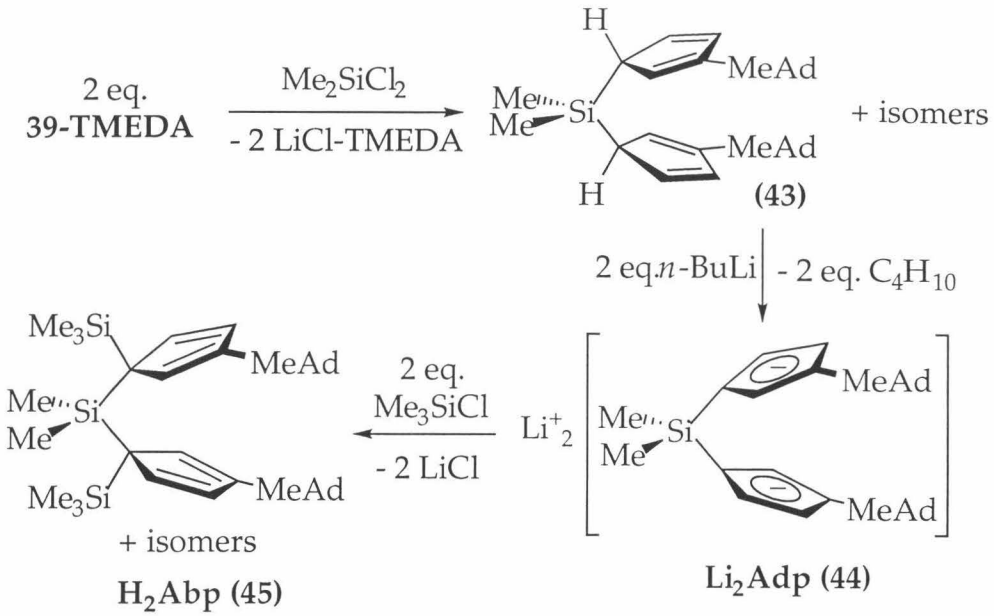

Figure 26. Syntheses of H_2Adp (**43**), Li_2Adp (**44**), H_2Abp (**45**).

As expected, the ^{1}H NMR of **45**, in either C_6D_6 or THF-d_8, indicates a mixture of isomers due to facile silyl- and hydrogen migrations about the cyclopentadiene rings. Treatment of this mixture with any of a variety of nucleophiles, however, results in the double deprotonation of H_2Abp to yield *a single isomer* of $[Abp]^{2-}$. Li_2Abp (**46**) and K_2Abp (**47**) may be obtained from the treatment of **45** with $LiCH_2SiMe_3$ or $KN(SiMe_3)_2$, respectively. The 500 MHz ^{1}H NMR spectra of the mixture of isomers of **45** and the single constitutional isomer **47** are shown in Figures 27 and 28, respectively. The

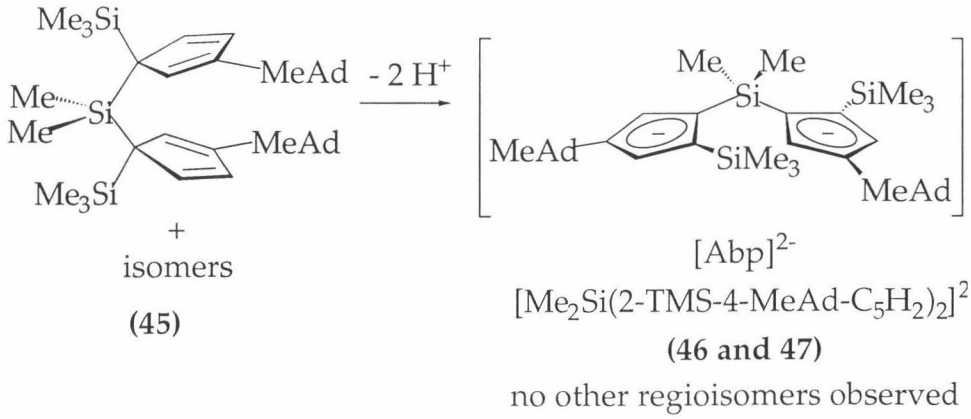

Figure 27. Deprotonation of H_2Abp (**45**) affords a single constitutional isomer of the desired 2-(2-methyl)-Adamantyl substituted ligand array.

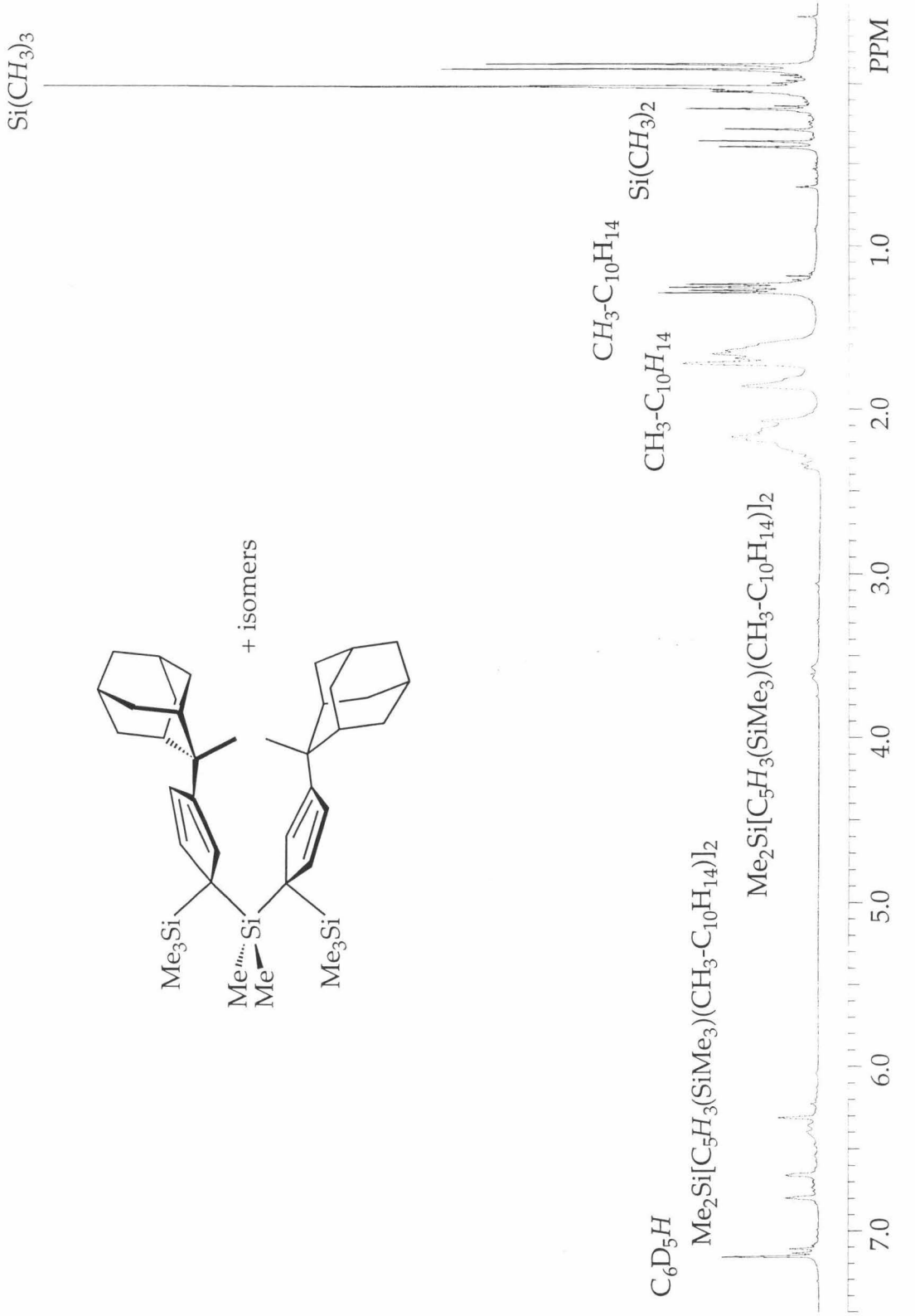

Figure 28. 500 MHz ^{1}H NMR spectra of H_2Abp (**45**) (C_6D_6).

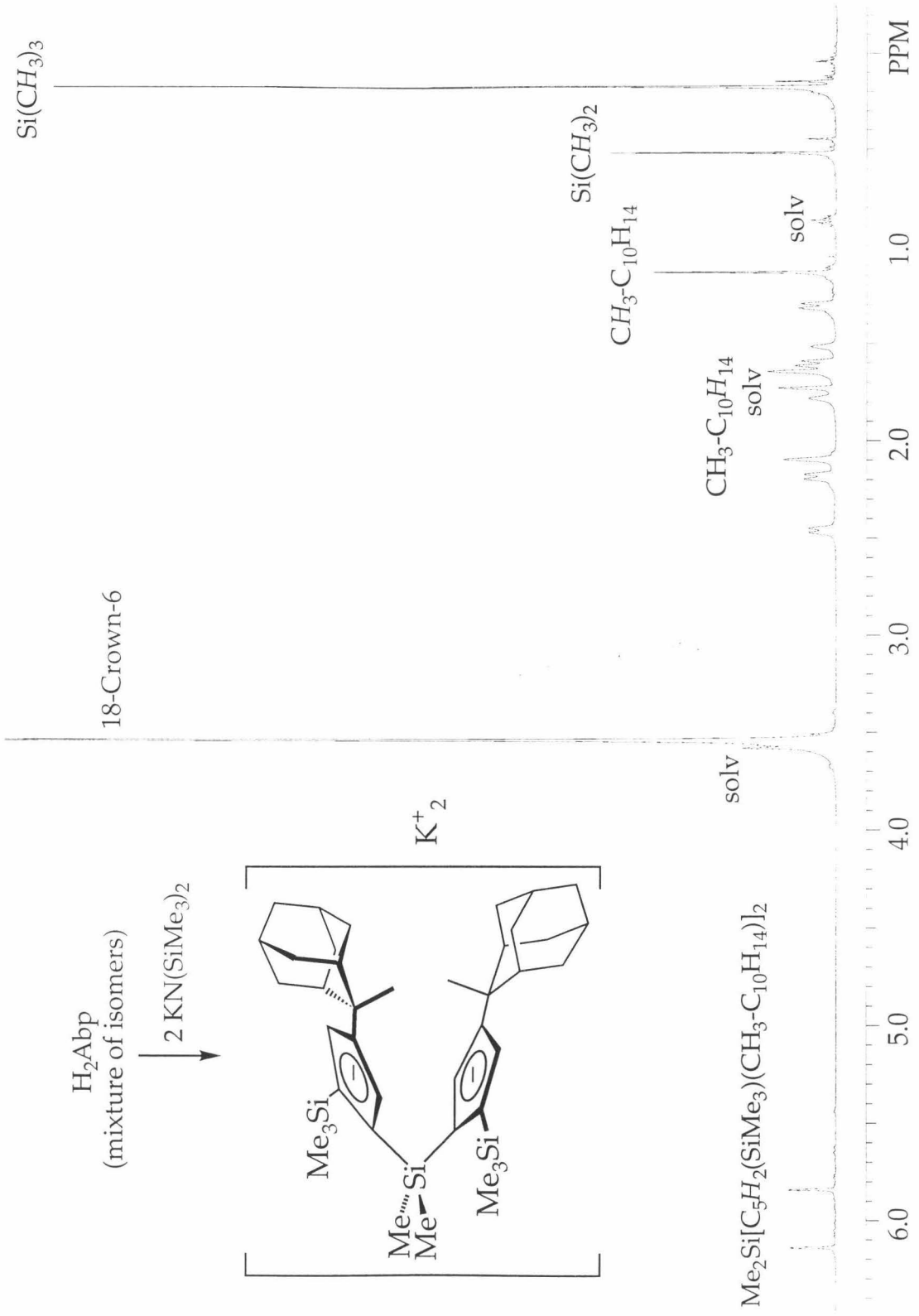

Figure 29. 500 MHz ^{1}H NMR spectra of K_2Abp (**47**) (THF-d_8, with added 18-crown-6).

1,2,4 substitution of **46** and **47** are assigned on the basis of similar chemical reactivities of Abp-derived metallocenes (*vide infra*) to related *tert*-butyl substituted complexes, whose 1,2,4-substitutions have been confirmed by single crystal X-ray crystallographic methods.[31,44]

The dilithio salt **37** is soluble not only in ethereal solvents such as THF and Et_2O, but also in hydrocarbon solvents such as toluene and petroleum ether, which precluded its isolation and purification. Analogous solubility problems are observed for the dilithio salt of the analogous *tert*-butyl substituted ligand; efforts to precipitate **46** through addition of coordinating bases are not undertaken because of previous difficulties encountered in the transmetallation of DME- and TMEDA-containing dianionic ligands.[32]

In contrast to the dilithio salt, **47** is insoluble in hydrocarbon solvents, and is almost completely insoluble in ethereal solvents such as THF. Only upon addition of stoichiometric quantities of the K^+-coordinating crown ether 18-Crown-6 could **47** be rendered sufficiently soluble in THF for characterization by ^1H NMR spectroscopy. Addition of potential donor ligands such as DME fails to enhance the solubility properties of **47**.

Efforts to obtain Group III metallocenes of both **44** and **47** were undertaken in order to assess the ability of the methyladamantyl groups and the α- trimethylsilyl groups to induce formation of *racemo*- metallocenes.

The reaction of Li_2Adp (**44**) with $ScCl_3(THF)_{3.5}$ proceeds readily in THF over 12 hours at room temperature. Examination of the crude product mixture indicates the formation of exclusively *meso*-AdpScCl-LiCl-$(THF)_2$ (**48**) (Figure 30), as evidenced by the inequivalent linking silyl-methyl resonances in the ^1H NMR spectra of **48**; no *racemo* products are observed.

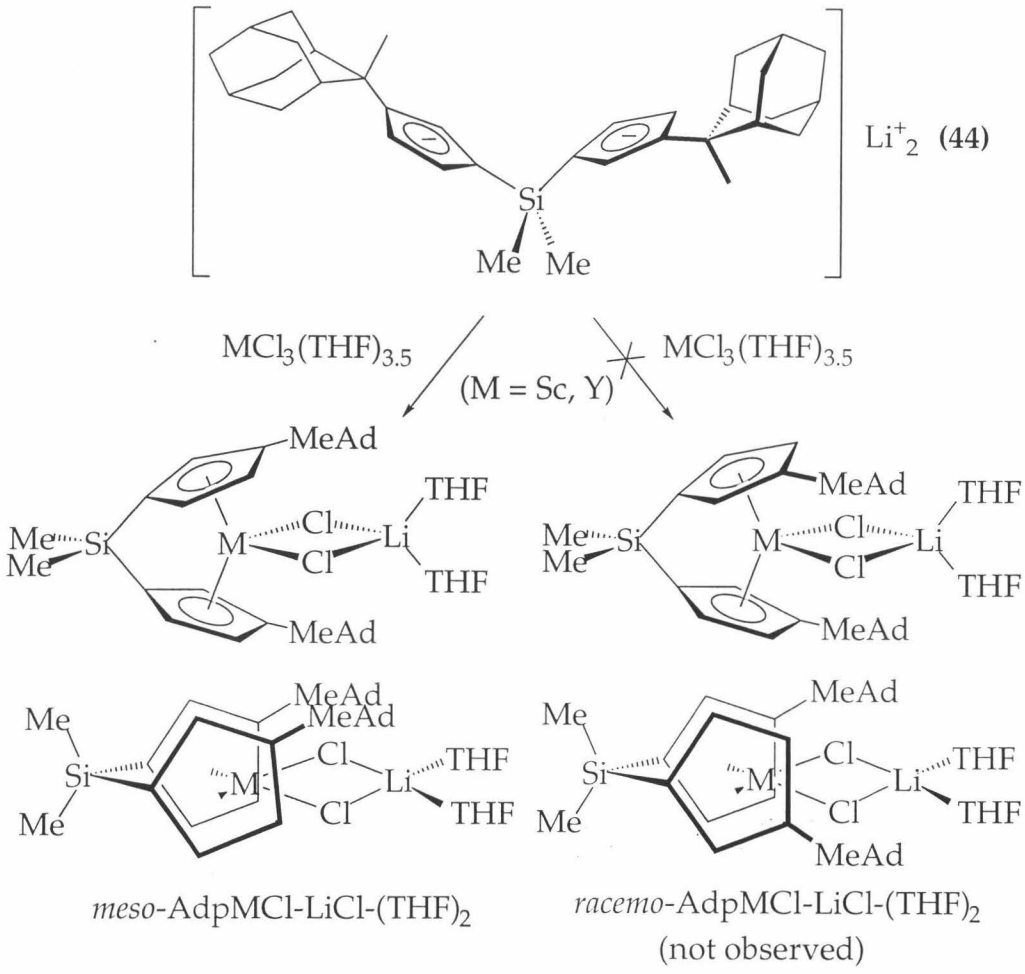

Figure 30. Formation of exclusively *meso*- AdpMCl-LiCl-(solvent)$_2$ complexes; M = Sc (**48**), Y (**49**).

Although NMR spectroscopy of the crude reaction mixture indicates a high (>85%) yield of **48**, separation of **48** from LiCl generated during transmetallation proved problematic, as both **48** and LiCl are soluble in THF and insoluble in toluene and diethyl ether.

An identical selectivity for *meso*- metallocene formation is observed in the reaction between **44** and $YCl_3(THF)_{3.5}$ (48 hours, 25 °C, THF). *meso*-AdpYCl-LiCl-(THF)$_2$ (**49**) is obtained as a tan solid (56% yield) after removal of LiCl through a series of toluene and Et_2O washes and filtrations. A small amount (~18%) of the tetrahydrofuran originally coordinated in **49** is replaced by diethyl ether over the course of these washings; two equivalents of solvent appear coordinated to Li throughout the workup procedure.

The assignment of **48** and **49** as LiCl-bis(solvent) adducts is based on the established tendency of highly Lewis acidic group III and lanthanide metallocenes to coordinate Li-halides,[49] and the observation of two equivalents of coordinating solvent in the metallocenes' ^{1}H NMR spectra. Repeated attempts to grow single crystals of **48** and **49** suitable for X-ray diffraction to confirm the solid state structures were unsuccessful.

The formation of exclusively *meso*-metallocenes is consistent with previous findings that even relatively bulky alkyl substituents residing in the β- positions of singly linked cyclopentadienes do not necessarily lead to an increased selectivity for formation of *racemo*- complexes. Increasingly bulky β- substituents, in fact, seem to *favor* the formation of *meso*- complexes; analogous transmetallations using the *tert*-butyl substituted ligand array $[Me_2Si(3\text{-}CMe_3\text{-}C_5H_3)_2]Li_2$ (abbreviated $[Dp]Li_2$) showed exclusive formation of [*meso*-DpScCl]$_n$, and a 1:1 *meso*:*racemo* ratio in the formation of $[DpYCl]_n$.[28] The thermodynamic preference for formation of *meso*- metallocenes of singly silyl-linked bis(3-alkyl-cyclopentadienyl) ligand arrays has been demonstrated previously by Jordan and co-workers.[50]

The transmetallation of $[Abp]^{2-}$ (**46**/**47**), which contains trimethylsilyl substituents adjacent to the Me_2Si linker to generate group III metallocenes proceeds with diastereoselectivities opposite to those observed for [Adp]. Treatment of K_2Abp (**47**) with either $ScCl_3(THF)_{3.5}$ or $YCl_3(THF)_{3.5}$ (refluxing THF, 48 hours) results in the formation of exclusively *racemo*- metallocenes. Steric interactions in the narrow portion of the metallocene wedge apparently disfavor formation of the *meso*- complexes, in which the $SiMe_3$ groups adopt eclipsed conformations.

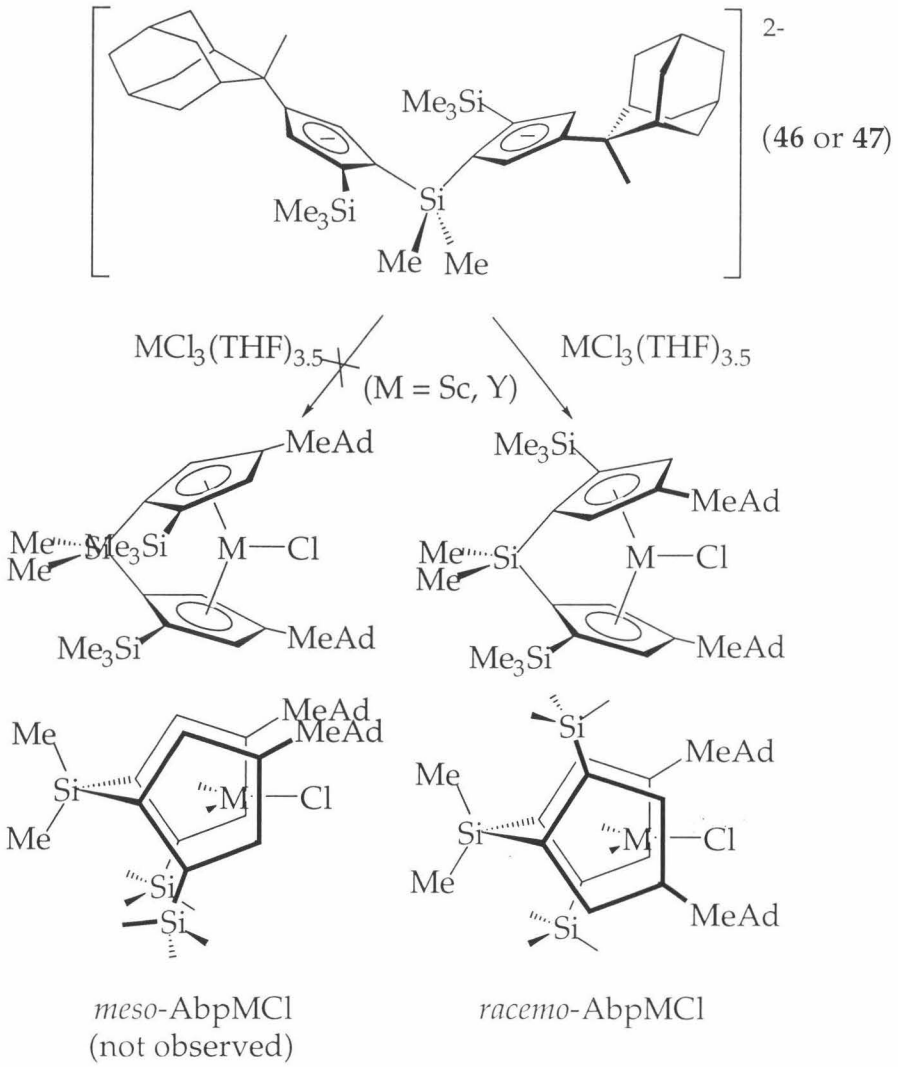

Figure 31. Metallation using the [Abp] dianion results in exclusively *racemo*-metallocenes (M = Sc or Y).[51]

Solutions of refluxing THF are required to promote transmetallation; the metallations are unsucessful when attempted in toluene or benzene. The limited solubility of K_2Abp in THF is undoubtedly a factor contributing to the extended periods of heating required to drive the metallations to completion.

When followed by ^{1}H NMR spectroscopy, treatment of K_2Abp and $ScCl_3(THF)_{3.5}$ in THF-d_8 results in the formation of a C_2-symmetric kinetic product, assigned as the KCl-bis(solvent) adduct *rac*-AbpScCl-(KCl)-$(THF)_2$ (**50**) (Figure 32),[52] which is then converted to two new products, each of which contains exclusively *racemo*-metallocenes (**51**, **52**).

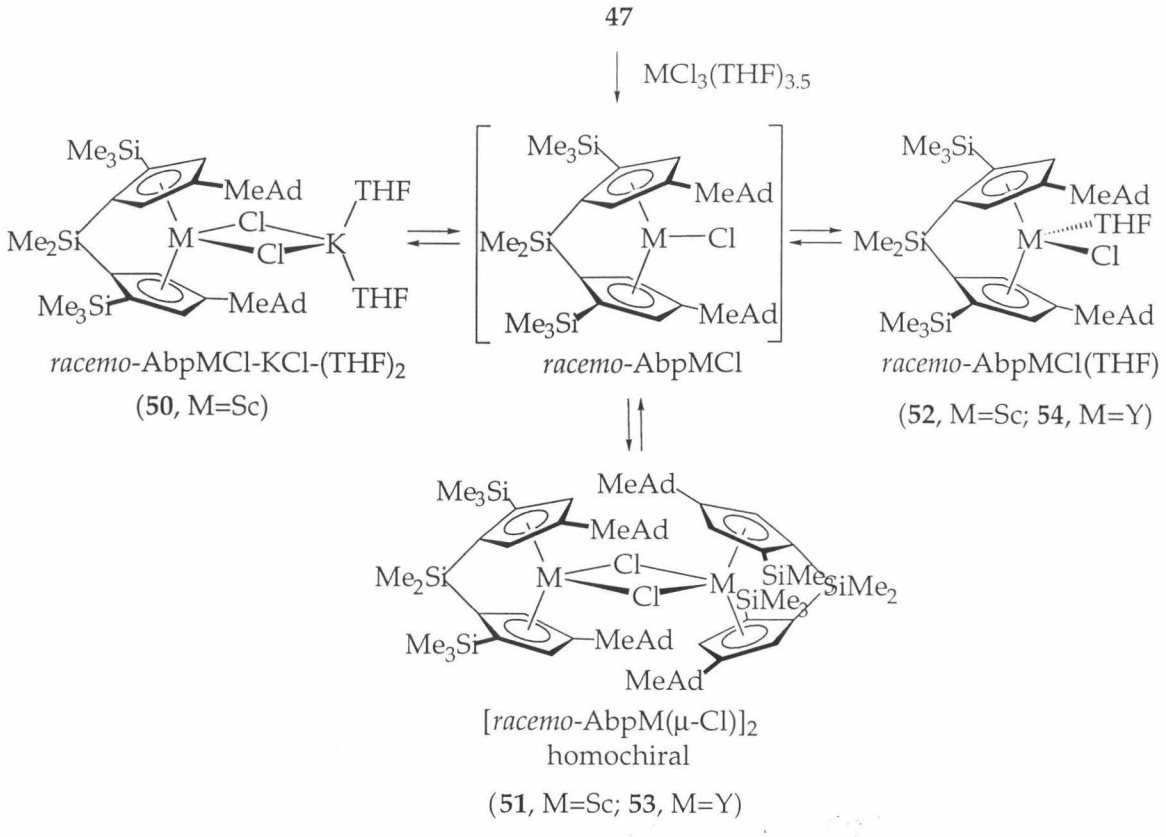

Figure 32. Metalation of **47** affords *rac*-AbpMCl-(KCl)-$(THF)_2$, which is subsequently converted to *rac*-AbpMCl(THF) and [*rac*-AbpM(μ-Cl)]$_2$ (M=Sc, Y).

51 and **52** are assigned as the THF adduct *rac*-AbpScCl(THF) and the chloride bridged dimer [*racemo*-AbpSc(μ-Cl)]$_2$.[51] These assignments are supported by the previous observation of multiple transmetallation products for $[Me_2Si(2\text{-}SiMe_3\text{-}4\text{-}CMe_3)_2]K_2$ with $ScCl_3(THF)_{3.5}$, which are assigned as the analogous THF adducts and $(\mu\text{-}Cl)_2$ dimers.[30] Also possible, however, are equilibria involving homochiral and heterochiral dimers of [*rac*-AbpYCl]. As the transmetallations are performed in THF, it is unlikely that the monmeric, base-free [*rac*-AbpYCl] is a stable metallation product under the observed conditions.

Conversion of the kinetic product to **51** and **52** begins prior to total consumption of the starting materials, and the ratio of **51** to **52** does not deviate from the 1:3 ratio attained after 48 hours at 80 °C. Removal of solvent (THF) followed by extended heating in benzene-d_6 does not result in

additional conversion of **51** to **52**; decomposition to unidentifiable products is, instead, observed.

A similar mixture of products is observed in the transmetallation of **47** with $YCl_3(THF)_{3.5}$; the 2:1 mixture of thermodynamic products observed upon treatment of **47** with $YCl_3(THF)_{3.5}$ (THF, 48 hours, 80 °C) are assigned as the homochiral chloride-bridged dimer [*rac*-AbpY(μ-Cl)]$_2$ (**53**) and *rac*-AbpYCl(THF) (**54**). Alternate possible transmetallation products, however, include the homochiral and heterochiral dimers of [*racemo*-AbpYCl] and *rac*-AbpYCl-(KCl)-(THF)$_2$.

Nonstoichiometric quantities of THF (~0.2 equivalents THF-d_0 per Y) accompany the yttrocenes (as determined by ^{1}H NMR spectroscopy), despite repeated lyophilizations and exposures to dynamic vacuum. Although the ratio of major:minor products varies somewhat depending on the workup conditions, the ratio is largely independent of the amount of residual THF present.

A single *racemo*- organometallic product is observed (^{1}H and ^{13}C NMR spectroscopy), however, when the [AbpYCl] product mixture is dissolved in C_6D_6. Based, in part, on the previously observed thermodynamic stabilities of (μ-Cl)$_2$ dimers,[30,32,44] this product is assigned as the chloride-bridged dimer **53**. When benzene is removed *in vacuo* and replaced by THF-d_8, the two *racemo*- products **53** and **54** are observed in a c.a. 2:1 ratio. This disruption of (μ-Cl)$_2$ dimers in the presence of donor ligands (THF-d_8) may serve as preliminary evidence for the ability of the methyladamantyl substituents to destabilize dimer formation relative to monomeric (albeit donor-stabilized) complexes.

Conclusions

The syntheses of a series of multiply silylated cyclopentadienes incorporating either cyclohexyl- (**25**), 2-adamantyl- (**28**, **38**), or 2-(2-methyl)-adamantyl groups (**45**) are described. These cyclopentadienes exist in solution as a mixture of rapidly interconverting isomers as result of the ability of silylated cyclopentadienes to undergo spontaneous hydrogen and silyl

migrations. Mixtures of constitutional isomers result from the double deprotonation of the cyclohexyl- and 2-adamantyl-substituted ligand arrays. The products of these deprotonations are believed to be constitutional isomers of the desired dianionic ligands. Double deprotonation of the 2-(2-methyl)-adamantyl substituted cyclopentadienes results in exclusive formation of the $[Me_2Si\{2\text{-}(SiMe_3)\text{-}4\text{-}[2\text{-}(2\text{-}CH_3\text{-}C_{10}H_{14})]\text{-}C_5H_2\}_2]M_2$ regioisomer (M = Li (**46**); K (**47**)). These results show that a tertiary alkyl group is required in order to direct the trimethylsilyl substituents selectively to the position adjacent to the silyl linker.

The incorporation and 2,4-disposition of trimethylsilyl and alkyl substituents is essential for the formation of chiral metallocenes. Transmetallation of **47** with $MCl_3(THF)_{3.5}$ result in exclusively *racemo*-metallocenes. Steric interactions between the trimethylsilyl substituents in the narrow portion of the metallocene wedge are believed to preclude formation of the *meso*- (achiral) conformer. Transmetallation of $Me_2Si\{3\text{-}[2\text{-}(2\text{-}CH_3\text{-}C_{10}H_{14})]\text{-}C_5H_3\}_2]Li_2$ (**46**) proceeds with enantioselectivity opposite to that of **47**, resulting in exclusively *meso*- metallocenes **48** and **49**.

Experimental Section

General Considerations: All air and/or moisture sensitive compounds were manipulated using standard high vacuum line, Schlenk, or cannula techniques or in a dry box under a nitrogen atmosphere, as described previously.[53] Argon and hydrogen gases were purified and dried by passage over columns of MnO on vermiculite and activated molecular sieves. Solvents were stored under vacuum over titanocene[54] or sodium benzophenone ketyl.

Pentamethylenefulvene was prepared according to the procedure of Stone and Little.[45] $ScCl_3(THF)_{3.5}$ was prepared using the procedure of Manzer;[55] $YCl_3(THF)_{3.5}$ was prepared by an identical route. $LiCH(SiMe_3)_2$ was prepared according to the procedure of Cowley.[56] $SiCl_4$, Me_2SiCl_2, Me_3SiCl, and Et_3N were dried over CaH_2 and stored under vacuum. $LiCH_2SiMe_3$, $KOCMe_3$ and $KN(TMS)_2$ were purchased from Aldrich and sublimed prior to

use. $LiAlH_4$ was purchased from Aldrich and dissolved in diethyl ether prior to use. TMEDA was stored over Na, and DME was dried first over sodium benzophenone ketyl and then stored over potassium benzophenone ketyl. 18-crown-6 was dried over activated 4Å sieves and sublimed twice prior to use. Vitride was purchased from Kodak and used as received. All other reagents were purchased from Aldrich and used as received.

NMR spectra are recorded on a Bruker AM500 (500.13 MHz for ^1H, 125.76 MHz for ^{13}C) or a GE QE-300 (300 MHz for ^1H, 75.5 MHz for ^{13}C) spectrometer. All shifts reported for proton and carbon NMR are referenced to solvent. NMR tube reactions are carried out using flame sealed NMR tubes or J. Young type Teflon-valved NMR tubes purchased from Wilmad. Mass spectra were acquired with the help of Dr. Peter G. Green at the Caltech Environmental Analysis Center using an HP 59880B Particle Beam LC/MS Interface to an HP 5989A Mass Spectrometer Engine; air/water exclusion was attempted using the HP 1090 Liquid Chromatograph's Solvent Delivery System and Variable Volume Injector. Elemental analyses were performed at the Caltech Elemental Analysis Facility by Fenton Harvey.

Preparation of [Cy-C_5H_4]K-B(*sec*-Bu)$_3$ (21-BR_3): A 50 ml roundbottom flask is charged with 2.0 g (13.7 mmol) of pentamethylenefulvene, and is attached to a small frit with a 50 ml receiving roundbottom flask. After evacuation, 25 ml Et_2O is vacuum transferred into the flask, affording a clear yellow solution upon warming to room temperature. After cooling the roundbottom and its contents to 0 °C with an ice-water bath, 13.6 mmol potassium tri-*sec*-butylborohydride (K-Selectride, 13.6 ml, 1.0 M solution in THF) is injected into the flask against an argon counterflow. The ice bath is removed, and the resulting pale yellow solution is allowed to stir at 25 °C for 10 hours. Solvent is removed *in vacuo*, and the resulting tan solid is dried under dynamic vacuum for 1 hour. Diethyl ether (25 ml) is vacuum transferred onto the solid, and a small amount of finely divided white solid is filtered away from the ether solution, and is washed twice with diethyl ether. Solvent is removed in vacuo, leaving a tacky tan solid in the receiving roundbottom flask. A new 50 ml flask is attached to the frit assembly in the glove box, and petroleum ether (35 ml) is vacuum transferred onto the solid. The petroleum ether (PE) insoluble material is isolated by filtration, and is washed twice with PE, affording 2.037 grams of beige powder (10.9 mmol, 80% yield).

Preparation of $(SiMe_3)(Cy)C_5H_4$: A 250 ml roundbottom flask is charged with 17.2 mol of **21** and is attached to a swivel frit assembly. THF (250 ml) is transferred onto the solid. Chlorotrimethylsilane (2.5 ml, 19.7 mmol, 1.15 eq.) is added at -78 °C. The solution is warmed 55 °C and stirred for three hours. After cooling to room temperature, solvent is removed *in vacuo*, and petroleum ether (15 ml) is distilled into the flask. LiCl is removed by filtration, and is washed twice with petroleum ether. Solvent is removed *in vacuo*, leaving a clear yellow oil. A short path distillation (60 °C, <1μ) yielded 1.76 g (8.0 mmol, 47% yield) of a yellow oil.

Preparation of $[1\text{-}SiMe_3\text{-}3\text{-}Cy\text{-}C_5H_3]K$ (24): In a glove box, a 250 ml roundbottom flask is charged with 1.75 g (8.0 mmol) of $(SiMe_3)(Cy)C_5H_4$ and 120 ml THF. Potassium *tert*-butoxide (888 mg, 7.92 mmol) is added slowly to the stirred solution. After stirring for 21 hours at room temperature, solvent is removed from the clear orange solution *in vacuo*. Excess *tert*-butanol is removed by heating under dynamic vacuum (6 hrs, 65 °C). The flask is attached to a swivel frit assembly, and 1.59 g of a white petroleum ether solid is isolated (6.15 mmol, 77% yield).

Preparation of $[Cy\text{-}C_5H_4]Li$ (20): In a 250 ml roundbottom flask is placed 40 mmol of pentamethylenefulvene, and the flask is attached to a medium porosity swivel frit assembly. Diethyl ether (125 ml) is vacuum transferred onto the fulvene and is warmed to 0 °C, resulting in a clear yellow solution. LAH (1.0 M in Et_2O, 50 ml, 50 mmol) is syringed into the flask against an Ar counterflow over the course of 30 minutes, and the solution is stirred at 0 °C for 25 minutes. The 0 °C bath is removed, and the solution is stirred at 25 °C for an additional 12 hours. The white diethyl ether-insoluble material is isolated by filtration and is dried *in vacuo*, affording 3.998 g of a flocculent white solid (26 mmol, 65% yield).

Preparation of $Me_2Si(Cy\text{-}C_5H_4)_2$ (22): A 100 ml roundbottom flask is charged with 3.934 g (25.5 mmol) of **20**, and is attached to a medium porosity swivel frit. Tetrahydrofuran (80 ml) is distilled onto the solid, and the solution kept at -78 °C while 1.15 ml (9.46 mmol) Me_2SiCl_2 is vacuum transferred first into a graduated cold finger and then into the THF solution. The solution is stirred

for 11 hours as the dry ice/acetone bath slowly warmed to room temperature, leaving a yellow solution with grey precipitate. Solvent is removed *in vacuo*, and the resulting material is dried under dynamic vacuum for 4 hours. Petroleum ether (60 ml) is distilled into the roundbottom, and a grey solid (LiCl) is removed from the yellow solution by filtration; the solid is washed 5 times will small portions of PE. The petroleum ether is removed *in vacuo*, leaving 3.062 g (8.68 mmol) of a yellow oil (92%).

Preparation of $[Me_2Si(3\text{-}Cy\text{-}C_5H_3)_2]Li_2$ (26a): A 500 ml roundbottom flask is charged with 7.999 g (22.7 mmol) of **22**, and is attached to a large swivel frit equipped with a 90° needle valve and a 500 ml receiving roundbottom. Petroleum ether (250 ml) is distilled onto the yellow oil, producing a clear yellow solution when warmed to 0 °C. A 1.6 M solution of *n*-butyllithium (31 ml, 49.6 mmol) is syringed into the solution against an argon counterflow, and the solution is stirred at 0 °C for 2 hours. The resulting solution, containing a large amount of white precipitate, is stirred at 25 °C for an additional 2 hours, at which time the solution is filtered, and the solid washed is washed 5 times with small aliquots of petroleum ether. Solvent is removed and the white solid is dried *in vacuo* , affording approximately 5.66 g (15.5 mmol) of **26a** (68%).

Preparation of $[Me_2Si(3\text{-}Cy\text{-}C_5H_3)_2]K_2$ (26b): In the glove box, a 25 ml roundbottom flask is charged with 570 mg (1.62 mmol) **22**, and 15 ml of THF is added *via* pipet. To this clear yellow solution is added 357 mg $KOCMe_3$ (sublimed, 3.18 mmol, 1.96 eq.); the frit assembly is placed on the vacuum line, and the solution is stirred at 25 °C for 16 hours. Solvent is removed *in vacuo* , and the resultant brown solid is dried under vacuum (70 °C) for 9 hours. Petroleum ether (20 ml) is distilled into the flask, and 404 mg of a tan PE insoluble solid is isolated after filtration (0.93 mmol, 57%).

Preparation of $Me_2Si[(SiMe_3)(Cy)C_5H_3]_2$ (25): A medium porosity swivel frit is affixed with a 90° needle valve and two 100 ml roundbottom flasks, one of which contains 1.214 g (3.33 mmol) of **26a**. The frit assembly is evacuated, and 50 ml of THF is distilled onto the solid. Trimethylchlorosilane (1.05 ml, 8.27 mmol) is vacuum transferred into a graduated cold finger, and is then transferred into the reaction flask at -78 °C. The dry ice/actone bath is

removed, and the solution allowed to warm with stirring to room temperature; solvent is removed from the solution after approximately 44 hours of stirring at 25 °C. Petroleum ether (50 ml) is distilled onto the product mixture, and the resulting white precipiate (LiCl) is filtered easily from the bright yellow solution. The solid is washed three times with petroleum ether, and then PE is removed *in vacuo*, affording 1.293 g (2.60 mmol) of orange oil after Kugelröhr distillation (79%). Mass spectroscopy on the mixture provides a parent peak at (m/z) = 496 (expected for $C_{30}H_{52}Si_3$ = 497.09 g/mol).

Preparation of Admantylfulvene (30): To a stirred solution of 2-adamantanone (24.85 g, 165.4 mmol) and freshly cracked cyclopentadiene (66.0 ml, 800.6 mmol) in 500 ml of methanol is added 17.0 ml (204 mmol) of pyrrolidine. Yellow solid began precipitating from the burgundy-colored solution within several hours of pyrrolidine addition. After stirring for 11 days, the solution is acidified with 33 ml of glacial acetic acid and diluted with 400 ml of water and 100 ml of diethylether. The liquids are transferred to a 2-liter separatory funnel, to which is added an additional 100 ml of water and 400 ml ether. The aqueous layer is washed three times with 375 ml and once with 75 ml of ether, and the combined organic layers are washed once with 150 ml water and once with 150 ml brine. After drying over and gravity filtering from magnesium sulfate, the organic solution is rotovapped to dryness, leaving an orange-brown solid. Bright yellow crystals (28.69 g, 144.7 mmol, 88% yield) are obtained upon recrystallization from petroleum ether. Elemental analysis: Calculated (Found, with V_2O_5 added) C: 90.83 (90.97, 90.92); H: 9.17 (8.97, 9.05).

Preparation of [(2-Ad)-C_5H_4]Li (31a): Adamantylfulvene (**30**) (10.829 g, 55 mmol) is placed in a 500 ml roundbottom flask on a large swivel frit assembly, and 250 ml Et_2O is distilled in from Na/benzophenone ketyl. At 0 °C, 60 ml of a 1.0 M solution of $LiAlH_4$ (Et_2O) is syringed into the clear yellow solution against an Ar counterflow. The solution is stirred at 0 °C for 30 minutes, and then at room temperature overnight. A large amount of white solid is isolated by filtration, washed 3 times with Et_2O, and dried under vacuum, affording 12.27 g of **31a**-$(Et_2O)_{0.2}$ (55 mmol, 100%). The solid may be then subjected to an aqueous workup by making a suspesion of **31a** in diethyl

ether (3.85 g **31a**/150 ml Et_2O, 250 ml roundbottom flask), adding water (2.5 ml) via syringe pump (0.17-0.25 µl/min) (**USE EXTREME CAUTION WHEN QUENCHING RESIDUAL AlH_3**), followed by 2.5 ml of an aqueous 15% NaOH solution. More water (15 ml) is added to the flask, and the contents of the flask are transferred to a 250 ml separatory funnel. The aqueous layer is washed once with 20 ml Et_2O, and the combined organics are dried over magnesium sulfate and filtered. Solvent is removed *in vacuo*, leaving a light green oil ((2-Ad)-C_5H_5) in ~70% yield. Deprotonation with *n*-butyllithium proceeds by adding 40 ml petroleum ether to a solution of 1.4606 g (7.29 mmol) of (2-Ad)-C_5H_5, cooling the solution to 0 °C, and syringing 4.0 ml of a 2.0 M solution of *n*-BuLi in pentane into the cooled roundbottom flask against an Ar counterflow. The solution is stirred at room temperature for three hours, during which time white solid precipitates from solution. Solvent is removed *in vacuo*, and 930 mg of a white petroleum ether insoluble material is isolated and washed once with fresh pet ether (4.30 mmol, 59% yield of **31a**). Elemental analysis: Calculated (Found, with V_2O_5 added) C: 83.26 (86.55, 87.81); H: 13.54 (9.70, 10.41). Calculated (Found, without added oxidant) C: 83.26 (85.48, 84.80); H: 13.54 (9.90, 9.77).

Preparation of [(2-Ad)-C_5H_4]Na (31b): A 100 ml roundbottom flask is charged with 1.027 g (5.18 mmol) **30**. Petroleum ether (50 ml) is distilled onto the yellow solid and is warmed to 0 °C. Vitride ($NaAl(OCH_2CH_2OCH3)_2H_2$, 70% solution in toluene, 2.0 ml, 7.22 mmol) is syringed into the clear yellow solution against an Ar counterflow, and the solution stirred at 0 °C for approximately 10 minutes. After warming to room temperature and stirring for an additional 18 hours, solvent is removed *in vacuo*, and the resulting solid is washed twice with petroleum ether and then filtered from toluene. **31b** is isolated as a toluene-insoluble white solid (599 mg, 2.69 mmol) in 52% yield.

Preparation of ($SiMe_3$)(2-Ad)C_5H_4 (32): A 500 ml roundbottom flask equipped with a 180° needle valve is charged with 6.765 g (32.8 mmol) of **31a**. Onto this white solid is distilled 200 ml of THF. Trimethylchlorosilane (4.9 ml, 38.6 mmol) is vacuum transferred onto the suspension at -78 °C. The solution is stirred at -78 °C for 30 minutes, and then warmed to room temperature and stirred overnight. Solvent is removed *in vacuo* , and the flask is brought into

the glove box and attached to a large swivel frit assembly. Petroleum ether (250 ml) is vacuum transferred onto the crude reaction mixture, generating a colorless solution with a small amount of white precipitate. The solid (LiCl) is filtered away from the colorless solution, and is washed twice with small portions of petroleum ether. Removal of solvent from the clear, colorless solution gave 8.773 g (32.2 mmol) of a viscous oil (98%).

Preparation of $(SiMe_2Cl)(2\text{-}Ad)C_5H_4$ (33): A 100 ml roundbottom flask is charged with 559 mg (2.71 mmol) of **31a** and attached to a medium porosity swivel frit assembly. THF (40 ml) is distilled onto the solid, giving a clear and colorless solution. The solution is cooled to -78 °C, onto which dimethylchlorosilane (0.5 ml, 4.12 mmol, 1.53 eq.) is transferred. The solution is allowed to warm slowly to room temperature as the dry ice/acetone bath slowly evaporates. After 12 hours of stirring at 25 °C, volatiles are removed from the solution *in vacuo*. A grey petroleum ether (25 ml) insoluble solid is removed by filtration, leaving a clear yellow liquid. Solvent is removed, affording 780 mg of a clear yellow oil (2.67 mmol, 98% yield).

Preparation of $[1\text{-}SiMe_3\text{-}3\text{-}(2\text{-}Ad)\text{-}C_5H_3]Li$ (34): **32** (8.773 g, 32.2 mmol) is placed in a 500 ml roundbottom flask attached to a 180 °C needle valve. Petroleum ether (300 ml) is transferred into the flask, and the solution brought to 0 °C. n-Butyllithium (1.6 M in hexanes, 24.0 ml, 38.4 mmol) is syringed dropwise into the solution against an Ar counterflow followed by 60 minutes of stirring at 0 °C. After warming to room temperature, the solution is stirred for 22 hours, accompanied by the evolution of gas and precipitation of a large amount of white solid. The solution is degassed and brought into a glove box, where the solid is washed and suction filtered 4 times through a coarse filter frit with a total of 175 ml of petroleum ether. The petroleum ether-insoluble white solid is dried *in vacuo*, affording 8.77432 g (31.4 mmol) of **34** (98%). Elemental analysis: Calculated (Found) C: 77.63 (75.56, 74.97); H: 9.79 (9.50, 9.56); N: 0.00 (0.00, 0.00).

Preparation of $(SiMe_2Cl)(SiMe_3)(2\text{-}Ad)C_5H_3$ (35): In a glove box, a J-Young NMR tube is charged with 15.3 mg (0.0550 mmol) of **34**. The teflon valve is sealed and the NMR tube evacuated on the vacuum line. THF-d_8 (0.4 ml) is distilled onto the solid and the solution is warmed to room temperature,

giving a clear and colorless solution. The tube is cooled with a LN_2 bath, and (using a calibrated gas bulb) 0.0275 mmol of Me_2SiCl_2 is vacuum transferred into the tube from CaH_2. The tube is sealed and warmed slowly to room temperature. Half of the starting **34** had reacted within 15 hours at room temperature. No further reaction was observed (3 days at room temperature). Heating the NMR tube resulted in decomposition to unidentifiable products (days, 80 °C).

Preparation of $(SiCl_3)(SiMe_3)(2\text{-}Ad)C_5H_3$ (36): A 25 ml roundbottom flask is charged with 136 mg (0.49 mmol) **34** and is placed on a small medium porosity swivel frit. Toluene (13 ml) is distilled onto the solid and the suspension warmed to room temperature, then cooled to -78 °C. Silicon tetrachloride (0.24 mmol) is measured into a calibrated 42.5 ml gas bulb, and is then transferred into the reaction flask at -78 °C. The dry ice/acetone bath is allowed to warm to room temperature and the solution is stirred at 25 °C for 4 days. The white solid is filtered away from the yellow solution and is washed three times with small aliquots of toluene. Solvent and volatiles are removed *in vacuo* from the clear yellow toluene solution, leaving 136 mg of a clear yellow oil (0.38 mmol, 78%). Elemental analysis: Calculated (Found) C: 67.34 (63.64, 62.90); H: 8.49 (8.21, 8.53); N: 0.00 (0.00, 0.00). Mass spectral analysis indicates a parent peak at (m/z) = 406 ($C_{18}H_{27}Si_2Cl_3$ = 405.98), with no peak at (m/z) = 643 (corresponding to $Cl_2Si(AdTMSCpH)_2 = C_{36}H_{54}Si_3Cl_2$). Also present in the mass spectrum are smaller peaks at m/z = 389 and 369, corresponding to the products resulting from hydrolyses of one and two, respectively, of the Si-Cl bonds in **36**, during introduction into the spectrometer.

Preparation of $Cl_2Si[(SiMe_3)(2\text{-}Ad)C_5H_3]_2$ (37): A 25 ml roundbottom flask is charged with 303 mg (1.09 mmol) of **34**. Tetrahydrofuran (12 ml) is distilled onto the white solid, giving a clear and colorless solution at 35 °C. Silicon tetrachloride (0.535 mmol) is transferred into a 42.5 ml gas bulb and then into the reaction flask, which had been cooled to -78 °C. The dry ice/acetone bath is allowed to warm slowly to 25 °C as the solution is stirred overnight. Solvent and volatiles are removed *in vacuo*, and the roundbottom flask is attached to a medium porosity swivel frit assembly. Petroleum ether (13 ml) is distilled onto the light yellow solid, resulting in a yellow solution and fine

white precipitate. The white solid (LiCl) is removed by filtration and is washed three times with small portions of petroleum ether. Solvent is removed *in vacuo* from the solution, leaving 245 mg (0.382 mmol) of a faint yellow microcrystalline solid (72% yield). Elemental analysis: Calculated (Found) C: 67.34 (66.97, 66.84); H: 8.49 (8.54, 8.59); N: 0.00 (0.00, 0.00). Mass spectroscopy indicates a parent peak at (m/z) = 642 (expected for $C_{36}H_{54}Si_3Cl_2$ = 642.07).

Preparation of $Me_2Si[(SiMe_3)(2\text{-}Ad)C_5H_3]_2$ (28): A 250 ml roundbottom flask is charged with 2.366 g (3.67 mmol) of **37** and placed on a fine porosity swivel frit assembly. Diethyl ether (150 ml) is distilled onto the solid, and the solution is warmed to 0 °C. Methyllithium (1.4 M in Et_2O, 13.0 ml, 18.2 mmol) is syringed into the flask against an Ar counterflow and the ice bath is allowed to warm slowly to room temperature as the solution is stirred overnight. The faint yellow solution with white precipitate is cooled to -78 °C and 0.8 ml (19.74 mmol) CH_3OH is syringed into the flask. The solution is stirred and warmed slowly to room temperature for 4 hours. Solvent and volatiles are removed *in vacuo* and 20 ml petroleum ether is distilled onto the product mixture. The white solid (LiCl) is removed from the light yellow solution by filtration, and is washed twice with petroleum ether. Solvent is removed *in vacuo*, affording 986 mg (1.64 mmol) of a light yellow microcrystalline solid (45% yield). Elemental analysis: Calculated (Found) C: 75.91 (76.90, 77.56); H: 10.08 (10.24, 10.42); N: 0.00 (0.00, 0.00). The yellow solid is placed in a small sublimator and yellow solid began collecting on the cold finger as the heating bath temperature reached 147 °C. The sublimator is heated at 165 °C for 4 hours, at which time 407 mg (0.41 mmol) of light yellow solid could be scraped from the cold finger.

Preparation of $[(\pm)C_{20}H_{12}O_2]Si[(SiMe_3)(2\text{-}Ad)C_5H_3]_2$ (38): A 100 ml roundbottom flask is charged with 976.5 mg (1.521 mmol) of **37** and 433.2 mg (1.513 mmol, 1.00 eq.) of (±)1,1'-bi-2-naphthol, attached to a 180° needle valve, and degassed on a vacuum line. THF (50 ml) is distilled into the flask (-78 °C), as is 0.6 ml Et_3N (4.305 mmol, 2.85 eq.). The solution is allowed to warm to room temperature for 10 hours. Solvent is removed and the resultant yellow solid dried *in vacuo*. The flask is attached to a medium porosity frit assembly (in the glove box); 50 ml of diethyl ether is distilled onto the solid, resulting

in a yellow solution and a considerable amount of white solid. Et_3N-HCl is removed by filtration, and the remaining Et_2O-soluble yellow solid is dried under dynamic vacuum and then subjected to an Et_2O filtration through a fine frit. Solvent is removed in vacuo, leaving 974.3 mg of a microcrystalline yellow solid (^{1}H NMR indicates the presence of 0.71 equivalents of residual diethyl ether); 1.07 mmol, 71% yield.

Preparation of [(MeCy)C_5H_4]Li: A 100 ml roundbottom flask is charged with 1.359 g (8.58 mmol) of pentamethylenefulvene, and is attached to a medium porosity swivel frit assembly. Petroleum ether (50 ml) is distilled onto the solid, generating a clear yellow solution. The solution is cooled to -78 °C and 6.5 ml 1.4 M CH_3Li (9.1 mmol) is syringed, dropwise, into the solution against an Ar counterflow. The resulting cloudy yellow solution is stirred at -78 °C for 15 minutes, and is allowed to warm slowly to room temperature with stirring. After 26 hours of stirring, the solution is filtered, leaving a tan petroleum ether-insoluble powder, which is dried *in vacuo* (1.266 g, 7.52 mmol, 88% yield).

Preparation of {[2-(2-Me-$C_{10}H_{14}$)]-C_5H_4}Li-DME ([MeAd-C_5H_4]Li-DME) (39-DME). A 100 ml roundbottom flask equipped with a 180° needle valve is charged with 1.427 g (7.19 mmol) of **30**. Diethyl ether (50 ml) and dimethoxyethane (1.1 ml, 10.6 mmol) are distilled onto the solid and the resulting clear yellow solution is cooled to 0 °C. Methyllithium (1.4 M in Et_2O, 6.0 ml, 8.4 mmol) is syringed into the solution against an Ar counterflow and the solution is stirred at 0 °C for 20 minutes. After warming to room temperature, the yellow solution with white precipitate is stirred at 25 °C for 70 hours. Solvent is removed *in vacuo* and the reaction flask is affixed to a coarse swivel frit; 50 ml of petroleum ether is vacuum transferred into the flask and a white solid is removed from the colorless solution by filtration. The petroleum ether insoluble material is washed 3 times with aliquots of petroleum ether, and dried *in vacuo*, yielding 1.947 g of a flocculent white solid. ^{1}H NMR spectroscopy (THF-d_8) indicates that the solid is **39** accompanied by a non-stoichiometric amount of DME (0.55 equivalents); isolated yield = 6.50 mmol, 90%. Elemental analysis: Calculated (Found) C: 80.99 (77.98, 78.44); H: 9.92 (10.06, 10.19); N: 0.00 (0.00, 0.00); these elemental

analysis numbers are more consistent with the presence of 0.88 equivalents of coordinated DME: C: 78.21; H: 10.04; N: 0.00.

Preparation of [MeAd-C_5H_4]Li-TMEDA (39-TMEDA): A 2-liter, 3-necked roundbottom flask, equipped with a rubber septum and a 180° needle valve, is charged with 83.30 g (420 mmol) of **30**. With stirring, 1100 ml of diethyl ether and 64 ml (424 mmol, 1.01 eq.) of N,N,N',N'-tetramethylethylenediamine are cannulaed into the flask. The solution is cooled to 0 °C and 300 ml of 1.4 M methyllithium (Et_2O, 420 mmol, 1.00 eq.) is cannulaed into the flask over 1 hour. White solid began to precipitate from the otherwise clear and bright yellow solution during the methyllithium addition. The solution is allowed to warm slowly to 25 °C and is stirred at 25 °C for approximately 6 days. Solvent is removed in vacuo, and the remaining white solid is washed four times with 150 ml aliquots of petroleum ether. The petroleum ether insoluble material is dried *in vacuo* for 6 hours, providing 132.5 g (393.7 mmol, 94% yield) of a fluffy white solid. Elemental analysis: Calculated (Found, with V_2O_5 added) C: 78.51 (77.95, 78.43); H: 11.10 (10.30, 11.03); N: 8.33 (8.29, 8.46).

Preparation of ($SiMe_3$)(MeAd)C_5H_4: A 100 ml roundbottom flask is charged with 1.537 g (4.57 mmol) of **39-TMEDA** and attached to a small, fine porosity swivel frit assembly. Tetrahydrofuran (50 ml) is distilled onto the solid, yielding a clear light yellow solution at 0 °C. The solution is cooled to -78 °C, and 0.8 ml (6.30 mmol) of Me_3SiCl is vacuum transferred into a graduated cold finger, and then into the reaction flask. The -78 °C bath is removed and the solution allowed to warm to room temperature and stir for 12 hours. Solvent is removed *in vacuo* and 50 ml petroleum ether is distilled onto the tan solid. White solid (LiCl) is removed by filtration and is washed twice with petroleum ether. Solvent and volatiles are removed from the clear yellow solution, leaving 1.282 g (4.47 mmol) of tan solid (98%).

Preparation of [1-$SiMe_3$-3-MeAd-C_5H_3]Li-DME (40-DME): II-125 & 129 In the glove box, a 1-liter roundbottom flask is charged with a magnetic stir bar, 23.475 g (81.91 mmol) of ($SiMe_3$)(MeAd)C_5H_4 and 450 ml of petroleum ether. A 180° needle valve is attached to the flask and the apparatus is placed on the vacuum line and cooled to 0 °C. *n*-Butyllithium (1.6 M in hexanes, 60 ml, 96

mmol) is syringed into the flask against an argon counterflow over the course of 25 minutes. The solution is stirred at 0 °C for 10 minutes, at which time the ice bath is removed and the solution allowed to warm to room temperature and stirred overnight, leaving an extremely viscous brown paste at the bottom of the otherwise pale yellow solution. Solvent is removed *in vacuo*, leaving 25.8623 g of tan powder. The flask is brought into a glove box, and 2.0636 grams of the powder is removed for other reactivity studies. To the remaining 23.799 g (~80 mmol) of tan powder is added 250 ml of petroleum ether. Dimethoxyethane (9.4 ml, 90.4 mmol) is pipetted dropwise into the colorless solution containing the gooey orange solid, accompanied by the immediate precipitation of white solid. The solution is stirred vigorously overnight in order to break up clumps of starting material. The white solid formed is isolated by suction filtration, is washed three times with 50-60 ml portions of petroleum ether, and is dried *in vacuo*, affording 26.8962 g of flocculent white solid (93% yield). Elemental analysis: Calculated (Found) C: 72.19 (71.82, 72.29); H: 10.29 (10.23, 10.39); N: 0.00 (0.00, 0.00).

Preparation of $(SiMe_2Cl)(SiMe_3)(MeAd)C_5H_3$: In the glove box, a J-Young NMR tube is charged with 14.2 mg (0.037 mmol) of **40**. Into the tube is vacuum transferred 0.4 ml THF-d_8 (-78 °C), and the contents of the tube warmed to room temperature, affording a clear yellow solution. The contents of the NMR tube are frozen with a liquid nitrogen bath, and 0.018 mmol Me_2SiCl_2 is vacuum transferred from CaH_2 to a calibrated 3.3 ml gas bulb to the J-Young tube. The contents of the NMR tube are warmed to room temperature and agitated overnight. After 15 hours at room temperature, ^1H NMR spectroscopy indicated that all of the Me_2SiCl_2 had reacted, as had approximately half of the starting Li salt. This product mixture changed neither after an additional 6 hours of agitation at 25 °C, nor after 16 additional hours of heating at 80 °C. The presence of diastereotopic Me_2SiCl methyl groups, and the absence of allylic cyclopentadiene resonances, in the ^1H NMR spectrum of the new compound are characteristic of a doubly silylated, alkyl-substituted cyclopentadiene.

Preparation of $(SiCl_3)(SiMe_3)(MeAd)C_5H_3$: In the glove box, a J-Young NMR tube is charged with 13.0 mg (0.044 mmol) of **40**. THF-d_8 (0.4 ml) is vacuum transferred into the tube, and the contents of the tube shaken and warmed to

room temperature. Using a calibrated 3.3 ml gas bulb, 0.045 mmol of $SiCl_4$ is vacuum transferred into the tube (LN_2); the contents of the tube are warmed to room temperature and are agitated for 90 minutes, at which time ^1H NMR spectroscopy indicates that all of the starting material has been consumed.

Preparation of $(SiMe_3)_2(MeAd)C_5H_3$ (41): In the glove box, a J-Young NMR tube is charged with 18.9 mg (0.049 mmol) of **40-DME**. THF-d_8 (0.5 ml) is transferred into the tube, and the solution warmed to room temperature. The contents of the NMR tube are then cooled with a liquid nitrogen bath, and Me_3SiCl (0.062 mmol) is vacuum transferred from CaH_2 into a calibrated 42.5 ml gas bulb, and then into the cooled NMR tube. The contents of the tube are warmed quickly to room temperature, and the resulting clear, pale yellow solution is agitated overnight. After 11.5 hours of stirring, ^1H NMR spectroscopy indicates that all of the starting material had been consumed.

Preparation of [1,2-$(SiMe_3)_2$-4-MeAd-C_5H_2]Li (42): II-151 A J-Young tube containing 0.049 mmol of $MeAd(TMS)_2CpH$ and 0.5 ml of THF-d_8 is brought into a glove box, and 9 mg (0.083 mmol) of CH3Li-LiBr is added to the clear, very pale yellow solution. After 4 hours of stirring at room temperature, ^1H NMR spectroscopy indicated that all of the starting material had been consumed. The presence of a single vinylic cyclopentadiene resonance (relative intensity 2H), one singlet for the trimethylsilyl groups (18H), and one **Me**Ad resonance (singlet, 3H), are diagnostic for the assigned 1,2-$(TMS)_2$-4-MeAd substitution about the Cp ring.

Preparation of $Me_2Si(MeAd\text{-}C_5H_4)_2$ (H_2Adp, 43): A 2-liter, 3-necked roundbottom flask, equipped with a 180° needle valve and a rubber septum, is charged with 80.82 grams (237.7 mmol) of **39-TMEDA**. THF (400 ml) is added via cannula, and the contents of the flask are cooled to -78 °C. Dichlorodimethylsilane (13.5 ml, 111.1 mmol, 0.46 eq.) is vacuum transferred from CaH_2 into an evacuated 50 ml roundbottom flask/180° needle valve assembly. After filling the small flask with argon, the Me_2SiCl_2 is syringed slowly into the 2-liter flask containing the white THF suspension. The THF solution is slowly warmed to room temperature, and is stirred at room temperature for an additional 36 hours. THF is removed in vacuo, leaving a viscous yellow oil, which is brought into a dry box. The petroleum ether

insoluble white solid (LiCl-TMEDA) is removed by suction filtration, and the bright yellow petroleum ether solution is transferred to a 1 L roundbottom flask with a 180° needle valve. Solvent is removed in vacuo, leaving a large quantity of viscous orange oil. MeAd-C_5H_5, a side product from the linking reaction, is removed by Kugelröhr distillation (15 hours, 100 °C, <1 μ), affording 88 mmol of **43** (79% yield) as a dark orange/brown glassy solid upon cooling to room temperature. Elemental analysis: Calculated (Found, with V_2O_5 added) C: 84.21 (83.15, 82.97); H: 10.00 (10.30, 9.75); N: 0.00 (0.00, 0.00); (Found, without added oxidant) C: (83.22, 83.12); H: (8.73, 8.58); N: (0.00, 0.00).

Preparation of [Me_2Si(3-MeAd-C_5H_3)$_2$]Li_2 (Li_2Adp, 44): A 500 ml roundbottom flask equipped with a 180° needle valve is charged in a dry box with 18.0 mmol of **43**. Petroleum ether (160 ml) is vacuum transferred onto the orange solid and the solution is cooled to 0 °C. A 1.6 M solution of *n*-butyllithium in hexanes (24 ml, 38.4 mmol, 2.1 eq.) is syringed into the roundbottom against an argon counterflow over a period of five minutes. The solution is warmed slowly to room temperature and is then stirred at 25 °C for 16 hours. Volatiles are removed from the suspension of white solid in a faint yellow solution and residual solvent is removed from the beige solid by an additional 2 hours of drying under dynamic vacuum. The flask is brought into a dry box and attached to a fine porosity swivel frit and a 500 ml roundbottom flask. Petroleum ether (175 ml) is vacuum transferred onto the solid and the solution is filtered after warming to room temperature. Solvent is removed and the beige petroleum ether insoluble material is dried in vacuo for 8 hours, yielding 8.20 grams of a pale peach-colored solid. **43** is recrystallized from Et_2O, producing an initial crop of 4.76 g (9.58 mmol, 53.2% yield) of ligand; additional ligand may probably be recovered from the remaining 1.95 grams of Et_2O soluble material through additional recrystallizations. Elemental analysis: Calculated (Found, with V_2O_5 added) C: 82.20 (79.91, 78.31); H: 9.35 (10.00. 9.54); N: 0.00 (0.00, 0.00).

Preparation of Me_2Si[($SiMe_3$)(MeAd)-C_5H_3)$_2$] (H_2Abp, 45): A 1-liter roundbottom flask is charged with 22.0336 g (42.8 mmol) of **43** and 500 ml of THF. A 180° needle valve is attached to the flask and the solution is degassed on a vacuum line and then cooled to -78 °C. Trimethylchlorosilane (13.2 ml, 104 mmol, 2.43 equivalents) is vacuum transferred from CaH2 into a

graduated cold finger and then onto the Li_2Adp suspension. The solution is stirred at -78 °C for 3 hours, and is then allowed to warm to room temperature and stirred at 25 °C for 12 hours. Volatiles are removed *in vacuo*, leaving a large amount of yellow foam; the foam is dried overnight by exposure to dynamic vacuum, and then brought into a glove box. A bright yellow solution and white solid result from the addition of 350 ml of petroleum ether to the foam. The solid (LiCl) is removed by filtration and is washed twice with small aliquots of petroleum ether. Solvent is removed from the combined organics, leaving a large amount of yellow foam. The low boiling (<110 °C) species are removed by Kugelröhr distillation, leaving 20.17 g of a dark orange glassy solid that could be crushed into an orange solid (32.1 mmol, 75% yield). Elemental analysis: Calculated (Found, with V_2O_5 added) C: 76.34 (75.49, 75.17); H: 10.27 (8.73, 9.44); N: 0.00 (0.00, 0.00). Calculated (Found, without added oxidant) C: 76.34 (75.50, 75.51); H: 10.27 (10.27, 10.52); N: 0.00 (0.00, 0.00).

Use of the following purification procedure results in improved isolated yields of yttrocenes: 18.0 mmol of the once-Kugelröhred **45** is placed in a 500 ml roundbottom flask, to which is added 275 ml of THF. $KOCMe_3$ (4.312 g, 38.4 mmol, 2.13 eq.) is added slowly to the clear yellow solution; white solid began precipitating from the solution within several minutes. Solvent is removed in vacuo after stirring at room temperature for 45 hours, and the resultant tan solid dried *in vacuo*. Diethyl ether (225 ml) is transferred onto the resulting solid, and the suspension is cooled to 0 °C. A 0.5 M aqueous solution of NH_4Cl (110 ml) is syringed slowly into the suspension, and allowed to warm to room temperature. The orange organic layer is washed three times with 30 ml aliquots of water, and the combined aqueous layers are washed once with 30 ml of ether. The combined organics are dried over magnesium sulfate and filtered. Solvent is removed from the clear yellow solution, leaving an orange foam,. Removal of low boiling species is attained by a lengthy Kugelröhr distillation (15 hours of heating at 100-110 °C), leaving 7.52 g (12 mmol) of **45** (38% yield based on **44**).

Li_2Abp (46) A 50 ml roundbottom flask is charged with 789.9 mg **45** and 247.0 mg $LiCH_2SiMe_3$, and the flask is attached to a coarse frit assembly. THF (25 ml) is distilled onto the solids (-78 °C), and the solution is warmed to -40 °C.

After stirring at -40 °C for three hours, the solution is allowed to warm slowly to room temperature, and is stirred at 25 °C overnight. Volatiles are removed and the resulting foam dried *in vacuo*. Petroleum ether (25 ml) is distilled onto the foam, resulting in an almost completely clear orange solution, thus precluding removal of **46**. Solvent is removed from the flask, and 936 mg of tan solid is isolated. ^{1}H NMR spectrosopy indicates one equivalent of residual THF accompanying the doubly deprotonated **46**/LiCl mixture.

K_2Abp (47): A 100 ml roundbottom flask is charged with 2.5001 g (3.97 mmol) of **45** and 1.6056 g (8.05 mmol, 2.03 eq.) of $KOCMe_3$. The flask is attached to a 180° needle valve and degassed on the vacuum line. Toluene (50 ml) is distilled onto the solids (-78 °C) and the solution allowed to warm to room temperature. After stirring at 25 °C for 32 hours, solvent is removed *in vacuo*, leaving a brown solid. The flask is attached to a medium porosity swivel frit and 40 ml petroleum ether are distilled onto the reaction mixture. A light brown petroleum ether insoluble material is isolated by filtration from the dark brown solution and the solid is washed twice with small aliquots of pet ether. The solid is dried by heating (9 hours, 130 °C) under dynamic vacuum (<1μ), affording 2.2815 g (3.22 mmol) of **47** as a pale tan solid (81% yield). Elemental analysis: Calculated (Found, with V_2O_5 added) C: 68.09 (67.33, 67.18); H: 8.88 (9.13, 8.59); N: 0.00 (0.00, 0.00). Calculated (Found, without added oxidant) C: 68.09 (65.64, 65.56); H: 8.88 (9.59, 9.48); N: 0.00 (0.00, 0.00).

Preparation of *meso*-AdpScCl-LiCl-$(THF)_2$ (48): In a 100 ml roundbottom flask attached to a medium porosity swivel frit is placed 2.09 g (11.79 mmol) of **47** and 1.54 g of $ScCl_3(THF)_{3.5}$. THF (50 ml) is vacuum transferred into the flask, and the resulting solution is allowed to warm to room temperature. After 45 minutes of stirring, all the reagents had fully dissolved, producing a clear orange solution. THF is removed after stirring at room temperature for 12 hours, and the resulting tan foam is dried in vacuo. In a glove box, the foam is crushed into a finely divided solid and the frit assembly is brought back to the vacuum line, where 50 ml of petroleum ether is transferred onto the solid and allowed to warm to 25 °C. The finely divided tan and white petroleum ether-insoluble species are removed by filtration and are washed three times with small portions of PE. Removal of solvent from the

petroleum ether solution provided 374 mg (0.52 mmol) of AdpScCl-LiCl-$(THF)_2$. Additional AdpScCl-LiCl-$(THF)_2$ comprised much of the 1.86 g of white petroleum ether insoluble solid (as evidenced by ^1H NMR); the exact quantity of PE insoluble AdpScCl is not determined. As subsequent reactions with allylmagnesium bromide prove tolerant of LiCl, these alkylations are often run using the crude **48** product mixture.

Preparation of *meso*-AdpYCl-LiCl-(solv)$_2$ (49): A 500 ml roundbottom flask, equipped with a magnetic stir bar and a 180° needle valve, is charged with 11.1465 grams of Li_2Adp (22.44 mmol) and 9.2344 grams of $YCl_3(THF)_3$ (22.43 mmol, 1.0 eq.). The flask is evacuated and 250 ml THF is vacuum transferred onto the solids at -78°C. The solution is stirred and allowed to warm to room temperature. After 4 days, 150 ml of solvent is removed in vacuo. The remaining THF is removed in vacuo after an additional 12 hours of stirring at room temperature, leaving approximately 19.65 grams of tan solid. From that 19.7 grams of solid, 13.73 grams are placed in a 500 ml roundbottom flask, which is attached to a fine porosity frit and another 500 ml flask. Diethyl ether (150 ml) is vacuum transferred onto the solid, warmed to room temperature with stirring, and then removed in vacuo. This procedure is repeated with one 150 ml aliquot of toluene, and then with two aliquots of Et_2O. Another 150 ml of diethyl ether is vacuum transferred onto the solid, and the Et_2O insoluble material is removed by filtration, and is washed twice with small portions of Et_2O. Solvent is removed from the dark yellow ether solution, and the resulting tan foam is washed with an additional 75 ml Et_2O, which is removed *in vacuo*. After drying the resulting foam for 5 hours under dynamic vacuum, 7.19 grams of a tan solid is isolated. NMR spectroscopy indicates the presence of 0.16 equivalents of toluene, 0.37 equivalents of THF, and 1.74 equivalents of Et_2O, providing a yield of 8.76 mmol of AdpYCl-LiCl (56%, based on Y).

Preparation of *rac*-AbpScCl (50, 51, 52): A J-Young tube is charged with 15.7 mg (0.022 mmol) of **49** and 8.4 mg (0.022 mmol, 1.0 eq.) $ScCl_3(THF)_3$ and is degassed on the vacuum line. THF-d_8 (0.4 ml) is vacuum transferred onto the solids and the tube is warmed to room temperature, resulting in a suspension of white solid. The presence of **50** in solution is evident after 20 hours at room temperature (^1H NMR). The cloudy white suspension is then placed in

an 85 °C bath, and NMR spectra taken periodically. Resonances attributed to **51** and **52** appear as those of **50**. Total conversion of **50** to **51** and **52** is observed after 24 hours at 85 °C.

Preparation of *rac*-AbpYCl (53 and 54): A 500 ml roundbottom flask, equipped with a water cooled condensor and a 180° needle valve, is charged with 8.529 g (12.05 mmol) of **47** and 4.95 g (12.0 mmol) of $YCl_3(THF)_3$ and is evacuated on the vacuum line. THF (230 ml) is distilled onto the solids and the solution is heated to reflux. After 60 hours of refluxing, the solution is cooled to room temperature and solvent is removed *in vacuo*. Benzene (20 ml) is vacuum transferred onto the solid, the solution cooled to -78 °C, and benzene removed *in vacuo*. The apparatus is brought into a glove box, and the flask attached to a medium porosity swivel frit assembly. The petroleum ether soluble species are isolated by extraction into 200 ml of pet ether; 15% of the petroleum ether soluble species are set aside for other experiments. The diethyl ether insoluble portion of the remaining PE soluble species are washed with diethyl ether and isolated by a cold (-78 °C) filtration from 25 ml of Et_2O, leaving a tan solid which is dried *in vacuo*. Benzene (100 ml) is distilled onto the petroleum ether soluble and diethyl ether insoluble material, warmed to room temperature, and the volume of the solution reduced *in vacuo* to ~40 ml. The clear burgundy-colored solution is cooled to -10 °C with an ice/NaCl/water bath, and benzene is removed *in vacuo*. After 5 hours, the flask is heated to 55 °C under exposure to dynamic vacuum, affording 3.3325 g of pale tan solid. ^{1}H NMR spectroscopy indicates 0.22 equivalents of residual THF (per Y), 0.07 equivalents of residual C_6H_6, and a 1.5:1 ratio of **53**:**54** (4.31 mmol of Y, 42% yield).

Elemental analysis does little to confirm the assignment of **53** and **54** in the solid state. More than one permutation of *rac*-AbpYCl-(KCl)-$(THF)_2$, *rac*-AbpYCl(THF), and [*rac*-AbpY(μ-Cl)]$_2$ (in quantities consistent with the observed ^{1}H NMR [Abp] ligand intensities) provide virtually identical %C and %H values (see below). Furthermore, these permuations of *rac*-AbpYCl-(KCl)-$(THF)_2$, *rac*-AbpYCl(THF), and [*rac*-AbpY(μ-Cl)]$_2$ are inconsistent with the amount of residual THF observed by ^{1}H NMR; inclusion of the observed quantity of THF results in expected %C and %H values that equally poorly fit the observed data.

	%C	%H
Observed (with added V_2O_5)	61.96, 61.80	8.14, 8.11
Observed (without added oxidant)	61.65, 61.94	8.36, 8.40
mixture of homo- and heterochiral $[AbpY(\mu\text{-}Cl)]_2$	64.71	8.54
1.5 $[AbpY(\mu\text{-}Cl)]_2$ + 1 AbpYCl(THF)	64.18	8.39
1.5 $[AbpY(\mu\text{-}Cl)]_2$ + 1 AbpYCl-(KCl)-$(THF)_2$	61.81	8.70
0.5 $[AbpY(\mu\text{-}Cl)]_2$ + 3 AbpYCl(THF)	64.28	8.52
0.5 $[AbpY(\mu\text{-}Cl)]_2$ + 3 AbpYCl-(KCl)-$(THF)_2$	57.08	7.41
3 AbpYCl(THF) + 1 AbpYCl-(KCl)-$(THF)_2$	62.10	8.33
1 AbpYCl(THF) + 3 AbpYCl-(KCl)-$(THF)_2$	58.32	7.90
stoichiometry of $[AbpYCl](THF)_{0.22}$	64.13	8.34
stoichiometry of $[AbpYCl](KCl)_{0.11}(THF)_{0.22}$	63.05	8.24

References and Notes

1. Brintzinger, H. H.; Fischer, D.; Mulhaupt, R.; Rieger, B.; Waymouth, R. N. *Angew. Chem. Int. Ed. Eng.* **1995**, *34*, 1143.

2. Willoughby, C. A.; Buchwald, S. L. *J. Am. Chem. Soc.* **1992**, *114*, 7562.

3. Willoughby, C. A.; Buchwald, S. L. *J. Org. Chem.* **1993**, *58*, 7627-7629.

4. Lee, N. E.; Buchwald, S. L. *J. Am. Chem. Soc.* **1994**, *116*, 5985.

5. Broene, R. D.; Buchwald, S. L. *J. Am. Chem. Soc.* **1993**, *115*, 12569-12570.

6. Carter, M. B.; Scihott, B.; Gutirrez, A.; Buchwald, S. L. *J. Am. Chem. Soc.* **1994**, *116*, 11667.

7. Erker, G.; Nolte, R.; Aul, R.; Wilker, S.; Krüger, C.; Noe, R. *J. Am. Chem. Soc* **1991**, *113*, 7594.

8. Erker, G.; Aulbach, M.; Knickmeier, M.; Wingbermühle, D.; Krüger, C.; Nolte, M.; Werner, S. *J. Am. Chem. Soc.* **1993**, *115*, 4590.

9. See also a) Erker, G; Temme, B. *J. Am. Chem. Soc.*, **1992**, *114*, 4004. b) Chen, Z.; Eriks, K.; Halterman, R. L. *Organometallics*, **1991**, *10*, 3449.

10. Coates, G. W.; Waymouth, R. M. *Science* **1995**, *267*, 217.

11. Hauptman, E.; Waymouth, R. M.; Ziller, J. W. *J. Am. Chem. Soc.* **1995**, *117*, 11586.

12. The latin prefix "ansa", meaning "handle", has been used by Brintzinger to describe such a tethered arrangement of cyclopentadienyl rings. Smith, J. A.; Von Seyerl, J.; Huttner, G.; Brintzinger, H. H. *J. Organomet. Chem.*, **1979**, *173*, 175.

13. Giardello, M. A.; Conticello, V. P.; Brard, L.; Gagne, M. R.; Marks, T. J. *J. Am. Chem. Soc.* **1994**, *116*, 10241.

14. Giardello, M. A.; Conticello, V. P.; Brard, L.; Sabat, M.; Rheingold, A. L.; Stern, C. L.; Marks, T. J. *J. Am. Chem. Soc.* **1994**, *116*, 10212.

15. Giardello, M. A.; Eisen, M. S.; Stern, C.; Marks, T. J. *J. Am. Chem. Soc.* **1993**, *115*, 3326-7.

16. Mengele, W.; Diebold, J.; Troll, C.; Roll, W.; Brintzinger, H. H. *Organometallics* **1993**, *12*, 1931.

17. Grossman, R. B.; Tsai, J. C.; Davis, W. M.; Gutiérrez, A.; Buchwald, S. L. *Organometallics* **1994**, *13*, 3892.

18. Herrmann, W. A.; Morawietz, M. J. A.; Priermeier, T. *Angew. Chem. Int. Ed. Engl.* **1994**, *33*, 1946.

19. Burger, P.; Diebold, J.; Gutmann, S.; Hund, H. U.; Brintzinger, H. H. *Organometallics* **1992**, *11*, 1319.

20. Piemontesi, F.; Camurati, I.; Resconi, L.; Balboni, D.; Sironi, A.; Moret, M.; Ziegler, R.; Piccolrovazzi, N. *Organometallics* **1995**, *14*, 1256.

21. For alternate means of synthesizing metallocenes see a) Diamond, G. M.; Rodewald, S.; *Organometallics*, **1995**, *14*, 5. b) Jordan, R. F. Diamond, G. M.; Jordan, R. F.; Petersen, J. L. *Organometallics*, **1996**, *15*, 4030. c) Jordan, R. F. Diamond, G. M.; Jordan, R. F.; Petersen, J. L. *Organometallics*, **1996**, *15*, 403045.

22. Collins, S.; Hong, Y.; Taylor, N. J. *Organometallics* **1990**, *1990*, 2695.

23. Collins, S.; Hong, Y.; Ramachandran, R.; Taylor, N. J. *Organometallics* **1991**, *10*, 2349.

24. Gutmann, S.; Burger, P.; Hund, H. U.; Hofmann, J.; Brintzinger, H. H. *J. Organomet. Chem.* **1989**, *369*, 343.

25. Wiesenfeldt, H.; Reinmuth, A.; Barsties, E.; Evertz, K.; Brintzinger, H. H. *J. Organomet. Chem.* **1989**, *369*, 359-370.

26. Chacon, S. T.; Coughlin, E. B.; Henling, L. M.; Bercaw, J. E. *J. Organomet. Chem.* **1995**, *497*, 161.

27. Jutzi, P. *Chem. Rev.* **1986**, *86*, 983.

28. Bunel, E. E., Ph.D. Thesis, California Institute of Technology, **1989**.

29. Bunel, E. E.; Bercaw, J. E. *Unpublished results*.

30. Mitchell, J. P.; Bercaw, J. E. , unpublished results.

31. Coughlin, E. B.; Bercaw, J. E. *J. Am. Chem. Soc.* **1992**, *114*, 7606.

32. Coughlin, E. B., Ph.D. Thesis, California Institute of Technology, **1994**.

33. Miya, S.; Mise, T.; Yamazaki, H., in *Catalytic Olefin Polymerization*; Tominaga, K. and Soga, K., Eds.; Elsevier: Amsterdam, **1990**, p. 531.

34. Kaminsky, W.; Külper, K.; Brintzinger, H. H.; Wild, F. R. W. P. *Angew. Chem. Int. Ed. Engl.* **1985**, *24*, 507.

35. Spaleck, W.; Antberg, M.; Rohrmann, J.; Winter, A.; Bachmann, B.; Kiprof, P.; Behm, J.; Herrmann, W. A. *Angew. Chem. Int. Ed. Engl.* **1992**, *31*, 1347.

36. Alternate syntheses of these complexes have been reported in which no *rac*:*meso* ratios are reported. Stehling, U.; Diebold, J.; Kirsten, R.; Röll, W.; Brintzinger, H. H.; Jüngling, S.; Mülhaupt, R.; Langhauser, F. *Organometallics*, **1994**, *13*, 964.

37. Spaleck, W.; Küber, F.; Winter, A.; Rohrmann, J.; Bachmann, B.; Antberg, M.; Dolle, V.; Paulus, E. F. *Organometallics* **1994**, *13*, 954.

38. Rheingold, A. L.; Robinson, N. P.; Whelan, J.; Bosnich, B. *Organometallics* **1991**, *11*, 1869.

39. Bandy, J. A.; Green, M. L. H.; Gardiner, I. M.; Prout, K. *J. Chem. Soc. Dalton Trans.* **1991**, *11*, 2207.

40. Burk, M. J.; Coletti, S. L.; Halterman, R. L. *Organometallics* **1991**, *10*, 2998.

41. Hollis, T. K.; Rheingold, A. L.; Robinson, N. P.; Whelan, J.; Bosnich, B. *Organometallics* **1992**, *11*, 2812.

42. Huttenloch, M. E.; Diebold, J.; Rief, U.; Brintzinger, H. H.; Gilbert, A.; Katz, T. J. *Organometallics* **1992**, *11*, 3600-3607.

43. Chen, Z.; Halterman, R. L. *J. Am. Chem. Soc.* **1992**, *114*, 2276.

44. Mitchell, J. P.; Hajela, S.; Brookhart, S. K.; Hardcastle, K. I.; Henling, L. M.; Bercaw, J. E. *J. Am. Chem. Soc.* **1996**, *118*, 1045.

45. Stone, K. J.; Little, R. D. *J. Org. Chem.* **1984**, *49*, 1849.

46. Fendrick, C. M.; Schertz, L. D.; Day, V. W.; Marks, T. J. *Organometallics* **1988**, *7*, 1828.

47. Molle, G.; Bauer, P. *J. Am. Chem. Soc* **1982**, *104*, 3481.

48. Molle, G.; Bauer, P.; Dubois, J. E. *J. Org. Chem* **1983**, *48*, 2975.

49. Edelmann, F. T., in *Comprehensive Organometallic Chemistry II*; Abel, E. W., Stone, F. G. A., Wilkinson, G. and Lappert, M. F., Eds.; Pergamon Press: Tarrytown, NY, **1995**; *Vol. 4*, p. 11.

50. Diamond, G. M.; Jordan, R. J.; Petersen, J. L. *Organometallics* **1996**, *15*, 4045.

51. Although presumably equimolar quantities of the (R) and (S) enantiomers of the chiral *rac*-AbpYMCl metallocenes are formed during metalation, for clarity only the (S) metallocenes are drawn explicitly.

52. The stability of KCl-(solvent)$_2$ adducts of group III *ansa*- metallocenes has been observed previously. Zubris, D. L.; Bercaw, J. E. Unpublished results.

53. Burger, B. J.; Bercaw, J. E. *New Developments in the Synthesis, Manipulation, and Characterization of Organometallic Compounds*; ACS Symposium Series, **1987** *357*,

54. Marvich, R. H.; Brintzinger, H. H. *J. Am. Chem. Soc.* **1971**, *93*, 2046.

55. Manzer, L. E. *Inorg. Synth.* **1982**, *21*, 135.

56. Cowley, A. H.; Kemp, R. A. *Synth. React. Inorg. Metal-Org. Chem.* **1981**, *11*, 591.

Appendix A: ^{1}H and ^{13}C NMR Data For 19-54

Table 1. Proton NMR assignments for **19-54** (500 MHz, C_6D_6, 25 °C unless otherwise noted)

Compound	Assignments	δ (ppm)	J_{H-H}
Pentamethylenefulvene	Cy (2H)	1.28 (m)	
(19)	(4H)	1.41 (m)	
(300 MHz)	(4H)	2.35 (m)	
	Cp (4H)	6.59 (m)	
$(SiMe_3)(Cy)C_5H_4$	**$SiMe_3$ (9H)**	**-0.07 (s)**	
(300 MHz)	$SiMe_3$	0.19 (d)	
(≥2 isomers)	**Cy (10H)**	**1.10-1.40 (overlapping)**	
		1.60-1.75 (overlapping)	
		1.90-2.00 (overlapping)	
	(1H)	**2.38 (m)**	
	Cp, allylic	2.88, 2.94 (m)	
	Cp, allylic (1H)	**3.20 (s)**	
	Cp, vinylic (3H)	**6.11 (s), 6.42 (s), 6.63 (m)**	
	Cp, vinylic	6.19 (m), 6.24 (m), 6.79 (m), 6.88 (m)	
[1-$SiMe_3$-3-Cy-C_5H_3]K	$SiMe_3$ (9H)	0.27 (s)	
(24)	Cy (11H)	1.27, 1.49, 1.79, 1.93 (overlapping)	
(THF-d_8, 300 MHz)	(1H)	2.44 (m)	
	Cp (3H)	5.65, 5.72, 5.80 (m)	
[Cy-C_5H_4]Li **(20)**	Cy (7H)	1.20-1.40 (overlapping)	
(THF-d_8, 300 MHz)	(3H)	1.60-1.80 (overlapping)	
	(1H)	1.90 (d)	
	(1H)	2.39 (m)	
	Cp (4H)	5.45 (s)	

Table 1. (continued)

Compound	Assignments	δ (ppm)	J_{H-H}
[Cy-C_5H_4]K	Cy (10H)	1.21, 1.26, 1.31, 1.35, 1.39,	
(THF-d_8, 300 MHz)		1.42, 1.67, 1.74 , 1.83, 1.90	
		(m)	
	(1H)	2.37 (t of t)	11.8,
			3.7
	Cp (2H)	5.32 (m)	
	(2H)	5.35 (m)	
Me_2Si(Cy-C_5H_4)$_2$ **(22)**	**Me_2Si (3H)**	**-0.18 (s)**	
(≥2 isomers)	Me_2Si (2H)	0.13 (s), 0.15 (s)	
	Cy (10H)	**1.10 - 1.40 (m)**	
	(6H)	**1.60 - 1.85 (m)**	
	(3H)	**1.95 (m), 1.97 (m)**	
	(2H)	2.27 (t of t), **2.37 (t of t)**	
	Cp, allylic (0.5H)	2.92 (s), 2.97 (m), 3.44 (d)	
	Cp, allylic (0.5H)	**3.36 (s)**	
	Cp, vinylic (4H)	**6.14, 6.47, 6.62 (m)**	
	Cp, vinylic (1H)	6.19, 6.21, 6.80, 6.91 (m)	
[Me_2Si(3-Cy-C_5H_3)$_2$]Li_2	Me_2Si (6H)	0.46 (s)	
(26a)	Cy (20H)	1.16, 1.20, 1.22, 1.28, 1.34,	
(THF-d_8, 300 MHz)		1.63, 1.68, 1.80 (m)	
	(1H)	2.32 (t of t)	12.0,
			3.2
	Cp (1H)	5.50 (m)	2.6
	(1H)	5.58 (m)	2.6
	(1H)	5.65 (m)	2.6
[Me_2Si(3-Cy-C_5H_3)$_2$]K_2	Me_2Si (6H)	0.85 (s)	
(26b)	Cy (12H)	1.15 - 1.50 (m)	
(THF-d_8)	(4H)	1.70 - 1.80 (m)	
	(4H)	1.87 - 1.95 (m)	
	(2H)	2.43 (m)	
	Cp (6H)	5.72, 5.75, 5.78 (m)	

Table 1. (continued)

Compound	Assignments	δ (ppm)	J_{H-H}
$Me_2Si[(SiMe_3)(Cy)C_5H_3]_2$ **(25)** (>2 isomers)	Me_3Si (18H)	-0.04, -0.03, -0.02, 0.02, 0.03 (s)	
	Me_2Si (6H)	0.10, 0.14, 0.18, 0.22, 0.27, 0.28, 0.32 (s)	
	Cy (14H)	1.15 - 1.42 (m)	
	(7H)	1.60 - 1.80 (m)	
	(2H)	1.86 - 2.20 (m)	
	Cp, allylic	2.95, 3.03, 3.17, 3.20 (m)	
	Cp, vinylic (4H)	6.15, 6.23, 6.29, 6.36, 6.44, 6.50, 6.54, 6.59, 6.69, 6.75 (m)	
$\{Me_2Si[Cy(SiMe_3)Cp]_2\}K_2$ (major isomer, THF-d_8/18-crown-6)	Me_3Si (18H)	0.04 (s)	
	Me_2Si (6H)	0.33 (s)	
	Cy (22H)	1.20 - 1.35, 1.60 - 1.75, 2.47 (m)	
	Cp (4H)	5.79, 5.80 (m)	
Adamantylfulvene (**30**)	Ad (2H)	1.65 (t)	2.8
	(2H)	1.72 (quartet)	2.0
	(8H)	1.75 (t)	2.6
	(2H)	3.11 (s)	
	Cp (4H)	6.62, 6.65 (m)	
$[(2\text{-Ad})\text{-}C_5H_4]Li$ **(31a)** (THF-d_8)	Ad (10H)	1.42, 1.67, 1.75, 1.89, 1.91, 1.93, 1.94, 2.20 (s)	11.5
	(2H)	2.21 (d)	11.8
	(1H)	2.96 (s)	
	Cp (4H) (degenerate)	5.58 (s)	
$[(2\text{-Ad})\text{-}C_5H_4]Na$ **(31b)** (THF-d_8)	Ad (2H)	1.39 (d)	11.7
	(3H)	1.66, 1.75 (s)	
	(7H)	1.87, 1.89, 1.91, 1.92, 2.21 (m)	
	(2H)	2.28 (d)	11.9
	(1H)	3.02 (s)	
	Cp (4H) (degenerate)	5.59 (s)	

Table 1. (continued)

Compound	Assignments	δ (ppm)	J_{H-H}
$(SiMe_3)(2\text{-}Ad)C_5H_4$ **(32)**	**$SiMe_3$**	**-0.05 (s)**	
(2 isomers)	$SiMe_3$	0.21, 0.19 (s)	
	Ad	**1.54, 1.56, 1.71, 1.74, 1.81, 1.83, 1.88, 1.90, 2.10, 2.24, 2.29 (m)**	
	Cp, allylic	2.62 (s), 2.66 (s), 2.82 (s), 3.00 (s)	
	Cp, allylic	**2.86 (s), 3.25 (s)**	
	Cp, vinylic	**6.22 (s), 6.49 (s), 6.66 (s)**	
	Cp, vinylic	6.26 (s), 6.28 (s), 6.83 (m), 6.91 (m)	
$(SiMe_2Cl)(2\text{-}Ad)C_5H_4$	**$SiMe_2Cl$ (3H)**	**0.12 (s)**	
(33)	**(3H)**	**0.15 (s)**	
(2 isomers)	$SiMe_2Cl$	0.43 (s)	
		0.44 (s)	
	Ad (2H)	**1.47 (m)**	
	(14H)	**1.71, 1.77, 1.79, 1.85, 1.87, 1.91 (m)**	
	(3H)	**2.17 (m)**	
	(1H)	**2.77 (s)**	
		2.89 (s)	
	Cp, allylic	3.03 (m)	
	Cp, allylic (1H)	**3.42 (s)**	
	Cp, vinylic (1H)	**6.12 (s)**	
	Cp, vinylic	6.15, 6.21 (m)	
	Cp, vinylic (1H)	**6.42 (m)**	
	Cp, vinylic (1H)	**6.57 (m)**	
	Cp, vinylic	6.83 (m)	
		6.92 (m)	
[1-$SiMe_3$-3-(2-Ad)-C_5H_3]Li **(34)**	$SiMe_3$ (9H)	0.10 (s)	
(THF-d_8)	Ad (2H)	1.43 (d)	11.8
	(14H)	1.68, 1.76, 1.88, 1.90, 1.91, 2.19, 2.21, 2.96 (s)	
	Cp (1H)	5.76 (m)	2.5
	(1H)	5.79 (m)	2.1
	(1H)	5.82 (m)	2.6

Table 1. (continued)

Compound	Assignments	δ (ppm)	J_{H-H}
$(SiMe_2Cl)(SiMe_3)(2\text{-}Ad)C_5H_3$ **(35)** (THF-d_8)	Me_3Si (9H)	0.04 (s)	
	Me_2Si (6H)	0.22, 0.26 (s)	
	Ad	1.42, 1.56, 1.68, 1.56, 1.68, 1.72, 1.75, 1.78, 1.88, 1.90, 1.92, 1.95, 1.97 (m)	
		2.21 (s)	
	Cp, allylic (1H)	2.83 (s)	
	Cp, vinylic (3H)	6.28, 6.57, 6.79 (m)	
$(SiCl_3)(SiMe_3)(2\text{-}Ad)C_5H_3$ **(36)**	$SiMe_3$ (9H)	0.05 (s)	
	Ad (2H)	1.47, 1.49, 1.51 (s)	
	(5H)	1.69 (s), 1.72 (m)	
	(3H)	1.75, 1.80, 1.83 (m)	
	(1H)	1.93 (d)	12.6
	(1H)	1.99 (d)	10.8
	(2H)	2.14, 2.72 (s)	
	Cp (3H)	6.28, 6.41, 6.72 (m)	
$Cl_2Si[(SiMe_3)(2\text{-}Ad)C_5H_3]_2$ **(37)** ≥2 isomers	Me_3Si (8H)	-0.06 (d)	16.0
	(10H)	0.17 (s)	
	Ad (5H)	1.47, 1.49, 1.51, 1.53 (m)	
	(44H)	1.73, 1.79, 1.82, 1.87, 1.89, 1.98, 2.01, 2.05, 2.22 (m)	
	(1H)	2.63 (s)	
	(1H)	2.78 (d)	13.6
	Cp (3H)	6.52, 6.70, 6.76 (m)	
$Me_2Si[(SiMe_3)(2\text{-}Ad)C_5H_3]_2$ **(28)** ≥2 isomers	Me_3Si (18H)	-0.06, -0.02, 0.00, 0.02, 0.04, 0.05 (s)	
	Me_2Si (16H)	0.14, 0.17, 0.36, 0.38 (s)	
	Ad (2H)	1.52 (d), 1.62 (d), 1.66 (d)	
	(15H)	1.77, 1.88, 1.92 (m)	
	(5H)	2.24 (d), 2.38 (m)	
	Cp, allylic (2H)	2.94 (s), 2.74 (s)	
	Cp, vinylic (3H)	6.45, 6.53, 6.64, 6.77, 6.82 (m)	

Table 1. (continued)

Compound	Assignments	δ (ppm)	J H-H
[(±)$C_{20}H_{12}O_2$]Si[(SiMe_3)(2-Ad)C_5H_3]$_2$ **(38)**	Me3Si (18H)	-0.42, -0.27, -0.21, -0.04, 0.02, 0.08, 0.10, 0.12, 0.14, 0.17, 0.19, 0.21, 0.23	
	Ad (2H)	0.83 - 1.04 (overlapping)	
	(5H)	1.21 - 1.49	
	(1H)	1.50 - 1.70	
	(18H)	1.70 - 2.10	
	(3H)	2.10 - 2.50	
	Cp, allylic (2H)	2.50 - 3.45	
	Cp, vinylic (2H) (overlaps with Bn)	6.21 - 6.70	
	Bn (4H)	6.70 - 7.04	
	(2H)	7.05 - 7.14	
	(8H)	7.18 - 7.78	
MeCyCpLi (THF-d_8)	**Me**Cy (3H)	1.14 (s)	
	Me**Cy** (6H)	1.42 - 1.49 (m)	
	(2H)	1.52 - 1.55 (m)	
	(2H)	1.83 m	
	Cp (2H)	5.50 (m)	2.7
	(2H)	5.53 (m)	2.7
[MeAd-C_5H_4]Li-DME **(39-DME)** (THF-d_8)	**Me**Ad (3H)	1.27 (s)	
	Me**Ad** (2H)	1.43 (m)	11.0
	(8H)	1.59, 1.66, 1.68, 1.84, 2.08 (m)	
	(2H)	2.24 (m)	10.4
	(2H)	2.39 (m)	10.0
	CH_3O**CH_2CH_2**OCH_3	3.27 (s)	
	CH_3 OCH_2CH_2O**CH_3**	3.43 (s)	
	Cp (4H)	5.55, 5.56 (m)	

Table 1. (continued)

Compound	Assignments	δ (ppm)	J_{H-H}
[MeAd-C_5H_4]Li-TMEDA **(39-TMEDA)**	**Me**Ad (3H)	1.30 (s)	
	Me**Ad** (2H)	1.42 (d)	5.9
	(12H)	1.59, 1.65, 1.69, 1.83, 2.07, 2.22 (s)	
	(2H)	2.39 (d)	5.7
	Me_2NCH_2CH_2N**Me_2**	2.13 (s)	
	(12H)		
	Me_2N**CH_2CH_2**NMe_2	2.26 (s)	
	(4H)		
	Cp (4H)	5.56, 5.57 (m)	
($SiMe_3$)(MeAd)C_5H_4	Me_3Si (9H)	-0.05 (s)	
	MeAd (3H)	1.24 (s)	
	Me**Ad** (2H)	1.58 (d)	12.4
	(2H)	1.64 (d)	12.8
	(5H)	1.70, 1.78, 1.85 (s)	
	(1H)	2.04 (d)	11.1
	(2H)	2.15 (d)	12.8
	(1H)	2.20 (d)	12.3
	(1H)	2.26 (d)	12.0
	Cp, allylic (1H)	3.21 (s)	
	Cp, vinylic (3H)	6.12, 6.48, 6.65 (m)	
[1-$SiMe_3$-3-MeAd-C_5H_3]Li-DME **(40-DME)**	Me_3Si (9H)	0.46 (s)	
	MeAd (3H)	1.44 (s)	
	Me**Ad** (1H)	1.65 (d)	12.0
	(1H)	1.70 (d)	10.3
	(4H)	1.85, 1.84, 1.82 (m)	11.9
	(1H)	2.00 (s)	
	(overlaps w/DME)	2.35, 2.41 (m)	
	(1H)	2.57 (d)	11.8
	(overlaps w/DME)	2.72 (m)	
	CH_3O**CH_2CH_2**OCH_3	2.39 (s)	
	CH_3 OCH_2CH_2O**CH_3**	2.76 (s)	
	Cp (3H)	6.16, 6.19, 6.35 (m)	

Table 1. (continued)

Compound	Assignments	δ (ppm)	J_{H-H}
$(SiMe_2Cl)(SiMe_3)(MeAd)C_5H_3$ (THF-d_8)	Me_3Si (9H)	0.04 (s)	
	Me_2Si (6H)	0.23, 0.27 (s)	
	MeAd (3H)	1.20 (s)	
	Me**Ad** (10H)	1.56 (s), 1.86 (s), 2.06 (m), 2.08 (m), 2.23 (m)	
	Cp (3H)	6.23, 6.57, 6.79 (m)	
$(SiCl_3)(SiMe_3)(MeAd)C_5H_3$ (THF-d_8)	Me_3Si (9H)	0.13 (s)	
	MeAd (3H)	1.21 (s)	
	Me**Ad** (2H)	1.57 (d)	11.3
	(6H)	1.72 (br), 1.87 (s)	
	(1H)	1.99 (d)	13.0
	(3H)	2.11 (s)	
	(2H)	2.22 (d)	10.4
	Cp (3H)	6.25, 6.61, 6.97 (m)	
$(SiMe_3)_2(MeAd)C_5H_3$ **(41)** (THF-d_8, 300 MHz)	Me_3Si (18H)	-0.03 (s)	
	MeAd (3H)	1.19 (s)	
	Me**Ad** (2H)	1.55 (d)	9.8
		1.68 (m)	
	(1H)	1.86 (s)	
	(4H)	2.10 (m)	
	(2H)	2.22 (d)	10.5
	Cp (3H)	6.17, 6.49, 6.67 (m)	
[1,2-$(SiMe_3)_2$-4-MeAd-C_5H_2]Li **(42)** (THF-d8)	Me_3Si (18H)	0.17 (s)	
	MeAd (3H)	1.26 (s)	
	Me**Ad** (2H)	1.42 (d)	11.5
	(2H)	1.59 (s)	
	(2H)	1.65 (d)	17.3
	(5H)	1.68, 1.82, 2.09 (s)	
	(2H)	2.22 (d)	11.0
	(2H)	2.27 (d)	11.9
	Cp (2H)	6.11 (s)	

Table 1. (continued)

Compound	Assignments	δ (ppm)	J_{H-H}
$Me_2Si(MeAd\text{-}C_5H_4)_2$ (H_2Adp) **(43)**	Me_2Si (5H)	-0.18, -0.14, -0.13, 0.14, 0.17 (s)	
	MeAd (6H)	1.13, 1.20, 1.22, 1.24, 1.25 (s)	
	Me**Ad** (43H)	1.58, 1.60, 1.63, 1.65, 1.71, 1.78, 1.85, 2.06, 2.11, 2.14, 2.16, 2.20, 2.26, 2.27 (m)	
	Cp, allylic (2H)	3.01, 3.04, 3.31 (s)	
	Cp, vinylic (6H)	6.18, 6.53, 6.66	
Li_2Adp **(44)** ($THF\text{-}d_8$)	Me_2Si (6H)	0.24 (s)	
	MeAd (6H)	1.27 (s)	
	Me**Ad** (28H)	1.41 (d)	5.9
		1.58 (s)	
		1.66 (d)	6.4
		1.69 (s), 1.83 (s), 2.10 (s)	
		2.24 (d)	5.6
		2.41 (d)	4.9
	Cp (2H)	5.70 (t)	2.6
	(2H)	5.90 (t)	2.1
	(2H)	5.91 (t)	2.5
$Me_2Si[(SiMe_3)(MeAd)\text{-}C_5H_3)_2]$ (H_2Abp) **(45)** (≥2 isomers)	Me_3Si (18H)	-0.10, -0.07, 0.37 (s)	
	Me_2Si (6H)	0.17, 0.30, 0.37, 0.41 (s)	
	MeAd (9H)	1.24, 1.26, 1.28, 1.29 (s)	
	Me**Ad** (23H)	1.65 - 1.72 (m)	
	(6H)	1.86 (m)	
	(23H)	2.08 - 2.36 (m)	
	Cp, allylic (1H)	3.57, 3.64 (s)	
	Cp, vinylic (4H)	6.31, 6.66, 6.79, 7.10, 7.13 (m)	

Table 1. (continued)

Compound	Assignments	δ (ppm)	J_{H-H}
Li_2Abp **(46)**	Me_3Si (18H)	-0.17	
(THF-d_8)	Me_2Si (6H)	0.41	
	MeAd (6H)	1.27	
	Me**Ad** (9H)	1.60, 1.69 (m)	
	(2H)	1.83 (m)	
	(4H)	2.12 (m)	
	(5H)	2.23 (m)	
	(2H)	2.38 (m)	
	(2H)	2.54 (m)	
	Cp (2H)	6.04 (m)	
	(2H)	6.24 (m)	
K_2Abp **(47)**	Me_3Si (18H)	0.18 (s)	
(THF-d_8/18-Crown-6)	Me_2Si (6H)	0.52 (s)	
	MeAd (6H)	1.14 (s)	
	Me**Ad** (4H)	1.30 (m)	11.8
	(2H)	1.52 (m)	
	(8H)	1.60 (d), 1.65 (s)	12.1
	(2H)	1.78 (m)	
	(4H)	2.10 (s)	
	(4H)	2.18 (d)	11.6
	(4H)	2.48 (d)	11.0
	Cp (4H)	5.84, 6.14 (m)	
meso-AdpScCl-LiCl-	Me_2Si (3H)	0.41 (s)	
$(THF)_2$ **(48)**	(3H)	0.55 (s)	
(THF-d_8)	Me**Ad** (25H)	1.42, 1.47, 1.49, 1.53, 1.63. 1.69, 1.72, 2.22, 2.25, 2.29, 2.32, 2.50 (m)	
	MeAd (6H)	2.16 (s)	
	Cp (2H)	5.79 (t)	2.7
	(2H)	5.89 (t)	2.1
	(2H)	6.23 (t)	2.5

Table 1. (continued)

Compound	Assignments	δ (ppm)	J_{H-H}
meso-AdpYCl-LiCl-(solv)$_2$ **(49)**	Me_2Si (3H)	0.44 (s)	
	(3H)	0.57 (s)	
	MeAd (6H)	1.69 (s)	
	Me**Ad** (28H)	1.28, 1.43, 1.55, 1.59, 1.82, 2.15, 2.22, 2.24, 2.29, 2.49 (m)	
	Cp (2H)	5.84 (m)	2.7
	(2H)	5.92 (m)	2.0
	(2H)	6.20 (m)	2.5
rac-AbpScCl-(KCl)-(THF)$_2$ **(50)** (THF-d_8)	Me_3Si (18H)	0.26 (s)	
	Me_2Si (6H)	0.56 (s)	
	MeAd (6H)	1.18 (s)	
	Me**Ad**	1.19, 1.22, 1.28, 1.40, 1.56, 1.66, 2.11, 2.21 (m)	
	Cp (4H)	5.97 (s), 6.23 (s)	
[*rac*-AbpSc(μ-Cl)]$_2$ **(51)** (THF-d_8)	Me_3Si (18H)	0.28 (s)	
	Me_2Si (6H)	0.77 (s)	
	MeAd	1.20 - 1.70	
		2.05 - 2.35	
	Cp (2H)	6.28 (d)	1.6
	(2H)	6.59 (d)	1.7
rac-AbpScCl(THF) **(52)** (THF-d_8)	Me_3Si (18H)	0.26 (s)	
	Me_2Si (6H)	0.84 (s)	
	MeAd (6H)	1.56 (s)	
	Me**Ad**	overlap with those of **51**	
	Cp (2H)	6.23 (d)	1.0
	(2H)	6.56 (d)	1.7
[*rac*-AbpY(μ-Cl)]$_2$ **(53)**	Me_3Si (18H)	0.56 (s)	
	Me_2Si (6H)	0.99 (s)	
	MeAd	1.70 (s)	
	Me**Ad**	1.29, 1.46, 1.50 - 2.00, 2.20 - 2.25 (br, overlap)	
	Cp (3H)	6.65 (s), 6.87 (br)	

Table 1. (continued)

Compound	Assignments	δ (ppm)	J_{H-H}
[*rac*-AbpY(μ-Cl)]$_2$ **(53)** (THF-d_8)	Me_3Si (18H)	0.27 (s)	
	Me_2Si (6H)	0.77 (s)	
	MeAd	1.74 (s)	
	Me**Ad**	1.28 (d)	9.8
		1.36 (d)	10.2
		1.43 (d)	12.0
		1.50, 1.52, 1.57, 1.61, 1.69 (overlapping)	
		1.73 (s)	
		2.11 (s)	
		2.19 (d)	12.1
		2.25 (d)	12.5
		2.48 (d)	12.5
	Cp (4H)	6.28 (d)	2.0
		6.54 (d)	2.0
rac-AbpYCl(THF) **(54)** (THF-d_8)	Me_3Si	0.29 (s)	
	Me_2Si	0.84 (s)	
	MeAd	1.74 (s)	
	Me**Ad**	overlap with major product resonances	
	Cp	6.31 (d)	2.0
		6.58 (d)	1.9

Table 2. Proton decoupled ^{13}C assignments for **53** (125 MHz, 25 °C)

Cmpd	solvent	Assignments	δ (ppm)
[*rac*-AbpY(μ-Cl)]$_2$ **(53)**	C_6D_6	Me_2Si	1.13
		Me_3Si	3.34
		MeAd	28.58, 28.77, 29.94, 34.44, 34.57, 34.65, 35.37, 37.15, 40.29, 40.91, 42.00
		Cp	118.67, 120.44, 124.29, 130.70, 147.70
[*rac*-AbpY(μ-Cl)]$_2$ **(53)**	THF-d_8	Me_2Si	1.05
		Me_3Si	3.06
		MeAd	29.20, 29.32, 29.40, 34.67, 34.89, 34.97, 35.47, 35.77, 37.03, 40.96, 41.57
		Cp	117.37, 119.53, 122.40, 131.17, 146.47

Chapter 3

Reactivity of C_s- and C_2-Symmetric Group III Metallocenes with Dihydrogen and with Unsaturated Organic Substrates

Abstract

The reaction of *meso*- $Me_2Si\{3\text{-}[2\text{-}(2\text{-}CH_3\text{-}C_{10}H_{14})]\text{-}C_5H_3\}_2MCl\text{-}(LiCl)\text{-}(THF)_2$ (*meso*-AdpMCl-(LiCl)-$(THF)_2$) with allylmagnesium bromide afford *meso*-AdpM(η^3-C_3H_5) (M = Sc, Y) in good yield. The allyl ligands appear η^3-coordinated in solution, but variable temperature NMR spectroscopy indicates fluzinal behavior associated with the allyl moieties. The results of hydrogenolysis of *meso*-AdpM(η^3-C_3H_5) are consistent with σ-bond metathesis to generate propene and highly reactive *meso*-AdpMH monomers. The use of methyladamantyl groups as metallocene β-substituents effectively prevents formation of bridging hydride ($(\mu\text{-}H)_2$) dimers; [*meso*-AdpM(μ-$H)_2$] account for only ~3% of the overall organometallic hydrogenolysis products. The highly reactive [*meso*-AdpMH] monomers react readily with available C-H bonds in solution; intermolecular cyclopentadienyl C-H activation is believed to be the predominant [*meso*-AdpMH] decomposition mechanism. Treatment of $[rac\text{-}Me_2Si\{2\text{-}SiMe_3\text{-}4\text{-}[2\text{-}(2\text{-}CH_3\text{-}C_{10}H_{14})]\text{-}C_5H_2\}_2Y(\mu\text{-}Cl)]_2$ ([*rac*-AbpY(μ-$Cl)]_2$) with $LiCH(SiMe_3)_2$ affords the bulky yttrium-alkyl complex *rac*-AbpY$CH(SiMe_3)_2$ (**18**). Although ethylene is readily polymerized by **18**, no reaction is observed between α-olefins and **18**. Hydrogenolysis of **18** results in the formation of **20**, the homochiral dimer of [*rac*-AbpY(μ-$H)]_2$. Neither the monomeric *rac*-AbpYH (**19**) nor the heterochiral [*rac*-AbpY(μ-$H)]_2$ dimer are observed in solution. Although variable temperature NMR studies indicate that dissociation of **20** into **19** is not rapid on the NMR timescale at 25 °C, evidence for the dissociation of **20** at room temperature is obtained from H/D scrambing experiments. Dimer **20** is an active α-olefin polymerization catalyst, but does not oligomerize or polymerize α-olefins. The allenyl complex **21** is formed from the C-H activation of allene by **19**. Treatment of **20** with 2-butyne results in alkyne insertion to generate the yttrium-butenyl complex **22**. Complex **22** readily undergoes β-H elimination from an sp^2-hybridized carbon to generate a methylallene- complex, the C-H bonds of which rapidly undergo σ-bond metathesis with **19** to generate methylallenyl complexes **25a**,**b**.

Introduction

The reactions of early transition metal metallocene-hydride and -alkyl complexes with unsaturated organic substrates have been studied extensively over the last 40 years.[1] Cationic group IV and the isoelectronic neutral group III 14-electron d^0 metallocenes have found extensive use as homogeneous α-olefin polymerization catalysts. Similar catalysts may often be employed to promote the oligomerization or polymerization of alkynes.[2-4] The ability of an olefin or alkyne to undergo insertion into or σ-bond metathesis with a given bis(cyclopentadienyl)metal complex depends considerably on the degree of substitution and saturation of the substrate and on the steric influences of the metallocene.

The often competing mechanisms of insertion chemistry and σ-bond metathesis dominate the reactivities of allene and alkynes with metallocene-based Ziegler-Natta catalysts. Cationic group IV metallocenes such as $[Cp^*_2ZrH(THF)][BPh_4]$ and $[Cp^*_2ZrCH_3][B(4\text{-}C_6H_5F)_4]$ favor insertion of allene to generate η^3-allyl and η^3-methallyl complexes (Figure 1).[5,6] Additional insertions of allene into and decomposition of **2** are observed in the presence of excess allene; subsequent insertions into **1** are not observed, presumably due to the nonlability of the THF ligand. Although insertion of allene is observed for the monomeric $Cp^*_2Sc\text{-}H$ (**3**),[7] allene does not insert into

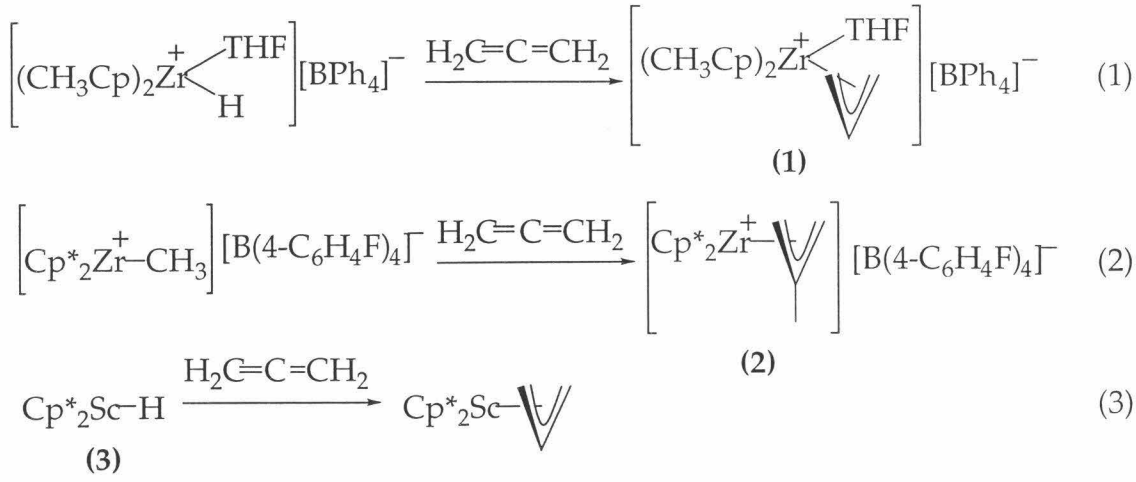

Figure 1. Insertion of allene to give η^3-allyl and η^3-methallyl complexes.

$[Cp^*_2Y(\mu\text{-}H)]_2$; σ-bond metathesis with one of the allene C-H bonds instead gives dihydrogen and the allenyl complex $Cp^*_2YCH{=}C{=}CH_2$ (Figure 2).[8]

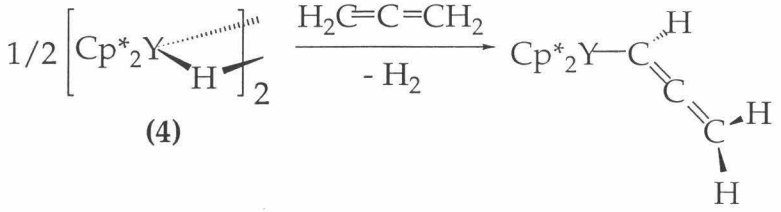

Figure 2. σ-bond metathesis of $[Cp^*_2Y(\mu\text{-}H)]_2$ with allene.

Subtle differences exist between the reactivities of cationic group IV complexes and those of neutral group III and Ln complexes with terminal alkynes. Terminal acetylenes undergo 1,2-insertion into cationic group IV-methyl complexes to generate M-vinyl species.[9] Although these vinyl complexes may be trapped in the presence of coordinating ligands,[10] they are usually quite reactive and undergo rapid σ-bond metathesis with C-H bonds of additional alkyne monomers to generate M-alkynyl complexes (Scheme 1).[11,12]

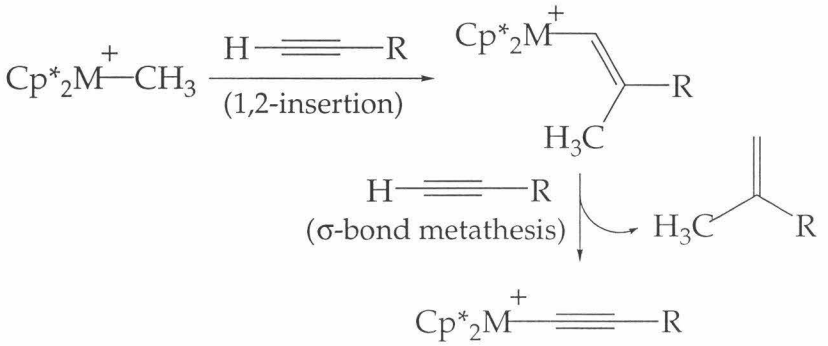

Scheme 1. Generation of cationic group IV M-alkynyl complexes.

Once generated, these metal-alkynyl species act as efficient catalysts for the dimerization of terminal olefins. The catalytic cycle, involving 1,2-insertion to give a metal-alkenyl-yne, followed by σ-bond metathesis to regenerate the alkynyl complex, is shown in Scheme 2 (**A**).

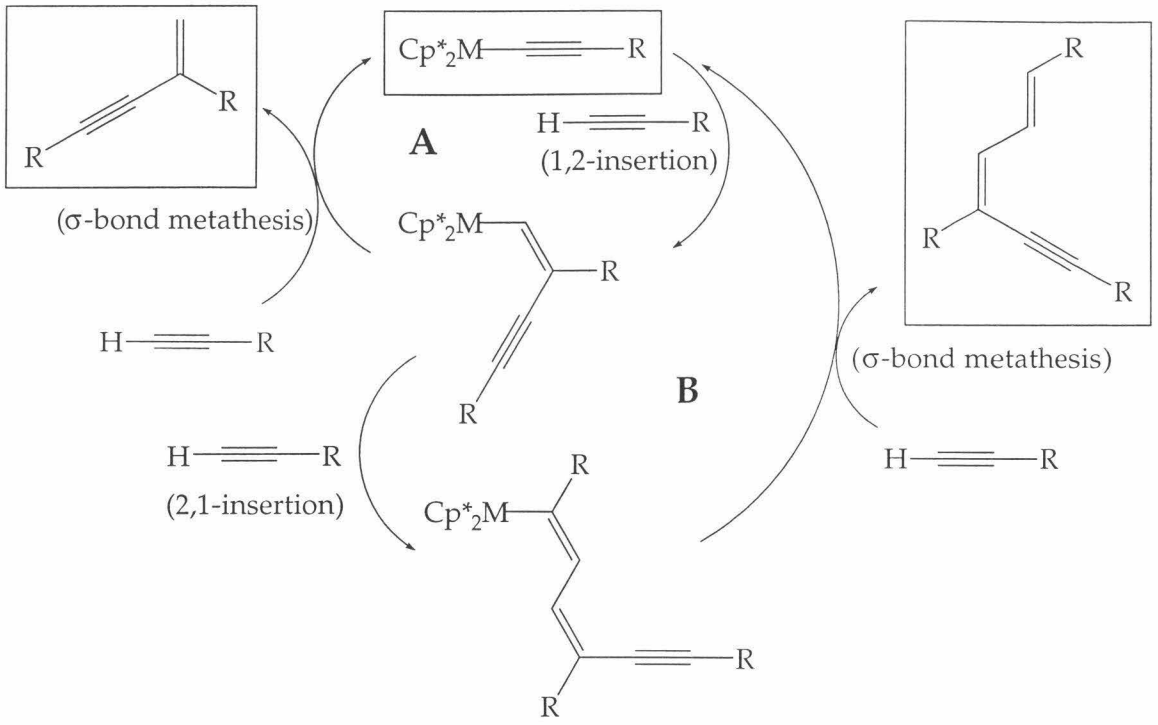

Scheme 2. Catalytic olefin oligomerization by Cp^*_2M-alkynyl complexes (M=Sc, Y, Zr^+).

Rather than initially undergoing 1,2-insertion, terminal alkynes undergo σ-bond metathesis with $Cp^*_2Sc\text{-}CH_3$ and $Cp^*_2YCH(SiMe_3)_2$ to generate M-alkynyl complexes and one equivalent of alkene.[7,13] Like their group IV counterparts, though, these alkynyl complexes rapidly catalyze the dimerization of alkynes (**A**, Scheme 1).

$$Cp^*_2Sc\text{–}CH_3 \xrightarrow{H\text{—}\equiv\text{—}R} Cp^*_2Sc\text{—}\equiv\text{—}R + CH_4 \qquad (3)$$

(5)

$$Cp^*_2Y\text{–}CH(SiMe_3)_2 \xrightarrow{H\text{—}\equiv\text{—}R} Cp^*_2Y\text{—}\equiv\text{—}R + H_2C(SiMe_3)_2 \qquad (4)$$

Variations to the R substituent and to the ligand array have marked effects on the ability of the metal complexes to oligomerize acetylenes. Use of alkynes with R=-CH_3 and -$CH_2CH_2CH_3$ provide both alkyne dimers (**A**, Scheme 2) and trimers (**B**, Scheme 2), while acetylenes with R=-CMe_3, -Ph, and -4-C_6H_4Me are only dimerized. Although trimethylsilylacetylene undergoes multiple insertions, it fails to undergo σ-bond metathesis to regenerate a catalytically active M-C≡R complex.[11] The less sterically

congested $(C_5H_5)_2$ framework permits formation of unusual bridged complexes upon additon of just one equivalent of the activator $[PhNMe_2H][B(4\text{-}C_6H_4F)_4]$ to $Cp_2Zr(CH_3)_2$ (Figure 3);[12] neither the starting materials nor the organometallic products react with additional equivalents of alkyne.

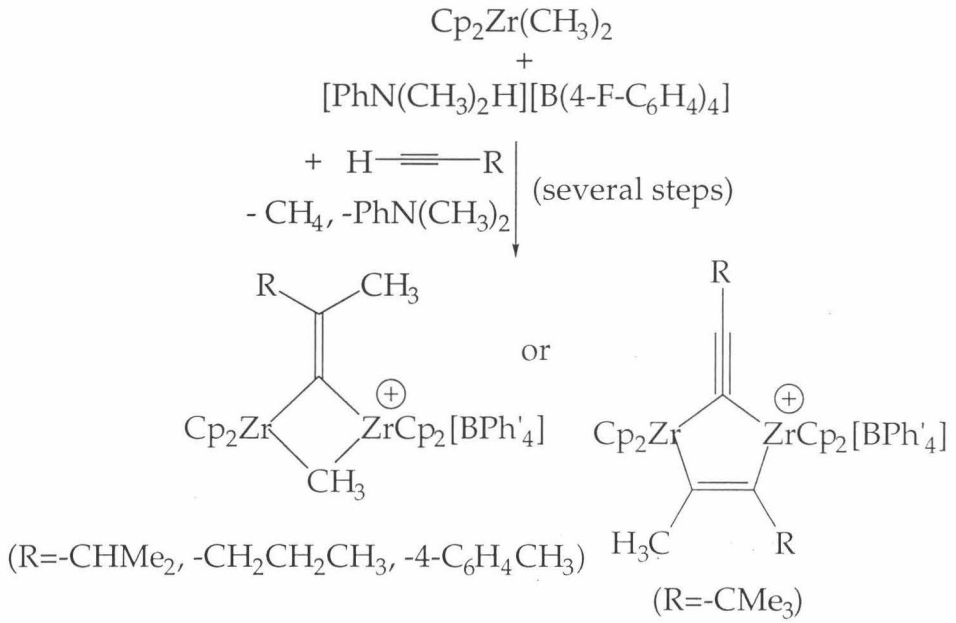

Figure 3. The relatively uncongested $(C_5H_5)_2$ ligand array permits formation of bimetallic complexes inactive for alkyne oligomerization.

The observed reactivity of internal alkynes towards Cp_2M-R (M=Sc, Y, Ln, Zr^+) is highly subject to subtle variations to the metal, ligand, and substrate.[14] The vast majority of cationic group IV-alkyl complexes insert 2-butyne and various other internal alkynes, affording M-alkenyl species (Scheme 3). In the absence of additional coordinating ligands, the relatively unhindered metallocenes (R_2=R_3=CH_3 or CH_2CH_3, $Cp_2M \neq Cp^*_2Zr$,) often permit insertion of a second equivalent of alkyne to generate η^5-pentadienyl complexes (Scheme 4).[15] By contrast, the sterically congested alkenyl complex $Cp^*_2Zr^+$-$C(CH_3)$=$C(CH_3)_2$ does not insert additional 2-butyne, instead activating a C-H bond of butyne by σ-bond metathesis to give $Cp^*_2Zr^+$-CH_2-C≡C-CH_3 and 2-methyl-2-butene.[15] $Cp^*_2Zr^+$-CH_3 also fails to react cleanly with H_3C-C≡C-$SiMe_3$, presumably due to the steric bulk of the substrate.[16]

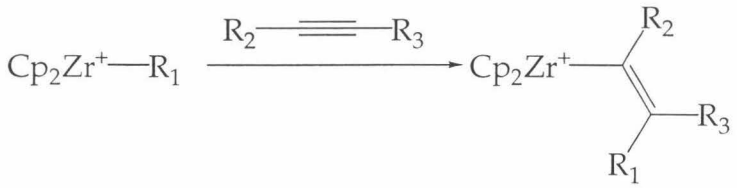

Scheme 3. Insertion of internal alkynes; $Cp_2 = (C_5H_5)_2$, $(CH_3Cp)_2$, $(Me_3SiCp)_2$, $(Me_3CCp)_2$, ethylenebis(indenyl), Cp^*_2; $(R_2,R_3) = (CH_3, CH_3)$, (CH_2CH_3, CH_2CH_3), (C_6H_5, C_6H_5), $(CH_3, Si(CH_3)_3)$.[5,15,16]

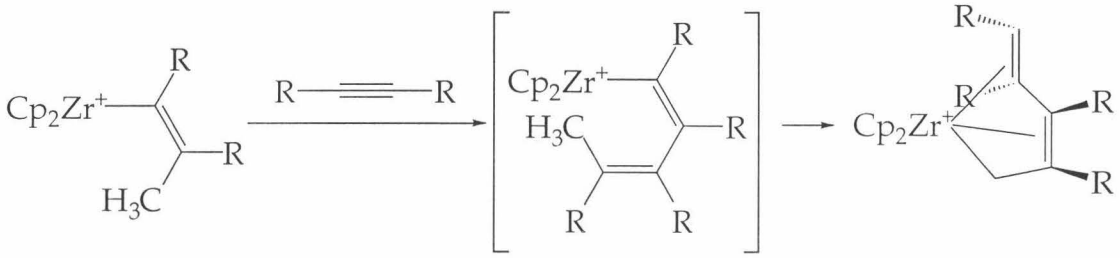

Scheme 4. Syntheses of η^5-pentadienyl complexes; R=CH_3 or CH_2CH_3.

Permethylyttrocene alkyl- and hydride- complexes show no insertion chemistry with internal alkynes. A C-H bond in 2-butyne undergoes σ-bond metathesis with $[Cp^*_2Y(\mu\text{-}H)]_2$ (**4**) to give dihydrogen and the propargyl complex $Cp^*_2YCH_2C{\equiv}CCH_3$,[17] which is unreactive towards additional equivalents of alkyne. The hindered $Cp^*_2YCH(SiMe_3)_2$ is completely unreactive towards 2-butyne.

Switching to larger lanthanides leads to a pronounced increase in reactivity. Both $Cp^*_2LaCH(SiMe_3)_2$ (**6**) and $Cp^*_2CeCH(SiMe_3)_2$ (**7**) undergo σ-bond metathesis with and catalyze the dimerization of internal alkynes (Scheme 5).[18] Bulky alkynes such as $H_3C\text{-}C{\equiv}C\text{-}C(CH_3)_3$ and $H_3C\text{-}C{\equiv}C\text{-}Si(CH_3)_3$ are not dimerized by **6** or **7**, although do react by α-methyl C-H bond activation. **6** and **7** do not react with 3-hexyne, even after several months at 80 °C.

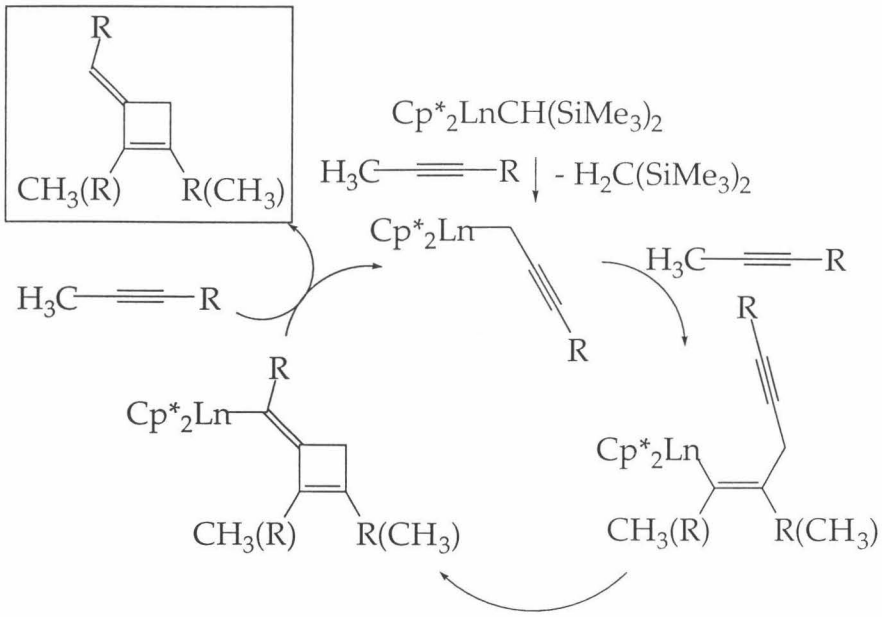

Scheme 5. Organolanthanide catalyzed dimerization of internal alkynes; Ln = La, Ce; R= Me, Et, *n*-Pr.

Considerably more research has focused on the use of metallocene catalysts in olefin polymerization than has touched on the area of alkyne insertion and oligomerization. The use of chiral metallocenes, such as ethylenebis(tetrahydroindenyl)$ZrCl_2$/MAO ((EBTHI)$ZrCl_2$, (**8/MAO**) as stereospecific Ziegler-Natta α-olefin polymerization catalysts is well documented.[19,20] Although mechanistic studies have been performed on selected cationic group IV systems, the fact that neutral group III metallocene complexes, such as *rac*-$Me_2Si(2\text{-}SiMe_3\text{-}4\text{-}CMe_3)_2Y$-H (*rac*-[Bp]YH, **9b**) and *rac*-$(C_{20}H_{12}O_2)Si(2\text{-}SiMe_3\text{-}4\text{-}CMe_3)_2Y$-H (*rac*-[BnBp]YH, **10b**), are single component catalysts (require no activator or cocatalyst) makes them particularly well suited for mechanistic studies.

Several factors contribute to the stereospecificity with which these C_2-symmetric catalysts promote olefin polymerization. The high isotacticities exhibited by the polymers produced indicate a very high degree of enantioselectivity for olefin insertion into M-alkyl bonds. Isotopic labelling studies on olefin hydrogenation, hydrodimerization, and oligomerization using *rac*-(EBTHI) complexes indicate a considerably lower (and opposite) enatiofacial selectivity for insertion into [Zr^+-H] bonds.[21-24] Similarly, although insertion of α-olefins into the Ti-ethyl bond of *rac*-

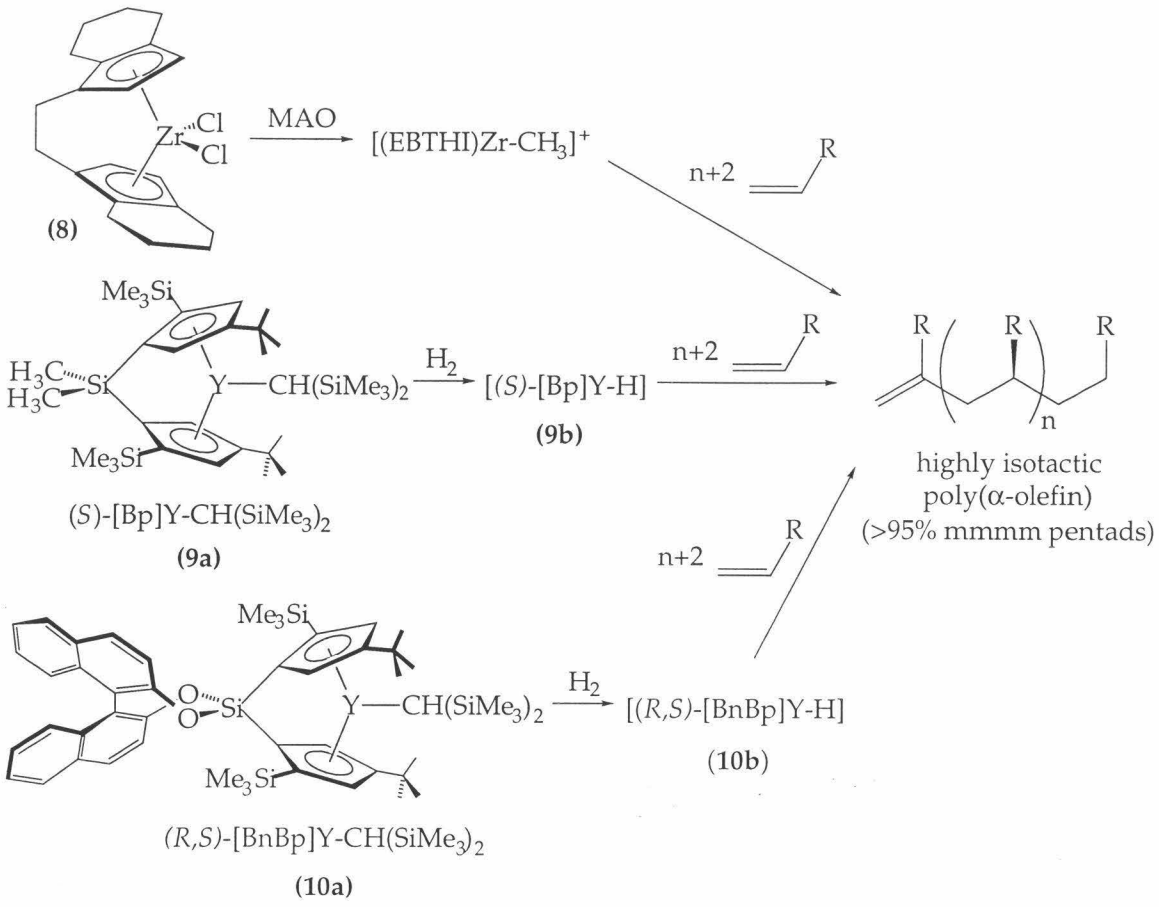

Figure 4. Isospecific Ziegler-Natta polymerization catalysts.[25]

ethylenebis(indenyl)Ti^{+}-$^{13}CH_2CH_3$ proceeds with high selectivity, analogous insertions into the Ti^{+}-$^{13}CH_3$ bond proceed with very *low* enantioselectivity.[26,27]

The use of an isotopically labelled and chiral 1-pentene ($D_3CCD_2CHDCH{=}CD_2$) in conjunction with the diastereomerically pure single component catalyst **10b** shows that insertion into the Y-H bond proceeds with low (34%) enantiomeric excess, and that subsequent insertion into the Y-pentyl species is achieved with high (>40:1) enantioselectivity.[28]

These results suggest the models for olefin insertion shown in Figure **5**. Steric interactions between the C_2-symmetric ligand array and incoming olefin are such that transition state **A**, in which the **R** group of the olefin is directed away from the bulky ligand *tert*-butyl group, is favored only slightly over that of **B**, resulting in low observed e.e.'s for insertion into the Y-hydride. The role of the ligand array is much more pronounced in

subsequent insertions, when the growing polymer chain (**P**) is directed into the open region, away from the *tert*-butyl groups. With the growing chain in this orientation, assisted by an α-agostic interaction with one of the two methylene hydrogens, the key steric interaction between the metallocene complex and the incoming monomer is that between the olefin alkyl group (**R**) and the C_α-C_β bond of the yttrium-alkyl; the favored transition state (**C**) is that in which the **R** group adopts a *trans*- orientation to the growing polymer chain.

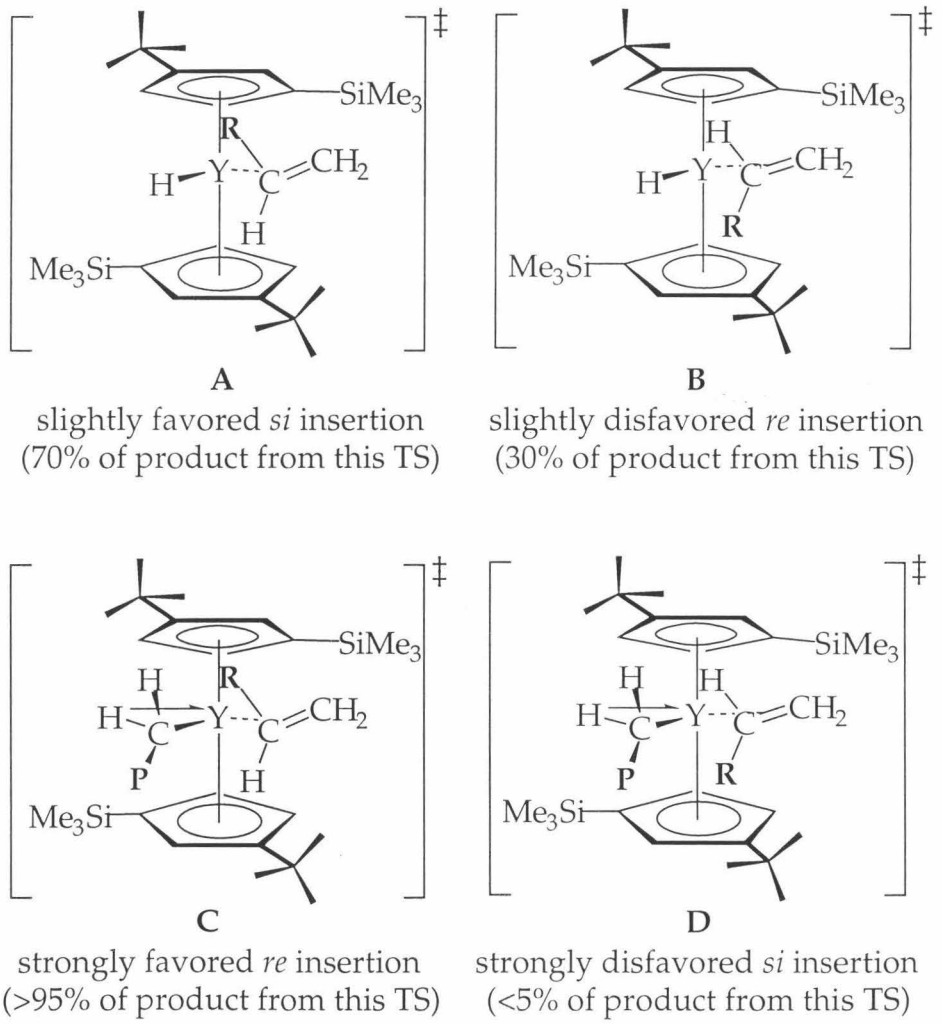

Figure 5. Transition states for olefin insertion into Y-H and Y-CH_2**P** bonds of (*R*,*S*)-BnBpY.[25]

Although useful in mechanistic studies, the practical use of group III complexes as Ziegler-Natta catalysts are complicated by the highly electron

deficient nature of the metal alkyls- and hydrides. Common pathways leading to catalyst deactivation are formation of bridging hydride ($(\mu\text{-H})_2$) dimers and activation of solvent, and often ligand C-H bonds by σ-bond metathesis.

Metal-alkyl species such as the bis(trimethylsilyl)methyl complexes **9a** and **10a** often initiate the polymerization of ethylene, but are too crowded to permit insertion of α-olefins. Hydrogenolysis of these M-alkyl complexes serves a convenient method for the formation of less congested M-H complexes which may serve as olefin polymerization catalysts.

In the absence of extreme steric congestion imparted by the Cp^*_2 ligand array, terminal group III metallocene-hydrides are extremely unstable, and dimerize to form $(\mu\text{-H})_2$ dimers (Figures 6 and 7). The monomer-dimer equilibria which interconvert the 14-electron monomer and the 16-electron dimers are so heavily weighted in favor of the inactive dimer that monomeric M-H species are never observed in solution for **9** and **10**. Rapid dissociation into monomeric M-H complexes is a prerequisite for active group III and Ln- hydride catalysts; the terminal hydrides are estimated to be 8 to 10 orders of magnitude more reactive than their $(\mu\text{-H})_2$ counterparts.[29]

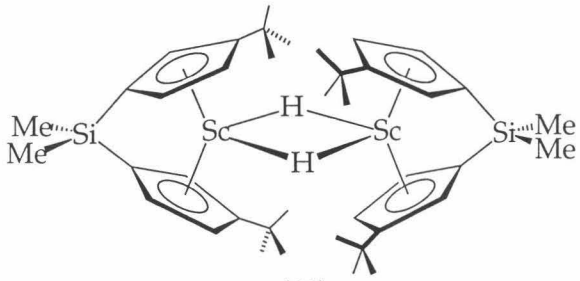

(11)

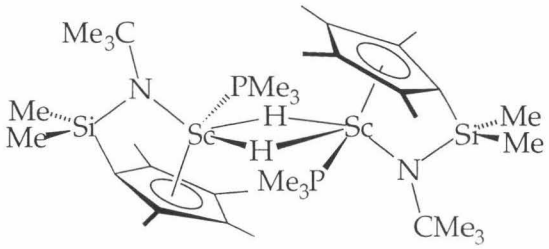

(12)

Figure 6. Group III bridging hydride dimers.

Careful investigation of the hydrides formed from the chiral **9a** and **10a** show two types of $(\mu\text{-H})_2$ dimers: homochiral (formed from the dimerization of two metallocenes of like chirality, **9c** and **10c**), and heterochiral (formed from dimerization of a pair of metallocenes of opposite chirality, **9d** and **10d**). When a mixture of (R) and (S) **9a** or **10a** metallocenes are used to generate Y-H complexes, a 1:1 mixture of the homochiral and heterochiral dimers are observed immediately upon hydrogenolysis; over the course of several hours,

the mixture is converted entirely to the thermodynamically stable homochiral dimer.

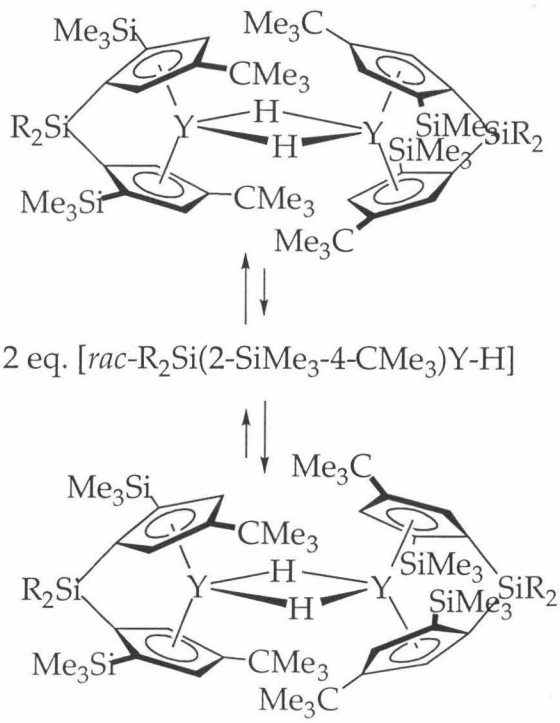

(9c, 10c)
homochiral $(\mu\text{-H})_2$ dimer

(9b, 10b)
never observed

(9d, 10d)
heterochiral $(\mu\text{-H})_2$ dimer

Figure 7. Monomeric/homochiral-/heterochiral hydride dimer equilibria; (R_2Si = Me_2Si, $(\pm)C_{20}H_{12}O_2Si$).

The use of sterically demanding pentamethylcyclopentadienyl ligands may be exploited to permit manipulation of monomeric M-H complexes. Hydrogenolysis of $Et_2Si(C_5Me_4)(C_5H_4)MCH(SiMe_3)_2$ (M=Lu, Y) permits observation of a monomeric Lu-H complex prior to formation of "flyover" $(\mu\text{-H})_2$ dimers; observation of the corresponding Y-H monomer is reported, although the doublet in the ^1H NMR diagnostic for a monomeric ^{89}Y-H species is not observed.[29] Although the monomeric Cp^*_2Y-H is not observed in solution, monomeric Cp^*_2Sc-H is the (moderately) stable hydrogenolysis product of Cp^*_2Sc-CH_3.[7]

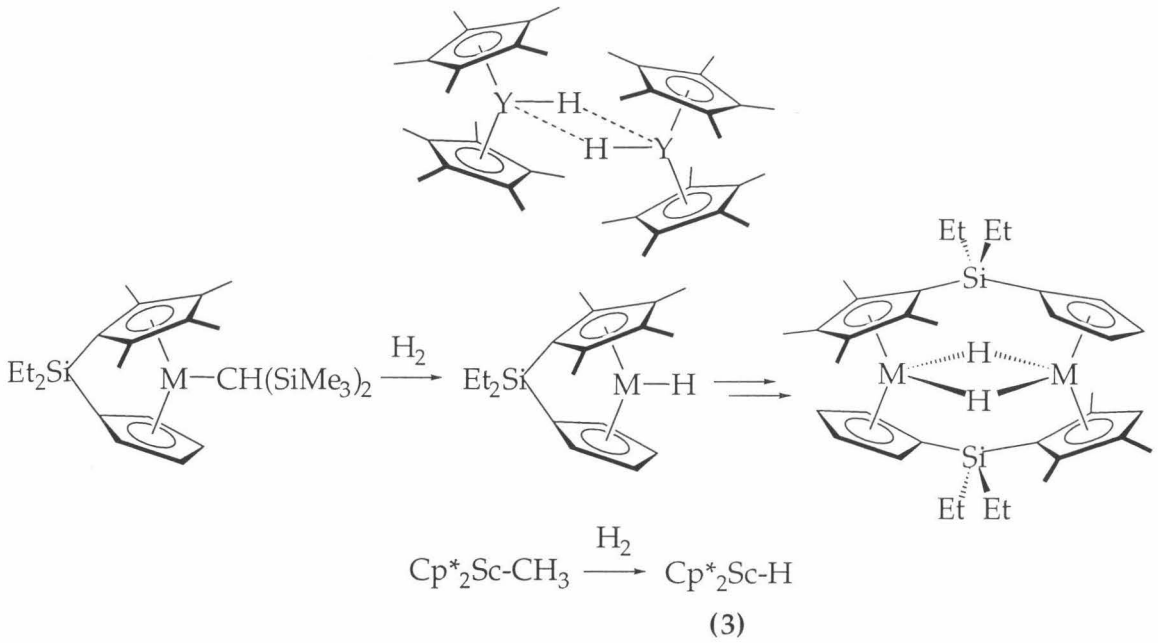

Figure 8. The results of increased steric crowding on formation of $(\mu\text{-H})_2$ dimers.

The destabilization of $(\mu\text{-H})_2$ dimers is generally accompanied by an increased reactivity towards H-H and C-H bonds. **3** reacts rapidly with H_2 in solution, even at -80 °C. Arene C-H bonds are also readily activated by **3**; although slow at -80 °C, H/D exchange between Cp^*_2Sc-D and C_6H_6 is >95% complete within 5 minutes at 25 °C. Activation of 1° C-H bonds also commonly leads to formation of M-R complexes such as Cp^*_2M-Ph (M=Sc,[7] Y,[31] Lu[32]) and Cp^*_2M-C_6H_4-MCp^*_2 (M=Lu[32]).

Electron deficient early transition metal complexes are also known to activate exposed C-H bonds of the metallocene ligand array, as shown in Figure 9. Although considerably slower than 1° C-H bond activation, examples of both inter- and intramolecular 2° C-H activation are well documented.[7,31,33-35]

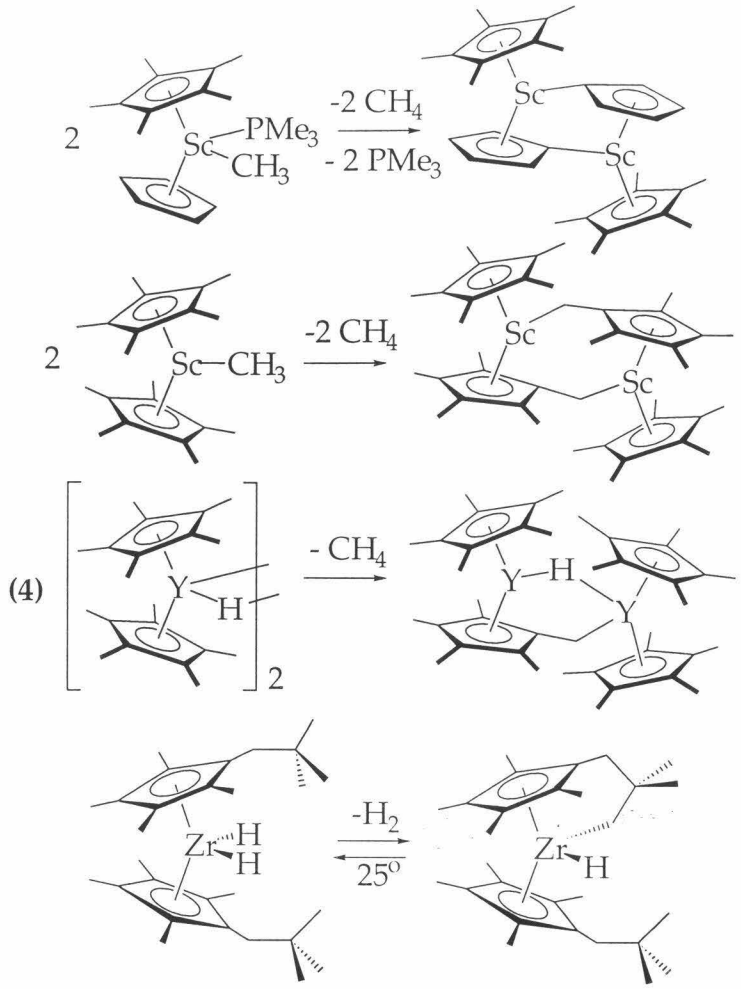

Figure 9. Intra- and intermolecular ligand C-H activation.

The attraction of using sterically congested pentamethyl cyclopentadienyl ligands to generate moderately stable monomeric 14-electron d^0 metal complexes is offset by the inability of these complexes to undergo multiple α-olefin insertions. The monomeric hydride **3** readily inserts one equivalent of propene at -80 °C; the resultant Sc-CH_2CH_3 complex, however, does not insert additional equivalents of olefin, and is subject to σ-bond metathesis with available C-H bonds to form Sc-vinyl complexes. In the presence of only one or two equivalents of olefin, or in the presence of excess olefin at elevated temperatures, $Cp^*_2Sc\text{-}CH_3$ is shown to insert one equivalent of propene to generate $Cp^*_2Sc\text{-}CH_2CH(CH_3)_2$. Both σ-bond metathesis with additional equivalents of propene and β-H elimination from

the isobutyl complex, however, are much faster than insertion of additional olefins.

Results and Discussion

The incorporation of bulky methyladamantyl groups as *ansa*-metallocene β-substituents is designed to perturb the monomer-dimer equilibria commonly observed for group III and Ln hydrides. Although they are unlikely to serve as stereospecific olefin polymerization catalysts, hydride complexes ultimately derived from C_s- symmetric scandocene **13** and yttrocene **14** (*meso*-AdpScCl-LiCl-$(THF)_2$ and *meso*-AdpYCl-LiCl-$(THF)_2$, respectively) should provide preliminary evidence for the ability of the methyladamantyl groups to disrupt formation of $(\mu\text{-H})_2$ dimers. Of greater interest, though, are the effects of incorporation of bulky β-substituents into chiral metallocenes such as those derived from the [Abp] ligand array. Disruption of the monomer-dimer equilibria may result in highly active and enantioselective α-olefin polymerization catalysts.

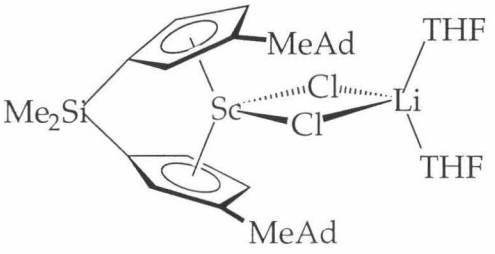

meso-AdpScCl-(LiCl)-$(THF)_2$
(**13**)

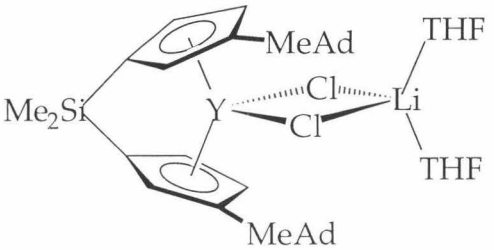

meso-AdpYCl-(LiCl)-$(THF)_2$
(**14**)

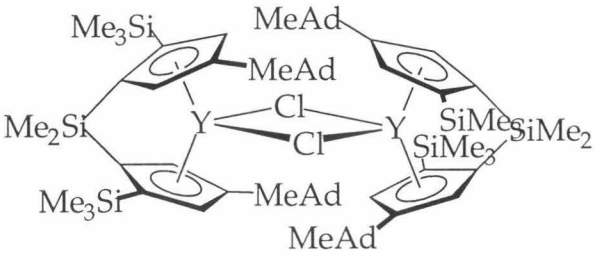

[*rac*-AbpY(μ-Cl)]$_2$
(**15**)

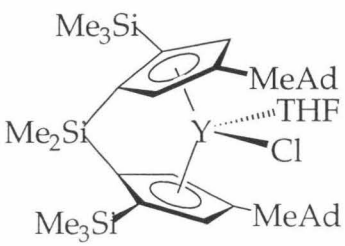

rac-AbpYCl(THF)

Treatment of Et_2O solutions of *meso*-AdpMCl-LiCl-$(THF)_2$ (M = Sc, Y) with a slight excess (~1.1 equivalents) of C_3H_5MgBr (-78 °C), followed by stirring at 25 °C, results in the formation of *meso*-AdpSc(η^3-C_3H_5), **16**, and *meso*-AdpY(η^3-C_3H_5), **17**, as yellow diethyl ether soluble solids. Residual THF and LiCl in **13** and **14** neither impede the alkylation nor coordinate to Sc or Y in the resulting η^3-allyl complexes, and may be removed from **16** and **17** by a series of petroleum ether and toluene washings. The η^3- coordination of the allyl moiety may serve to prevent coordination of donor solvent and Li/Mg-halide to the electrophilic metal centers.

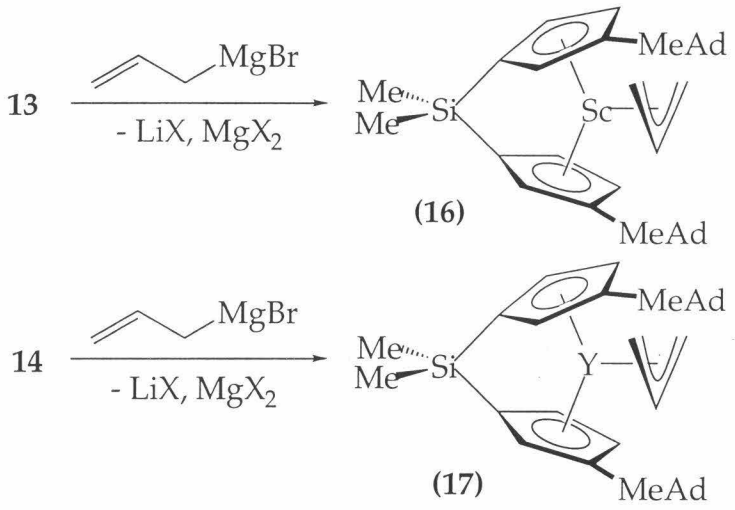

(5)

(6)

Although the allyl ligands appear η^3-coordinated in solution, variable temperature NMR spectroscopy indicates fluxional behavior associated with the allyl ligands. A detailed investigation of the fluxional behavior of these, and other, group III metallocene allyl complexes is described in the following chapter (*vide infra*). These studies indicate that η^1-allyl complexes are kinetically accessible, although η^1- complexes are never observed directly (Equation 7). Upper limits on the barriers to dissociation of the allyl C=C double bond (generation of an η^1-allyl species), as determined by lineshape analysis of the variable temperature NMR spectra, are found to be 12.0 kcal/mol (290 K, Et_2O-d_{10}) for **16**, and 15.6 kcal/mol (361 K, Et_2O-d_{10}) and 16.0 kcal/mol (370 K, toluene-d_8) for **17**.

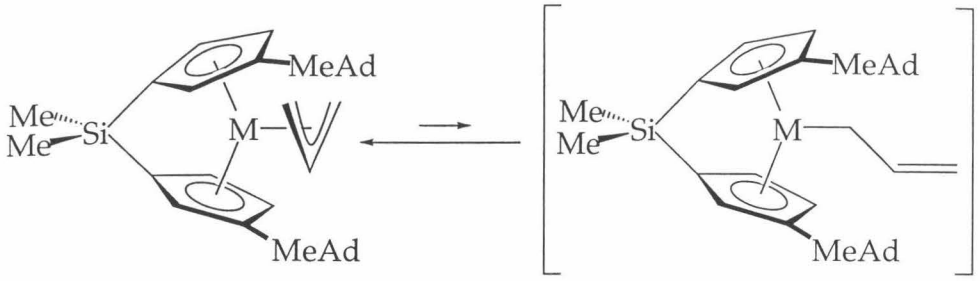

(7)

meso-AdpM(η^3-C_3H_5) *meso*-AdpM(η^1-C_3H_5)

The role of η^1-allyl complexes in the reactivity of *meso*-AdpM(C_3H_5) is not known. Although the 14-electron η^1-species generated by dissociation of the allyl C-C double bond are expected to be much more reactive than the ground state 16-electron η^3-complexes, reactions such as hydrogenolysis may proceed by associative mechanisms in which olefin displacement follows coordination of substrate to the metal center.

Treatment of **16** or **17** with excess H_2 (1 atm, 25 °C, C_6D_6) results in the generation of propylene from σ-bond metathesis of the allyl ligand with dihydrogen; the monomeric 14-electron metal hydride species *meso*-AdpMH, the initial organometallic product derived from hydrogenolysis, is not observed during or following hydrogenolysis. A small amount (~3%) of the overall product mixture from the hydrogenolysis of **17** is identified as the bridging hydride dimer [*meso*-AdpY(μ-H)]$_2$ on the basis of the appearance of a 1:3:1 triplet (δ 4.65, $^1J_{Y\text{-}H}$ = 31.1 Hz) due to coupling to the 100% natural abundance ^{89}Y (I = 1/2); no other resonances attributable to Y-H species were observed. The absence of a corresponding (μ-H)$_2$ resonance for the Sc hydrogenolysis product [*meso*-AdpSc(μ-H)]$_2$ is attributed to broadening from quadropolar ^{45}Sc.

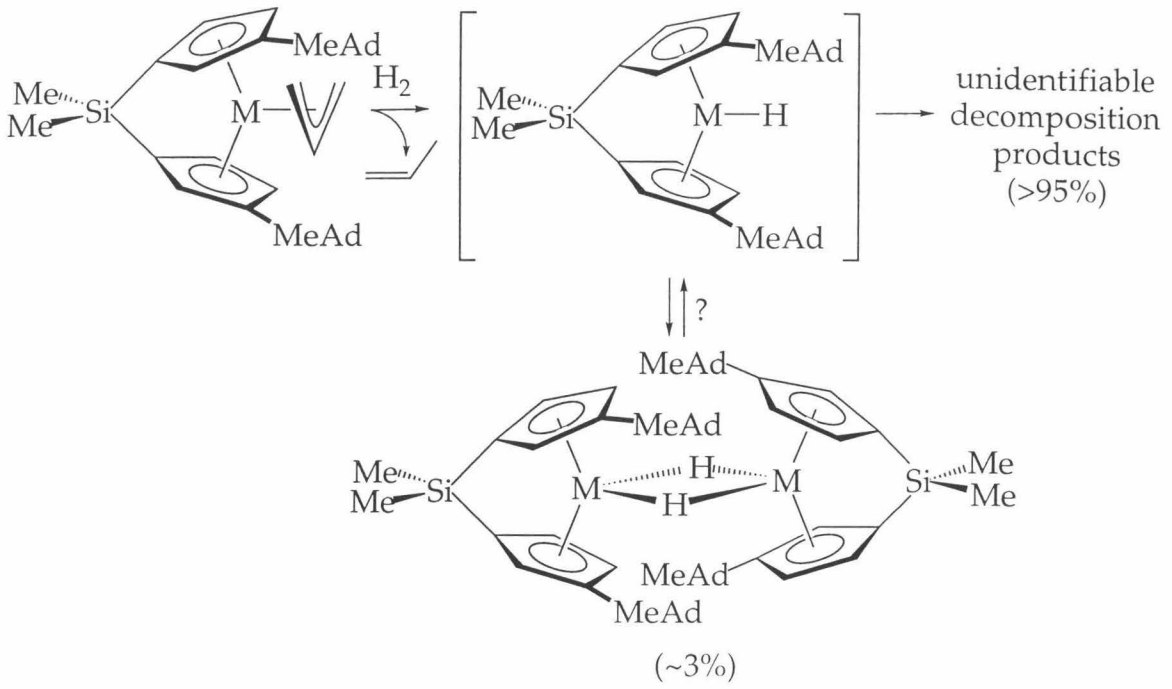

Figure 10. Only small quantities of $(\mu\text{-H})_2$ dimers are observed upon hydrogenolysis of *meso*-AdpM(C_3H_5) (M=Sc, Y)

The organometallic products resulting from hydrogenolysis of **16** and **17** do not react with α-olefins. The propylene generated from initial hydrogenolysis of the allyl ligand is never converted to propane via insertion into a M-H species and subsequent σ-bond metathesis with H_2, despite the presence of excess dihydrogen. No reaction is observed between the organometallic products and added olefinic substrates such as 1-pentene.

Identification of the major organometallic hydrogenolysis products is complicated by the number of possible decomposition pathways, including solvent C-H bond activation, intramolecular ligand C-H activation, and intermolecular ligand C-H activation. Deuterium labeling studies and hydrogenolyses in nonaromatic solvents (C_6D_{12}), intended to identify arene (solvent) C-H activation, are inconclusive.

Molecular models indicate that each methyladamantyl group in [Adp] has two sterically accessible C-H bonds which may undergo σ-bond metathesis (Figure 11; these products share structural similarities to the 2° C-H bond activation products observed previously by Bercaw (Figure 9).[35] Although hydrogenolysis with D_2 fails to result in an observable decrease in intensity of the methyladamantyl resonances (^{1}H NMR), these observations are

complicated by the multiple overlapping resonances of the thirty-four methyladamantyl protons.

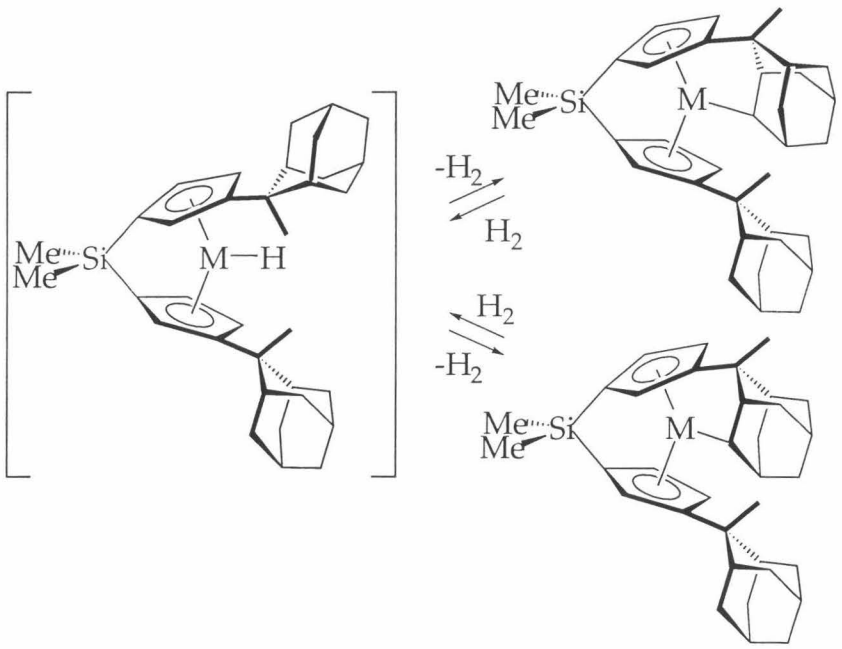

Figure 11. Possible intramolecular C-H bond activation.

Despite the presence of the bulky methyladamantyl substituents, the C_s-symmetry of the *meso*-Adp metallocenes results in exposed sp^2-hybridized cyclopentadienyl C-H bonds that may undergo σ-bond metathesis with M-H species to form dimers similar to those observed from [CpCp*$ScCH_3(PMe_3)$] (Figure 9).[33] Multiple complexes resulting from intermolecular C-H activation are possible as a result of the exposed vinylic C-H bonds in the 4- and 5- positions of the Cp rings; the possible dimer resulting from activation of the 4-CH bonds is shown in Figure 12.

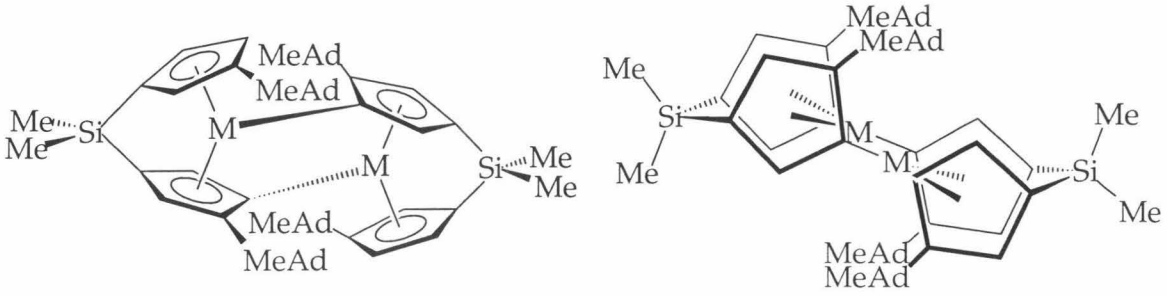

Figure 12. One of several possible dimers resulting from intermolecular C-H activation.

Efforts to trap [AdpYH] with a coordinating ligand are largely unsuccessful. Hydrogenolysis of a solution of **17** containing excess trimethylphopshine does not result in the clean formation of *meso*-AdpYH(PMe_3); a mixture of at least four products is obtained (^{1}H NMR). Dihydrogen and trimethylphosphine pressure dependencies of the relative ratios of the products suggest equilibria between species such as those shown in Figure 13, in addition to the possible C-H activation products outline above.

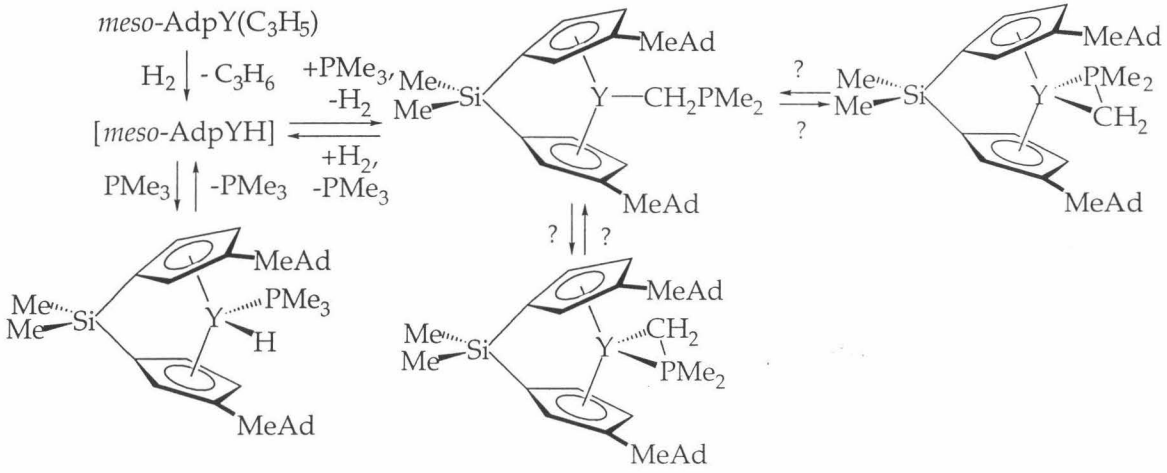

Figure 13. Possible equilibria involving *meso*-AdpM-H, trimethylphosphine, and dihydrogen (M = Sc, Y).

These overall results are consistent with the hydrogenolyses of *meso*-AdpM(C_3H_5) to generate extremely reactive 14-electron *meso*-AdpMH monomers, which appear to react with any of a variety of accessible C-H bonds. The incorporation of methyladamantyl groups as β- substituents appears to inhibit formation of $(\mu\text{-H})_2$ dimers, in contrast to the related *tert*-butyl complex [*meso*-$Me_2Si(3\text{-}CMe_3\text{-}C_5H_3)_2Sc(\mu\text{-H})]_2$ (**11**).

It was hoped that the *rac*- [Abp] ligand array resulting from the net addition of trimethylsilyl groups onto [Adp] would provide metallocene hydride species less prone to irreversible deactivation than those derived from **16** and **17**; molecular models indicated that the staggered conformations of the methyladamantyl and $SiMe_3$ groups in *rac*-AbpMH provide considerable steric hindrance to the approach of two M-H monomers, thus

rendering intermolecular ligand C-H activation less likely than that shown in Figure 12.

Although the use of $(C_3H_5)MgBr$ provides a facile means of generating *meso*- group III allyl complexes, analogous reactions with the [*rac*-AbpY(μ-Cl)]$_2$ / [*rac*-AbpYCl(THF)] mixture fails to reproducibly provide pure samples of AbpY(C_3H_5). Uncertainties in the Y:Mg stoichiometry may lead to formation of bis(allyl)yttrates along with the desired AbpY(C_3H_5).

Bis(trimethylsilyl)methyllithium reacts rapidly with [*rac*-AbpY(μ-Cl)]$_2$ (benzene or toluene) to generate AbpYCH($SiMe_3$)$_2$, **18**. A beige powder, **18** is isolated in 25-35% yield after removal of solvent, removal of KCl by Et_2O filtration, and recrystallization from cold (-78 °C) pentane. The loss of C_2-symmetry in the ^1H and ^{13}C NMR spectra of **18**, (benzene-d_6, toluene-d_6, cyclohexane-d_{12}, methylcyclohexane-d_{14}) evidenced by the inequivalence of the Cp rings and substituents, is indicative of hindered rotation about the Y-C bond (Figure 14).

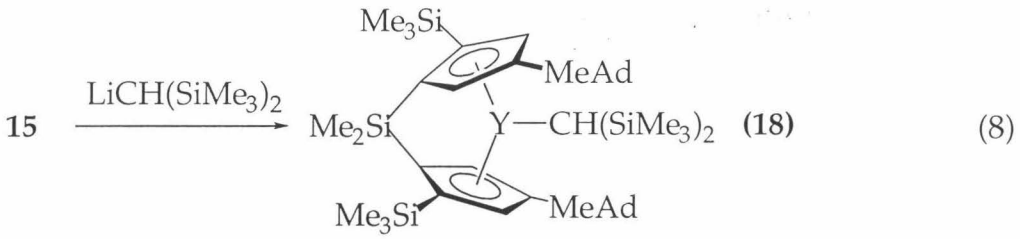

(8)

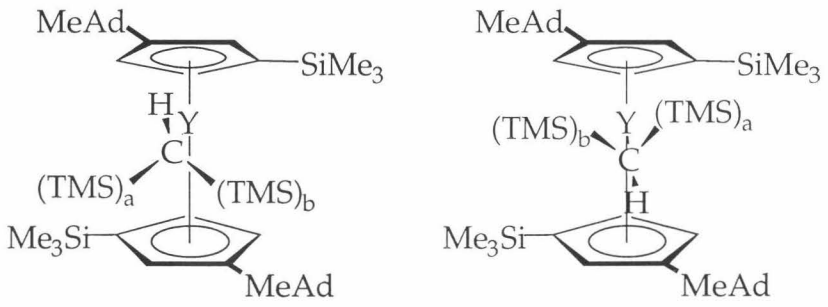

18 is an active catalyst for the polymerization of ethylene (1 atm. C_2H_4, 25 °C, toluene). No reaction is observed, however, between **18** and either 20 equivalents of 1-butene or 230 equivalents of 1-pentene (days, 25 °C, C_6D_6). Steric congestion at the metal center imparted by the methyladamantyl and bis(trimethylsilyl)methyl groups appears to prevent both olefin insertion and σ-bond metathesis.

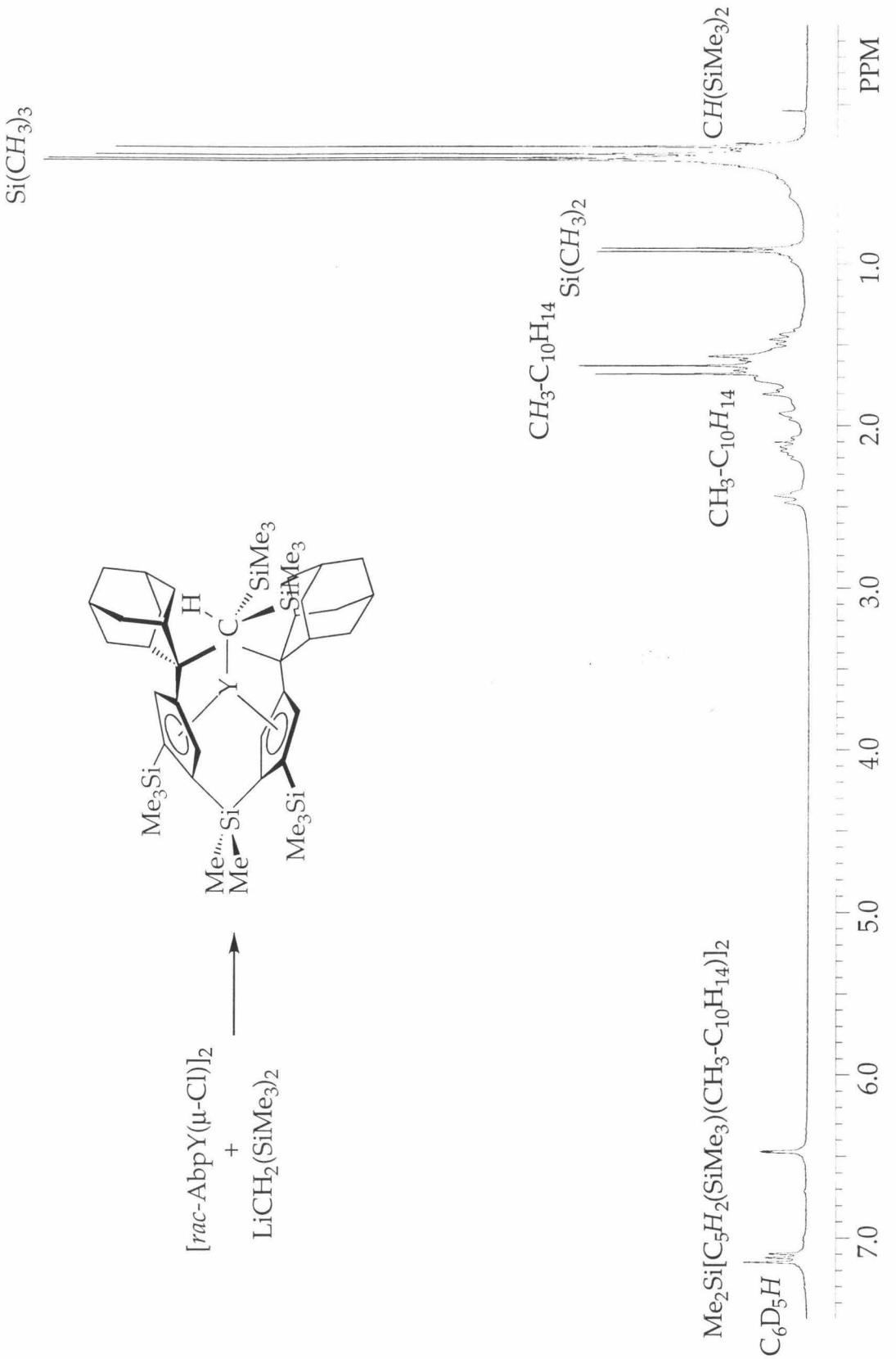

Figure 14. 500 MHz ^{1}H NMR spectra (C_6D_6) of *rac*-AbpYCH($SiMe_3$)$_2$ (**18**).

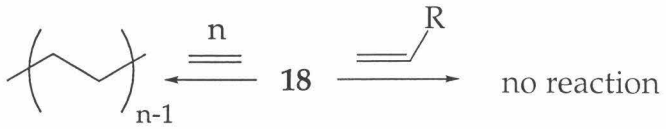

Figure 15. *rac*-AbpYCH($SiMe_3$)$_2$ (**18**) polymerizes ethylene but does not react with α-olefins.

18 also fails to react with bulky terminal alkynes such as trimethylsilylacetylene and *tert*-butylacetylene at room temperature. This is in marked contrast to Cp*$_2$YCH($SiMe_3$)$_2$, which rapidly undergoes σ-bond metathesis with terminal alkynes to generate Y-alkynyl species and $H_2C(SiMe_3)_2$.[36] Heating 1:1 **18**:alkyne solutions (80 °C, C_6D_6) results in the evolution of $H_2C(SiMe_3)_2$, although the resultant organometallic products can not been positively identified as either alkynyl products resulting from σ-bond metathesis or alkenyl-yne complexes arising from insertion of additional equivalents of alkyne to a Y-alkynyl complex.

The reaction of **18** with dihydrogen proceeds cleanly and quantitatively via σ-bond metathesis, resulting in the formation of $H_2C(SiMe_3)_2$ and a single hydride dimer, [*rac*-AbpY(μ-H)]$_2$ (**20**), as the sole organometallic product (Figure 16). The presence of a 1:2:1 triplet in the ^{1}H NMR spectra of **20** due to coupling to equivalent ^{89}Y nuclei is diagnostic for the presence of a symmetric, hydride-bridged yttrocene dimer (Table 1). None of the monomeric *rac*-AbpYH (**19**), which should exhibit a characteristic Y-H doublet and a distinct set of ligand resonances, is observed under any hydrogenolysis conditions.

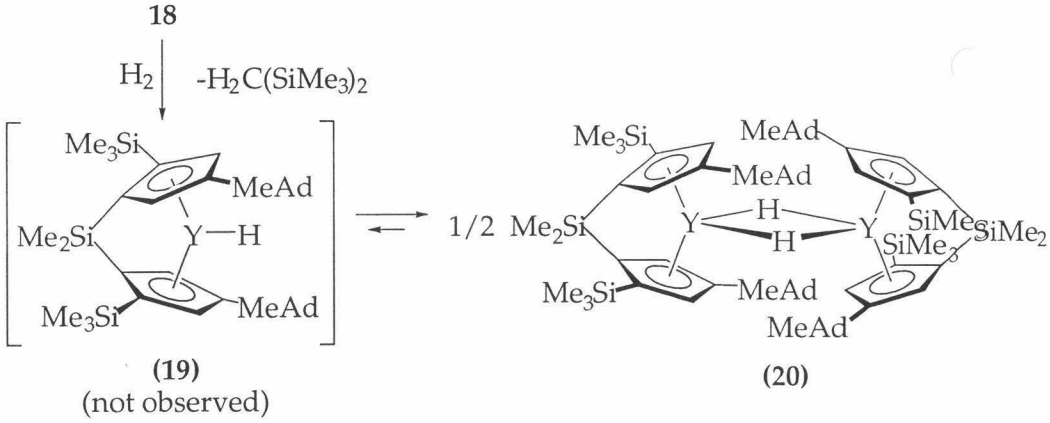

(9)

Solvent	δ (ppm)	$^1J_{Y\text{-}H}$ (Hz)
benzene-d_6	4.76	31.3
cyclohexane-d_{12}	4.48	31.0
methylcyclohexane-d_{14}	4.39	31.2

Table 1. 500 MHz ^{1}H NMR chemical shifts and one-bond Y-H coupling constants for the bridging hydride resonance of [*rac*-AbpY(μ-H)]$_2$ (**20**).

Variable temperature NMR studies rule out the possibility of an energetically accessible homochiral-heterochiral dimer equilibrium in methylcyclohexane. Hydrogenolysis of **18** at 246 K (C_7D_{14}) confirms that the triplet observed in the room temperature hydrogenolysis is the kinetic hydrogenolysis product as well as the thermodynamic product. Neither additional hydride resonances nor changes in the chemical shift of the observed (μ-H)$_2$ triplet, are observed upon cooling room temperature solutions of **20** to 213 K, indicating the absence of exchange between homochiral and heterochiral dimers on the NMR timescale. This result also indicates that dissociation of **20** to **19** is slow on the NMR timescale.

Assignment of **20** as the homochiral dimer is based, in part, on the previously observed stabilities of **9c** and **10c** (previous homochiral dimers), compared to the instabilities of the heterochiral dimers **9d** and **10d**.[37] Further support for the assignment of **20** as the homochiral dimer comes from the upfield chemical shift of the (μ-H)$_2$ resonance (cf. **9c**: δ 4.87, J=31 Hz, C_6D_6; **10c**: δ 4.98, J=31.4 Hz, C_6D_6; **10d**: δ 5.97, J=31.4 Hz, C_6D_6), Single crystals grown by cooling a concentrated cyclohexane solution of **20** show severe twinning, and are not suitable for study by X-ray diffraction techniques.

Efforts to trap the highly reactive **19** monomer by addition of donor ligands are only partially successful. Hydrogenolysis of **18** in the presence of 1.1 equivalents of THF shows a doublet (δ 5.52, J=72.8 Hz, C_6D_6) in the region of the ^{1}H NMR spectrum in which the Y(μ-*H*)$_2$Y and Y*H*(THF) resonances are typically observed, suggesting the formation of *rac*-AbpYH(THF) (cf. Cp*$_2$Y*H*(THF): δ 6.17, J=81.7 Hz, C_6D_6). Formation of *rac*-AbpYH(THF) is accompanied by the formation of an intractable mixture of additional organometallic products, as evidenced by the presence of multiple Cp, methyladamantyl, and Si-Me resonances. Following the hydrogenolysis by

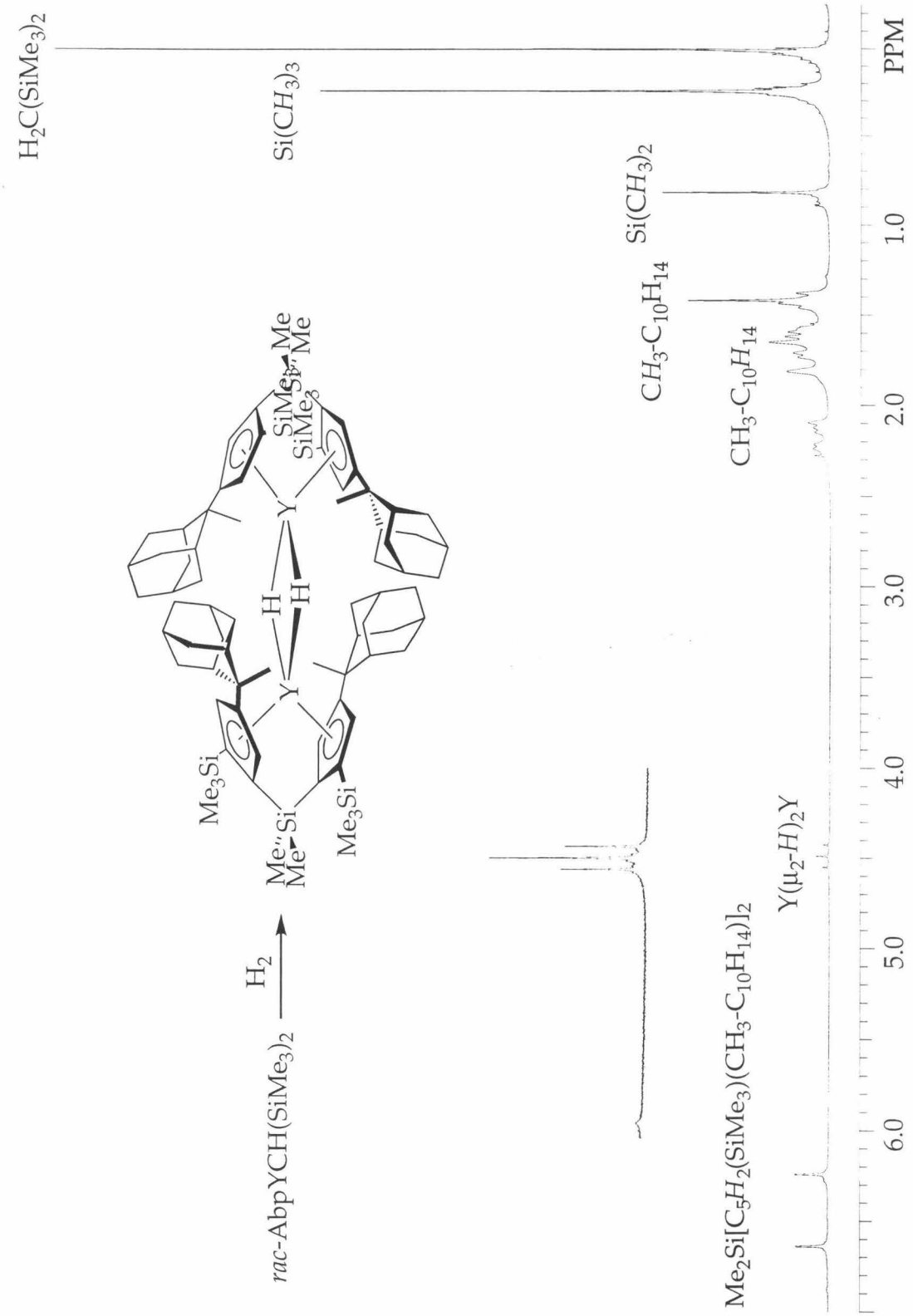

Figure 16. 500 MHz ^{1}H NMR spectra (cyclohexane-d_{12}) of [*rac*-AbpY(μ-H)]$_2$ (**20**).

^{1}H NMR in neat THF-d_8 does not provide additional information on the fate of [*rac*-AbpYH]. The hydride dimer **20** is not cleaved by added PMe_3; similarly, hydrogenolysis of **18** in the presence of excess PMe_3 results only in **20**, with no evidence for the formation of *rac*-AbpYH(PMe_3).

Evidence for dissociation of **20** into monomeric *rac*-AbpYH, however, is obtained from H/D scrambling experiments. The deuteride-bridged dimer **20-d_2** may be generated by placing **20-d_0** under one atmosphere of D_2. The NMR spectrum of **20-d_2**, which may also be obtained from treatment of **18** with D_2, is identical to that of **20-d_0**, save for the absence of the (μ-H)$_2$ triplet. Complete conversion from **20-d_0** to **20-d_2** is observed after several hours at room temperature, indicating a series of dimer dissociations and σ-bond metathesis steps outlined in Scheme 6.

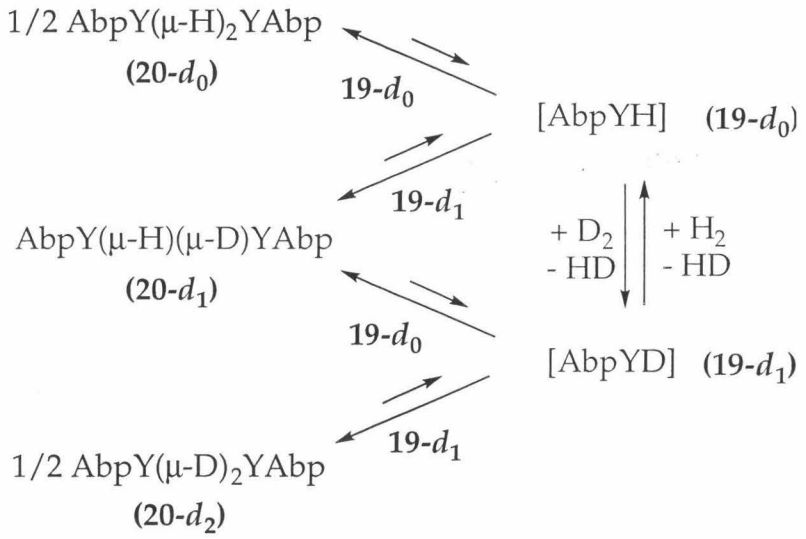

Scheme 6. Dimer dissociations and σ-bond metathesis steps required to account for H/D scrambling into **20**.

Dissociation of **20** into **19** and subsequent σ-bond metathesis with excess dihydrogen is, however, slow on the NMR timescale at 25 °C, as evidenced by the presence of a sharp singlet for free H_2 accompanying the characteristic (μ-H)$_2$ triplet of **20** (benzene-d_6, cyclohexane-d_{12}, methylcyclohexane-d_{14}, 25 °C). Rapid exchange would result in an averaged H_2 and M-hydride signal, as is observed for monomeric Cp^*_2ScH.[7] **20** is also relatively unreactive towards the C-H bonds of aromatic solvents. Whereas

the permethylscandocene hydride monomer readily undergoes σ-bond metathesis with the aryl C-H bonds of benzene, deuterium incorporation into **20** (in the absence of D_2) is not observed after several hours in C_6D_6 or C_7D_8 (25 °C).

Although **20** does not readily activate solvent C-H bonds, the overall stability of **20** is greatly diminished in aromatic solvents, compared to that in aliphatic hydrocarbons. Decomposition of **20** in C_6D_6 is observed within minutes in the absence of excess dihydrogen (25 °C). Under one atmosphere of H_2, **20** is stable in benzene-d_6 or toluene-d_8 for several (<12) hours. By contrast, cyclohexane-d_{12} and methylcyclohexane-d_{14} solutions of **20** are stable for weeks at room temperature.

The decomposition mechanisms operating are not currently understood, and are beyond the scope of this study. It does not appear that **19** or **20** activates the C-H bonds of benzene to afford Y-phenyl complexes, as no reaction is observed between **20** and excess C_6H_6 (10 equivalents per yttrium) after 24 hours at 25 °C in cyclohexane-d_{12}. The stability imparted by the introduction of trimethylsilyl substituents in **20** (either by virtue of the reduction in the number of available C-H bonds or due to steric hindrance provided by the *racemo*- conformations of the resultant metallocenes) compared to the rapid decomposition of [*meso*-AdpMH] indicates that decomposition of the *meso*- Adp complexes may occur primarily by intermolecular cyclopentadienyl C-H bond activation.

Hydrogenolysis of **18** in the presence of excess 1-butene (20 equivalents per Y) results in the formation of **20** and butane (<45 minutes, ^{1}H NMR). The proposed catalytic cycle for olefin hydrogenation is shown in Scheme 7.

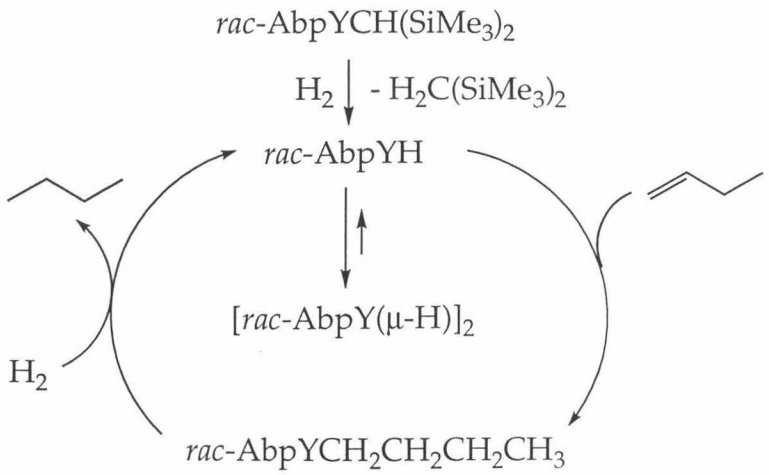

Scheme 7. Olefin hydrogenation catalyzed by [*rac*-AbpYH] (**19**).

The influence of the methyladamantyl groups on the reactivity of **19** is most easily observed by the introduction of α-olefins to solutions of **20**. Treatment of **20** with excess α-olefin does not result in the formation of poly(α-olefin). **20** fails to generate polymers even under reaction conditions analogous to those successfully employed in α-olefin polymerization by **9c** (90% v/v 1-pentene/cyclohexane, 11 days, 25 °C).

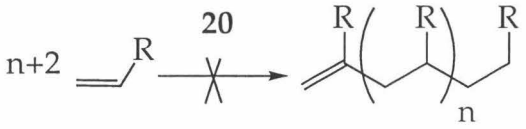

(10)

When followed by ^{1}H NMR, **20** begins to react within 20 minutes of the addition of excess 1-butene or 1-hexene (20 equivalents per Y) to a solution of **20**. Complete reaction/decomposition of **20** is observed within 120 minutes at 25 °C, although there is virtually no consumption of alkene. **20** is not converted cleanly to either an identifiable yttrium-alkyl or yttrium-alkenyl complex; the organometallic products of these reactions show broad and unassignable NMR resonances. The use of 3,3-dimethylbutene[38] does not result in significantly cleaner reactions with **20** than do the α-olefins mentioned above.

Deuterium labeling indicates that **19** does not insert α-olefins and then rapidly undergo β-H elimination from a transient yttrium-alkyl complex. Treatment of **20-d_2** with 2 equivalents of d_0-1-pentene (C_6D_{12}) shows neither H incorporation into the bridging deuteride positions of **20** nor a change in the

relative intensities of the vinylic resonances of the free olefin. A similar lack of H/D scrambling is observed for a 1:1 mixture of **20-d_2** and neohexene.

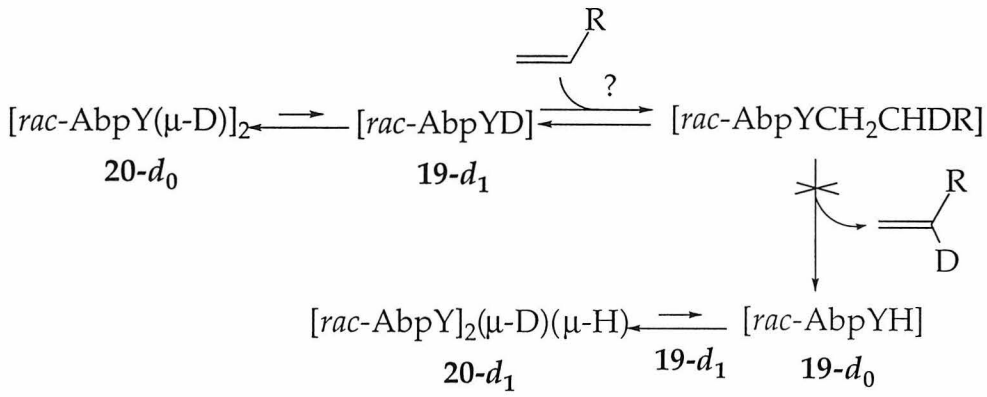

Scheme 8. H/D scrambling is not observed between **20-d_2** and perprotio 1-olefins (R=$CH_2CH_2C_3$, CMe_3).

In contrast, the reaction of **20** with allene proceeds smoothly over 24 hours at room temperature, affording the allenyl complex **21**. The proposed mechanism for formation of **21** is shown in Figure 17; dissociation of **20** into monomeric **19** is followed by σ-bond metathesis with a C-H bond of allene to generate dihydrogen and **21**. There is no evidence for insertion of allene into **19** to generate *rac*-AbpY(η^3-C_3H_5). The NMR spectrum of **21** (Figure 18) shows equivalent Cp rings and substituents, indicating rapid rotation about the Y-C bond. The C_2- symmetry of the [*rac*-Abp] ligand array renders the two terminal allenyl methylene hydrogens magnetically inequivalent, regardless of the rate of Y-C bond rotation.

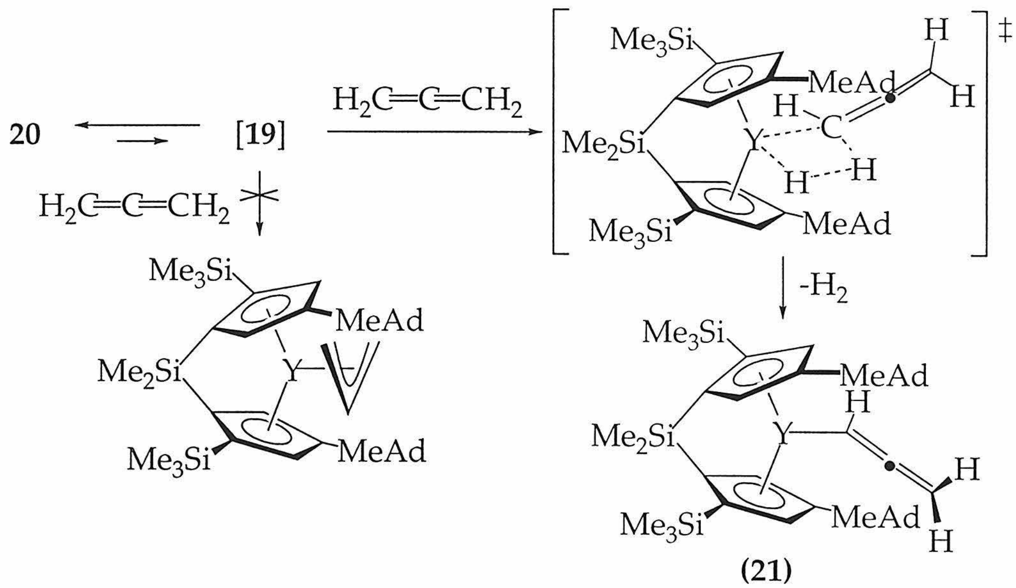

Figure 17. Allene undergoes σ-bond metathesis with **19.**

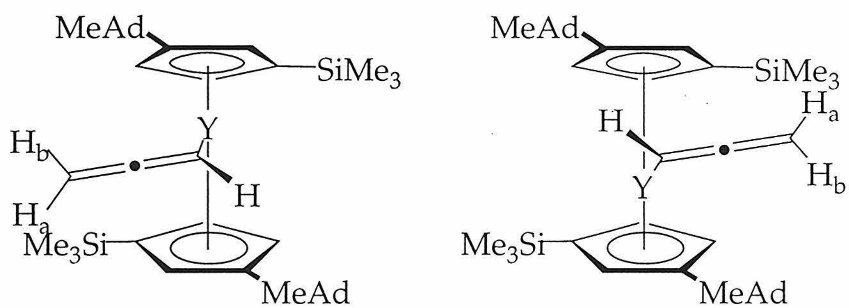

Catalytic amounts of trimethylphosphine are reported to catalytically induce dissociation of and equilibration between *rac*-BpLa(μ-H)$_2$ dimers, indicating an associative pathway for dimer dissociation[39] The observed rates of consumption of **20** and generation of **21** are not affected (qualitatively) by the addition of PMe_3.

Terminal alkynes such as H-C≡C-CMe$_3$ and H-C≡C-SiMe$_3$ do not react cleanly with **20,** instead resulting in the decomposition of **20** over several hours at room temperature. Particularly intriguing, though, is the reaction of **20** with 2-butyne. Given the observed preference for **20** to undergo σ-bond metathesis with rather than undergo insertion with allene, the propargylic product resulting from C-H activation was expected to be the kinetic product

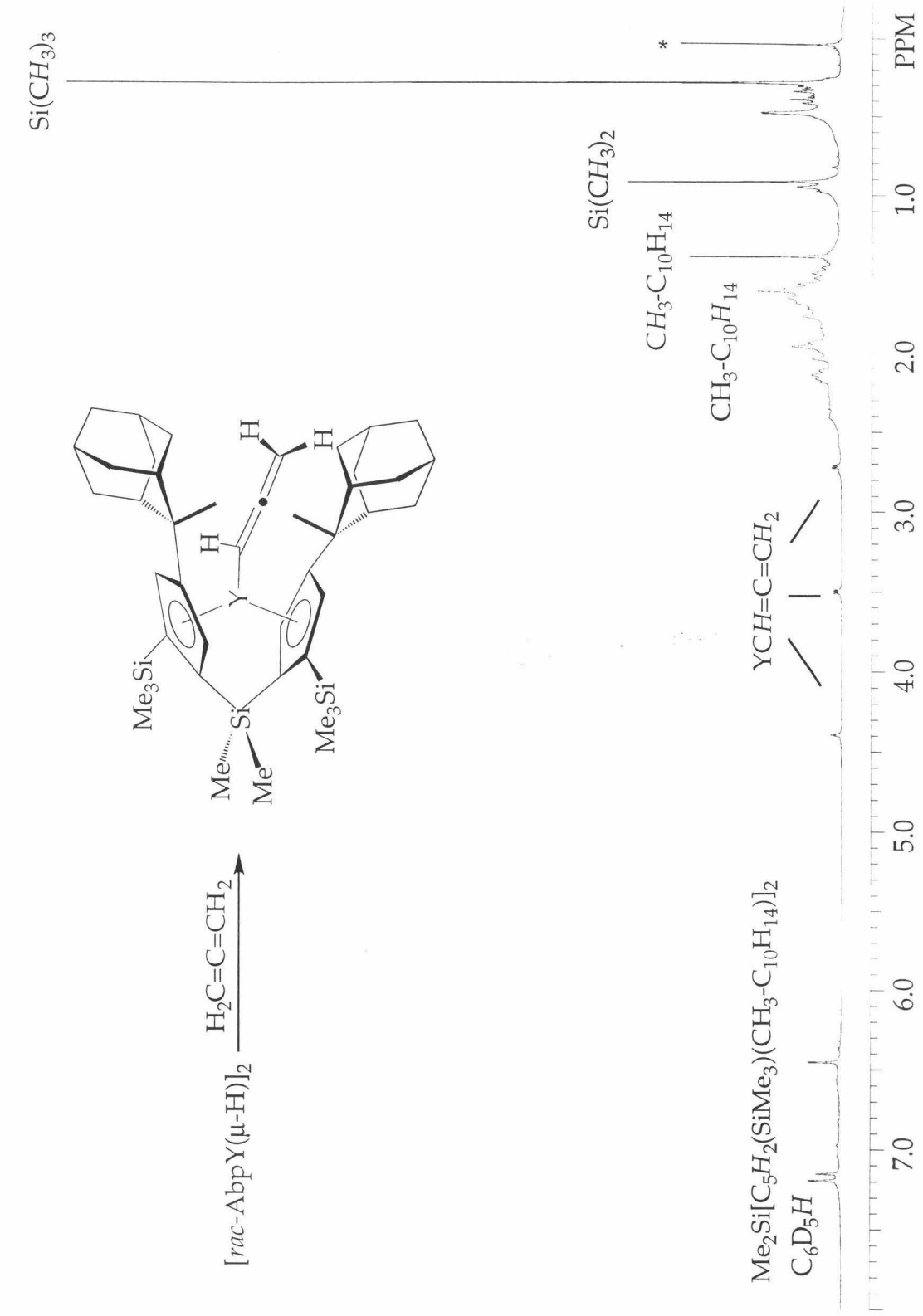

Figure 18. 500 MHz ^{1}H NMR spectrum (C_6D_6) of *rac*-AbpYCH=C=CH_2 (**21**); * = residual $H_2C(SiMe_3)_2$ from hydrogenolysis of **18**.

with the Y-CH_3 bond of $CnY(CH_3)_3$ to give an equilibrium mixture of the propargyl and allenyl complexes shown in Figure 19.

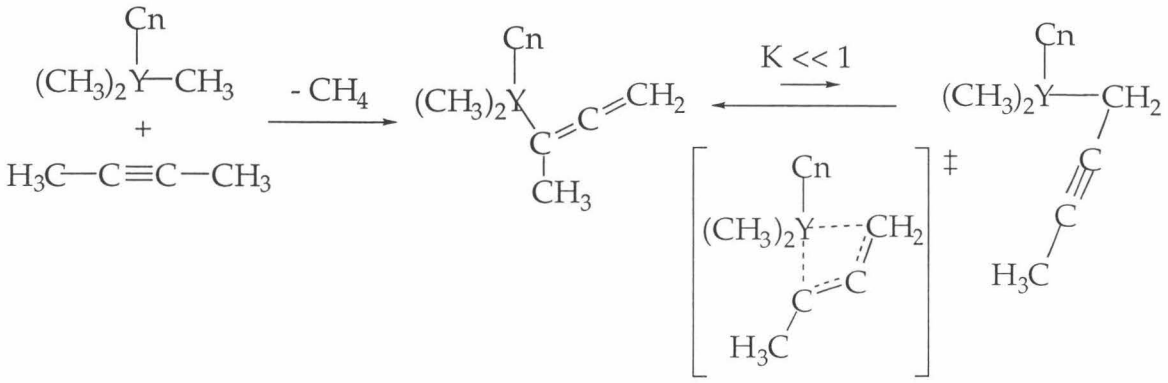

Figure 19. Formation of an equilibrating mixture of propargyl and allenyl complexes are observed from the reaction of 2-butyne with $CnY(CH_3)_3$.

Surprisingly, treatment of **20** with one equivalent of 2-butyne (C_6D_{12}) proceeds over the course of minutes at room temperature to generate the butenyl complex **22**, the product of alkyne insertion into the Y-H bond of **19** (Figure 20). The overall C_2-symmetry of **22** indicates rapid rotation about the Y-C bond. Formation of the propargyl complex **23** is unlikely based on the observed downfield chemical shift (^{1}H NMR) of the single proton assigned as H_a (4.76 ppm), the only vinylic proton resonance observed. The observed NMR spectrum is also inconsistent with the allenyl complex **24**. The C_2-symmetry of the *rac*-Abp ligand array renders the allenyl methylene hydrogens (H_{b1} and H_{b2}) magnetically inequivalent, regardless of the rate of rotation about the Y-C bond.

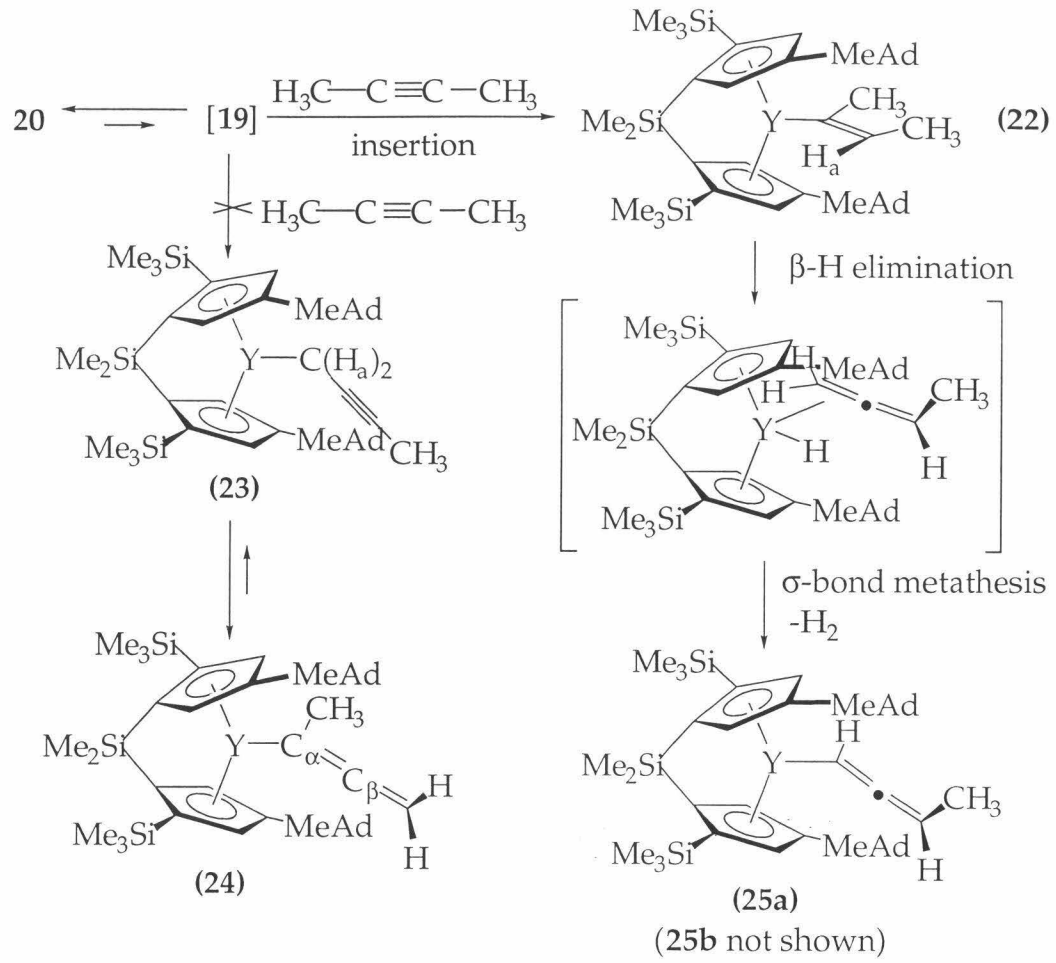

Figure 20. Alkyne insertion into **19**, followed by β-H elimination and subsequent σ-bond metathesis generates a pair of diastereomeric yttrium-methylallyl complexes.

The butenyl complex **22** undergoes a rearrangement over the course of 48 hours to give a ~1:1 mixture of two new complexes (**25a,b**) the NMR spectra of **25a,b** are consistent yttrium-methylallenyl complexes (Figure 21). A mechanism accounting for formation of **25a** and **25b** is given in Figure 20. β-Hydride elimination from **22** generates a 1,2-butadiene-complex, which then rapidly undergoes σ-bond metathesis with the available Y-H bond to generate dihydrogen and yttrium-methylallyl complexes. The β-hydride elimination step from an sp^2-hybridized carbon to generate methylallene has been noted for 2-butenyl derivatives of iridium[41] and molybdenum,[42] and is implicated in the observed rearrangements of $Cp^*_2M(C(CH_3)=CHCH_3)H$ (M=Zr, Hf) to the corresponding crotyl-hydrides (equation 11).[43]

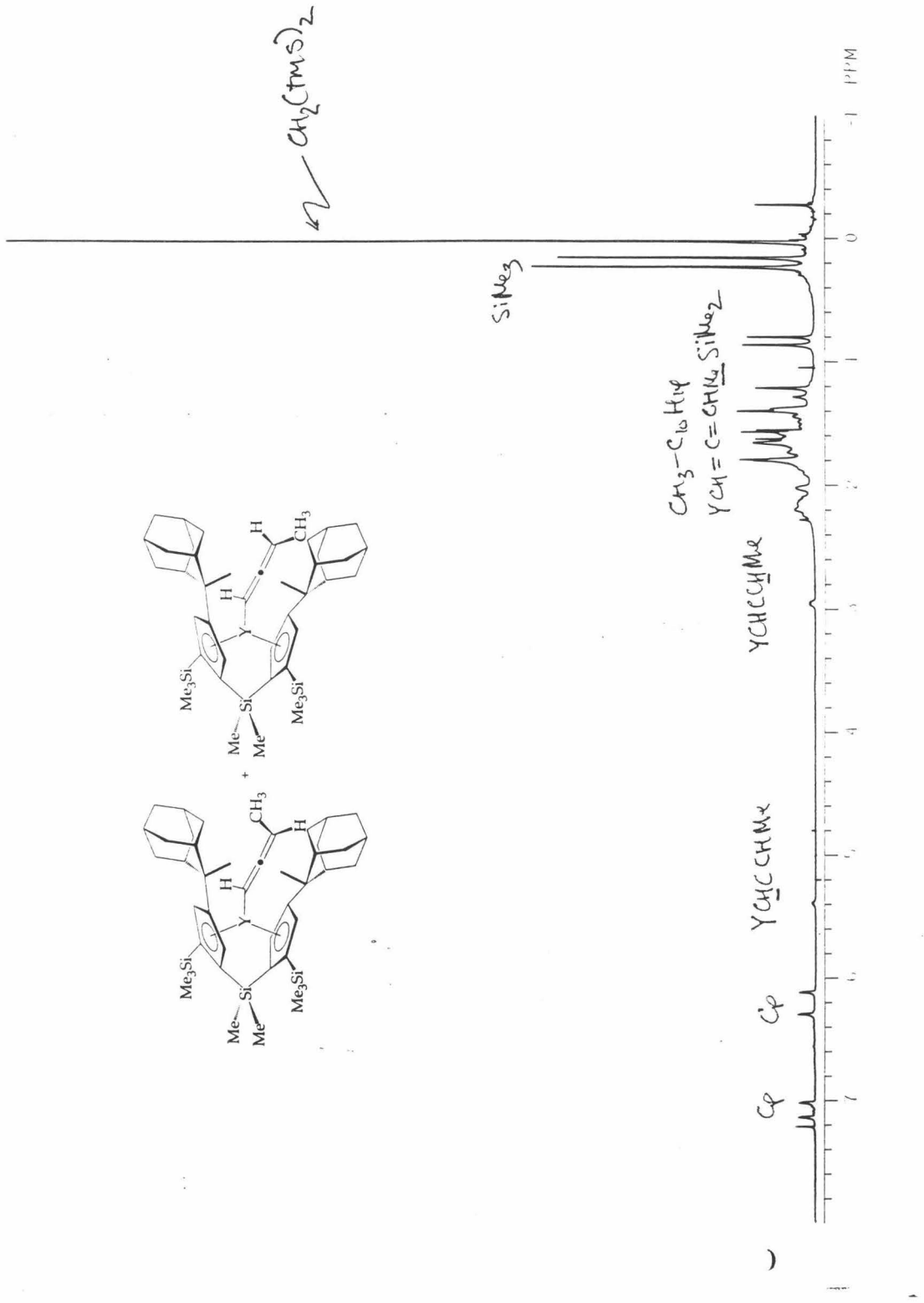

Figure 21. 300 MHz ^{1}H NMR spectra (cyclohexane-d_{12}) of *rac*-AbpYCH=C=CHMe (**25a,b**).

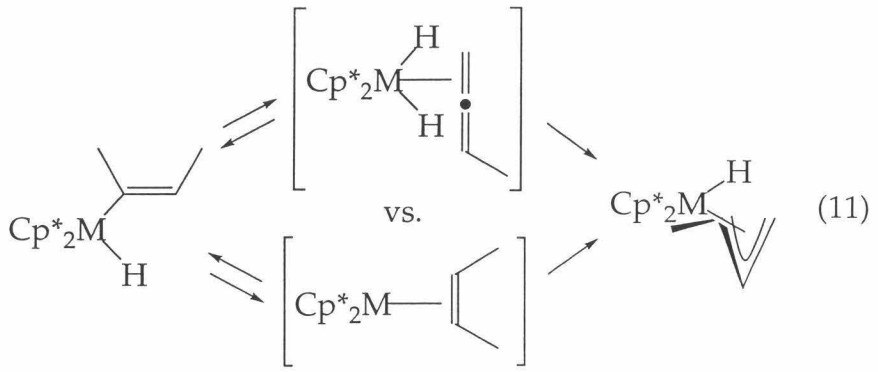

(11)

The mixture of observed final products arises from the two possible C-H bonds with which the chiral *rac*-AbpYH moiety can react.[44] The observed C_2- symmetry of the Abp ligand arrays of each of the diastereomers of **25** is indicative of rapid rotation about the Y-C bonds (Figure 22).

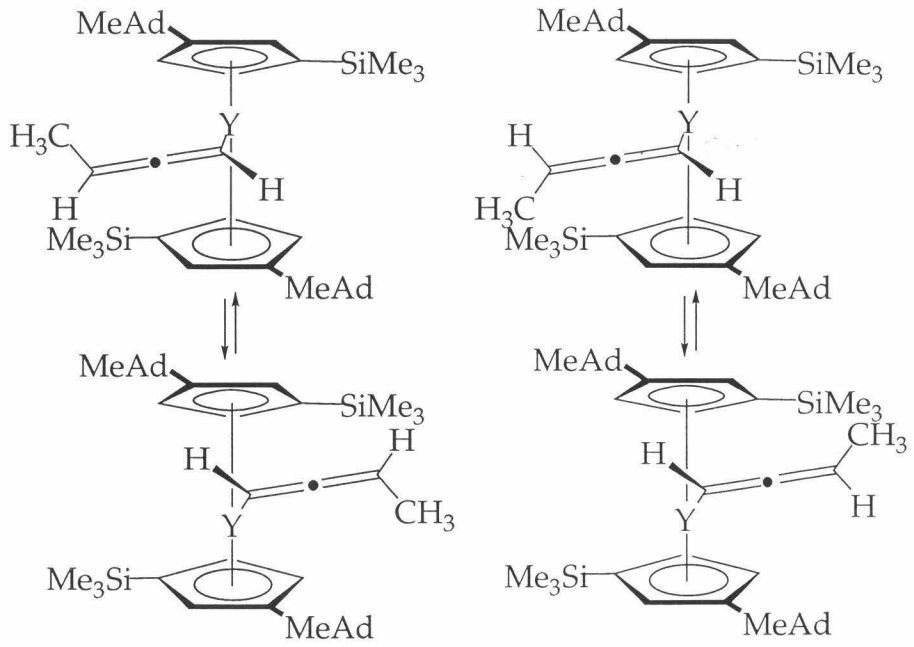

(25a) **(25b)**

Figure 22. Y-C bond rotation for the diastereomeric pair **25a,b**.

The observed ^{1}H NMR spectra are inconsistent with the formation of either **23** or **24**. The observed relative intensities of the vinylic Cp and methylallyl methylene hydrogens are inconsistent with both the propargyl complex **23** and the allenyl complex **24**. Furthermore, **23** should exhibit overall C_2- symmetry due to facile rotations about the Y-C bond; this is

inconsistent with the 4 Cp, 2 $SiMe_3$, 2 $SiMe_2$ (linker), and 2 *Me*Ad resonances actually observed. Similarly, rotation about the Y-C bond in the allenyl complex **24** (as is observed for **21**) would result in an observed C_2- symmetric complex by NMR, which runs contrary to the pairwise [Abp] ligand resonances observed. The possibility of hindered rotation about the Y-C bond in **24** accounting for a complex with overall C_1- symmetry is refuted on the basis of the pair of alkenyl-methyl resonances in the observed NMR spectra; the substitution of the alkenyl moiety in **24** is such that the methyl group resides in the plane defined by Y-C_α-C_β, which results in a single CH_3 resonance, regardless of the rate of Y-C bond rotation. An entirely coincidental 1:1 mixture of **24** and **25** accounting for the observed spectra is theoretically possible, although unlikely based on the extreme bias of the previously observed CnY equilibrium, which heavily favors the alkenyl complex at room temperature.

Conclusions

Incorporation of methyladamantyl substituents into the β-positions of group III *ansa*-metallocenes is a successful strategy for preventing the formation of bridging hydride dimers. Only very small quantities (~3% of the overall product mixture) of the $(\mu\text{-H})_2$ dimers are formed upon hydrogenolysis of *meso*-AdpM(C_3H_5). The observed reactivity of *meso*-AdpM(C_3H_5) with H_2 is consistent with formation of highly reactive 14-electron d0- metal-hydride species that, since formation of $(\mu\text{-H})_2$ dimers is disfavored because of the bulky methyladamantyl substituents readily activate available C-H bonds. Intermolecular Cp C-H bond activation is thought to be the preferred mode of decomposition for the *meso*- complexes, although other possible mechanisms include intramolecular (methyladamantyl) and solvent C-H activation.

rac-AbpYCH($SiMe_3$)$_2$ (**18**), obtained from the treatment of [*rac*-AbpY(μ-Cl)]$_2$, is an active ethylene polymerization catalyst. Although the monomeric [*rac*-AbpYH] (**19**) is not observed directly from the hydrogenolysis of **18**, the ability of the methyladamantyl groups to perturb the hydride monomer-dimer equilibria are evident from the formation of only a single $(\mu\text{-H})_2$ dimer,

20. Variable temperature NMR experiments show that the heterochiral [*rac*-AbpY(μ-H)]$_2$ dimer is not in equilibrium with **20** (the homochiral dimer) at 25 °C, and the heterochiral dimer is not formed even as a kinetic hydrogenolysis product en route to the thermodynamically stable **20**.

The methyladamantyl groups that prevent formation of the heterochiral dimer also appear to inhibit multiple α-olefin insertions and s-bond metathesis with arene substrates. The observation that **20** is a 1-butene hydrogenation catalyst indicates that the [Abp] ligand array is not too sterically bulky to prevent insertion of a single olefin monomer into **19**, although steric factors undoubtedly play a major role in the inability of **20** to act as olefin polymerization catalyst. Similar steric factors are believed to preclude the approach of arene C-H bonds, thus rendering **20** considerably more inert to H/D scrambling in perdeuterated aromatic solvents than are complexes such as Cp^*_2Sc-H.

Both allene and 2-butyne react cleanly with **20**. Activation of a C-H bond in allene results in the formation of the yttrium-allenyl complex **21**; no insertion of allene to generate η^3-allyl complexes is observed. Insertion of 2-butyne into the Y-H bond of **19** gives the butenyl complex **24**. This reactivity is somewhat surprising, given the tendency of allene to resist insertion into **19** and the previously observed C-H activation of 2-butyne with $CnY(CH_3)_3$ to generate an equilibrium mixture of yttrium-propargyl and yttrium-allenyl complexes. The [AbpY]-butenyl complex undergoes β-hydride elimination from an sp^2- hybridized carbon to generate a methylallenyl complex which rapidly undergoes σ-bond metathesis with available **19** to produce **25a,b**, a diastereomerically related pair of yttrium-methylallyl compounds.

Assessment of whether dissociation of **20** proceeds by a dissociative pathway or an associative pathway is complicated by the formation of only the homochiral dimer (thus precluding homochiral-heterochiral equilibration studies) and the fact that the observed reactivity of **20** is a function of both the dissociation of the (μ-H)$_2$ dimer and the subsequent reaction with substrate. Variable temperature NMR studies in the presence of excess dihydrogen show no evidence for a rapid dissociation of **20** into monomeric **19** at 25 °C. Decomposition of **20** occurs within minutes in the presence of substrates such as olefins, yet **20** reacts over the course of 24 hours in the presence of analogous concentrations of allene. The addition of trimethylphosphine fails to result in a marked increase in the observed rate

of the reaction with allene, suggesting a dissociative mechanism for formation of the 14-electron monomer **19**.

Experimental Section

General Considerations: All air and/or moisture sensitive compounds were manipulated using standard high vacuum line, Schlenk, or cannula techniques or in a dry box under a nitrogen atmosphere, as described previously.[45] Argon, hydrogen and deuterium gases were purified and dried by passage over columns of MnO on vermiculite and activated molecular sieves. Solvents were stored under vacuum over titanocene[46] or sodium benzophenone ketyl.

Allylmagnesium bromide was purchased from Aldrich and used as received. $LiCH(SiMe_3)_2$ was prepared using the method of Cowley[47] and sublimed prior to use. Ethylene was dried in a toluene solution of $(i\text{Bu})_3\text{Al}$ prior to use. 1-butene, 1-hexene, 3,3-dimethylpropene, 2-butyne, *tert*-butylacetylene, and trimethylsilylacetylene were stored over activated sieves, and 1-pentene was stored over Na/K. Allene was purchased from Aldrich and purified by several cycles of freeze-pump-thaw.

NMR spectra were recorded on a Bruker AM500 (500.13 MHz for ^1H, 125.76 MHz for ^{13}C) or a GE QE-300 (300 MHz for ^1H, 75.5 MHz for ^{13}C) spectrometer. All shifts reported for proton and carbon NMR were referenced to solvent. NMR tube reactions were carried out using flame sealed NMR tubes or J. Young type Teflon-valved NMR tubes purchased from Wilmad. Elemental analyses were performed at the Caltech Elemental Analysis Facility by Fenton Harvey.

Preparation of *meso*-AdpSc(η^3-C_3H_5) (16). In a 100 ml roundbottom flask was placed 2.5 mmol of AdpScCl-LiCl-$(THF)_2$ and a magnetic stir bar. Approximately 50 ml of Et_2O was vacuum transferred into the roundbottom, and the maroon-colored solution was warmed to room temperature with stirring. After cooling the solution back to -78 °C, 2.5 ml of allylmagnesium bromide (1.0 M solution in Et_2O, 1.0 eq.) was injected against a heavy argon counterflow. The solution was stirred at -78 °C for 15 minutes, after which time the cooling bath was removed and the solution was allowed to warm to room temperature. After stirring at 25 °C for 6 hours, Et_2O was removed from

the dark orange solution *in vacuo*, and the brown foam was left open to dynamic vacuum for 10 hours. The 100 ml roundbottom flask was brought into the glove box and attached to a medium porosity pencil frit equipped with a 100 ml roundbottom flask and a 90° needle valve. Two 20 ml aliquots of petroleum ether were successively vacuum transferred onto and off of the brown solid, followed by a similar procedure using 20 ml of toluene, and two additional petroleum ether washes (40 ml each); the purpose of these washings was to remove residual THF from the LiCl and Mg-halide byproducts prior to filtration. The final petroleum ether solution was filtered, and PE was removed in vacuo, leaving a dark yellow powder, which was dried in vacuo for approximately 6 hours, affording 480 mg (0.84 mmol, 34% yield) of AdpSc(η^3-C_3H_5). Contamination of the AdpScCl starting material with excess ,LiCl does not affect the purity or yield of the (η^3-C_3H_5) product, as the crude reaction mixture from Li_2Adp and $ScCl_3(THF)_3$ can also be alkylated cleanly with C_3H_5MgBr. Anal. Calcd. for $C_{37}H_{51}SiSc$: C, 78.11; H, 9.05. Found (with V_2O_5 added): C, 78.85, 75.78; H, 10.50, 9.98; (without oxidant) C, 74.90, 75.50; H, 9.13, 9.57.

Preparation of *meso*-AdpY(η^3-C_3H_5) (17). A 250 ml roundbottom flask, charged with 3.24 mmol of AdpYCl-LiCl-$(solv)_2$ is attached to a medium sized coarse frit; 115 ml of diethyl ether is vacuum transferred onto the solid and warmed slightly with stirring, giving a clear tan solution. Against a heavy counterflow of argon, 3.6 ml of allymagnesium bromide (1.0 M in Et_2O, 1.1 eq.) is syringed into the solution at -78 °C. After 10 minutes of stirring at -78 °C, the cooling bath is removed and the solution allowed to warm to room temperature. After three hours of stirring at room temperature, 60 ml of Et_2O is removed in vacuo, and the remaining orange solution was stirred at room temperature for another five hours. The solution is filtered, and the fine white insoluble material is washed once with a small portion of Et_2O. Ether is removed in vacuo, leaving a large amount of an orange foam, which is dried *in vacuo* overnight. The roundbottom flask containing the Et_2O soluble species is put on a fine pencil frit, and 40 ml of benzene is vacuum transferred onto the solid. The solution is warmed to room temperature and filtered. The benzene is removed in vacuo, and the benzene-soluble species is dried for 6 hours by exposure to dynamic vacuum, leaving a yellow microcrystalline solid (1.699 g, 2.77 mmol, 85% yield).

Preparation of *rac*-AbpYCH(SiMe$_3$)$_2$ (18): A 25 ml roundbottom flask is charged with 276.6 mg (0.358 mmol) of [*rac*-AbpY(μ-Cl)]2 and 166.38 mg (0.358 mmol) of LiCH(SiMe3)2 and attached to a 180° needle valve. The flask is evacuated on the vacuum line, and toluene (15 ml) is distilled onto the solids (-78 °C); the clear orange solution is warmed to room temperature and stirred at 25 °C for 4 hours. Toluene is removed from the yellow solution with white precipitate, and benzene (10 ml) is distilled onto the resulting white solid, cooled to -10 °C, and removed *in vacuo*. The flask is brought into the box, attached to a small swivel frit assembly, and evacuated. The diethyl ether (10 ml) soluble species are again dried by freezing a benzene solution (5 ml) and slowly removing solvent under reduced pressure. The pentane (1 ml) insoluble species are isolated by a cold (-78 °C) filtration, affording 77.1 mg of white solid (0.088 mmol, 25% yield). Elemental analysis: Calculated (Found, with added V_2O_5) C: 64.46 (61.00, 61.16); H: 9.34 (8.76, 8.45); N: 0.00 (0.00, 0.00), Calculated (Found, without added oxidant) C: 64.46 (60.61, 60.98); H: 9.34 (8.53, 9.08); N: 0.00 (0.00, 0.00).

Preparation of [*rac*-AbpYH]$_2$ (20): A J-Young NMR tube is charged with 15.2 mg of **18** and evacuated on the vacuum line. Cyclohexane-d_{12} (0.4 ml) is distilled on from titanocene. The solution warmed to room temperature affording a tan solution with a small amount of finely divided white precipitate, and one atmosphere of dihydrogen is admitted to the NMR tube. Within 2 minutes of the addition of H_2, the solution is clear and light tan. ^{1}H NMR indicates complete conversion to **20** within several minutes at 25 °C.

Preparation of *rac*-AbpYCH=C=CH$_2$ (21): A J-Young NMR tube is charged with 15.0 mg (0.0171 mmol) of **18**. Cyclohexane-d_{12} (0.4 ml) is distilled onto the solid from titanocene (-78 °C), and 1 atm H_2 admitted to the tube. The solution is warmed to room temperature, and agitated overnight. The contents of the NMR tube are frozen (-78 °C), and excess dihydrogen removed *in vacuo*. Allene (0.0690 mmol, 4.0 equivalents) is transferred into the NMR tube using a liquid nitrogen bath. The solution is warmed to room temperature, and ^{1}H NMR spectra are taken periodically. Half of the starting **18** has reacted after 3.5 hours at room temperature, and complete conversion to **21** is observed after 25 hours at 25 °C. Volatiles are removed *in vacuo*, and

cyclohexane-d_{12} (0.4 ml) is vacuum transferred back onto the light yellow solid.

Preparation of *rac*-AbpYC(CH_3)=CH(CH_3) (22) and *rac*-AbpYCH=C=CH(CH_3) (25): A J-Young tube is charged with 11.4 mg (0.0130 mmol) of **18** and is evacuated on the vacuum line. Cyclohexane-d12 (0.4 ml) is distilled onto the solid, the tube is sealed, and the solution warmed to room temperature with shaking. After cooling to -78 °C, 1 atmosphere of dihydrogen is admitted to the tube, the tube is sealed, warmed to room temperature and agitated for 30 minutes. The solution is cooled to -78 °C and volatiles are removed *in vacuo*. 2-Butyne (0.0135 mmol, 1.04 equivalents) is vacuum transferred into the tube from a calibrated gas bulb, the tube is sealed, and the solution is warmed to 25 °C. Proton NMR spectra are taken periodically to monitor the extent of the reaction. Conversion to **22** is observable within 20 minutes at room temperature; 25% of **20** is consumed after 60 minutes at 25 °C. Conversion of **22** to **25** is observed within 4 hours of addition of 2-butyne, and the reaction has gone to completion after 43 hours at 25 °C.

References and Notes

1. Collman, J. P.; Hegedus, L. S.; Norton, J. R.; Finke, R. G. *Principles and Applications of Organotransition Metal Chemistry*; University Science Books: Mill Valley, CA, **1987**, p. 577.

2. Edelmann, F. T., in *Comprehensive Organometallic Chemistry II*; Abel, E. W., Stone, F. G. A., Wilkinson, G. and Lappert, M. F., Eds.; Pergamon Press: Tarrytown, NY, **1995**; *Vol. 4*, p. 11.

3. Bochmann, M., in *Comprehensive Organometallic Chemistry II*; Abel, E. W., Stone, F. G. A. and Wilkinson, G., Eds.; Elsevier Science, Inc.: Tarrytown, NY, **1995**; *Vol. 4*, p. 273.

4. Guram, A. S.; Jordan, R. F., in *Comprehensive Organometallic Chemistry II*; Abel, E. W., Stone, F. G. A. and Wilkinson, G., Eds.; Elsevier Science, Inc.: Tarrytown, NY, **1995**, p. 589.

5. Jordan, R. F.; LaPointe, R. E.; Bradley, P. K.; Baezinger, N. *Organometallics* **1989**, *8*, 2892.

6. Horton, A. D. *Organometallics* **1992**, *11*, 3271.

7. Thompson, M. E.; Baxter, S. M.; Bulls, A. R.; Burger, B. J.; Nolan, M. C.; Santarsiero, B. D.; Schaefer, W. P.; Bercaw, J. E. *J. Am. Chem. Soc.* **1987**, *109*, 203.

8. Yoder, J. C.; Bercaw, J. E. , Unpublished results.

9. For examples of 2,1 insertions of acetylenes into M^+-R complexes, see: Guram, A. S.; Jordan, R. F.; Taylor, D. F. *J. Am. Chem. Soc.*, **1991**, *113*, 1833.

10. Guram, S. A.; Guo, Z.; Jordan, R. F. *J. Am. Chem. Soc.* **1993**, *115*, 4902.

11. Horton, A. D. *J. Chem. Soc. Chem. Commun.* **1992**, 185.

12. Horton, A. D.; Orpen, A. G. *Angew. Chem. Int. Ed. Engl.* **1992**, *31*, 876.

13. den Haan, K. H.; Wielstra, Y.; Teuben, J. **1987**.

14. For reactions of internal alkynes with non-Cp containing early transition metal complexes, see: a) Uhrhammer, R.; Black, D. G.; Gardner, T. G.; Olsen, J. D.; Jordan, R. F. *J. Am. Chem. Soc.*, **1993**, *115*, 8493. b) Hajela, S. P.; Schaefer, W. P.; Bercaw, J. E. *J. Organomet. Chem.* , **1997**, *532*, 45.

15. Horton, A. D.; Orpen, A. G. *Organometallics* **1992**, *11*, 8.

16. Horton, A. D.; Orpen, A. G. *Organometallics* **1991**, *10*, 3910.

17. Heeres, H. J.; Heeres, A.; Teuben, J. H. *Organometallics* **1990**, *9*, 1508.

18. Ionic radius (6 coordinate): Sc^{3+} 0.75Å; Y^{3+} 0.90Å; La^{3+} 1.03Å; Ce^{3+} 1.07Å; Zr^{4+} 0.72Å; Shannon, R. D. *Acta. Cryst., Sect. A*, **1976**, *32*, 751.

19. Brintzinger, H. H.; Fischer, D.; Mulhaupt, R.; Rieger, B.; Waymouth, R. N. *Angew. Chem. Int. Ed. Eng.* **1995**, *34*, 1143.

20. Bochmann, M. *J. Chem. Soc., Dalton Trans.* **1996**, 255.

21. Pino, P.; Galimberti, M. *J. Organomet. Chem.* **1989**, *370*, 1.

22. Krauledat, H.; Brintzinger, H. H. *Angew. Chem. Int. Ed. Engl.* **1990**, *102*, 1412.

23. Waymouth, R.; Pino, P. *J. Am. Chem. Soc.* **1990**, *112*, 4911.

24. Pino, P.; Cioni, P.; Wei, J. *J. Am. Chem. Soc.* **1987**, *109*, 6189.

25. The (R,S) designation refers to metallocenes derived from (R)-binaphthol, which results in metallocenes of (S) stereochemistry.

26. Longo, P.; Grassi, A.; Pellecchia, C.; Zambelli, A. *Macromolecules* **1987**, *20*, 1015-1018.

27. Zambelli, A.; Pellachia, C.; Oliva, L. *Makromol. Chem. Macromol. Symp.* **1991**, *48/49*, 297.

28. Gilchrist, J. H.; Bercaw, J. E. *J. Am. Chem. Soc.* **1996**, *118*, 12021.

29. Stern, D.; Sabat, M.; Marks, T. J. *J. Am. Chem. Soc.* **1990**, *112*, 9558.

30. den Haan, K. H.; Wielstra, Y.; Teuben, J. *Organometallics* **1987**, *6*, 2053.

31. Booj, M.; Deelman, B. J.; Duchateau, R.; Postma, D. S.; Meetsma, A.; Teuben, J. H. *Organometallics* **1993**, *12*, 3531.

32. Watson, P. L. *J. Chem. Soc. Chem. Commun.* **1983**, 276.

33. Bunel, E. E., Ph.D. Thesis, California Institute of Technology, **1989**.

34. Hajela, S.; Schaefer, W. P.; Bercaw, J. E. *Acta. Crystallogr.* **1992**, *C48*, 1771.

35. Bercaw, J. E. *Adv. Chem. Ser.* **1978**, *167*, 136.

36. den Haan, K. H.; Wielstra, Y.; Eshuis, J. J. W.; Teuben, J. H. *J. Organomet. Chem.* **1987**, *323*, 181.

37. Mitchell, J. P.; Hajela, S.; Brookhart, S. K.; Hardcastle, K. I.; Henling, L. M.; Bercaw, J. E. *J. Am. Chem. Soc.* **1996**, *118*, 1045.

38. Although the analogous reactions with 1-pentene are not clean, $Cp^*(C_5H_5BN(CHMe_2)_2)HfH(PMe_3)$ cleanly inserts neohexene to afford the $Hf\text{-}CH_2CH_2CMe_3$ complex. M.S. Thesis, California Institute of Technology, 1996.

39. Levy, C. J.; Bercaw, J. E. , Unpublished results.

40. Hajela, S.; Schaefer, W. P.; Bercaw, J. E. *J. Organomet. Chem.* **1997**, *532*, 45.

41. Schwartz, J.; Hart, D. W.; McGiffert, B. *J. Am. Chem. Soc.* **1974**, *96*, 5613.

42. Bottrill, M.; Green, M. *J. Am. Chem. Soc.* **1977**, *99*, 5795.

43. McDade, C.; Bercaw, J. E. *J. Organomet. Chem.* **1985**, *279*, 281.

44. Although only the reaction of 1,2-butadiene with metallocenes of (S) chirality are shown explicity, it is assumed that the (R) metallocenes react with both available 1,2-butadiene methylene hydrogens to give the enantiomeric pair of the diasteromeric pair of yttrium-butadienyl complexes shown.

45. Burger, B. J.; Bercaw, J. E. *New Developments in the Synthesis, Manipulation, and Characterization of Organometallic Compounds*; ACS Symposium Series, **1987** *357*,

46. Marvich, R. H.; Brintzinger, H. H. *J. Am. Chem. Soc.* **1971**, *93*, 2046.

47. Cowley, A. H.; Kemp, R. A. *Synth. React. Inorg. Metal-Org. Chem.* **1981**, *11*, 591.

Appendix B: ^{1}H and ^{13}C NMR Data For 16-25

Table 1. Proton NMR assignments for **16-25** (500 MHz, C_6D_6, 25 °C unless otherwise noted)

Compound	Assignments	δ (ppm)	J_{H-H}
meso-AdpSc(η^3-C_3H_5) (**16**)	Me_2Si (3H)	0.23 (s)	
	(3H)	0.69 (s)	
	MeAd (6H)	0.85 (s)	
	Me**Ad** (29H)	1.46, 1.49, 1.55, 1.57, 1.59, 1.62, 1.66, 1.67, 1.70, 1.78, 1.92, 2.06, 2.08, 2.39 (m)	
	Cp (2H)	5.54 (m)	2.6
	(2H)	5.98 (m)	2.4
	(2H)	6.55 (m)	2.5
	η^3-$H_2CC\mathbf{H}CH_2$ (1H)	7.19 (m)	12.3
meso-AdpY(η^3-C_3H_5) (**17**)	Me_2Si (3H)	0.41 (s)	
	(3H)	0.72 (s)	
	MeAd (6H)	0.97 (s)	
	Me**Ad** (29H)	1.45, 1.48, 1.51, 1.54, 1.56, 1.58, 1.60, 1.65, 1.78, 1.86, 1.94, 1.98, 2.00, 2.04 (m)	
	η^3-$\mathbf{H}_2CCHC\mathbf{H}_2$ (*syn*)	2.66 (s)	
	(2H)		7.4
	η^3-$\mathbf{H}_2CCHC\mathbf{H}_2$ (*anti*)	3.39 (d)	2.5
	(2H)		
	Cp (2H)	5.79 (m)	
	(2H)	5.98 (s)	7.7,
	(2H)	6.12 (s)	1.3
	η^3-$H_2CC\mathbf{H}CH_2$ (1H)	6.72 (m)	(J_{Y-H})
rac-AbpYCH($SiMe_3$)$_2$ (**18**)	$CH(SiMe_3)_2$	0.26	2.0
	Me_3Si (43H)	0.28, 0.32, 0.35, 0.36 (s)	(J_{Y-H})
	Me_2Si (6H)	0.91, 0.93 (s)	
	MeAd (51H total)	1.63, 1.68	
	Me**Ad**	1.43, 1.48, 1.59, 1.66, 1.71, 1.80, 1.92, 2.10, 2.14, 2.19, 2.43, 2.47 (br)	
	Cp (4H)	6.47, 6.46, 7.10, 7.12 (d)	

Table 1. (continued)

Compound	Assignments	δ (ppm)	J_{H-H}
rac-AbpYCH($SiMe_3$)$_2$ C_6D_{12}	C*H*($SiMe_3$)$_2$ Me_3Si (36H) Me_2Si (6H) **Me**Ad (6H) Me**Ad** (16H) (12H) Cp (4H)	not located 0.01, 0.03, 0.23, 0.24 (s) 0.89, 0.90 (s) 1.55, 1.56 (s) 1.58, 1.61, 1.66, 1.79, 1.81 (br) 2.20, 2.24, 2.27, 2.31 (br) 6.27 (d) 6.28 (d) 6.87 (d) 6.89 (d)	 1.9 1.9 1.7 1.5
rac-AbpYCH($SiMe_3$)$_2$ C_7D_{14}	C*H*($SiMe_3$)$_2$ Me_3Si (38H) Me_2Si (4H) **Me**Ad Me**Ad** Cp (3-4H)	not located 0.01, 0.03, 0.23, 0.24 (s) 0.89, 0.90 (s) 1.54, 1.56 (s) 1.60, 1.62, 1.66, 1.69, 1.79, 1.82, 2.17, 2,24, 2.32 (br) 6.27, 6.88 (d)	
rac-AbpYCH($SiMe_3$)$_2$ (**18**) C_7D_8	C*H*($SiMe_3$)$_2$ Me_3Si (36H) Me_2Si (6H) **Me**Ad (6H) Me**Ad** (7H) (11H) (6H) (4H) Cp (4H)	not located 0.24, 0.28, 0.34, 0.35 (s) 0.92, 0.94 (s) 1.60, 1.66 (s) 1.20 - 1.60 (br) 1.68 - 2.00 (br) 2.10 - 2.32 (br) 2.44 (m) 6.43, 6.44, 7.07, 7.09 (s)	
rac-[AbpY(μ-H)]$_2$ (**20**) C_6D_6 (300 MHz)	Me_3Si (18H) Me_2Si (6H) **Me**Ad (6H) Me**Ad** Y(μ-H)$_2$Y (1H) Cp (4H)	0.46 (s) 0.96 (s) 1.66 (s) 1.83, 1.97, 1.99, 2.06, 2.23, 2.30 (br, overlapping) 4.76 (t) 6.54, 6.92 (s)	 $^1J_{YH}$= 31.3

Table 1. (continued)

Compound	Assignments	δ (ppm)	J_{H-H}
rac-[AbpY(μ-H)]$_2$ (**20**)	Me_3Si (18H)	0.26 (s)	
C_6D_{12}	Me_2Si (6H)	0.83 (s)	
	MeAd (6H)	1.42 (s)	
	Me**Ad** (4H)	1.45 (d)	12.0
	(14H)	1.60, 1.62, 1.65, 1.71, 1.81 (overlapping)	
	(2H)	2.10 (s)	
	(4H)	2.13 (d)	12.0
	(4H)	2.23 (d)	10.7
	Y(μ-H)$_2$Y (1H)	4.48 (t)	$^1J_{YH}$= 31.0
	Cp (4H)	6.24, 6.64 (s)	
rac-[AbpY(μ-H)]$_2$ (**20**)	Me_3Si (18H)	0.17 (s)	
C_7D_{14}	Me_2Si (6H)	0.73 (s)	
	MeAd (6H)	1.31 (s)	
	Me**Ad** (18H)	1.50, 1.53, 1.55 (overlap)	
	(5H)	1.72 (br)	
	(3H)	2.02 (br)	
	(2H)	2.12 (br)	
	Y(μ-H)$_2$Y (1H)	4.39 (t)	$^1J_{YH}$=31.2
	Cp (4H)	6.15, 6.55 (s)	

Compound	Assignments	δ (ppm)	J_{H-H}
rac-AbpYCH=C=CH_2 (**21**)	Me_3Si (18H)	0.29 (s)	
	Me_2Si (6H)	0.91 (s)	
	MeAd (6H)	1.30 (s)	
	Me**Ad** (3H)	1.46, 1.49, 1.56 (overlapping)	
	(9H)	1.61, 1.65, 1.71 (overlapping)	
	(2H)	1.77	
	(6H)	1.93, 1.96	
	(2H)	2.04	
	(6H)	2.11, 2.14, 2.16, 2.18 (overlapping)	
	allenyl (1H)	2.71 (dd)	3.1, 7.7
	allenyl (1H)	3.50 (dd)	3.8, 7.7
	allenyl (1H)	4.39 (t)	2.9
	Cp (2H)	6.45 (d)	2.0
	Cp (2H)	7.19 (d)	1.9
rac-AbpYC(CH_3)=CH(CH_3) (**24**)	Me_3Si (18H)	0.23 (s)	
	Me_2Si (6H)	0.85 (s)	
	YC(CH_3)=CH(CH_3), MeAd (overlapping)	1.18 - 2.40	
	YC(CH_3)=C*H*(CH_3)	4.76 (m)	
	Cp (4H)	6.71, 6.29 (s)	

Table 1. (continued)

Compound	Assignments	δ (ppm)	J_{H-H}
rac-AbpYCH=C=CH(CH_3) (**25 a,b**)	Me_3Si (36H)	0.16, 0.23 (s)	
	Me_2Si (12H)	0.80, 0.86 (s)	
	MeAd	1.21, 1.40 (s)	
	YCH=C=CH(C*H*$_3$) (6H)	1.55, 1.62 (s)	
	Me**Ad** (overlapping)	1.40 - 2.40 (br)	
	YC*H*=C=C*H*(CH_3) (2H)	2.94, 2.96 (m)	
	YC*H*=C=C*H*(CH_3) (2H)	5.39, 7.10 (m)	
	Cp (8H)	6.12, 6.30, 7.02, 7.14 (s)	

Table 2. Proton decoupled ^{13}C NMR assignments for **18**, **20** (125 MHz, 25 °C unless otherwise noted)

Cmpd	solv	Assignments	δ (ppm)
rac-AbpYCH($SiMe_3$)$_2$ (**18**)	C_6D_6	Me_2Si	0.76, 0.96
		Me_3Si	3.05, 3.19, 6.08, 6.32
		Y-C	30.94 ($^1J_{(89Y-13C)}$ = 38.8 Hz)
		MeAd	28.24, 28.29, 28.38, 28.41, 31.13, 33.24, 33.59, 33.73, 33.89, 34.08, 34.48, 34.72, 34.74, 35.23, 37.06, 37.19, 38.95, 39.58, 39.94, 40.49, 41.82, 42.21
		Cp	121.40, 122.50, 125.79, 126.44, 127.89, 131.42, 151.57, 152.77

Table 2. (continued)

Cmpd	solv	Assignments	δ (ppm)
rac-AbpYCH(SiMe$_3$)$_2$ (**18**)	C_6D_{12}	Me_2Si	0.58, 0.72
		Me_3Si	2.74, 2.90, 5.71, 5.91
		Y-C	31.41 ($^1J_{(89Y\text{-}13C)}$ = 39.7 Hz)
		MeAd	27.00, 28.65, 28.76, 28.81, 31.17, 33.36, 33.90, 34.06, 34.20, 34.39, 34.60, 34.86, 34.91, 35.39, 37.25, 37.44, 39.13, 39.99, 40.32, 40.51, 41.86, 42.27
		Cp	121.45, 122.51, 125.81, 126.36, 127.97, 128.51, 128.56, 131.47, 151.52, 152.78
rac-(AbpYH)$_2$ (**20**)	C_6D_{12}	Me_2Si	1.03
		Me_3Si	3.12
		MeAd	28.75, 28.99, 34.23, 34.37, 34.55, 34.86, 34.98, 37.91, 38.76, 40.24, 42.02
		Cp	121.83, 122.18, 122.41, 126.00, 152.91

Chapter 4

Investigation of Intramolecular Allyl (C_3H_5) Rearrangement Mechanisms and Evaluation of the Strength of Olefin Binding in d^0-Metallocene - Alkyl - Olefin Complexes

Abstract

Variable temperature ^{1}H NMR spectroscopy indicates fluxional behavior for a number of group III metallocene allyl (η^3-C_3H_5) complexes. Rearrangement mechanisms in which allyl C=C double bond dissociation from the metal center are the rate determining steps are supported by simulation and lineshape analysis of the VT spectra. Activation barriers to olefin dissociation have been determined for $Cp^*_2Sc(\eta^3$-$C_3H_5)$ ($\Delta H^{\ddagger}$=8.0 kcal/mol, $\Delta S^{\ddagger}$=-14.4 e.u., toluene-d_8; $\Delta H^{\ddagger}$=5.5 kcal/mol, and $\Delta S^{\ddagger}$=-23.3 e.u., THF-d_8), *meso*-$Me_2Si\{3$-$[2$-$(2$-$CH_3)$-$C_{10}H_{14}]$-$C_5H_3\}_2Sc(\eta^3$-$C_3H_5)$ ($\Delta G^{\ddagger}$=12.0 kcal/mol, toluene-d_8), *meso*-$Me_2Si\{3$-$[2$-$(2$-$CH_3)$-$C_{10}H_{14}]$-$C_5H_3\}_2Y(\eta^3$-$C_3H_5)$ ($\Delta G^{\ddagger}$=15.6 kcal/mol, Et_2O-d_{10}; $\Delta G^{\ddagger}$=16.0 kcal/mol, toluene-d_8), and *meso*-$Me_2Si(3$-CMe_3-$C_5H_3)_2Sc(\eta^3$-$C_3H_5)$ ($\Delta G^{\ddagger}$=13.4 kcal/mol, toluene-d_8), *meso*-$Me_2Si(2,4$-$CHMe_2$-$C_5H_2)_2Sc(\eta^3$-$C_3H_5)$ ($\Delta G^{\ddagger}$=14.9 kcal/mol, toluene-d_8), *racemo*-$Me_2Si(2,4$-$CHMe_2$-$C_5H_2)_2Sc(\eta^3$-$C_3H_5)$ ($\Delta G^{\ddagger}$=14.7 kcal/mol, toluene-d_8; $\Delta G^{\ddagger}$=14.6 kcal/mol, THF-d_8), and (S,R)-$(C_{20}H_{10}O_2)Si(2$-$SiMe_3$-4-CMe_3-$C_5H_2)_2Sc(\eta^3$-$C_3H_5)$ ($\Delta G^{\ddagger}$=13.6 kcal/mol, toluene-d_8; $\Delta G^{\ddagger}$=12.4 kcal/mol, THF-d_8). The presence of donor solvents does not dramatically affect the rate of olefin dissociation. A second rearrangement mechanism, which involves 180° rotation of the intact η^3-allyl moiety, has been found to operate in those metallocenes whose ancillary ligand arrays adopt rigid *meso*-geometries. Lineshape analysis indicates that the rate of η^3-rotation is generally ≥1 order of magnitude faster than olefin dissociation for a given *meso* -metallocene. Experimental difficulties preclude confirmation of the η^3-rotation mechanism for the *racemo*-metallocenes.

Introduction

Formally d^0- early transition metal - alkyl - olefin complexes are of interest because of their possible roles in Ziegler-Natta catalysis.[1,2] Although they have not been observed directly, the existence of d^0 transition metal - alkyl - alkene complexes as genuine intermediates has been implicated in the chain propagation step of the Z-N polymerizations of ethylene and α-olefins (Figure 1).

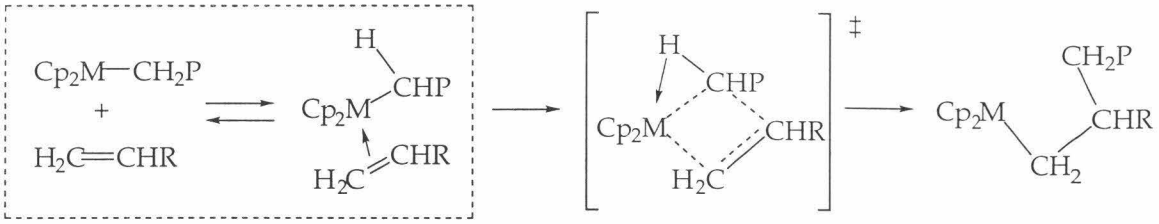

Figure 1. Transition metal-alkyl-alkene complexes as possible intermediates in Ziegler-Natta polymerization systems (M = 14-electron, d^0: Ti^+, Zr^+, Hf^+, Sc, Y, La; R = -H, $-CH_3$, $-CH_2CH_3$, etc.; P = growing polymer chain).

The few examples of structurally characterized d^0-metal - alkyl - olefin model complexes reported utilize olefinic groups linked by hydrocarbon or ether tethers to the metal center; the strengths of the M-olefin interactions were evaluated by dynamic NMR techniques. Olefin dissociation, followed by recoordination of the opposite face of the olefin, is believed to be rapid at -100 °C for the d^0 yttrocene - alkyl - alkene complex **1**, as evidenced by the equivalence of the diastereotopic Cp* and geminal-methyl groups in its ^1H NMR spectrum ($\Delta G^{\ddagger} \leq 10.4$ kcal/mol, toluene-d_8).[3,4] Similarly, olefin dissociation and subsequent recoordination is believed to be the process which renders the diastereotopic Cp* and *gem*-methyl groups equivalent in the ^1H NMR spectrum of the cationic zirconocene complex **2** ($\Delta G^{\ddagger} = 10.7$ kcal/mol, CD_2Cl_2),[5] although the extent to which solvent and counteranion assist this alkene displacement is unclear.

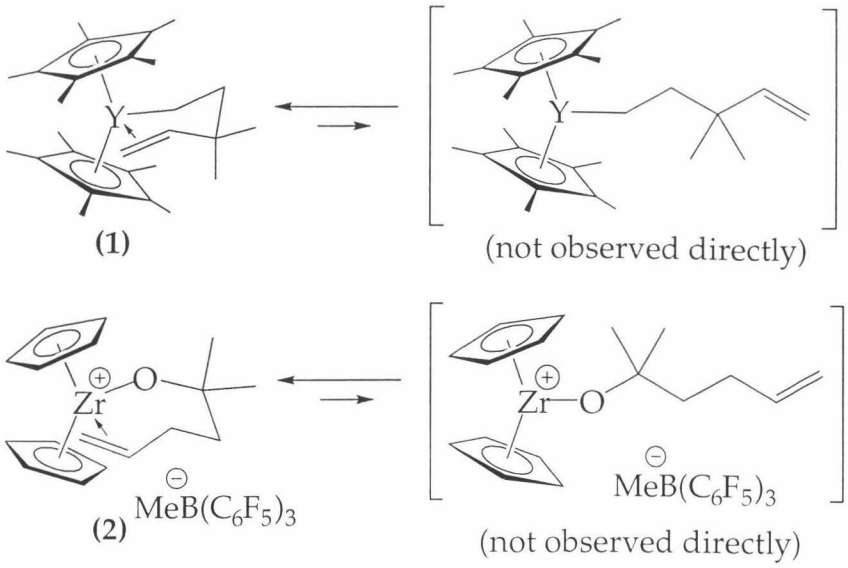

Figure 2. Spectroscopically characterized d^0 metal-alkyl-alkene complexes.

The allyl ($C_3H_5^-$) ligand is ubiquitous in organometallic chemistry, with η^3- or η^1-allyl complexes known for virtually every transition metal.[6-8] η^3-Allyl complexes are, themselves, special examples of tethered transition metal - alkyl - olefin complexes, where the barrier to the π-σ (η^3-η^1) rearrangement shown in Figure 3 may serve as an estimate of the strength of the M-olefin interaction. Variables such as the transition metal, ligand ensemble, and solvent utilized may, in principle, be varied in order to ascertain their relative effects on the strength of olefin binding.

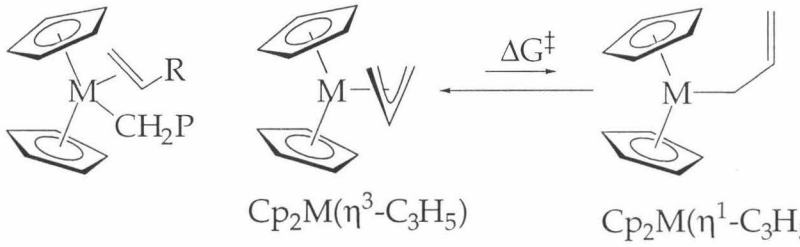

Figure 3. Use of η^3-allyl species as model complexes for estimating the strength of M-olefin interactions in metal-alkyl-alkene complexes.

Complicating the assessment of M-olefin bond strengths by NMR techniques is the fact that more than one mechanism may be contributing to dynamic behavior. The two most widely accepted unimolecular mechanisms for explaining the observed spectroscopic behavior of M-allyl complexes are:

An overall process involving dissociation of the allyl C=C double bond, rotation about the allyl C-C single bond, and subsequent recoordination of the C=C double bond to regenerate an η^3-fragment (mechanism (i), Figure 4);[9-11] and η^3-rotation,[9,10,12,13] which involves a 180° rotation of the intact η^3-fragment about an axis perpendicular to the plane of the allyl ligand (mechanism (ii), Figure 4).

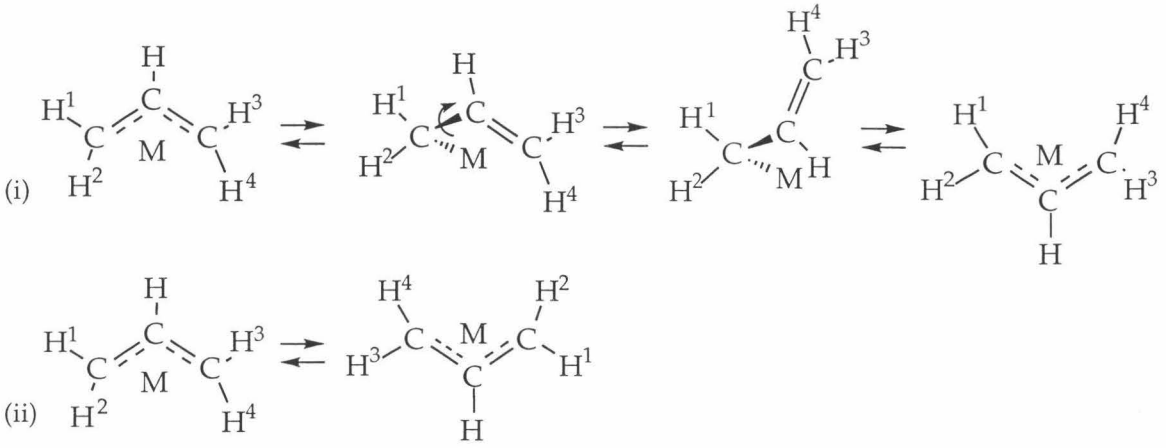

Figure 4. Proposed allyl rearrangement mechanisms: (i) dissociation of the allyl C=C double bond to generate an η^1-allyl complex, rotation about the allyl C-C single bond, and recoordination of the allyl alkene fragment, (ii) a 180° in-plane rotation of the coordinated allyl ligand.

Interestingly, only two complexes reported previously, the monomeric, homoleptic allyls of Mo(IV) (**3**) and W(IV) (**4**) have been unambiguously shown to undergo both η^3-η^1 and η^3-rotation. Detailed magnetization transfer experiments indicate that process (i) has been found to be faster than process (ii) for $Mo(C_3H_5)_4$,[10] and although both exchange processes are believed to occur for $W(C_3H_5)_4$,[10] no rate data for either (i) or (ii) has been reported. If the ground state structure of the related $Zr(C_3H_5)_4$ (**5**) is assumed to be thesame as that of the molybdenum and tungsten compounds, then both mechanisms (i) and (ii) operate in the Zr system. Although the slow exchange limit is not observed (-90 °C), η^3-rotation is reported to be the faster of the two processes.[9,14]

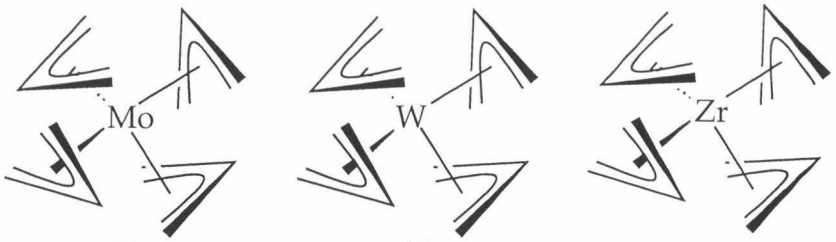

(3) (4) (5)

Of the bent-sandwich d^0- metallocene alkyl complexes reported previously, what is striking is the lack of understanding of the factors that promote fluxional allyl behavior. Although exceptions to these trends exist, the majority of the isolectronic group IV complexes, both neutral and cationic, possess static η^3-allyl ligands. Addition of strong σ-donor and weak π-acceptor ligands, such as THF, PMe_3, and methylimidazole, tends to induce fluxional behavior of the allyl ligand; addition of carbon monoxide, which acts as both a good σ-donor and π-acceptor, fails to induce fluxional allyl behavior in either the cationic Cp^*_2Zr complex **7b**[15] or the neutral aminoborole **9b**.[16]

Comparison of dynamic behavior for the isoelectronic d^0f^n Ln(allyl) complexes provides less definitive conclusions regarding the factors affecting allyl fluxionality; neither the presence nor absence of donor solvents and ligands can be used to reliably predict allyl fluxionality in related Ln(η^3-allyl) and (crotyl) complexes, shown in Figure 6.

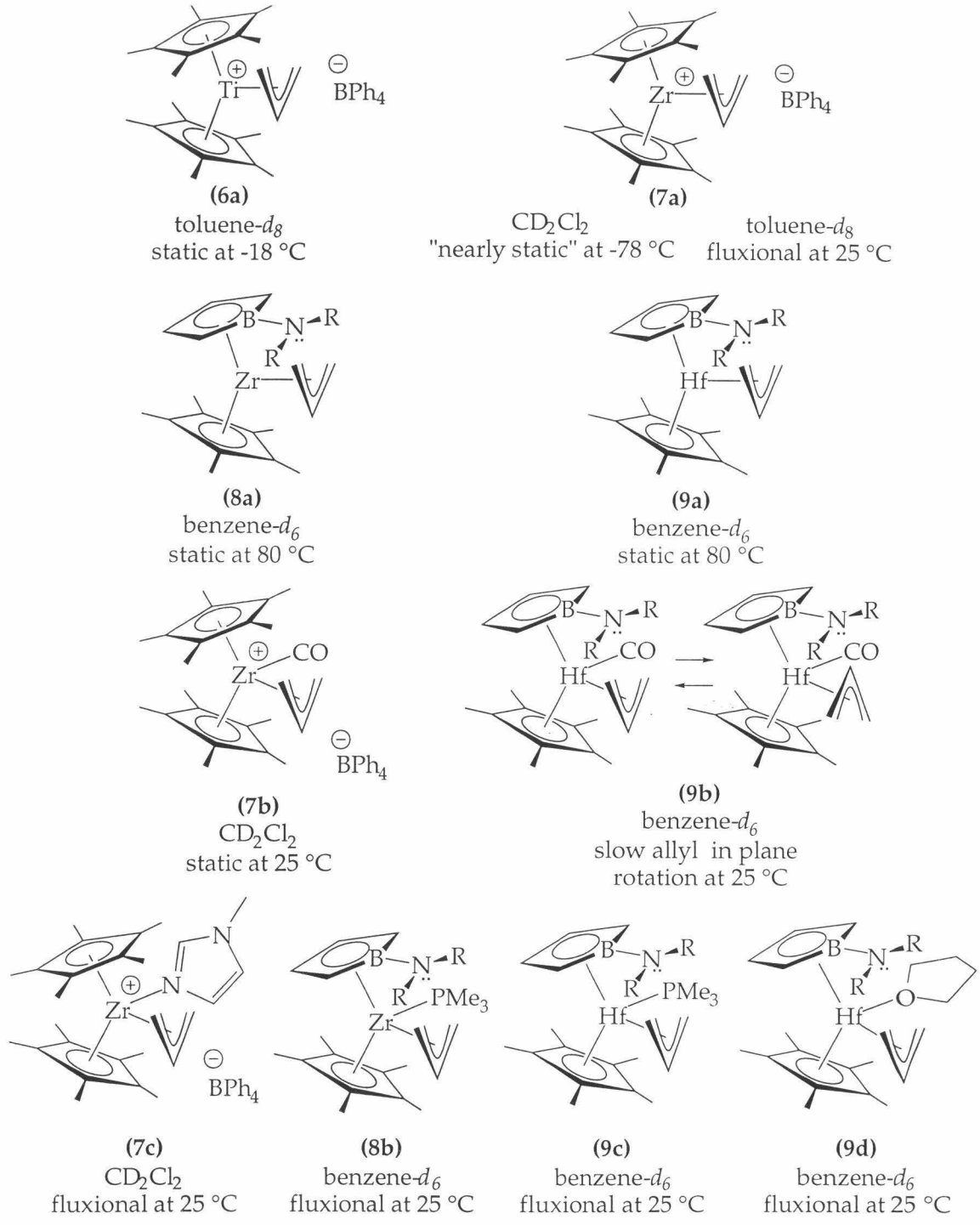

(6a)
toluene-d_8
static at -18 °C

(7a)
CD_2Cl_2
"nearly static" at -78 °C
toluene-d_8
fluxional at 25 °C

(8a)
benzene-d_6
static at 80 °C

(9a)
benzene-d_6
static at 80 °C

(7b)
CD_2Cl_2
static at 25 °C

(9b)
benzene-d_6
slow allyl in plane
rotation at 25 °C

(7c)
CD_2Cl_2
fluxional at 25 °C

(8b)
benzene-d_6
fluxional at 25 °C

(9c)
benzene-d_6
fluxional at 25 °C

(9d)
benzene-d_6
fluxional at 25 °C

Figure 5. d^0 Group IV metallocene η^3-allyl complexes.[15-17]

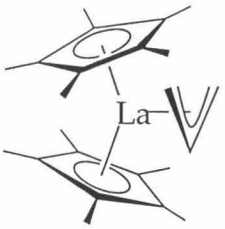

(10)
toluene-d_8
static at 25 °C

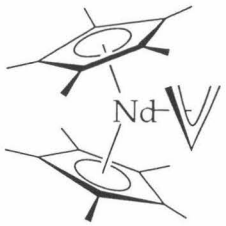

(11)
toluene-d_8
static at 90 °C on magnetization transfer timescale

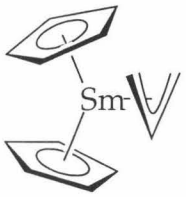

(12)
benzene-d_6 and THF-d_8
static at 25 °C

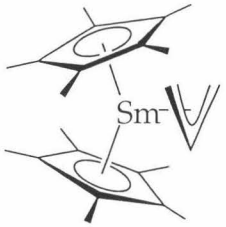

(13)
cyclohexane-d_{12} static at 25 °C
THF-d_8 fluxional at 25 °C

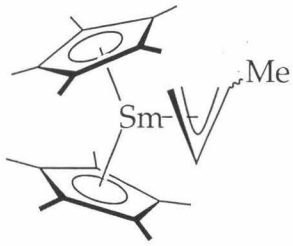

(14)
toluene-d_8
equivalent Cp* at -80 °C
THF-d_8
equivalent Cp* and *syn-anti* coalescence

Figure 6. Related metallocene d^0f^n Ln complexes.[13,18,19]

Results and Discussion

Reported herein is a mechanistic investigation of the fluxional behavior of d^0- metallocene complexes **15-21**. Variable temperature ^1H NMR spectra have been obtained for **15-21**, and lineshape analysis performed on these complexes in order to ascertain whether more than a single allyl

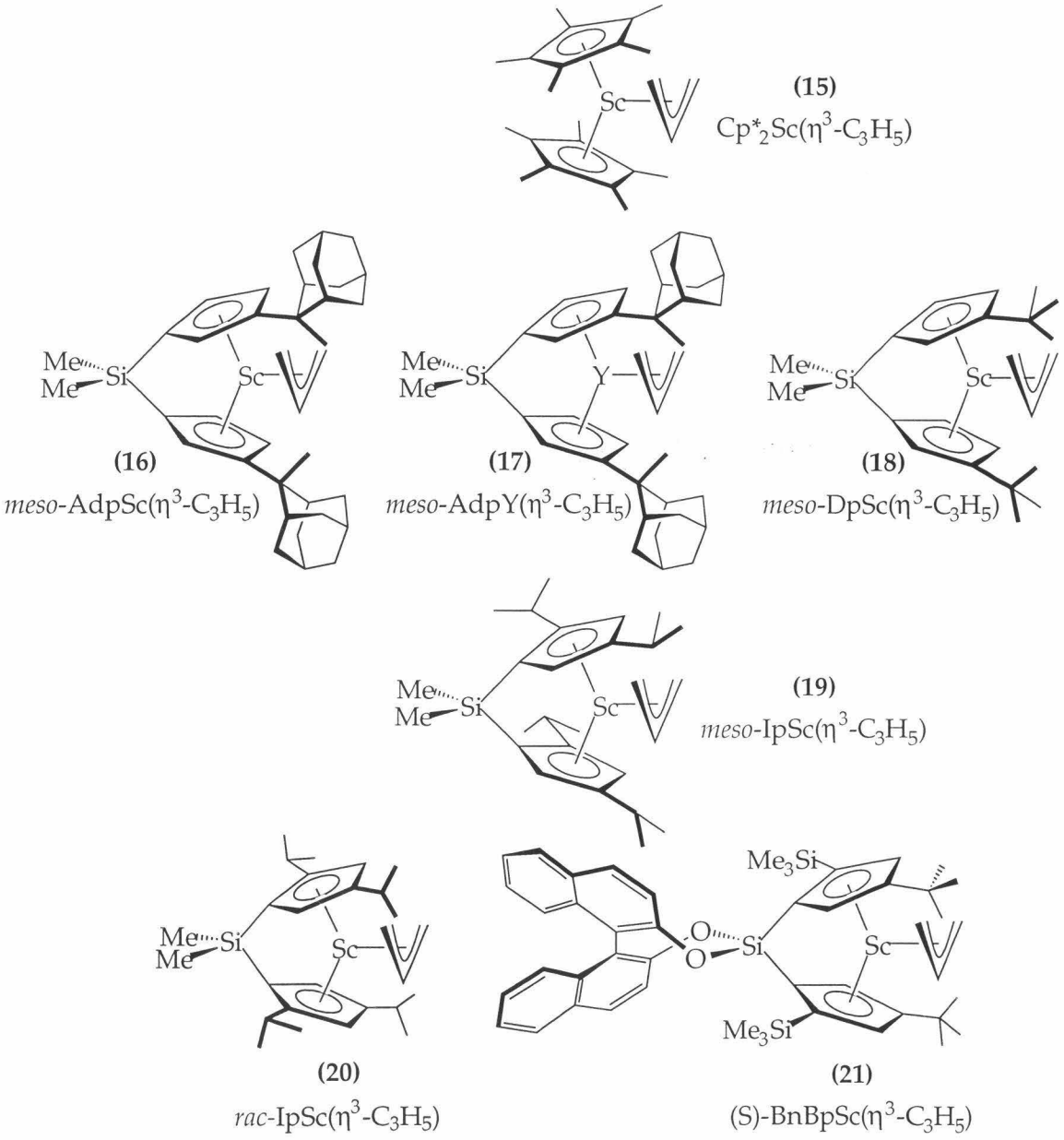

Figure 7. Group III metallocene allyl complexes investigated.

rearrangement mechanism is required to explain the observed temperature dependent behavior of $Cp^*_2Sc(\eta^3\text{-}C_3H_5)$ (**15**) and metallocene allyl complexes *meso*-$AdpSc(\eta^3\text{-}C_3H_5)$ (**16**), *meso*-$AdpY(\eta^3\text{-}C_3H_5)$ (**17**), and *meso*-$DpSc(\eta^3\text{-}C_3H_5)$ (**18**) [Adp = $Me_2Si\{3\text{-}[2\text{-}(2\text{-}CH_3)\text{-}C_{10}H_{14}]\text{-}C_5H_3\}_2$, Dp = $Me_2Si(3\text{-}CMe_3\text{-}C_5H_3)_2$]. In addition, lineshape analysis of the variable temperature spectral data has been performed for *meso*-$IpSc(\eta^3\text{-}C_3H_5)$ [Ip = $Me_2Si(2,4\text{-}CHMe_2\text{-}C_5H_2)_2$] (**19**), *racemo*-$IpSc(\eta^3\text{-}C_3H_5)$ (**20**), and (S,R)-$BnBpSc(\eta^3\text{-}C_3H_5)$ [BnBp = $(C_{20}H_{10}O_2)Si(2\text{-}SiMe_3\text{-}4\text{-}CMe_3\text{-}C_5H_2)_2$] (**21**), whose syntheses and NMR spectra have been reported elsewhere.[20,21] Activation parameters have been determined, when possible, for the barriers to olefin dissociation for complexes **15-21**, and for the barriers to in-plane allyl rotation for **16-19**, with the hope of correlating these rearrangement barriers with particular changes in metal, ligand array, and solvent.

Investigation of the Permethylscandocene System

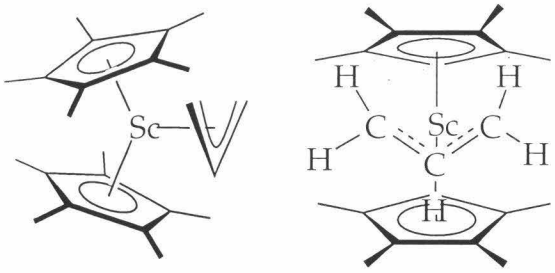

(15)

The 500 MHz ^1H NMR spectra (toluene-d_8) of $Cp^*_2Sc(\eta^3\text{-}C_3H_5)$ are shown as a function of temperature in Figure 8. At low temperatures (<225 K), the allyl ligand is clearly static on the NMR timescale, as evidenced by the inequivalent Cp* resonances (1.73 and 1.86 ppm) and an AM_2X_2 splitting pattern for the allyl moiety (H_a: 3.93 ppm; H_s: 2.05 ppm). As the probe temperature is raised, the Cp* resonances coalesce (257 K), followed by the appearance of an averaged Cp* signal at yet higher temperatures (>269 K). Accompanying the averaging of Cp* resonances are the broadening and coalescence (286 K) of the resonances for the *syn* and *anti* allyl methylenehydrogens, and the appearance of a new signal (T>309 K) at a chemical shift equal to the weighted average of the individual *syn* and *anti* resonances.

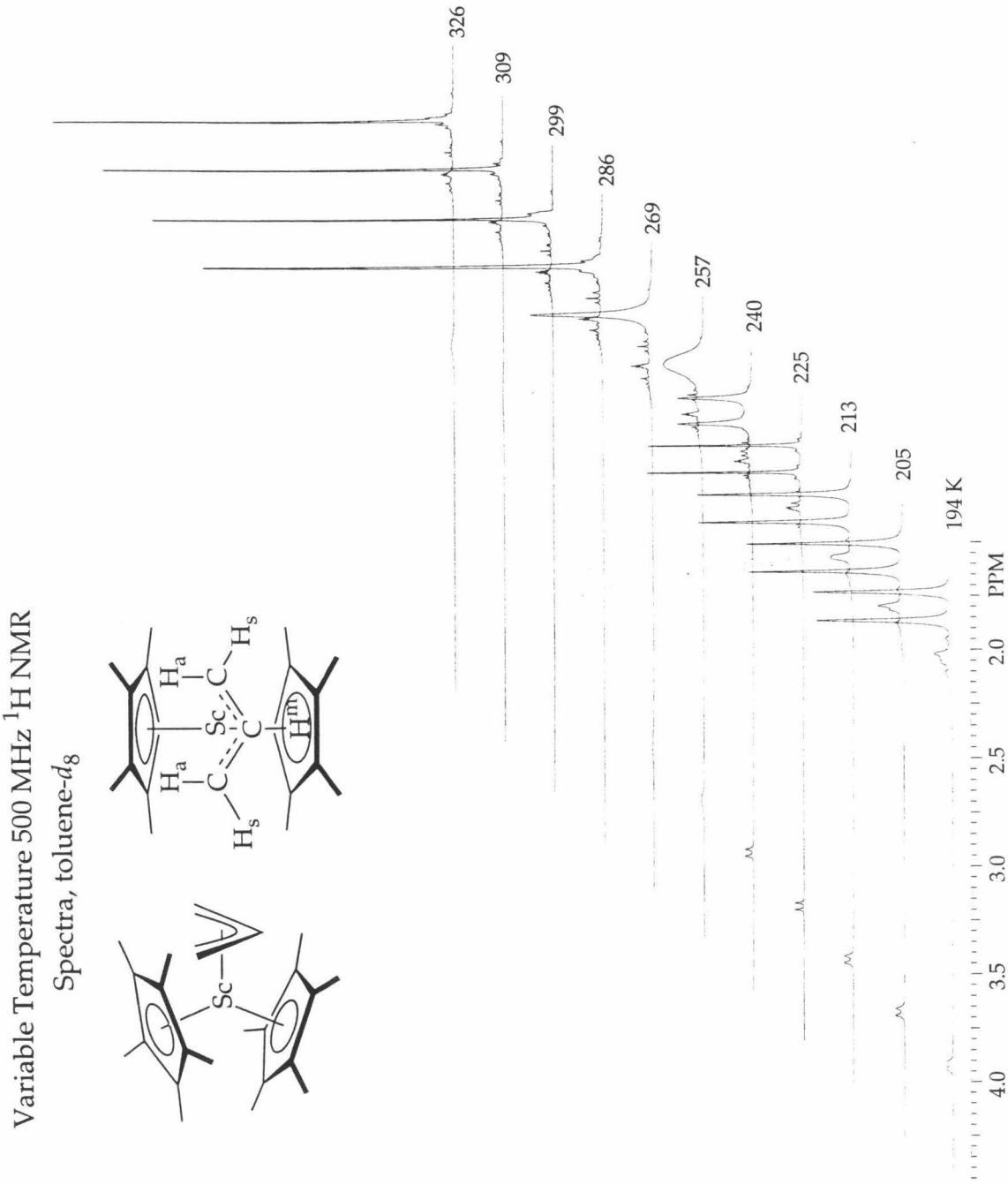

Figure 8. Variable temperature ^{1}H NMR spectra of $Cp^*_2Sc(C_3H_5)$ (**15**) (500 MHz, toluene-d_8).

Similar spectral trends are observed for **15** in THF-d_8; low temperature spectra (≤233 K) indicate a static η^3-allyl ligand, while fluxional behavior is observed as the probe temperature is raised. Coalescence of the Cp* signals is observed at 229 K, and the *syn* and *anti* allyl methylene averaging occurs with a coalescence temperature (T_c) of ~273 K (300 MHz).

The simplest explanation for the observed fluxional behavior of **15** involves the π-σ (allyl η^3-η^1) processes shown in Scheme 1. Dissociation of the allyl C=C double bond generates an η^1-allyl intermediate (**15**-η^1); rotation about the M-C single bond in **15**-η^1, followed by recoordination of the alkene fragment to form an η^3-species (pathway ia), exchanges the environments of the two Cp* rings. An alternate pathway from intermediate **15**-η^1 is rotation about the allyl C-C single bond, followed by recoordination of the alkene fragment (ib), serving not only to exchange the Cp* ligands, but also to exchange the *syn* and *anti* substituents on one of the allyl methylene carbons (that which remains coordinated to the metal throughout the transformation). As rotation about the M-C and C-C single bonds are expected to be facile in an η^1-allyl complex, both pathways (ia) and (ib) are likely upon generation of **15**-η^1.

Lineshape analysis[22] confirms that the combination of (ia) and (ib) may be used to simulate the observed ^{1}H NMR spectra of **15**. Using only the η^3-η^1 processes depicted in Scheme 1, the experimental data could be accurately modeled over the entire temperature range investigated solely varying the rate of alkene dissociation (k_1). Olefin dissociation to generate **15**-η^1 was modeled as the rate determining step, with subsequent rapid M-C and C-C single bond rotations occurring prior to regeneration of an η^3- complex. In addition, olefin dissociation from the left side of the metallocene wedge was modeled as occurring with equal probability as dissociation from the right side of the wedge.

A stackplot of the simulated NMR spectra (toluene-d_8) as a function of temperature is shown in Figure 9. At the limit of slow exchange ($k_1 = 0$), inequivalent Cp* signals and an AM_2X_2 splitting pattern for the allyl moiety are observed. As the rate of alkene dissociation is increased, averaging of the

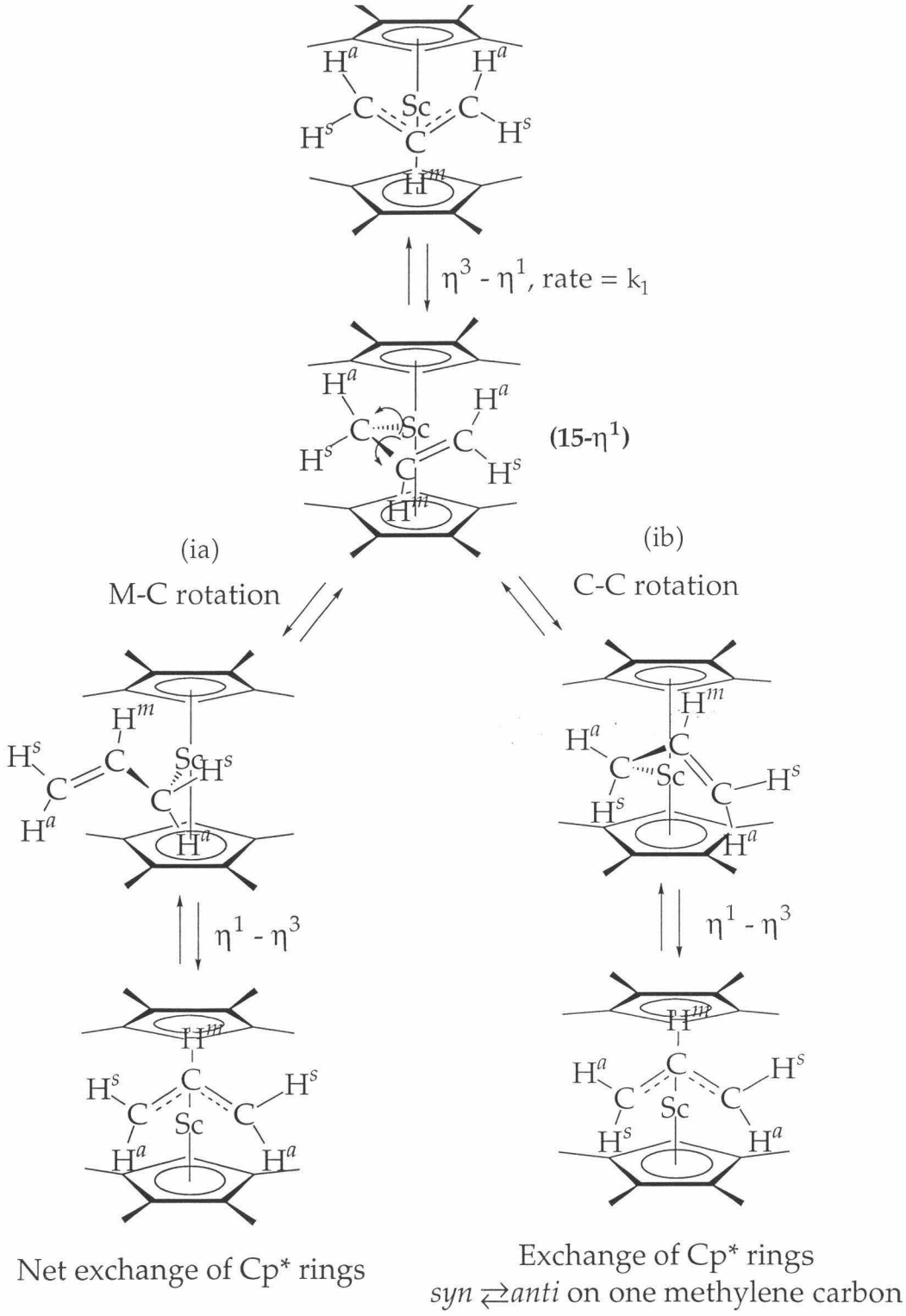

Scheme 1. η^3-η^1 Processes for $Cp^*_2Sc(C_3H_5)$ (**15**).

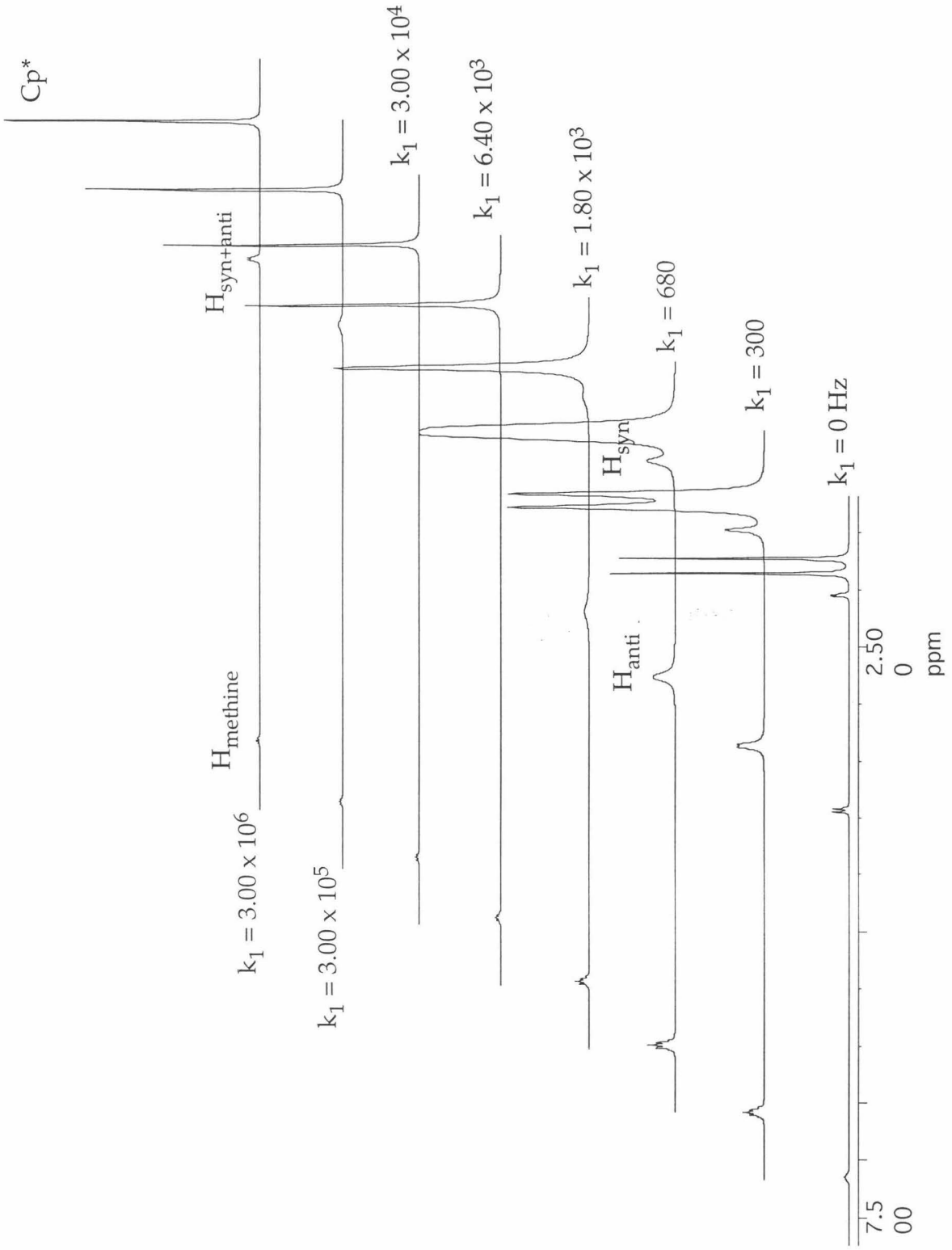

Figure 9. gNMR simulation of Cp* and (C_3H_5) resonances of **15** (500 MHz, toluene-d_8) using η^3-η^1 processes (ia) and (ib).

Cp* signals ($k_1 \approx 1.4 \times 10^3$ sec^{-1}) is followed by coalescence of the *syn* and *anti* signals ($k_1 \approx 1.3 \times 10^4$ sec^{-1}). Observation of a single, averaged allyl methylene resonance (an AX_4 splitting pattern) is observed at $k_1 > 2.0 \times 10^6$ sec^{-1}.

A linear Eyring plot for olefin dissociation (Figure 10) may be generated from the observed 300 and 500 MHz coalescence temperatures in conjunction with the corresponding rate constants obtained from gNMR simulations (Table 1). Activation parameters of $\Delta H^{\ddagger}_{\eta 3\text{-}\eta 1} = 8.0$ kcal/mol and $\Delta S^{\ddagger}_{\eta 3\text{-}\eta 1} = -14.4$ e.u. for olefin dissociation are obtained from the slope and intercept of this plot.

These activation parameters provide a $\Delta G^{\ddagger}_{\eta 3\text{-}\eta 1}$ of 11.7 kcal/mol at 259 K (the Cp*-Cp* coalescence temperature); this is in general agreement with the $\Delta G^{\ddagger}_{Cp^*\text{-}Cp^*}$ (12.4 ± 0.7 kcal/mol) obtained from application of the simple two-site exchange approximation **I** and equation **II**, where $k_{Cp^*\text{-}Cp^*,Tc}$ is the rate constant for Cp* exchange at T_c, and $\Delta\nu_\infty$ is the peak separation (in Hz) of the two averaging signals in the limit of slow exchange.

$$k_{Cp^*\text{-}Cp^*,Tc} = 2\pi/\sqrt{2}\,(\Delta\nu_\infty) \quad \textbf{(I)}$$

$$\Delta G^{\ddagger} = -RT[\ln(k/T) - 23.76] \quad \textbf{(II)}$$

Coalescence	Spectrometer Field Strength (MHz)	T_c (K)	k_1 (sec^{-1}) from gNMR	k_1 (sec^{-1}) from (**I**)
C_5Me_5	300	250	3.8×10^2	1.7×10^2
C_5Me_5	500	257	6.8×10^2	3.0×10^2
C_3H_5 *syn-anti*	300	292	4.8×10^3	*
C_3H_5 *syn-anti*	500	299	6.4×10^3	*

Table 1. Observed coalescence temperatures and gNMR-derived η^3-η^1 rate constants for **15** (toluene-d_8); * = not available using this method

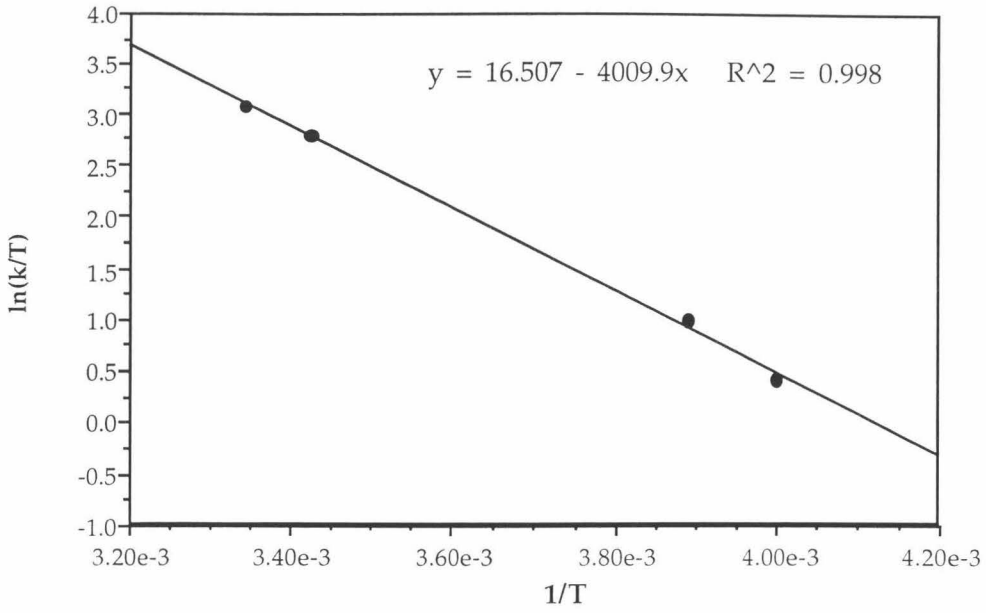

Figure 10. Eyring plot for olefin dissociation for **15** in toluene-d_8.

A statistical factor of two is included in equation I in order to account for the fact that, in addition to the (productive) processes shown in Scheme 1 which serve to exchange Cp* environments, there exist degenerate η^3-η^1 transformations in which the η^1-allyl simply recoordinates to M without net C-C or M-C bond rotations (Figure 11).

Simulation of **15** in THF-d_8, with olefin dissociation again modeled as the rate-determining step for the allyl rearrangement (tabulated in Table 2), provides activation parameters of $\Delta G^{\ddagger}_{\eta 3\text{-}\eta 1,\ 229\ K}$ = 10.8 kcal/mol, $\Delta H^{\ddagger}_{\eta 3\text{-}\eta 1}$ = 5.5 kcal/mol, and $\Delta S^{\ddagger}_{\eta 3\text{-}\eta 1}$ = -23.3 e.u.. For comparison, the two-site exchange approximation **I** provides $\Delta G^{\ddagger}$ = 11.3 (± 1.0) kcal/mol for Cp*-Cp* exchange.

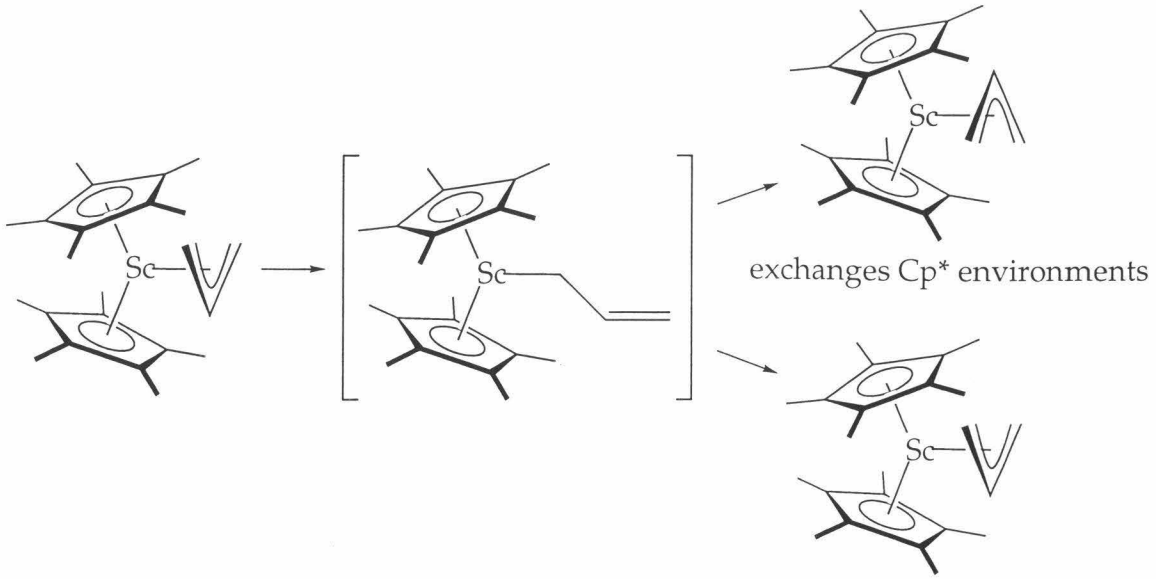

Figure 11. Origin of statistical factor included in two-site exchange approximation.

Coalescence	Spectrometer Field Strength (MHz)	T_c (K)	k_1 (sec^{-1}) from gNMR	k_1 (sec^{-1}) from (**I**)
C_5Me_5	300	233	2.9×10^2	1.4×10^2
C_3H_5 *syn-anti*	300	273	1.9×10^3	*

Table 2. Observed coalescence temperatures for **15** (THF-d_8) and gNMR-derived η^3-η^1 rate constants; * = not available using this method

The activation barriers to olefin dissociation of ~11-12 kcal/mol are comparable to the barriers observed for tethered olefin complexes **1** and **2** (≤ 10.4 kcal/mol and 10.7 kcal/mol, respectively). The activation barriers for **15** may be separated into enthalpy barriers of 5-8 kcal/mol, and large and negative entropy barriers (-14 to -23 e.u.). Unlike the previously observed group IV metallocene allyl complexes, the presence of donor solvents appears to have little effect on the rate of olefin dissociation; extrapolation of the $\Delta G^{\ddagger}$ values for olefin dissociation to 298 K (using the $\Delta H^{\ddagger}$ and $\Delta S^{\ddagger}$ obtained from the Eyring plots) provides $\Delta G^{\ddagger}_{\eta 3\text{-}\eta 1}$ = 12.3 kcal/mol (toluene) and 12.4 kcal/mol (THF).

The use of lineshape analysis does not provide a great deal of information regarding the rate of η^3-rotation for **15**. As simulations using only the η^3-η^1 processes (ia) and (ib) explain the observed data, process (ii) need not necessarily be invoked. Control experiments in which lineshape simulations include process (ii) (with $k_2 \leq (10 \times k_1)$) do not significantly alter the overall spectral simulations or fit to the observed spectra. Lineshape simulation using only the η^3-rotation process fails to provide the *syn-anti* averaging of the allyl methylene observed at high temperatures for **15**. Given the available data, though, it is possible that η^3-rotation is occurring, albeit at a rate considerably slower than is olefin dissociation.

Examination of the molecular orbital diagram for **15** provides one explanation for a slow rate of allyl rotation. The frontier MO diagram for a d^0-bent metallocene allyl complex is shown in Figure 12a.[23] Although rotation of the intact η^3-allyl fragment results in no net loss of overlap between the $1a_1$ frontier MOs, partial rotation does disrupt the bonding interaction of the $1b_1$ MO.

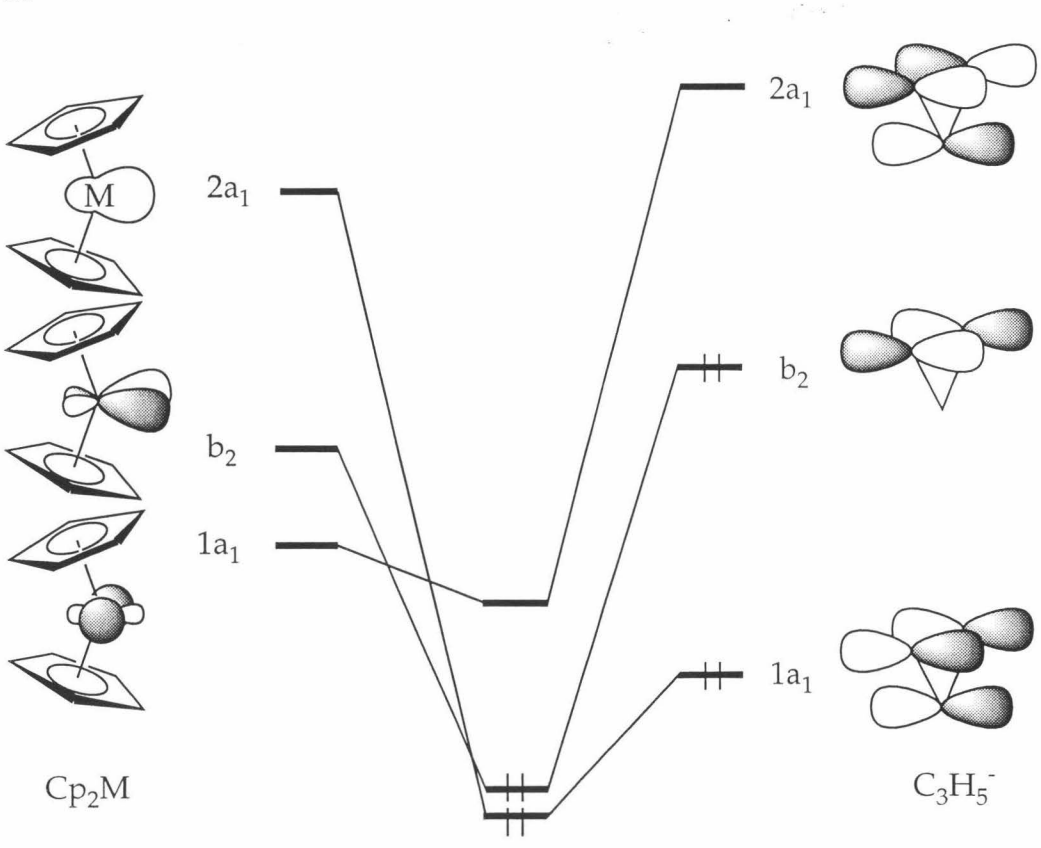

Figure 12. Frontier molecular orbital diagram for $Cp_2M(C_3H_5)$ (M=Sc, Y).

Investigation of *meso*-Metallocenes

The *ansa*-scandocene allyl complex AdpSc(C_3H_5) (**16**) exhibits markedly different temperature-dependent behavior from that of **15**, in part due to the C_s symmetry of the *meso*- ancillary ligand array, which places the 3- and 3'-Cp

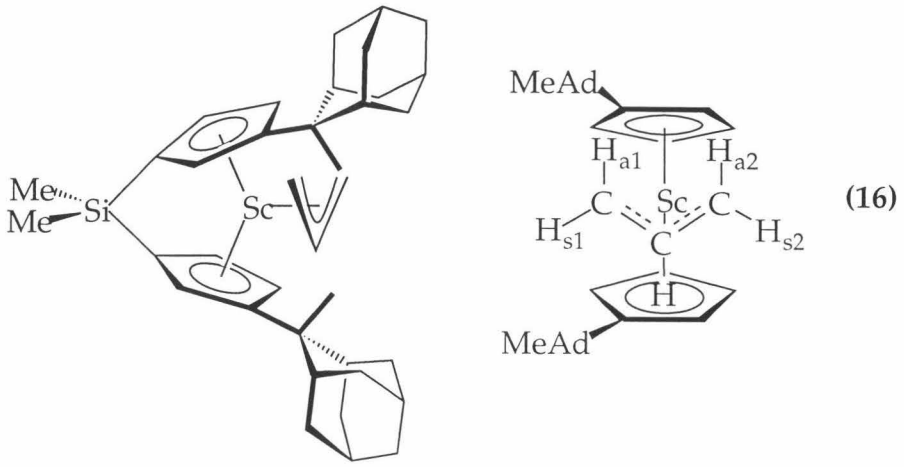

(16)

substituents [2-(2-CH_3)-$C_{10}H_{14}$ = 2-(2-Methyl)-Adamantyl = MeAd] on the same side of the metallocene wedge.

Shown in Figure 13 are the variable temperature ^{1}H NMR spectra of AdpSc(C_3H_5) in Et_2O-d_{10}. At low temperatures, an AGMPX splitting pattern is exhibited for the allyl ligand, indicating the absence of allyl rearrangement on the NMR timescale. This static structure is supported by the inequivalence of all of the vinylic cyclopentadienyl protons as well as the inequivalence of the methyladamantyl substituents in the low temperature (<194 K) NMR spectra.

As the probe temperature is raised, the resonances for the allyl *syn* hydrogens (H_{s1} and H_{s2}) broaden and coalesce, as do the resonances for the allyl *anti* hydrogens (H_{a1} and H_{a2}) (~215 K). Continuing to raise the temperature (246 K) results in the appearance of two new allyl resonances, one located midway between the previous signals for H_{s1} and H_{s2}, and the other resonance midway between those of H_{a1} and H_{a2}; the integrated areas of each of these new resonances are equal to twice those of the individual signals in the AGMPX spectra. This corresponds to averaging of *syn* and of *anti* hydrogens ($H_{s1} \rightleftarrows H_{s2}$, $H_{a1} \rightleftarrows H_{a2}$), with no *syn*-*anti* ($H_a \rightleftarrows H_s$) exchange. Accompanying these changes at higher temperatures are averaging of the Cp rings and substituents of the ancillary ligand array.

As the temperature of the sample is raised further, the averaged H_s and the averaged H_a resonances (2.28 ppm and 3.89 ppm, respectively) in the AM_2X_2 spectra broaden, coalesce, and a new signal appears, located equidistant from the previous resonances. This AX_4 splitting pattern, where all allyl methylene hydrogens are magnetically equivalent indicates not only rapid *syn-syn* (*anti-anti*) exchange, but also concurrent rapid exchange between the *syn* and *anti* allyl positions.

This progression from AGMPX - AM_2X_2 - AX_4 splitting patterns for *meso*-AdpSc(η^3-C_3H_5) is also observed for *meso*-AdpY(η^3-C_3H_5) (**17**), for *meso*-DpSc(η^3-C_3H_5) (**18**) (acquired from treatment of [*meso*-DpSc(μ-H)]$_2$ with excess allene), and for *meso*-IpSc(C_3H_5) (**19**), and holds true for all solvents in which spectra have been obtained.

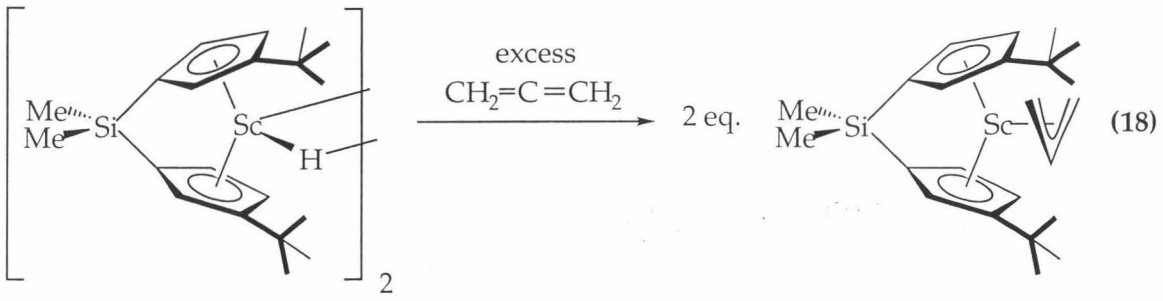

(18)

A 500 MHz spectrum of **18** exhibiting an AX_4 splitting pattern could not be obtained due to temperature limitations of the spectrometer employed for this study; the expected AX_4 splitting pattern is observed using a 300 MHz spectrometer at temperatures above 358 K. Similarly, the highest temperature spectra obtained for **17** (361 K, Et_2O-d_{10}), and **19** (377 K, toluene-d_8) are above the coalescence temperatures of the H_s and H_a resonances, and exhibit very broad features centered at approximately 2.80 ppm and 3.11 ppm (the predicted weighted averages of the chemical shifts for H_s and H_a), respectively. The highest temperature (355 K) at which spectra were recorded for **17** in toluene-d_8 is, as well, above the temperature required for the characteristic intermediate-temperature AM_2X_2 splitting pattern (298 K), where the allyl resonances observed are approaching, but have not quite reached, *syn-anti* coalescence.

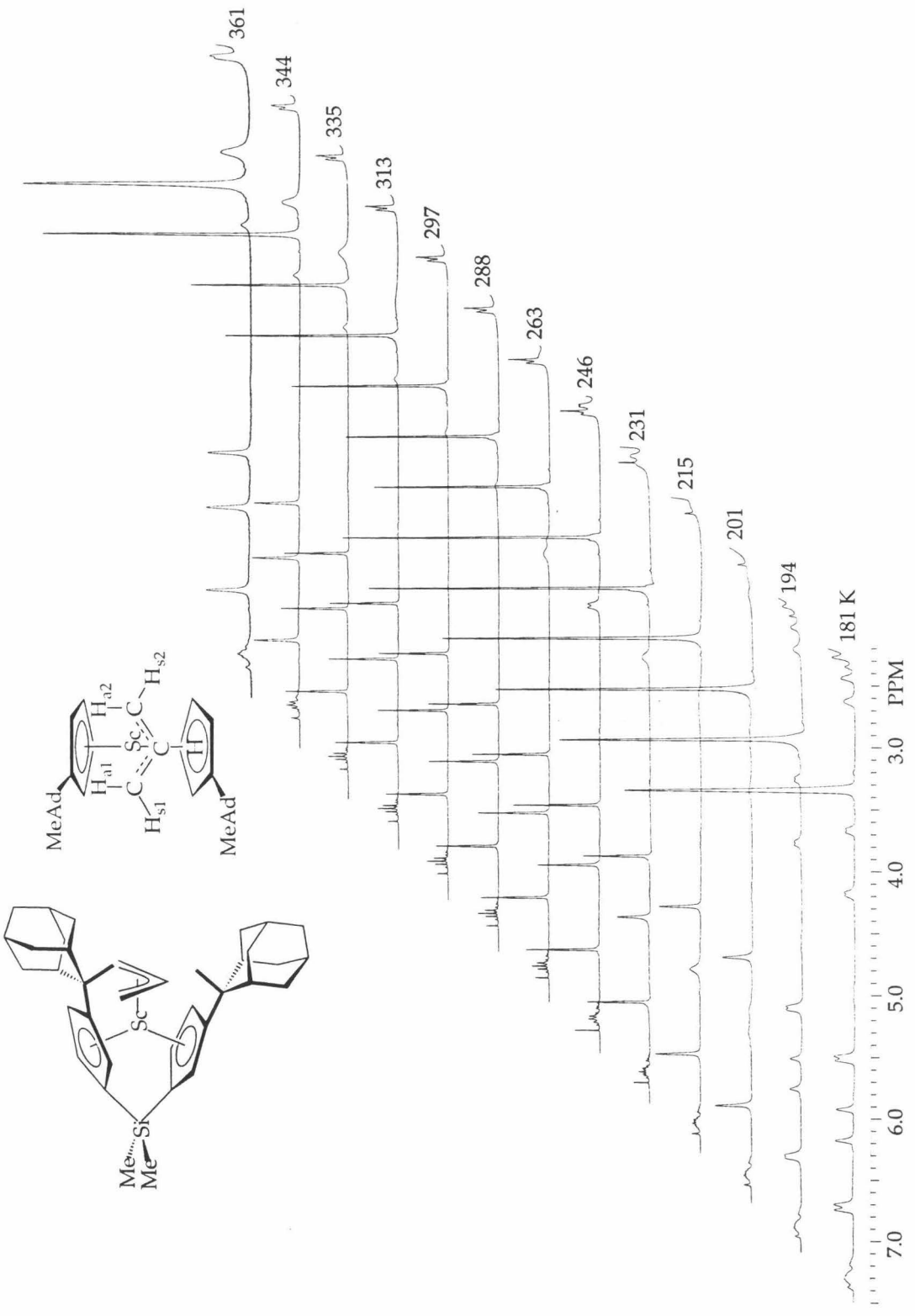

Figure 13. Variable temperature ^{1}H NMR spectra of AdpSc(C_3H_5) (**16**) (500 MHz, Et_2O-d_{10}).

All of the spectral differences resulting from temperature changes for **15-19** are reversible; cooling of the NMR samples after obtaining high temperature spectra results in the regeneration of the previously observed lower symmetry species. Decomposition is observed, though, after prolonged heating of solutions of any of these compounds.

The low temperature AGMPX splittings exhibited by **16-19** are indicative of nonfluxional allyl ligands on the NMR timescale; the C_s-symmetry of the *meso*-ligand arrays renders the two *syn* allyl substituents (H_{s1} and H_{s2}) as well as the two allyl *anti* substituents (H_{a1} and H_{a2}) inequivalent.

The high temperature AX_4 splitting patterns may be explained by π-σ rearrangement pathways analogous to those discussed earlier for the Cp^*_2Sc system. As shown in Scheme 2, rotation about the C-C single bond of an η^1-allyl complex serves to exchange the *syn* and *anti* substituents on one of the allyl methylene carbons (H_{a1} and H_{s1}, as drawn); multiple iterations of the η^3-η^1 processes will average all four of the methylene hydrogens.

There are *two* viable mechanistic possibilities, however, that will generate the AM_2X_2 allyl splitting patterns characteristic of the intermediate temperature range NMR spectra of all of the *meso* complexes.

Rotation about the M-C single bond of the η^1-allyl species (pathway ib), which serves only to exchange the Cp* rings for **15**, has the net effect for the *meso*- complexes of not only exchanging the magnetic environments of the two Cp rings, but of also exchanging the environments of the two *syn* allyl substituents ($H_{s1} \rightleftarrows H_{s2}$) and exchanging the two *anti* substituents ($H_{a1} \rightleftarrows H_{a2}$). The observation of *syn-anti* averaging at higher temperatures is indicative of the presence of an η^1 intermediate (pathway ib). As pathways ia and ib are expected to be facile from an η^1-intermediate, *syn-syn* (*anti-anti*) averaging via pathway (ib) is expected to accompany *syn-anti* exchange. The observed *syn-syn* and *anti-anti* averaging at lower temperatures than those where *syn-anti* averaging is seen may, therefore, simply result from the fact that $\Delta\nu_{Hs1\text{-}Hs2}$ and $\Delta\nu_{Hs1\text{-}Hs2}$ are both less than $\Delta\nu_{Hs1\text{-}Ha1}$ and $\Delta\nu_{Hs2\text{-}Ha2}$.

An alternate mechanism, however, may explain the existence of spectra which indicate *syn-syn* (and *anti-anti*) averaging but not *syn-anti* averaging. The in-plane rotation of an intact η^3-allyl complex (Scheme 3)

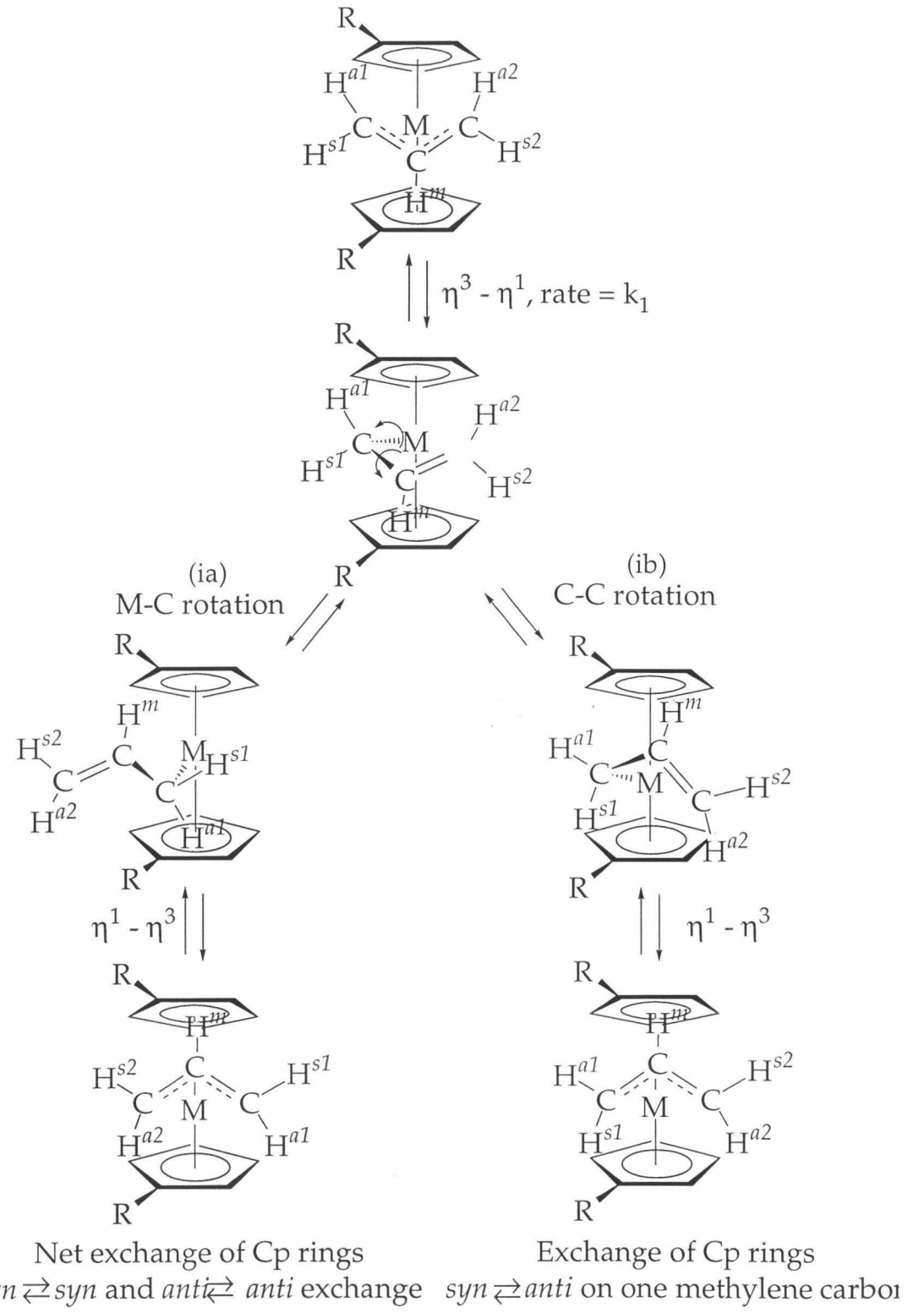

Scheme 2. η^3-η^1 Allyl rearrangements in *meso*-metallocenes.

serves to exchange the two *syn* hydrogens and to exchange the two *anti* hydrogens, as well as interchange the magnetic environments of the two Cp rings; this is identical to the net result of pathway (ia) shown in Scheme 2. The observed NMR spectra, therefore, could also be explained by the existence of two distinct rearrangement pathways, with both processes slow on the NMR timescale at low temperatures (resulting in AGMPX splitting patterns),η^3-rotation (providing Cp-Cp, *syn-syn*, and *anti-anti* averaging) rapid at intermediate temperatures, and the η^3-η^1 processes (ia) and (ib) (*syn-anti* exchange and the observed AX_4 allyl patterns) becoming rapid only at the higher temperatures investigated.

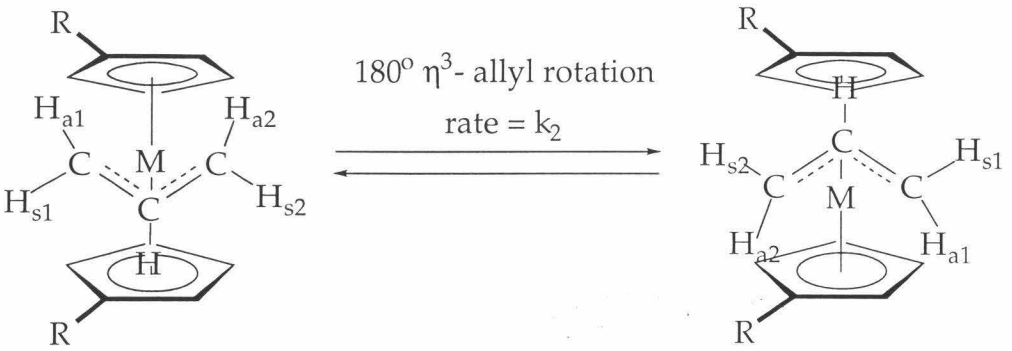

Scheme 3. η^3-Rotation for *meso*-metallocenes.

Distinguishing between these possibilities in the absence of lineshape analysis proved exceptionally difficult. The temperature range over which the Cp substituents coalesce was quite narrow; Eyring plots relying on these data points often showed considerable scatter and deviations from linearity, and, unsurprisingly, resulted in chemically nonsensical activation parameters. The utility of observing Cp or allyl coalescence temperatures on spectrometers of different field strength (300 vs. 500 MHz) was negated by the fact that the change in T_c was comparable to the uncertainty associated with the temperature measurement itself. As averaging of all four methylene hydrogens requires multiple iterations of the η^3-η^1 process, the fact that equation **I** applies rigorously only to two-site exchange processes dictates that **I** cannot be used to determine k_1 at the observed *syn-anti* T_c. Interpretation of the low temperature coalescences is further complicated by the fact that averaging of the ligand resonances may result from η^3-rotation, and the *syn-*

anti averaging from η^3-η^1 processes, a situation which can not be substantiated using only Equation **I** and Erying plots derived from its application.

Lineshape analysis, however, proved invaluable in distinguishing between the two mechanistic possibilities outlined in Schemes 2 and 3. Simulation of the *meso*-scandocenes and yttrocene allyl complexes using *only* the η^3-η^1 exchange process utilized in previous simulations of **15** *failed* to successfully model the entire temperature range investigated experimentally, indicating that the low temperature η^3-η^1 pathway observed for **15** is *not* the low energy allyl rearrangement pathway for *meso* complexes **16-19**. Representative NMR simulations generated using only the η^3-η^1 exchange processes are shown in Figure 14 for **16**. Although the observed low and high temperature spectra can be adequately simulated using only the η^3-η^1 mechanism, the characteristic AM_2X_2 splittings observed for the allyl ligands at intermediate temperatures can not be obtained solely by varying the rate of allyl double bond dissociation from the metal. Furthermore, Eyring plots obtained from the experimentally determined coalescence temperatures with the corresponding best-fitting rate constants (as determined using gNMR) were often plagued with the same problems associated with (previous) Eyring plots generated solely from the application of equation **I**.

Similarly, simulation of the VT NMR spectra using only the η^3-rotation mechanism did not mimic the experimental spectra over the entire temperature range investigated. Implementation of the η^3-rotation process as the sole rearrangement pathway successfully models both the low and intermediate temperature spectra, yet fails to generate the AX_4 splitting pattern observed experimentally at elevated temperatures, as shown for **16** in Figure 15.

The results of simulations using concurrent η^3-rotation and the η^3-η^1 pathways shown in Scheme 2 successfully mimic the observed spectra over the entire temperature range investigated. The simulated spectra for **16** using a low-energy η^3-rotation process and higher barrier η^3-η^1 rearrangement

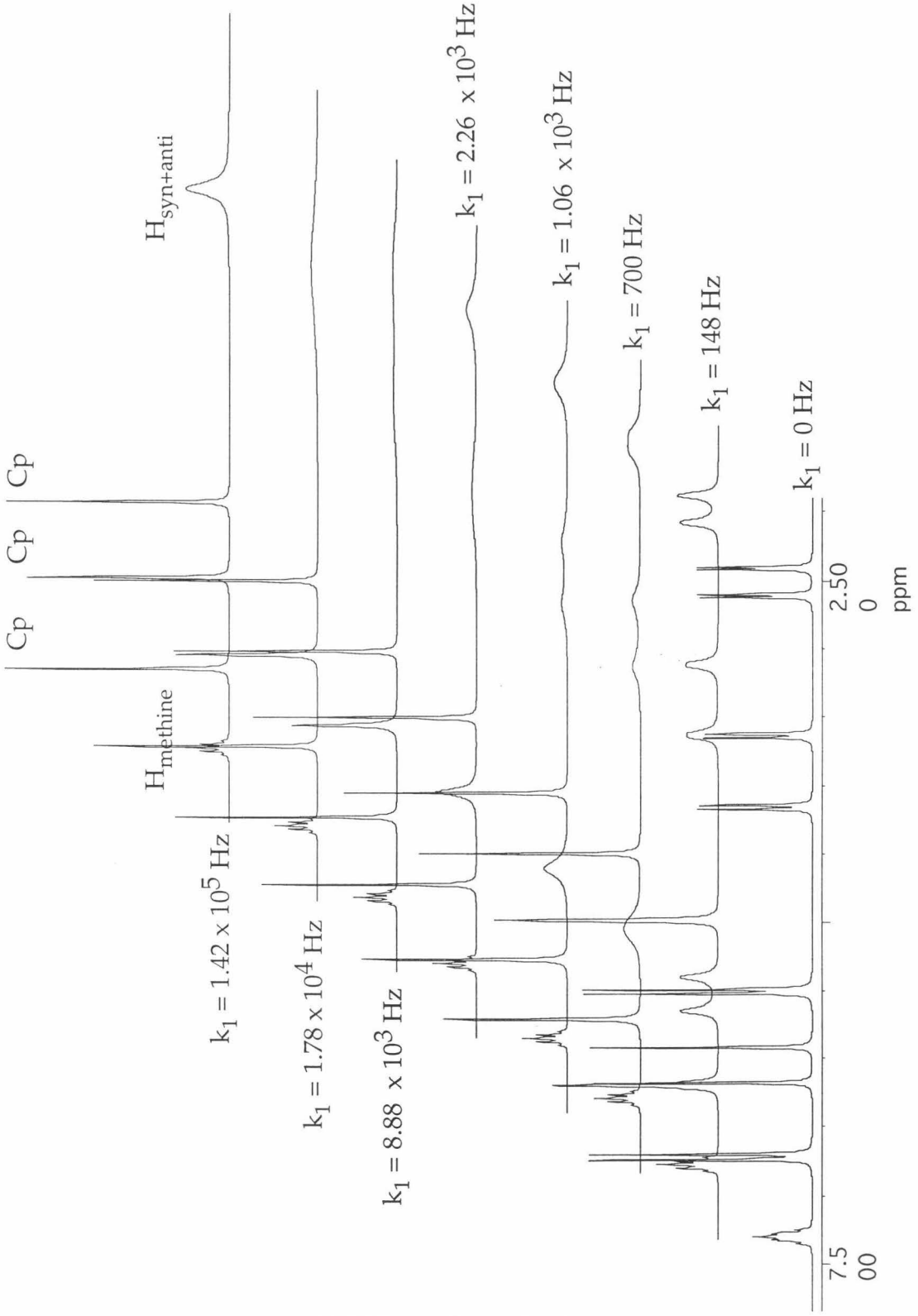

Figure 14. gNMR simulation of (C_3H_5) and vinylic Cp resonances of **16** (500 MHz, Et_2O-d_{10}) using only η^3-η^1 processes (ia) and (ib).

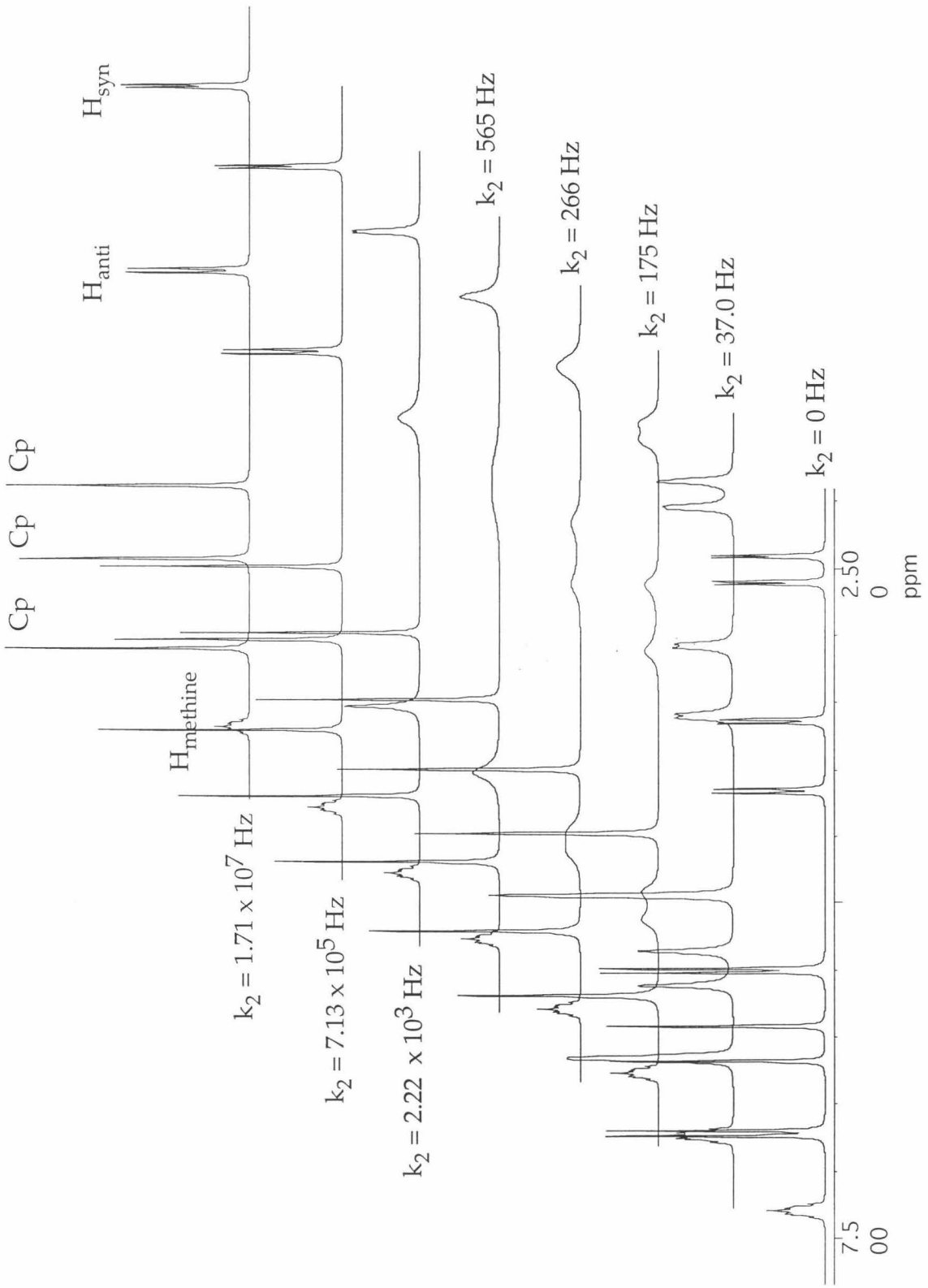

Figure 15. gNMR simulation of (C_3H_5) and vinylic Cp resonances of **16** (500 MHz, Et_2O-d_{10}) using only η^3-rotation.

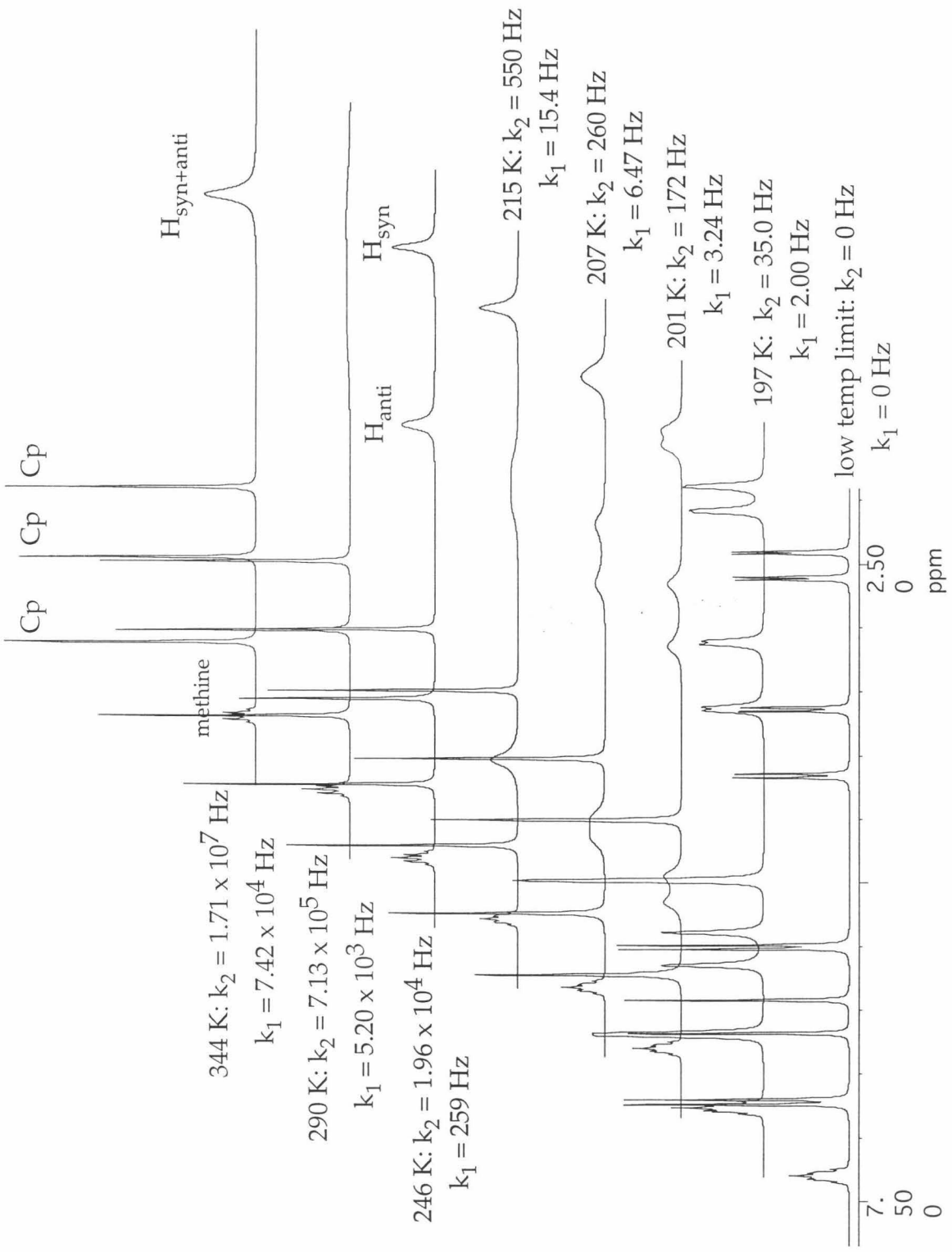

Figure 16. gNMR simulation of (C_3H_5) and vinylic Cp resonances of **16** (500 MHz, Et_2O-d_{10}) using η^3-η^1 processes (ia), (ib), and η^3-rotation.

mechanisms are shown in Figure 16. Only when η^3-rotation is fast relative to the η^3-η^1 processes, however, do the simulated spectra fit the observed spectra in all temperature regimes; making the η^3-η^1 processes the low energy rearrangement pathways fails to generate spectra containing sharp AM_2X_2 allyl splitting patterns.

It is worth noting that the use of spectral simulation is intended primarily as a means of judging whether the observed spectral trends could be explained qualitatively by a single rearrangement mechanism. Rate constants and activation parameters are obtained from these simulations, but caution must be exercised when interpreting these numbers, especially when extrapolating rate constants over large temperature ranges.

The temperature where the allyl *syn-anti* coalescence occurs (i.e. where the AM_2X_2 and AX_4 splitting patterns are averaged) is the key temperature at which to obtain information on the rate of olefin dissociation. As η^3-rotation does not provide a means of affecting *syn-anti* exchange, this coalescence is solely a result of pathway (ib).

Results of optimization of the rates of olefin dissociation for the various *meso*-complexes, as well as the associated $\Delta G^{\ddagger}$s calculated using equation **II** are given in Table 3. Activation barriers to olefin dissociation for the *meso*- complexes are all on the order of 14 kcal/mol. These $\Delta G^{\ddagger}$ values are each valid only at the T_cs indicated, which span a roughly 80 °C temperature range for the entire series of metallocene/solvent pairs.

Cmpd	solvent	T_c (K)	$\Delta G^{\ddagger}_{\eta 3\text{-}\eta 1, Tc}$ (kcal/mol)
16	Et_2O-d_{10}	290	12.0
17	Et_2O-d_{10}	361	15.6
17	toluene-d_8	370	16.0
18	toluene-d_8	327	13.4
19	toluene-d_8	362	14.9

Table 3. Olefin dissociation barriers for *meso*- metallocenes

When pathways (ia) and (ib) are slow (as was determined by lineshape analysis for **16-19**), η^3-rotation may be treated as a two-site exchange mechanism, and thus evaluated using equations **I** and **II**. Activation energies for η^3-rotation, determined using this approximation, for the *meso*-metallocenes are given in Table 4.

Cmpd	solvent	T_c (K)	$\Delta G^{\ddagger}_{\eta 3\text{-rot},Tc}$ (kcal/mol) Eqns **I**, **II**
16	Et_2O-d_{10}	215	9.7 (± 0.6)
17	Et_2O-d_{10}	208	9.9 (± 0.7)
17	toluene-d_8	207	10.6
18	toluene-d_8	246	12.2 (± 1.6)
19	toluene-d_8	259	12.2 (± 0.9)

Table 4. Activation barriers to η^3-rotation activation, obtained from two-site exchange approximation (I)

Extrapolation of Activation Barriers for Complexes 16-19

Complicating the direct comparison of olefin dissociation barriers is the fact that the $\Delta H^{\ddagger}$ and $\Delta S^{\ddagger}$ may not both be independently obtained from the observed NMR spectra.

Rate constants for olefin dissociation may then be extrapolated to various temperatures using Equation **III** (Table 5). Based primarily on the value obtained for **15** in toluene-d_8, a $\Delta S^{\ddagger}$ of -10 e.u. is utilized for these calculations.

$$k = T \exp [-(\Delta H^{\ddagger}/RT) + \Delta S^{\ddagger}/R + 23.76] \quad (\mathbf{III})$$

Incorporating the approximate η^3-η^1 rates, the rate of η^3-rotation may then be optimized in order to best approximate the observed NMR spectra at several temperatures, generally those where distinct coalescences could be observed. These optimizations were performed with the η^3-η^1 process operating at a rate determined by application of Equation III. After a series of k_2 had been evaluated, Eyring plots were generated for each of the

metallocene/solvent pairs; the activation parameters resulting from these plots are given in Table 6.

Cmpd	solvent	$\Delta S^{\ddagger}_{\eta 3\text{-}\eta 1}$ (e.u.)	$\Delta H^{\ddagger}_{\eta 3\text{-}\eta 1}$ (kcal/mol)	$\Delta G^{\ddagger}_{\eta 3\text{-}\eta 1,298\ K}$ (kcal/mol)	$k_{1,\ 298\ K}$ (sec^{-1})
16	Et_2O-d_{10}	-10	9.1	12.1	8.2×10^3
17	Et_2O-d_{10}	-10	12.0	14.9	6.8×10^1
17	toluene-d_8	-10	12.3	15.3	3.9×10^1
18	toluene-d_8	-10	10.1	13.1	1.6×10^3
19	toluene-d_8	-10	11.3	14.3	2.1×10^2

Table 5. Activation parameters for olefin dissociation, and 298 K rate constants obtained from extrapolation of estimated $\Delta H^{\ddagger}$, $\Delta S^{\ddagger}$

Cmpd	solvent	$\Delta S^{\ddagger}_{\eta 3\text{-rot}}$ (e.u.)	$\Delta H^{\ddagger}_{\eta 3\text{-rot}}$ (kcal/mol)	$\Delta G^{\ddagger}_{\eta 3\text{-rot,Tc}}$ (kcal/mol)
16	Et_2O-d_{10}	6.4	11	9.6
17	Et_2O-d_{10}	-24	5.1	10.1
17	toluene-d_8	-20	6.4	11.6
18	toluene-d_8	-13	9	12.2
19	toluene-d_8	9.9	14.5	11.9

Table 6. Activation parameters for in-plane rotation for *meso*- metallocenes obtained from Eyring plots of low temperature coalescence data

Despite the small temperature range over which ligand coalescences were observed, the considerable scatter observed in the Eyring plots, and the number of approximations required to arrive at the final activation free energies, comparison of the $\Delta G^{\ddagger}_{\eta 3\text{-}\ rot}$ resulting from extrapolation using the gNMR-derived $\Delta H^{\ddagger}_{\eta 3\text{-rot}}$ and $\Delta S^{\ddagger}_{\eta 3\text{-rot}}$ show a surprisingly good correlation with (are within experimental error of) those obtained from application of equations **I** and **II**.

As was performed for olefin dissociation, the evaluation of $\Delta H^{\ddagger}_{\eta 3\text{-rot}}$ and $\Delta S^{\ddagger}_{\eta 3\text{-rot}}$ permits extrapolation of $\Delta G^{\ddagger}_{\eta 3\text{-rot}}$ and k_2 for the various

metallocenes to a common temperature (Table 7), although these values are derived ultimately from estimated values of $\Delta H^{\ddagger}_{\eta 3\text{-}\eta 1}$ and $\Delta S^{\ddagger}_{\eta 3\text{-}\eta 1}$.

Cmpd	solvent	$\Delta G^{\ddagger}_{\eta 3\text{-rot},298\ K}$ (kcal/mol)	$k_{2,\ 298\ K}$ (sec^{-1})
16	Et_2O-d_{10}	9.1	1.33×10^6
17	Et_2O-d_{10}	12.3	6.42×10^3
17	toluene-d_8	12.4	5.35×10^3
18	toluene-d_8	12.9	2.25×10^3
19	toluene-d_8	11.5	2.10×10^4

Table 7. In-plane rotation barriers for **16 - 19**, extrapolated to 298 K

Regardless of the individual $\Delta H^{\ddagger}$ and $\Delta S^{\ddagger}$ values, judging only by qualitative assessment of the VT spectral trends, large differences exist between **15** and the *meso* metallocenes **16-19**. In the former, olefin dissociation is the lowest energy rearrangement pathway, whereas η^3-rotation is fast relative to η^3-η^1 (which becomes prominent at higher temperatures) for the latter. This may be explained by the relative congestion in the metallocene wedge imparted by the C_5Me_5 rings relative to the less-substituted *meso*- complexes, whose metal centers may additionally be more open as a result of "tying back" the Cp rings with the dimethylsilyl linking units.

Regarding the relative rates of η^3-rotation and η^3-η^1 for the *meso*-complexes **16-19**, qualitative assessment of the gNMR simulations indicates that the rate of η^3-rotation (k_2) is generally (usually $\geq$ 1 order of magnitude) greater than olefin dissociation (k_1). Extrapolations of the calculated $\Delta G^{\ddagger}$ to common temperatures (298 K, Table 2) are for the most part consistent with this observation. The one exception to this trend is **18** (toluene-d_8); the rate of η^3-rotation still exceeds that of η^3-η^1, but only by roughly a factor of two, as determined by extrapolation of the g-NMR derived activation parameters.

Caution must be exercised when comparing the 298 K values of k_1 and $\Delta G^{\ddagger}_{\eta 3\text{-}\eta 1}$, as these are extrapolations based on *estimated* values of $\Delta S^{\ddagger}_{\eta 3\text{-}\eta 1}$. Nonetheless, a pronounced increase in the rate of olefin dissociation (2 orders

of magnitude) is observed when switching from AdpY to the slightly more congested AdpSc system. The rate of olefin dissociation also appears largely independent of solvent at room temperature, with **17** exhibiting comparable η^3-η^1 activation barriers in both diethyl ether and toluene.

The rate of η^3-rotation appears largely independent of solvent (**17**, toluene vs. Et_2O), but large changes in k_1 (3 orders of magnitude) are observed when changing the transition metal (**16** vs. **17**, Et_2O), and smaller changes in rate are associated with variation of the Cp substituents (**18** vs. **19**). Some of the changes in rate may be easily rationalized, such as a decreased barrier to rotation when switching to a ligand with smaller alkyl substituents in the open portion of the metallocene wedge (3 and 3′ substituents) (**19** vs. **18**); other trends are more puzzling (such as the large decrease in the rate of η^3-rotation when switching from yttrium to the slightly smaller scandium, or the smaller decrease in rate when 3,3′ substituents are changed from MeAd to CMe_3).

As mentioned earlier, allyl C=C double bond dissociation was modeled as occurring with equal probability from each side of the metallocene wedge. Although this is a reasonable assumption for the Cp^*_2 ligand array, its validity in the cases of the *meso-* complexes is less certain, as the C_s-symmetry of the ligand array makes dissociation from the two sides of the wedge energetically inequivalent. The η^3-η^1 process was modeled assuming olefin dissociation from exclusively one side of the metallocene wedge, in order to determine whether such a preference might be observed experimentally. Although there is undoubtedly some lateral preference for dissociation, the fact that η^3-rotation, which provides *syn-syn* and *anti-anti* exchange, was determined to occur rapidly with respect to C=C dissociation leads to the observation that dissociation from one side of the metallocene wedge is, using the available NMR data, indistinguishable from dissociation from both sides of the wedge. Modeling C=C dissociation from one side of the wedge in the *absence* of η^3-rotation provided spectra that bore little likeness to any of the experimentally observed spectra.

The clockwise and counterclockwise rotations of the η^3-allyl ligand pass through energetically inequivalent transition states in the framework of a *meso-* ligand array (Figure 17). The η^3-rotation $\Delta G^{\ddagger}$s given in Tables 6 and 7, therefore, technically reflect only the pathway with the lower energy

activation barrier. Not enough is currently known about the precise steric interactions between the allyl ligand and the 3,3′ metallocene alkyl substituents in order to determine which of the two possible transition states is of lower energy. The availability of two possible rotation pathways does not significantly affect the analyses presented above, as the two pathways are experimentally indistinguishable for *meso*- complexes.

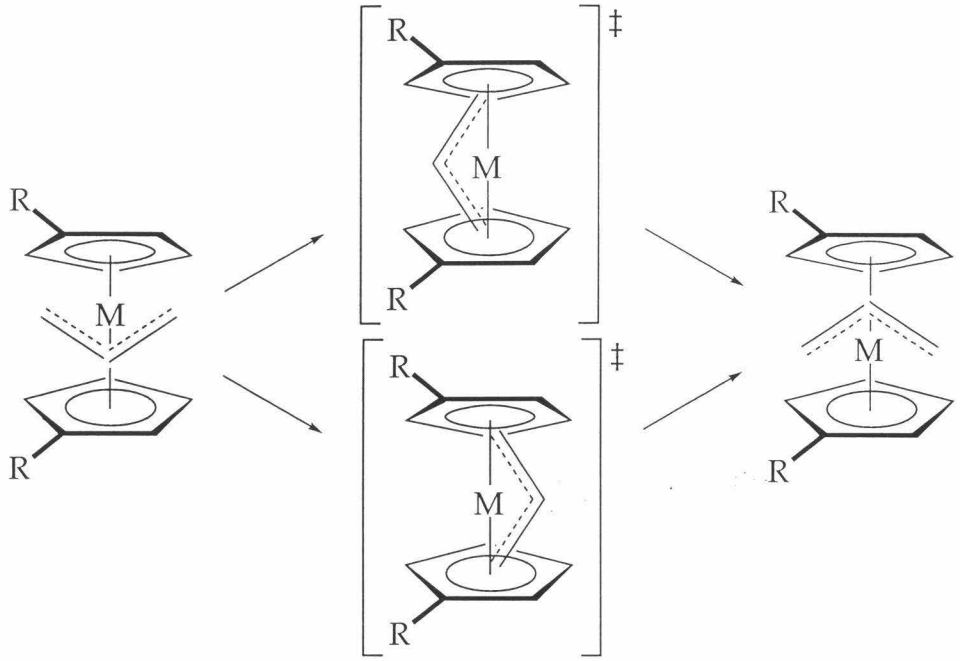

Figure 17. Possible η^3-rotation transition states for *meso*-metallocenes.

Lineshape Analyses of *racemo* -Metallocenes 20-21

Spectral simulations were undertaken in order to try to understand the rather complicated variable temperature NMR spectra exhibited by two d^0 scandocenes whose ancillary ligand arrays exhibit C_2-symmetry: *rac*-IpSc(C_3H_5) (**20**), and the enantiomerically pure (R,S)-BnBpSc(C_3H_5) (**21**) (the (R) refers to

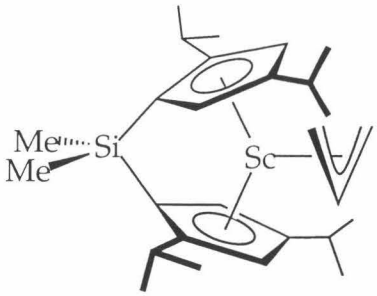

(20)

rac-IpSc(η^3-C_3H_5)

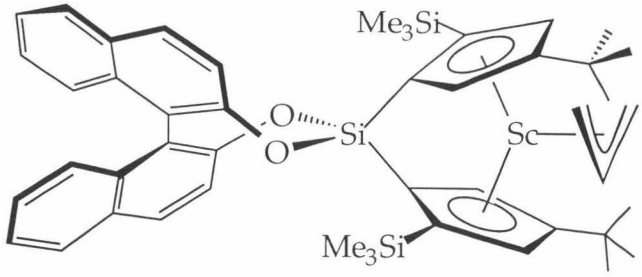

(21)

(R,S)-BnBpSc(η^3-C_3H_5)

the chirality of the binaphthol moiety, and the (S) to the configuration at the metal center).[24] The C_2- symmetries of the ligand arrays lead to pronounced differences in the observed NMR spectra, compared to either **15** or **16-19**.

The NMR spectra of **20** and **21** at low temperatures show AGMPX allyl splitting patterns and inequivalent Cp rings and substituents (Figure 18), consistent with static allyl moieties. As the probe temperature is raised, the Cp rings and substituents are rendered equivalent. As the temperature is increased further, there is a simultaneous broadening of all four of the allyl methylene hydrogen resonances. After a wide temperature range in which the allyl methylene hydrogens are broadened out into the baseline, a single resonance appears at a chemical shift equal to the weighted average of the four previously inequivalent methylene hydrogen signals (an AX_4 splitting pattern) with no sign of the intermediate AM_2X_2 spectra previously observed for the *meso*- complexes.

This behavior may be explained, in part, by observing the results of the η^3-rotation and η^3-η^1 rearrangement processes in a C_2-symmetric ligand framework. A single iteration of the in-plane η^3-rotation mechanism (Scheme 4) provides Cp-Cp exchange simply by a change in directionality of the allyl methine carbon. Inspection of the allyl ligand before and after the transformation shows no change in the magnetic environments of the individual methylene hydrogens; the fact that η^3-rotations affect no change in the environments of the allyl methylene hydrogens results in an AGMPX allyl splitting pattern, regardless of the rate of η^3-rotation.

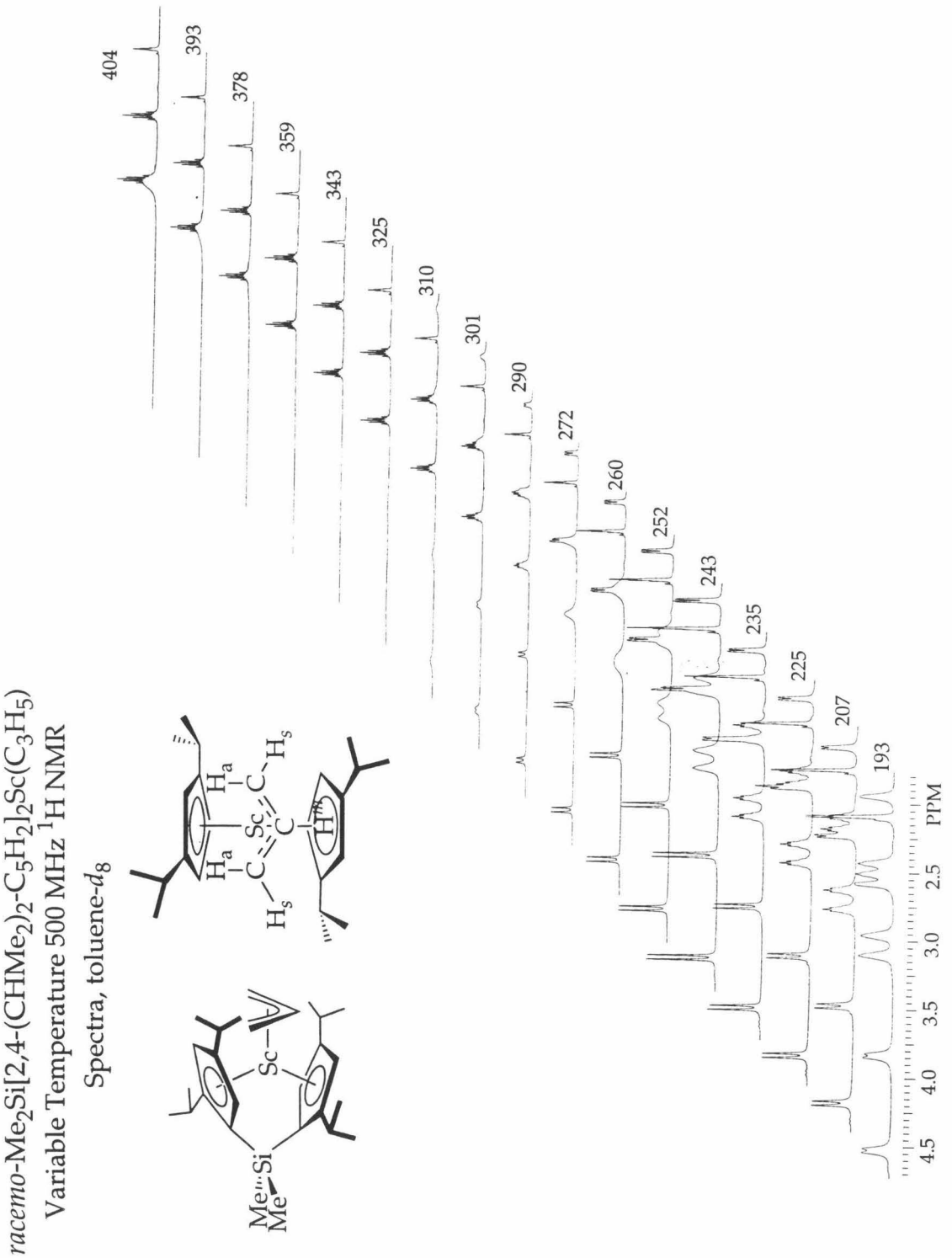

Figure 18. Variable temperature ^{1}H NMR spectra of *rac*-IpSc(C_3H_5) (**20**) (500 MHz, toluene-d_8).

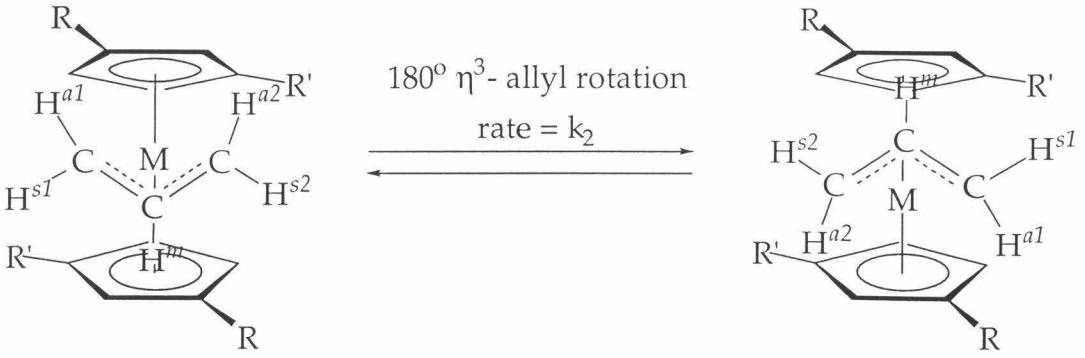

Scheme 4. 180° In-plane rotation for C_2-symmetric *ansa*-metallocenes.

The results of olefin dissociation followed by rotation about the allyl C-C single bond for **20** and **21**, however, are quite different from the systems investigated previously; a non-pairwise exchange of hydrogens (i.e. $H_{a1} \rightarrow H_{s2}$; $H_{a2} \rightarrow H_{a1}$; $H_{s1} \rightarrow H_{a2}$; $H_{s2} \rightarrow H_{s1}$) is observed for the *racemo*- complexes (Scheme 5).

Olefin dissociation followed by rotation about the M-C single bond has the same net effect as in-plane η^3-rotation; for the *racemo*-complexes **20** and **21**, this is manifested by exchange of the Cp rings and no net effect on the allyl resonances.

Again, spectral simulation must be used to obtain information on the rate of olefin dissociation, which exchanges allyl substituents by non-two-site exchange mechanisms. A stackplot of the gNMR-derived spectra for **20** using only the η^3-η^1 processes is shown in Figure 19. The values of $\Delta G^{\ddagger}$ and k_1 obtained from lineshape analysis similar to that performed on **15-19** are given in Table 8. As the $\Delta G^{\ddagger}$ values are valid only at the coalescence temperatures indicated, direct comparison of the *rac*-Ip and BnBp systems is not possible. Consistent with the results obtained for **15** and **17**, the nearly identical coalescence temperatures and $\Delta G^{\ddagger}$s in THF and toluene indicates a lack of solvent dependence on the rate of olefin dissociation.

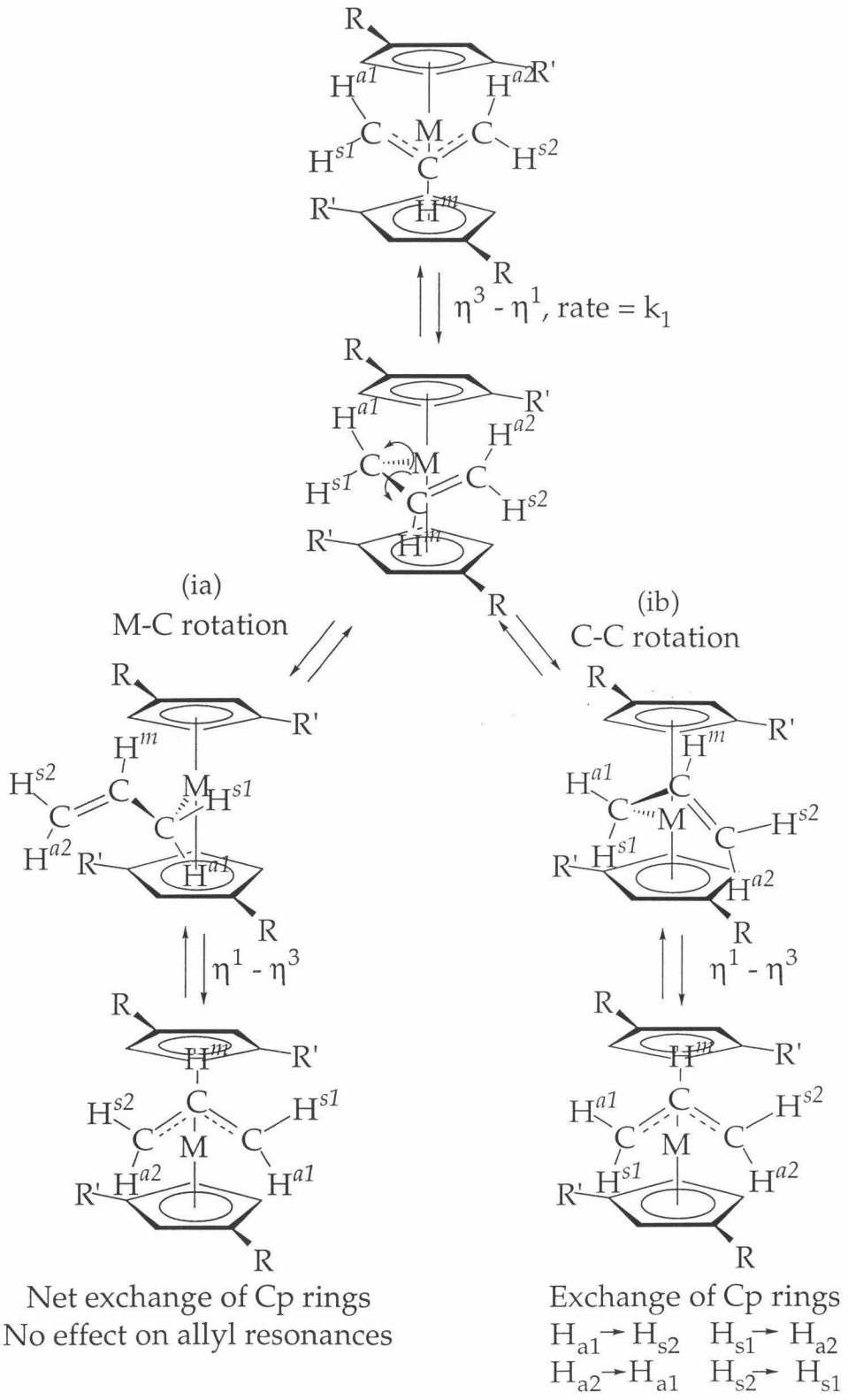

Scheme 5. Implications of olefin dissociation and subsequent M-C and C-C single bond rotations for C_2-symmetric metallocenes.

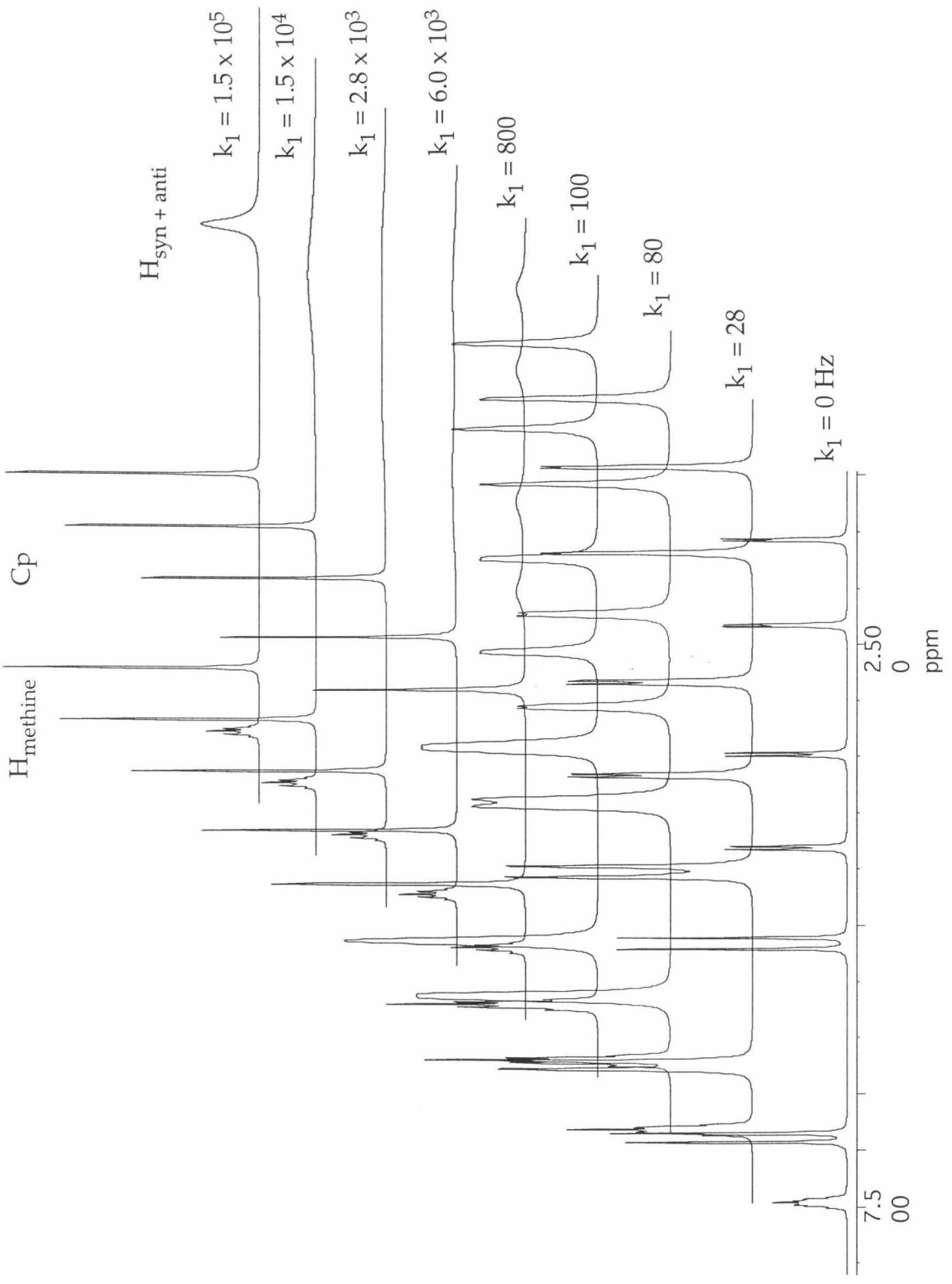

Figure 19. gNMR simulation of Cp and (C_3H_5) resonances of **20** (500 MHz, toluene-d_8) using η^3-η^1 processes (ia) and (ib).

Compound	Solvent	T_c (K)	$k_{1,\,Tc}$ (sec^{-1})	$\Delta G^{\ddagger}_{\eta 3\text{-}\eta 1,\,Tc}$ (kcal/mol)
20	toluene-d_8	359	8400	14.7
20	THF-d_8	350	5200	14.6
21	toluene-d_8	330	6400	13.6
21	THF-d_8	335	6800	13.8

Table 8. Olefin dissociation activation energies for *racemo*- metallocenes

Although it is clear that the η^3-η^1 processes are operating for **20** and **21** at higher temperatures, it is not possible to determine whether this process is responsible for the averaging of the ligand resonances at low temperatures (as was seen for **15**), or whether in-plane rotation is operating as the low energy rearrangement pathway (as was observed for the *meso*- metallocenes). The errors associated with extrapolating rate constants over considerably large temperature ranges precludes the identification of the rearrangement mechanism operating at low temperatures.

Conclusions

The variable temperature NMR spectra of d^0-metallocene allyl complexes **15-21** indicate static η^3-allyl ligands at low temperatures. Common to **15-21** is olefin dissociation to generate transient η^1-allyl species. Lineshape analysis of the observed spectra provides activation barriers to olefin dissociation of ~10-14 kcal/mol for all of these complexes, although the coalescence temperatures at which the $\Delta G^{\ddagger}$ were obtained span a 140 degree temperature range.

The symmetry constraints imposed by rigid *meso*-metallocenes **16-19** permits confirmation of a second type of allyl rearrangement: in-plane rotation of the intact η^3-allyl moiety. Although conclusive evidence of the existence of the latter process could not be obtained for *racemo*-complexes **20-21**, in-plane rotation was found, qualitatively, to be fast (rate constants

generally ≥1 order of magnitude larger) relative to olefin dissociation for **16-19**.

Rate constants derived from the activation parameters obtained for olefin dissociation and η^3-allyl rotation for **16-21** are rigorously valid only at the observed coalescence temperatures; this fact, coupled with the inability to independently determine $\Delta H^{\ddagger}$ and $\Delta S^{\ddagger}$, precludes a quantitative comparison of rate constants for the various processes and metallocene/solvent pairs at a common temperature, especially when the comparisons require extrapolation over large temperature ranges.

Experimental Section

General Considerations: All air and/or moisture sensitive compounds were manipulated using standard high vacuum line techniques or in a dry box under a nitrogen atmosphere, as described previously.[25] Argon and hydrogen gases were purified and dried by passage over columns of MnO on vermiculite and activated molecular sieves. Solvents were stored under vacuum over titanocene[26] or sodium benzophenone ketyl. Allene was purchased from Aldrich and used as received. $Cp^*_2Sc(\eta^3\text{-}C_3H_5)$,[27] *meso*-AdpSc($\eta^3$-$C_3H_5$), *meso*-AdpY($\eta^3$-$C_3H_5$),[28] and [*meso*-DpScH]$_2$,[29] were prepared according to published procedures. *meso*-IpSc(η^3-C_3H_5) and *rac*-IpSc(η^3-C_3H_5)[21] were synthesized and characterized by Jeffrey C. Yoder. Cyrille Loeber was responsible for the synthesis of (R,S)-BnBpSc(η^3-C_3H_5)[20].

Unless otherwise specified, all NMR spectra were recorded on a Bruker AM500 (500.13 MHz for ^{1}H) spectrometer. Lineshape analyses were performed on a 7300/180 Power Macintosh using gNMR (Cherwell Scientific Publishing, 1992-1996) version 3.6 for Macintosh.

Preparation of *meso*-$Me_2Si(3\text{-}CMe_3\text{-}C_5H_3)_2Sc(\eta^3\text{-}C_3H_5)$ [$DpSc(\eta^3\text{-}C_3H_5)$] (15). A J-Young NMR tube was charged with approximately 15 mg (0.0218 mmol) of [DpScH]$_2$ and 0.4 ml C_6D_6. The contents of the tube were cooled to -78 °C, and volatiles were removed on a high vacuum line. Allene (0.111 mmol, 5.1 eq) was transferred from a lecture bottle into the NMR tube at -78 °C via a 42.5 ml gas bulb, the NMR tube sealed, and the contents of the tube was brought to

room temperature. After heating for 6 hours at 80 °C, ^{1}H NMR spectroscopy indicated that all of the [DpScH] had been consumed. Volatiles were removed from the NMR tube *in vacuo*, and the residual yellow solid was dried under dynamic vacuum for 30 minutes. ^{1}H NMR (25 °C, C_6D_6): δ 7.50 (H_m, m, J=12.3 Hz, 1H), 6.75 (C_5H_3, t, J=2.5 Hz, 2H), 5.96 (C_5H_3, br, 2H), 5.29 (C_5H_3, t, J=2.6 Hz, 2H), 4.33 (H_a, br, 2H), 2.25 (H_s, br, 2H), 1.08 (CMe_3, s, 18H), 0.70 ($SiMe_2$, s, 3H), 0.22 ($SiMe_2$, s, 3H).

Lineshape Simulations

Spectral simulations using gNMR version 3.6 are based on general NMR theory.[30-32] Dynamic spectra are determined using a standard Liouville representation of quantum dynamics, as described by Binsch.[33,34] Lorentzian lineshapes with HWHM = 5.00 Hz were utilized, unless otherwise noted. Control experiments showed that changes to the linewidth did not visibly affect the rate of a particular exchange required to produce a given coalescence.

As systems with more than 12 exchanging nuclei may not be simulated using gNMR v.3.6, complicated systems such as **16-22** are generally broken down into two separate simulations: that of the allyl ligand and vinylic cyclopentadienyl fragments, and that of the silyl- and alkyl- substituents on the Cp rings. Frameworks for **16-22** were drawn on C.S. Chemdraw Pro v.3.5.1 (CambridgeSoft Corporation, 1995) and then cut and pasted into gNMR. The experimentally determined low temperature (slow exchange) chemical shifts and coupling constants were then entered for the various metallocene complexes. Exchange permutations then determined for each complex and then entered into the appropriate "Exchange" subroutine. Simulated spectra were obtained by entering the appropriate rates into the individual permutation routines and then using the "Calculate" function. Stackplots were generated by cutting and pasting a series of individual optimized spectra from gNMR into a single MacDraw Pro 1.5v1 file; this transfer causes a reduction in the resolution of the simulated spectra of a factor of 4.

For each combination of ligand array and solvent, ^{1}H NMR spectra were evaluated for **15-22** using the η^3-η^1 processes (rate = k_1) as the sole exchange mechanisms. The rate constant k_1 was evaluated as the rate of

olefin dissociation from an η^3-complex. Contributing to k_1 were processes involving rotations about both the resultant allyl C-C and the M-C single bonds. Each of these two types of rotations has the possibility of resulting in a productive rearrangement (one in which there is a net change in the allyl or Cp magnetic environments), or a nonproductive rearrangement (where there are no net changes in the allyl or Cp magnetic environments). Consequently, k_1 is the sum of the rates of four distinct exchange processes: generation of an η^1-intermediate and (1) a "productive" rotation about the C-C single bond; (2) a "non-productive" rotation about the C-C single bond; (3) a "productive" rotation about the M-C single bond; (4) a "non-productive" rotation about the M-C single bond.

To simplify the lineshape analyses, only "productive" rearrangements were utilized to generate the simulated spectra; k_1 was adjusted to take into account "nonproductive" rearrangements, which were modeled as occurring with equal likelihood as the "productive" rearrangements. Unless otherwise noted, generation of η^1-intermediates were modeled as occurring with equal probability from both sides of the metallocene wedge; rotation about the M-C single bonds of these η^1-intermediates result in identical exchanges of allyl and cyclopentadienyl hydrogens. In order to further simplify calculations, only a single M-C rotation permutation was utilized, with appropriate statistical factors and included in the reported value of k_1.

Control experiments were performed in which both "productive" and "nonproductive" rearrangements were explicitly simulated; excluding the identity operation(s) ("nonproductive" rearrangements), when appropriate, resulted in no observable change to the NMR spectrum for a given value of k_1 when the appropriate correction factor is applied to the remaining contributor to k_1. Similarly, control experiments showed no visible change in the value of k_1 required to generate a given coalescence when utilizing either one or two distinct processes to simulate the two possible M-C single bond rotations.

The variable temperature NMR spectra for **16-22** were simulated using the following procedure:

(1) k_1 was optimized to best simulate the high temperature (*syn-anti*) coalescence, with k_2 (the rate of η^3-rotation) set temporarily equal to 0.

(2) $\Delta H^{\ddagger}_{\eta 3 - \eta 1}$ was evaluated using equations (**II**) and (**III**), with $\Delta S^{\ddagger}_{\eta 3 - \eta 1} = -10$ e.u.

(3) k_1 was calculated at several temperatures using the $\Delta H^{\ddagger}_{\eta 3 - \eta 1}$ and $\Delta S^{\ddagger}_{\eta 3 - \eta 1}$ from step (2)

(4) k_2 was optimized to best fit the observed spectra at the temperatures used in step (3); these optimizations of k_2 were performed with concurrent olefin dissociation, using the k_1 rates determined in step (3).

(5) Activation parameters for η^3-rotation were derived from Eyring plots of the k_2 values from step (4)

(6) An approximate rate of η^3-rotation was calculated for the high temperature (*syn-anti*) coalescence using the activation enthalpy and entropy values derived in step (5)

(7) k_1 values were reoptimized to simulate the observed spectra, this time including concurrent η^3-rotation (k_2 rates from steps (4) and (6))

References and Notes

1. Bochmann, M. *J. Chem. Soc. Dalton. Trans* **1996**, 255.

2. Brintzinger, H. H.; Fischer, D.; Mulhaupt, R.; Rieger, B.; Waymouth, R. N. *Angew. Chem. Int. Ed. Eng.* **1995**, *34*, 1143.

3. Casey, C. P.; Hallenbeck, S. L.; Pollock, D. W.; Landis, C. R. *J. Am. Chem. Soc.* **1995**, *117*, 9770.

4. Casey, C. P.; Hallenbeck, S. L.; Wright, J. M.; Landis, C. R. *J. Am. Chem. Soc.* **1997**, *119*, 9680.

5. Wu, Z.; Jordan, R. F.; Petersen, J. L. *J. Am. Chem. Soc.* **1995**, *117*, 5867.

6. Collman, J. P.; Hegedus, L. S.; Norton, J. R.; Finke, R. G. *Principles and Applications of Organotransition Metal Chemistry*; University Science Books: Mill Valley, CA, **1987**, p. 175.

7. Jolly, P. W.; Mynott, R. *Adv. Organomet. Chem.* **1981**, *19*, 257.

8. Vrieze, K., in *Dynamic Nuclear Magnetic Resonance Spectroscopy;* Jackman, L. and Cotton, F. A., Eds.; Academic Press: New York, **1975**, p. 441.

9. Kreiger, J. K.; Deutch, J. M.; Whitesides, G. M. *Inorg. Chem.* **1973**, *12*, 1535.

10. Benn, R.; Rufinska, A.; Schroth, G. *J. Organomet. Chem* **1981**, *217*, 91.

11. Becconsall, J. K.; Job, B. E.; O'Brien, S. *J. Chem. Soc., A* **1967**, 423.

12. Faller, J. W.; Chen, C.-C.; Mattina, M. J.; Jakubowski, A. *J. Organomet. Chem*. **1973**, *52*, 361.

13. Evans, W. J.; Ulibarri, T. A.; Ziller, J. W. *J. Am. Chem. Soc.* **1990**, *112*, 2314.

14. Landis, C. R.; Cleveland, T.; Casey, C. P. *Inorg. Chem.* **1995**, *34*, 1285.

15. Tjaden, E. B.; Casty, G. L.; Stryker, J. M. *J. Am. Chem. Soc.* **1993**, *115*, 9814.

16. Pastor, A.; Kiely, A. F.; Henling, L. M.; Day, M. W.; Bercaw, J. E. *J. Organomet. Chem.* **1997**, *528*, 65.

17. Antonelli, D. M.; Tjaden, E. B.; Stryker, J. M. *Organometallics* **1994**, *13*, 763.

18. Jeske, G.; Lauke, H.; Mauermann, H.; Swepston, P. N.; Schumann, H.; Marks, T. J. *J. Am. Chem. Soc.* **1985**, *107*, 8091.

19. Tsutsui, M.; Ely, N. *J. Am. Chem. Soc.* **1975**, *97*, 3551.

20. Abrams, M. B.; Yoder, J. C.; Loeber, C.; Day, M. W.; Bercaw, J. E. , Manuscript in preparation.

21. Yoder, J. C.; Day, M. W.; Bercaw, J. E. *Manuscript in preparation*, .

22. Lineshape analysis was perfomed using gNMR Version 3.6 for Macintosh as described in the Experimental Section and in Appendix B.

23. Lauher, J. W.; Hoffmann, R. *J. Am. Chem. Soc.* **1976**, *98*, 1729.

24. Schlögl, K. *Top. Stereochem.* **1967**, *1*, 39.

25. Burger, B. J.; Bercaw, J. E. *New Developments in the Synthesis, Manipulation, and Characterization of Organometallic Compounds*, 1987; 357, .

26. Marvich, R. H.; Brintzinger, H. H. *J. Am. Chem. Soc.* **1971**, *93*, 2046.

27. Thompson, M. E.; Baxter, S. M.; Bulls, A. R.; Burger, B. J.; Nolan, M. C.; Santarsiero, B. D.; Schaefer, W. P.; Bercaw, J. E. *J. Am. Chem. Soc.* **1987**, *109*, 203.

28. Abrams, M. B., Ph.D. Thesis, California Institute of Technology, **1998**.

29. Bunel, E. E., Ph.D. Thesis, California Institute of Technology, **1989**.

30. Pople, J. A.; Schneider, W. G.; Bernstein, H. J. *High Resolution Nuclear Magnetic Resonance*; McGraw-Hill: New York, **1959**, p. 1.

31. Binsch, G., in *Dynamic Nuclear Magnetic Resonance Spectroscopy*; Jackman, L. M. and Cotton, F. A., Eds.; Academic Press: London, **1975**, p. 45.

32. Steigel, A., in *NMR, Basic Principles and Progress*; Diehl, P., Fluck, E. and Kosfeld, R., Eds.; Springer-Verlag: Berlin, **1978**; *Vol. 15*, p. 1.

33. Binsch, G. *J. Am. Chem. Soc.* **1969**, *91*, 1304.

34. Binsch, G. *J. Magn. Res.* **1978**, *30*, 625.

Appendix C: Variable Temperature ^{1}H NMR Data for 15-18

Table 1. Variable temperature 300 and 500 MHz ^{1}H NMR data for $Cp^*_2Sc(C_3H_5)$ (**15**)

Solvent	Temp (K)	δ (ppm)	J_{H-H} (Hz)	Assignment
toluene-d_8	326	7.06 (quintet, 1H) 2.89 (s, 4H) 1.85 (s, 30H)	12.9	$H_2CC\mathbf{H}CH_2$ $\mathbf{H}_2CCHC\mathbf{H}_2$ C_5Me_5
	194	7.15 (m, 1H) 3.93 (d, 2H) 2.05 (m, 2H) 1.86 (s, 15H) 1.73 (s, 15H)	14.8	$H_2CC\mathbf{H}CH_2$ $\mathbf{H}_2CCHC\mathbf{H}_2$, *anti* $\mathbf{H}_2CCHC\mathbf{H}_2$, *syn* C_5Me_5 C_5Me_5
Et_2O-d_{10} (300 MHz)	333	6.97 (quintet, 1H) 2.74 (d, 4H) 1.90 (s, 30 H)	12.6 (avg) 12.0	$H_2CC\mathbf{H}CH_2$ $\mathbf{H}_2CCHC\mathbf{H}_2$ C_5Me_5
	210	6.97 (m, 1H) 3.62 (d, 2H) 1.88 (d, 2H) 1.93 (s, 15H) 1.83 (s, 15H)	 15.6 4.6	$H_2CC\mathbf{H}CH_2$ $\mathbf{H}_2CCHC\mathbf{H}_2$, *anti* $\mathbf{H}_2CCHC\mathbf{H}_2$, *syn* C_5Me_5 C_5Me_5

Table 2. Variable temperature 500 MHz ^{1}H NMR data for *meso*-AdpSc(C_3H_5) (**16**)

Solvent	Temp (K)	δ (ppm)	J_{H-H} (Hz)	Assignment
Et_2O-d_{10}	181	7.30 (m, 1H)		$H_2CC\mathbf{H}CH_2$
		6.74 (1H)		Cp
		6.70 (1H)		Cp
		6.18 (1H)		Cp
		5.92 (1H)		Cp
		5.52 (1H)		Cp
		5.49 (1H)		Cp
		4.16 (d, 1H)	16	$\mathbf{H}_2CCHC\mathbf{H}_2$, *anti*
		3.64 (d, 1H)	15	$\mathbf{H}_2CCHC\mathbf{H}_2$, *anti*
		2.61 (d, 1H)	11	$\mathbf{H}_2CCHC\mathbf{H}_2$, *syn*
		2.41 (d, 1H)	9	$\mathbf{H}_2CCHC\mathbf{H}_2$, *syn*
		2.27, 2.16, 2.08, 1.88, 1.68,		
		1.57, 1.47, 1.32 (m, 28H)		Me**Ad**
		0.95 (s, 3H)		**Me**Ad
		0.84 (s, 3H)		**Me**Ad
		0.74 (s, 3H)		Me_2Si
		0.25 (s. 3H)		Me_2Si
	246	7.22 (m, 1H)		$H_2CC\mathbf{H}CH_2$
		6.67 (m, 2H)	2.3	Cp
		5.98 (m, 2H)		Cp
		5.50 (m, 2H)	2.6	Cp
		3.89 (d, 2H)	14.3	$\mathbf{H}_2CCHC\mathbf{H}_2$, *anti*
		2.28 (br, 2H)		$\mathbf{H}_2CCHC\mathbf{H}_2$, *syn*
		2.35, 2.17, 1.83, 1.76, 1.70,		
		1.67, 1.62, 1.47 (m, 28 H)		Me**Ad**
		0.90 (s, 6H)		**Me**Ad
		0.71 (s, 3H)		Me_2Si
		0.24 (s, 3H)		Me_2Si

	344	7.15 (m, 1H)		$H_2CC\mathbf{H}CH_2$
		6.62 (2H)		Cp
		5.96 (2H)		Cp
		5.51 (2H)		Cp
		3.07 (4H)		$\mathbf{H}_2CCHC\mathbf{H}_2$
		2.30, 2.18, 2.16, 1.81, 1.79, 1.70, 1.64, 1.48 (m, 28H)		Me**Ad**
		0.92 (s, 6H)		**Me**Ad
		0.69 (s, 3H)		Me_2Si
		0.22 (s, 3H)		Me_2Si

Table 3. Variable temperature 500 MHz ^{1}H NMR data for *meso*-AdpY(C_3H_5) (**17**)

Solvent	Temp (K)	δ (ppm)	J_{H-H} (Hz)	Assignment
Et_2O-d_{10}	263	6.67 (m, 1H)		$H_2CC\mathbf{H}CH_2$
		6.19 (m, 2H)		Cp
		5.97 (br, 2H)		Cp
		5.68 (m, 2H)	3	Cp
		3.19 (d, 2H)	15	$\mathbf{H}_2CCHC\mathbf{H}_2$, *anti*
		2.48 (d, 2H)	7.5	$\mathbf{H}_2CCHC\mathbf{H}_2$, *syn*
		2.15, 2.10, 1.95, 1.85, 1.81, 1.68, 1.58, 1.48 (m)		Me**Ad**
		1.70 (s, 6H)		**Me**Ad
		0.67 (s, 3H)		Me_2Si
		0.36 (s, 3H)		Me_2Si

	194	6.72 (m, 1H)		$H_2CC\mathbf{H}CH_2$
		6.24 (1H)		Cp
		6.20 (1H)		Cp
		6.13 (1H)		Cp
		5.93 (1H)		Cp
		5.67 (2H)		Cp
		3.34 (d, 1H)	13	$\mathbf{H}_2CCHC\mathbf{H}_2$, *anti*
		3.12 (d, 1H)	13	$\mathbf{H}_2CCHC\mathbf{H}_2$, *anti*
		2.56 (br, 1H)		$\mathbf{H}_2CCHC\mathbf{H}_2$, *syn*
		2.41 (br, 1H)		$\mathbf{H}_2CCHC\mathbf{H}_2$, *syn*
		2.13, 2.02, 1.93, 1.87, 1.55, 1.46 (m)		Me**Ad**
		1.69 (s, 6H)		**Me**Ad
		0.70 (s, 3H)		Me_2Si
		0.38 (s, 3H)		Me_2Si
toluene-d_8	186	**6.68 (m, 1H)??**		$H_2CC\mathbf{H}CH_2$
		6.03 (br, 2H)		Cp
		5.91 (s, 1H)		Cp
		5.86 (s, 1H)		Cp
		5.77 (s, 1H)		Cp
		5.75 (s, 1H)		Cp
		3.53 (d, 1H)	14.3	$\mathbf{H}_2CCHC\mathbf{H}_2$, *anti*
		3.39 (d, 1H)	13.4	$\mathbf{H}_2CCHC\mathbf{H}_2$, *anti*
		2.81 (br, 1H)		$\mathbf{H}_2CCHC\mathbf{H}_2$, *syn*
		2.64 (br, 1H)		$\mathbf{H}_2CCHC\mathbf{H}_2$, *syn*
		2.45, 2.00, 1.87, 1.76, 1.59, 1.38, 1.26 (m, 28H)		Me**Ad**
		0.93 (s, 3H)		**Me**Ad
		0.87 (s, 3H)		**Me**Ad
		0.78 (s. 3H)		Me_2Si
		0.50 (s, 3H)		Me_2Si

	309	6.66 (m, 1H)	12.3	$H_2CC\mathbf{H}CH_2$
		6.09 (m, 2H)	2.4	Cp
		5.95 (m, 2H)		Cp
		5.74 (m, 2H)	2.6	Cp
		3.32 (d, 2H)	15.1	$\mathbf{H}_2CCHC\mathbf{H}_2$, *anti*
		2.61 (d, 2H)	6.6	$\mathbf{H}_2CCHC\mathbf{H}_2$, *syn*
		2.05, 2.02, 1.99, 1.93, 1.90, 1.85, 1.78, 1.65, 1.61, 1.59, 1.57, 1.55, 1.52, 1.44 (m)		Me**Ad**
		0.98 (s, 6H)		**Me**Ad
		0.70 (s, 3H)		Me_2Si
		0.38 (s, 3H)		Me_2Si

Table 4. Variable temperature 500 MHz ^{1}H NMR data for *meso*-DpSc(C_3H_5) (**18**)

Solvent	Temp (K)	δ (ppm)	J_{H-H} (Hz)	Assignment
toluene-d_8	210	7.41 (m, 1H)		$H_2CC\mathbf{H}CH_2$
		6.66 (t, 1H)	2.2	Cp
		6.54 (s, 1H)		Cp
		5.91 (m, 1H)	br	Cp
		5.70 (m, 1H)	br	Cp
		5.17 (m, 1H)	2.5	Cp
		5.11 (m, 1H)	2.5	Cp
		4.48 (d, 1H)	15.3	$\mathbf{H}_2CCHC\mathbf{H}_2$, *anti*
		4.16 (d, 1H)	15.3	$\mathbf{H}_2CCHC\mathbf{H}_2$, *anti*
		2.31 (d, 1H)	7.3	$\mathbf{H}_2CCHC\mathbf{H}_2$, *syn*
		2.04 (d, 1H)		$\mathbf{H}_2CCHC\mathbf{H}_2$, *syn*
		1.05 (s, 9H)		CMe_3
		1.00 (s, 9H)		CMe_3
		0.67 (s, 3H)		Me_2Si
		0.20 (s, 3H)		Me_2Si

	297	7.44 (quintet, 1H)	12.3	$H_2CC\mathbf{H}CH_2$
		6.91 (m, 2H)		Cp
		5.90 (2H)	br	Cp
		5.23 (t, 2H)	2.7	Cp
		4.28 (d, 2H)	12.5	$\mathbf{H}_2CCHC\mathbf{H}_2$, *anti*
		2.52 (s, 2H)		$\mathbf{H}_2CCHC\mathbf{H}_2$, *syn*
		1.07 (s, 18H)		CMe_3
		0.68 (s, 3H)		Me_2Si
		0.21 (s, 3H)		Me_2Si
	373	7.44 (quintet, 1H)	12.4	$H_2CC\mathbf{H}CH_2$
		6.75 (t, 2H)	2.6	Cp
		5.95 (t, 2H)	2.2	Cp
		5.28 (t, 2H)	2.8	Cp
		3.22 (br)		$\mathbf{H}_2CCHC\mathbf{H}_2$
		1.09 (s, 18H)		CMe_3
		0.69 (s, 3H)		Me_2Si
		0.22 (s, 3H)		Me_2Si

Appendix D: Selected gNMR Data

Table 1. gNMR Parameters for $Cp^*_2Sc(\eta^3\text{-}C_3H_5)$ (**15**), toluene-d_8, 500 MHz

Molecule # 1 (Concentration = 1.00000) (C_5Me_5)

Nucleus Name	Group # n	Shift (ppm)	W (Hz)	J (Hz) 1	2	3	4
1H	1 1	7.150	5.00				
	2 1	2.050	5.00	7.00			
	3 1	3.930	5.00	14.80	0.00		
	4 1	2.050	5.00	7.00	0.00	0.00	
	5 1	3.930	5.00	14.80	0.00	0.00	0.00

Molecule # 2 (Concentration = 5.00000) (C_5Me_5)

Nucleus Name	Group # n	Shift (ppm)	W (Hz)	J (Hz)
1H	1 3	1.860	5.00	

Molecule # 3 (Concentration = 5.00000) (C_3H_5)

Nucleus Name	Group # n	Shift (ppm)	W (Hz)	J (Hz)
1H	1 3	1.730	5.00	

Permutations

Mol #	Nucl Name	Group # n	η^3-rotation	η^3-η^1, C-C	η^3-η^1, C-C	η^3-η^1, M-C
1	1H	1 1	1-1	1-1	1-1	1-1
1	1H	2 1	1-4	1-3	1-2	1-4
1	1H	3 1	1-5	1-2	1-3	1-5
1	1H	4 1	1-2	1-4	1-5	1-2
1	1H	5 1	1-3	1-5	1-4	1-3
2	1H	1 3	3-1	3-1	3-1	3-1
3	1H	2 3	2-1	2-1	2-1	2-1

Table 2. gNMR Parameters for *meso*-AdpSc(η^3-C_3H_5) (**16**), Et_2O-d_{10}, 500 MHz, Allyl and Vinylic Cyclopentadienyl Protons

Molecule # 1 (Concentration = 1.00000) (C_3H_5)

Nucleus Name	Group # n	Shift (ppm)	W (Hz)	J (Hz) 1	2	3	4
1H	1 1	2.610	5.00				
	2 1	4.160	5.00	0.00			
	3 1	7.300	5.00	11.00	16.00		
	4 1	2.410	5.00	0.00	0.00	9.00	
	5 1	3.640	5.00	0.00	0.00	15.00	0.00

Molecule # 3 (Concentration = 1.00000) (C_5H_3)

Nucleus Name	Group # n	Shift (ppm)	W (Hz)	J (Hz) 1	2
1H	1 1	6.740	5.00		
	2 1	6.180	5.00	0.00	
	3 1	5.520	5.00	0.00	0.00

Molecule # 4 (Concentration = 1.00000) (C_5H_3)

Nucleus Name	Group # n	Shift (ppm)	W (Hz)	J (Hz) 1	2
1H	1 1	6.700	5.00		
	2 1	5.920	5.00	0.00	
	3 1	5.490	5.00	0.00	0.00

Permutations

Mol #	Nucl Name	Group # n	η^3-rotation	η^3-η^1, C-C	η^3-η^1, C-C	η^3-η^1, M-C
1	1H	1 1	1-4	1-2	1-1	1-4
1	1H	2 1	1-5	1-1	1-2	1-5
1	1H	3 1	1-3	1-3	1-3	1-3
1	1H	4 1	1-1	1-4	1-5	1-1
1	1H	5 1	1-2	1-5	1-4	1-2
3	1H	1 1	4-1	4-1	4-1	4-1
3	1H	2 1	4-2	4-2	4-2	4-2
3	1H	3 1	4-3	4-3	4-3	4-3
4	1H	1 1	3-1	3-1	3-1	3-1
4	1H	2 1	3-2	3-2	3-2	3-2
4	1H	3 1	3-3	3-3	3-3	3-3

Table 3. gNMR Parameters for *rac*-IpSc(η^3-C_3H_5) (**20**), toluene-d_8, 500 MHz, Allyl and Vinylic Cyclopentadienyl Protons

Molecule # 1 (Concentration = 1.00000) (C_3H_5)

Nucleus Name	Group # n	Shift (ppm)	W (Hz)	J (Hz) 1	2	3	4
1H	1 1	7.420	5.00				
	2 1	2.550	5.00	8.00			
	3 1	3.780	5.00	15.00	0.00		
	4 1	1.910	5.00	8.00	0.00	0.00	
	5 1	4.510	5.00	15.00	0.00	0.00	0.00

Molecule # 2 (Concentration = 1.00000) (C_5H_2)

Nucleus Name	Group # n	Shift (ppm)	W (Hz)	J (Hz) 1	2
1H	1 1	6.370	5.00		
	2 1	5.230	5.00	0.00	

Molecule # 3 (Concentration = 1.00000) (C_5H_2)

Nucleus Name	Group # n	Shift (ppm)	W (Hz)	J (Hz) 1	2
1H	1 1	6.550	5.00		
	2 1	5.160	5.00	0.00	

Permutations

Mol #	Nucl Name	Group # n	η^3-rotation	η^3-η^1, C-C	η^3-η^1, C-C	η^3-η^1, M-C
1	1H	1 1	1-1	1-1	1-1	1-1
1	1H	2 1	1-2	1-4	1-5	1-2
1	1H	3 1	1-3	1-5	1-4	1-3
1	1H	4 1	1-4	1-3	1-2	1-4
1	1H	5 1	1-5	1-2	1-3	1-5
2	1H	1 1	3-1	3-1	3-1	3-1
2	1H	2 1	3-2	3-2	3-2	3-2
3	1H	1 1	2-1	2-1	2-1	2-1
3	1H	2 1	2-2	2-2	2-2	2-2

Table 4. gNMR Parameters for *rac*-IpSc(η^3-C_3H_5) (**20**), toluene-d_8, 500 MHz, Isopropyl Protons

Molecule # 1 (Concentration = 1.00000)

Nucleus Name	Group # n	Shift (ppm)	W (Hz)	J (Hz) 1	2
1H	1 1	3.100	5.00		
	2 3	1.320	5.00	7.00	
	3 3	1.320	5.00	7.00	0.00

Molecule # 2 (Concentration = 1.00000)

Nucleus Name	Group # n	Shift (ppm)	W (Hz)	J (Hz) 1	2
1H	1 1	2.960	5.00		
	2 3	1.160	5.00	7.00	
	3 3	1.160	5.00	7.00	0.00

Molecule # 3 (Concentration = 1.00000)

Nucleus Name	Group # n	Shift (ppm)	W (Hz)	J (Hz) 1	2
1H	1 1	2.530	5.00		
	2 3	1.100	5.00	7.00	
	3 3	1.100	5.00	7.00	0.00

Molecule # 4 (Concentration = 1.00000)

Nucleus Name	Group # n	Shift (ppm)	W (Hz)	J (Hz) 1	2
1H	1 1	2.430	5.00		
	2 3	1.060	5.00	7.00	
	3 3	1.060	5.00	7.00	0.00

Permutations

Mol #	Nucl Name	Group # n	η^3-rotation	η^3-η^1, C-C	η^3-η^1, C-C	η^3-η^1, M-C
1	1H	1 1	2-1	2-1	2-1	2-1
1	1H	2 3	2-2	2-2	2-2	2-2
1	1H	3 3	2-3	2-3	2-3	2-3
2	1H	1 1	1-1	1-1	1-1	1-1
2	1H	2 3	1-2	1-2	1-2	1-2
2	1H	3 3	1-3	1-3	1-3	1-3
3	1H	1 1	4-1	4-1	4-1	4-1
3	1H	2 3	4-2	4-2	4-2	4-2
3	1H	3 3	4-3	4-3	4-3	4-3
4	1H	1 1	3-1	3-1	3-1	3-1
4	1H	2 3	3-2	3-2	3-2	3-2
4	1H	3 3	3-2	3-2	3-2	3-2